WRPS-66074
Revision 0

FY2020 ILAW Glass Ion-Exchange Rate Testing
Final Report VSL-20R4820-2, Rev. 0, 10/05/2020

Prepared for the U.S. Department of Energy
Assistant Secretary for Environmental Management

Contractor for the U.S. Department of Energy
Office of River Protection under Contract DE-AC27-08RV14800

P.O. Box 850
Richland, Washington 99352

FY2020 ILAW Glass Ion-Exchange Rate Testing
Final Report VSL-20R4820-2, Rev. 0, 10/05/2020

I. L. Pegg
The Catholic University of America

I. S. Muller
The Catholic University of America

R. S. Skeen
Washington River Protection Solutions

C. Viragh
The Catholic University of America

K. Gilbo
The Catholic University of America

Date Published
February 2021

Department of Energy

Prepared for the U.S. Department of Energy
Assistant Secretary for Environmental Management

Contractor for the U.S. Department of Energy
Office of River Protection under Contract DE-AC27-08RV14800

P.O. Box 850
Richland, Washington 99352

APPROVED
By Lynn M Ayers at 2:55 pm, May 25, 2021

Release Approval Date

VSL-20R4820-2

Final Report

FY2020 ILAW Glass Ion-Exchange Rate Testing

prepared by

Isabelle S. Muller, Charles Viragh, Konstantin Gilbo, and Ian L. Pegg

Vitreous State Laboratory
The Catholic University of America
Washington, DC 20064

for

Atkins Energy Federal EPC, Inc.
Columbia, MD 21046

and

Washington River Protection *Solutions*, LLC
Richland, WA

September 1, 2020

Rev. 0, 10/5/20

Completeness of Testing:

This report describes the results of work and testing specified by WRPS. The work and any associated testing followed established quality assurance requirements. The descriptions provided in this test report are an accurate account of both the conduct of the work and the data collected. Results required by the test program are reported. Also reported are any unusual or anomalous occurrences that are different from the starting hypotheses. The test results and this report have been reviewed and verified.

I. L. Pegg: _____ **Date:** 10/6/20
VSL Program Director/Principal Investigator

I. Joseph: Innocent Joseph **Date:** 10/6/2020
Atkins Sub-Contract Manager

TABLE OF CONTENTS

List of Tables

List of Figures

List of Abbreviations

ANL-LRM	Argonne National Laboratory – Low-Activity Waste Reference Material
ASME	American Society of Mechanical Engineers
ASTM	American Society for Testing and Materials
CCC	Canister Centerline Cooling
CERCLA	Comprehensive Environmental Response, Compensation, and Liability Act
CUA	The Catholic University of America
DCP-AES	Direct Current Plasma Atomic Emission Spectroscopy
DOE	Department of Energy
DWPF-WA	Defense Waste Processing Facility – Environmental Assessment Glass
EDS	Energy Dispersive X-ray Spectroscopy
HLW	High Level Waste
ICP-AES	Inductively Coupled Plasma-Atomic Emission Spectroscopy
IDF	Integrated Disposal Facility
ILAW	Immobilized Low Activity Waste
IHLW	Immobilized High Level Waste
IX	Ion Exchange
LAW	Low Activity Waste
LFRG	Low-Level Waste Disposal Facility Federal Review Group
NDR	Normalized Dissolution Rate
NIST	National Institute of Standards and Technology
NQA	Nuclear Quality Assurance
ORP	Office of River Protection
PA	Performance Assessment
PCT	Product Consistency Test
PFT	Pulsed-Flow Test
PUF	Pressurized Unsaturated Flow
QA	Quality Assurance
QARD	Quality Assurance Requirements and Description
RCRA	Resource Conservation and Recovery Act
ROD	Record of Decision
S/V	Ratio of Surface Area to Solution Volume
SEM	Scanning Electron Microscopy
SPFT	Single-Pass Flow-Through
SRL-EA	Savannah River Laboratory-Environmental Assessment
TC&WM EIS	Tank Closure & Waste Management Environmental Impact Statement
Tris	tris(hydroxymethyl)aminomethane
TST	Transition State Theory
US	United States
VHT	Vapor Hydration Test
VSL	Vitreous State Laboratory
WRPS	Washington River Protection *Solutions*, LLC
WTP	Hanford Tank Waste Treatment and Immobilization Plant
XRF	X-Ray Fluorescence

SECTION 1.0
INTRODUCTION

1.1 Background

About 50 million gallons of high-level mixed waste is currently stored in underground tanks at The United States Department of Energy's (DOE's) Hanford site in the State of Washington. The Hanford Tank Waste Treatment and Immobilization Plant (WTP) will provide DOE's Office of River Protection (ORP) with a means of treating this waste by vitrification for subsequent disposal. The tank waste will be separated into low- and high-activity waste fractions, which will then be vitrified respectively into Immobilized Low Activity Waste (ILAW) and Immobilized High-Level Waste (IHLW) products. The ILAW product will be disposed of in an engineered facility – the Integrated Disposal Facility (IDF) – on the Hanford site, while the IHLW product will be directed to the national deep geological disposal facility for high-level nuclear waste. The ILAW and IHLW products must meet a variety of requirements with respect to protection of the environment before they can be accepted for disposal.

The Record of Decision (ROD) from the Tank Closure & Waste Management Environmental Impact Statement (TC&WM EIS) establishes the current waste streams to be disposed of at the IDF to be located in the 200 East Area which include ILAW, secondary waste associated with ILAW production, and other on-site Hanford non-Comprehensive Environmental Response, Compensation, and Liability Act (CERCLA) waste. In accordance with the DOE order on radioactive waste management (DOE Order 435.1), the IDF performance assessment (PA) is intended to analyze the long-term impacts on human health and the environment of the disposition of waste placed into the facility. Evaluation of the impact of disposed waste requires the ability to predict the long-term release of key radionuclides from the engineered system. In the case of the IDF, the engineered system includes a number of components including the proposed Resource Conservation and Recovery Act (RCRA) cap, back fill material, ILAW glass, leachate collection system, etc.

Since 1998, the IDF PA (formerly the ILAW PA) has been supported by a PA maintenance plan focused on collecting the critical data needed to predict long-term performance: site geology, recharge, hydrology, geochemistry (measurement of site specific K_d values for key contaminants of concern), and waste form release. The purpose of the PA maintenance plan is to allow PA revisions to reflect new scientific information that reduces the technical uncertainty associated with critical aspects of the PA. Although many of the components contained in the engineered system and addressed in previous IDF PAs are important in minimizing radionuclide release, arguably the most important, protective, and uncertain aspect of the engineered system is the long-term performance of the ILAW glass. The ILAW glass serves as a primary barrier that minimizes radionuclide release. Therefore,

developing robust, scientifically defensible predictions of long-term glass performance for the IDF PA is critical. The technical approach that is currently used to predict long-term release from ILAW glass for the IDF PA has gained acceptance from the Low-Level Waste Disposal Facility Federal Review Group (LFRG) and the international community evaluating the long-term corrosion of waste glass. It has also been peer reviewed and approved by a panel of independent experts during development of the 1998 IDF PA.

In the early IDF PAs, three prototypic glasses that spanned the range of glass compositions expected to be produced by the WTP were selected based upon specific processing constraints and composition projections that were current at the time. However, subsequent work has expanded the range of glass compositions that may be produced at the WTP and this type of composition range expansion is likely to continue through the life of the project. Thus, while the basic technical approach is well developed, there is a need to expand the range of glasses tested in order to span the composition range expected to be disposed of in the IDF and to develop an understanding of the dependence of the underlying model parameters and reaction network on the ILAW glass composition. Consequently, more recent testing has been directed towards addressing that need. Results from that work have identified a number of areas for potential improvement of the glass corrosion model that has been developed to support the ILAW PA, including the need to better understand and quantitatively describe the alkali-hydrogen ion exchange (abbreviated as ion exchange or IX). The need to relate the quantified ion exchange properties to glass composition is also evident. In Fiscal Year (FY) 19, the team of Atkins and the Vitreous State Laboratory (VSL) of The Catholic University of America (CUA) completed a series of tests to evaluate the ability of a fed batch-type reactor system (termed a Pulsed-Flow Test, or PFT) to elucidate the time dependence of ILAW glass ion exchange [1]. That work was important not only in demonstrating the performance of the PFT as an efficient method for expanding the available data on LAW glass ion exchange, but also because many researchers believe, and that work confirmed, that ion exchange is a diffusion limited process and will decrease with time. In contrast, the current IDF PA models ion exchange as a time-independent rate process. The results of the FY19 Atkins/VSL tests were much more successful than anticipated and the work has resulted in a large volume of data representing some of the most detailed information on ion exchange for LAW glasses obtained to date.

To capitalize on the success of the FY19 test results, Washington River Protection *Solutions*, LLC (WRPS) tasked Atkins/VSL to collect ion exchange data on three more ILAW glasses using the PFT, the results of which are the subject of the present Report. The work described herein was performed according to a Test Plan [2] that is responsive to the corresponding WRPS scope of work [3].

The following sections provide a brief review of the current approach for modeling ILAW release; the alternative ion exchange modeling approach that was evaluated in the previous [1] and present work; and an overview of the testing approach. Details and results are provided in the subsequent sections of this report.

1.2 ILAW Release Approach for the IDF PA

The technical approach that is currently used to predict long-term release from ILAW glass for the IDF PA has been developed, refined, and updated over the past decade or so. The approach and the supporting test data for ILAW glasses have been extensively documented [4 - 20]. A brief summary is presented in this section.

The underlying premise of the IDF PA is that the source term for radionuclide release is controlled by the long-term weathering of the glass matrix. This engineering-based approach has been used in previous PAs to provide the defense-in-depth required to defend the above premise and demonstrate through computer simulations that the proposed glass waste form will meet the regulatory requirements put forth by regulators and evaluated by the LFRG. The focus of this engineering-based approach is on estimating the model parameters and chemical reaction network needed to provide a robust simulation of glass weathering and the corresponding release of radionuclides over the period of performance (the compliance period specified in DOE M 435.1-1 is 1,000 years with 9,000 years of simulation beyond that point, completed to provide information to decision makers about potential long-term doses and to assess whether modeled peaks beyond the compliance period could potentially occur within the compliance period). The overall model incorporates the effects of chemical affinity and ion exchange. The model parameters $\vec{k}_o, \eta, E_a,$ and K_g are used to populate a chemical affinity-based kinetic rate law that is based upon Transition State Theory (TST) [21]:

$$r = \vec{k}_0 10^{\eta pH} \exp\left(\frac{-E_a}{RT}\right)\left[1-\left(\frac{Q}{K_g}\right)\right]^{\sigma} \tag{1.1}$$

where

- r is the dissolution rate of the glass [g/(m^2 d)], which is estimated after normalizing the measured concentration of each dissolved glass component to its concentration in the glass (value dependent on component since glass dissolves incongruently[1]),
- $\vec{k}_o$ is the forward rate constant [g /(m^2 d)],
- pH is the negative of the logarithm to base 10 of the hydrogen ion activity,
- η is the power law coefficient, which is unitless,

[1] If species are found in solution in proportion to their stoichiometry in the glass, dissolution is congruent. This is usually the case for boron for which the rate of release from the glass is often proportional to the glass dissolution rate because it is typically not retained in any reaction product formed during leaching. However, to address the possible diffusive release of boron, molybdenum and rhenium spiked into the glass also are used as indicators of matrix dissolution. When alkali and boron in the leachate have similar normalized concentrations, their release is congruent.

- E_a is the apparent activation energy (kJ/mol),
- R is the gas constant [8.314 . 10^{-3} kJ/(mo1 K)],
- T is the temperature (K),
- Q is the ion activity product (unitless[2]), K_g is the pseudo-equilibrium constant for the rate controlling phase or phases (unitless[2]), and σ is the Temkin coefficient, which has been theoretically shown to equal one [22, 23].

Equation (1.1) relates the effect of: (1) pH, (2) temperature, and (3) the activities of species that affect the rate of glass dissolution via Q. Equation (1.1) is based on the kinetic rate equation developed by Åagaard and Helgeson [22], as applied to glass by Grambow [24] wherein orthosilicic acid (H_4SiO_4) is the only rate controlling species in Q.

In addition to the dissolution rate equation, a term is included in the IDF PA calculations to represent the ion-exchange rate (r_{IEX}) between sodium in the glass and hydrogen ions in the aqueous phase, as the glass-water reaction proceeds. In general, the ion exchange rate is a function of temperature, glass composition, and reaction progress (stage of the glass-water reaction), as well as solution pH [1]. The potential importance of the contribution from ion exchange in the long-term corrosion mechanism had been emphasized previously by Feng and Pegg [25 - 27]. In previous glass testing work in support of the IDF PA, the standard approach to estimate this parameter has been that of McGrail et al. [6] and Pierce et al. [10] whereby r_{IEX} is obtained by subtraction of the boron dissolution rate from the sodium dissolution rate. Measurement of the temperature dependence of r_{IEX} also permits estimation of the activation energy E_{ad} of the Na ion exchange reaction. More recently, various issues with this approach have been identified [28, 29] including: (i) the reliability of this subtraction approach in view of the diffusive release of boron [14, 16]; (ii) an error in the calculation of r_{IEX} that has been propagated through previous work [29]; and (iii) the use of an r_{IEX} term that is independent of time and solution composition [28, 29]. In view of these issues, WRPS commissioned studies of potential alternative approaches for incorporation of ion exchange into the rate law [28, 29].

The use of Equation (1.1) with suitably estimated parameters, together with $r_{IEX,}$ solution speciation, and secondary phase formation, (as is typically performed with geochemical model codes with appropriate secondary phase data), allows for the source-term to be estimated within a reactive chemical transport modeling framework that takes into account the coupled effects of fluid flow and glass-water reactions on the chemistry of fluids percolating through the disposal facility. Coupling the fluid chemistry with the kinetic rate equations allows the simulations to describe the response of the glass corrosion rate to changes in fluid composition as a function of time and space.

---

[2] Note that although Q and K_g are unitless, their values are dependent on the standard state that is used for the underlying activities (typically, a hypothetical ideal solution at a concentration of 1 mol per liter in this work). Consequently, their numerical values are of no use unless these units are specified.

In previous work, the model parameters for Equation (1.1) have been obtained from the analysis of data produced using a variety of experimental techniques. The single-pass flow through (SPFT) test has been the primary technique used to estimate the coefficients of Equation (1.1). The results of recent work [1] show that Pulsed-Flow tests can also be used to obtain K_g and likely other parameters of Equation (1.1). Other tests used to evaluate glass durability are long-term high surface to volume ratio (S/V) product consistency tests (PCT-B), vapor hydration tests (VHT), and pressurized unsaturated flow (PUF) tests. This suite of tests evaluates different aspects of the glass-water reaction over the course of the various regimes of glass weathering: the initial forward rate regime; the decreasing rate regime; the residual rate regime; and the alteration rate renewal regime. These regimes are described below.

The initial forward rate consists of both ion-exchange and hydrolysis reactions. In dilute to near-saturated solutions, the TST-based model (without the ion-exchange term) successfully accounts for silicate dissolution in terms of temperature, pH, and reactive surface area because hydrolysis is the controlling reaction. However, as the glass-water reaction proceeds and the concentrations of glass components (particularly the dissolved silicic acid concentration) increase in solution, the rate of dissolution decreases. For ILAW glasses tested under alkaline conditions, it has been observed that, consistent with previous work [27], ion exchange becomes the dominant process controlling glass weathering under these near-saturated conditions [9]. The data collected from SPFT experiments conducted as a function of pH, temperature, and silicic acid concentration have been used to study these processes and to obtain the model parameters $\bar{k}_o, \eta, E_a, \text{and} K_g$.

As the glass continues to dissolve, the aqueous concentration of dissolved components approaches saturation with respect to the formation of a hydrated surface layer. The hydrated surface layer forms when relatively insoluble glass components (e.g., Al, Fe, and Si) accumulate in the bulk solution and condense at the glass-water interface. The rate of dissolution then continues at a relatively constant residual rate consistent with a process controlled by diffusion through the hydrated surface layer [30, 31]. The key alteration phase is often a clay mineral, such as a smectite or chlorite [14, 32, 33]. The precipitation kinetics associated with these phases can be complex, but in general the rate of secondary phase growth increases in response to an increase in the magnitude of supersaturation [23, 34]. In cases where an appreciable level of ion exchange is present, the data collected from SPFT experiments conducted as a function of temperature and silicic acid concentration can be used to evaluate the residual rate and obtain the model parameter r_{IEX}. Variable temperature experiments can also permit the determination of the activation energy for r_{IEX} and extrapolation of r_{IEX} to a specific repository temperature.

Finally, depending on the type of alteration phases that form, the glass-water reaction can increase from the residual rate and return to an elevated rate. This type of behavior has been observed in accelerated testing with high temperatures and high solid surface area to volume ratios for various glasses including United State (US) high level waste (HLW) glasses [32, 35-39], other HLW glasses [30, 31, 40-48], as well as Hanford low-activity waste (LAW) glasses

[14, 18, 33, 38, 49-52].

The combined H^+/Na^+ ion exchange and hydrolysis of the silicate network lead to the formation of a multi-layered reaction zone including a hydrated layer, a porous gel layer, and crystalline phases that precipitate on the surface [42, 47]. Increasing the S/V (PCT-B) is one method to explore higher reaction progresses and identify the secondary phases that are associated with resumption.

The data collected from VHT [14, 51], PCT-B [33, 38, 49-52], and PUF experiments [11] along with geochemical modeling and solid-phase characterization have been used to identify the key alteration phases formed as the glass weathers. The results from these tests provide the additional information needed to identify and constrain the appropriate chemical reaction network required for model simulations.

The above elements of the glass-water interactions are incorporated into the conceptual model that is used in the IDF PA to model glass dissolution, as described in more detail elsewhere [53].

1.3 Alternative Ion Exchange Approach

As described above, the current approach for modeling the release of contaminants from glass dissolution in the IDF PA employs a chemical affinity-based kinetic rate law that is used in combination with a term (r_{IEX}) that is intended to represent H^+/Na^+ ion exchange, together with the formation of secondary solid phases. Historically, the ion-exchange term has been assumed to be a constant for any given glass and depends only on temperature. As in the previous FY19 work [1], the present work addresses the need for an improved methodology for including ion exchange and for measuring the relevant H^+/alkali ion exchange parameters. The approach follows the recommendations provided in reference [28], which are in turn based on the findings of Feng and Pegg [27]. Thus, specific features of the present approach include:

- Recognition that ion exchange is a diffusive process and therefore the rate is expected to decrease as the square root of time;
- Recognition that ion exchange involves the exchange of an alkali ion by a hydronium ion or a proton and therefore the rate is expected to depend on the concentration of those species in solution. In other words, the ion exchange rate is expected to depend on the solution pH and to decrease as the pH increases;
- Recognition that ion exchange involves an activation energy and the rate is therefore expected to show an Arrhenius dependence on temperature;
- Recognition that all alkalis are subject to ion exchange, not just sodium. While sodium is the major alkali in LAW glasses, lithium becomes increasingly important

as the sulfur content in the waste increases since lithium (and other species such as vanadium and calcium) is added in increasing amounts to the glass formulations. Significant amounts of potassium are present in some wastes, which may also need to be considered.

As stated earlier, in comparison, the present approach used in the IDF PA employs an ion exchange rate that is constant with respect to time and solution composition, and for sodium only.

The approach of Feng and Pegg [27], together with the recognition that ion exchange and diffusive processes are expected to show an Arrhenius dependence on temperature, addresses all of the above issues and provides a rational basis for improvement of the manner in which ion exchange is incorporated into the IDF PA modeling. In that approach, release of alkalis by ion exchange is governed by the following rate equation [27]:

$$\frac{d[R^+]}{dt} = \frac{1}{2} k_d \frac{S}{V} \left(\frac{[H^+]}{[H^+]_0} \right)^{\alpha} t^{-1/2} \quad , \tag{1.2}$$

where $[R^+]$ is the solution concentration of alkali R, k_d is a rate constant, S is the glass surface area, V is the solution volume, $[H^+]$ is the H^+ concentration, $[H^+]_0$ is a scaling factor, t is time, and α is a constant (set equal to one half in [27] based on consistency with the data set). It should be noted that this provides a separate release mechanism for alkali above and beyond that provided by Equation (1.1).

Mathematically, both the time dependence and the pH dependence in Equation (1.2) are equivalent to those later described by Ojovan et al. [54] and subsequently implemented in the GRAAL model [55, 56], which together provide further underpinning of the basis for this approach. However, the interpretation is somewhat different in the GRAAL model (diffusion of all species through a protective layer in the GRAAL model [55, 56] versus diffusion-controlled release of alkali via ion exchange in [27] and [54]).

Finally, the temperature dependence is included by replacing k_d by $k_d(T)$ and writing:

$$k_d(T) = k_{d0} \exp\left(-\frac{E_{ad}}{RT} \right) \tag{1.3}$$

where $k_d(T)$ is the temperature dependent rate constant, k_{d0} is a constant, E_{ad} is an effective activation energy for ion exchange, R is the gas constant, and T is the absolute temperature. As noted previously [14, 28], if the ion exchange process is further interpreted in terms of the Doremus interdiffusion model [57], the rate constants are interpreted as diffusion constants and the term RT is replaced by $2RT$ in Equation (1.3); as in previous work [1], we adopt the rate constant approach and effective activation energy shown in Equation (1.3) for the present work.

As noted above, in the present IDF PA, sodium ion exchange is incorporated via an ion exchange rate that is assumed to be a constant (though sometimes temperature dependent) for any given glass. That rate, r_{IEX}, is expressed as moles of sodium released from the glass per unit time per unit glass surface area (typically mol m^{-2} s^{-1}). Clearly, that quantity can be obtained from Equation (1.2) by simply dividing by S/V. Thus, combining all of these results, the proposed new ion exchange rate is given by:

$$r_{IEX} = \frac{1}{2} k_{d0} \exp\left(-\frac{E_{ad}}{RT} \right) \left(\frac{[H^+]}{[H^+]_0} \right)^{\alpha} t^{-\frac{1}{2}} \tag{1.4}$$

Setting $[H^+]_0$ = 1 mol per liter and using pH = -log $[H^+]$, where "log" denotes the logarithm to base ten, we obtain:

$$r_{IEX} = \frac{1}{2} k_{d0} \exp\left(-\frac{E_{ad}}{RT} \right) 10^{-\alpha pH} t^{-\frac{1}{2}} \tag{1.5}$$

and therefore:

$$\log r_{IEX} = A + \frac{B}{T} + CpH - \frac{1}{2} \log t \tag{1.6}$$

where $A = \log(k_{d0}/2)$, $B = -(E_{ad}/R) \log e$, and C = - α.

We can also generalize Equation (1.4) to allow for deviation from square-root-of-time behavior by writing:

$$r_{IEX} = \frac{1}{2} k_{d0} \exp\left(-\frac{E_{ad}}{RT} \right) \left(\frac{[H^+]}{[H^+]_0} \right)^{\alpha} t^{-\gamma} \tag{1.7}$$

which yields:

$$\log r_{IEX} = A + \frac{B}{T} + CpH + D \log t \tag{1.8}$$

where D = - γ.

Equations (1.6) and (1.8) were used for the regression analysis of the PFT data, as described in Section 5.

The above approach could potentially address many of the shortcomings in the present IDF PA rate law and should be relatively simple to implement. However, any such approach requires a supporting test program that is designed to determine, over the range of ILAW glass compositions of interest, the new model parameters that are introduced. The work described herein further demonstrates the viability of this approach, which was verified for three glasses in the FY19 work [1], and expands the ion exchange data set to cover more of the LAW glass composition range.

It should be noted that ion exchange and matrix dissolution do not occur independently but are coupled processes that occur simultaneously, as described previously [27]. Thus, while in isolation, Equation (1.2) indicates that the ion exchange rate goes to zero as time goes to infinity, that is not the case when that process is coupled with matrix dissolution, described, for example, by Equation (1.1). Essentially, the velocity with which the diffusive alkali depletion front propagates into the glass is proportional to Equation (1.2) and that velocity decreases as that depletion layer increases in thickness. However, the glass is also being dissolved at the outer surface (the surface in contact with the solution) via matrix dissolution and, therefore, that surface propagates inwards at a velocity proportional to Equation (1.1); this process tends to thin the alkali depletion layer. This is a classic moving boundary problem, which has a steady-state solution wherein the two velocities become equal and the depletion layer moves inwards but with a constant thickness [27]. As a result, the time dependence will change from that typical for a diffusive system ($t^{-1/2}$) to a time independent system (t^{0}). Finally, other processes, such as the evolution of the solution composition and secondary phase formation, also modify the overall reaction trajectory. Thus, in implementation, Equations (1.1) and (1.5) (or the corresponding version of (1.7)) are coupled through the solution chemistry and speciation and precipitation reactions, which are typically handled in a geochemical code that forms part of the overall model. In the original work of Feng and Pegg [27], this coupling of the solution chemistry (but not secondary phase formation) was performed explicitly for silicon species only. Furthermore, the moving boundary aspects of the problem were handled in an approximate fashion by noting that, within this model, the velocity of the ion exchange front cannot fall below the velocity of the matrix dissolution front; therefore, if the calculated velocity of the ion exchange front does fall below the velocity of the matrix dissolution front, the former should be replaced by the latter, which leads to corresponding criteria for the ion exchange rate and matrix dissolution rate. Feng and Pegg [27] describe the various regimes in this overall process as these two rates approach each other and, ultimately, become equal.

1.4 Test Overview

Per the Test Plan [2] and WRPS work scope [3], this work addressed the measurement of ion exchange rates for selected LAW glasses using the PFT approach described in Section 1.3 The test conditions included variations in temperature, pH, and time in order to further test the alternative ion exchange model described in Section 1.3 and to determine the parameters in the ion exchange model for each glass.

As described in the glass selection document provided to WRPS for review [58] and subsequently approved by WRPS, the first two glasses selected for this work were formulated for LAW from tank AP-107 according to the two glass formulation algorithms developed previously by VSL: Glass AP107WDFL was formulated using the WTP Baseline LAW Glass Correlation [59] and ORLECAP107 was formulated using the Enhanced LAW Glass Correlation for high waste loading glasses [60]. The third glass ORLEC44 was also formulated with the Enhanced LAW Glass Correlation [60].

The work included fabrication, heat treatment, and confirmation of the composition of the selected glasses followed by testing to determine ion exchange rates using the Pulsed-Flow method. The data were analyzed to test the applicability of the ion exchange model form proposed by Feng and Pegg [27], as described in Section 1.3. Tests were conducted at three temperatures (70°C, 40°C, and 23°C) and five different buffer compositions covering a pH range from 7 to 11 (at room temperature) with ten sampling times for each experiment. The leachants were spiked with silicic acid in order to decrease the rate of matrix dissolution so that the relative ion exchange contribution to the overall glass dissolution rate was enhanced.

SECTION 2.0
GLASS SELECTION AND FABRICATION

2.1 Glass Selection

Two of the three glasses that were considered candidates for this work are LAW glasses that are important to the near-term DFLAW operations since they are designed for the LAW from the likely commissioning tank AP-107. They were also selected to avoid redundancy with any of the glasses for which SPFT testing has been conducted previously and, therefore, estimates of the ion exchange rates have not yet been made for these glasses. For convenience, a list of glasses previously tested by SPFT is included in Table 2.1. Also included in the table are the three glasses subjected to PFT in FY19 to elucidate the time, pH, and temperature dependence of ion exchange of various alkalis: LAWC22, IDF1-B2, and ORLEC28. A summary of prior PFT results is included in Table 2.2.

Two of the glasses selected for PFT in the present work, AP107WDFL and ORLECAP107, were formulated for LAW from tank AP-107 according to the two glass formulation algorithms developed previously by VSL [59, 60]. Glass AP107WDFL was formulated using the WTP Baseline LAW Glass Correlation [59] and ORLECAP107 was formulated using the ORP Enhanced LAW Glass Correlation for high waste loading glasses [60].

The third glass that was selected, ORLEC44 [60], is of interest because it has the same Na_2O content as LAWA44 but has a much higher SO_3 content. The higher sulfate solubility is accomplished by the introduction of V_2O_5 (2.44 wt%) together with higher levels of CaO (5.49 wt%) and Li_2O (0.99 wt%) as glass former additives. Consequently, testing of this glass offers additional insight into the effects of these changes, which are characteristic of the differences between the baseline and enhanced high waste loading glass formulations.

The compositions of the three glasses selected for testing in the present work are given in Table 2.3. As shown in Figure 2.1, the three selected glasses also further cover the LAW compositional space of glasses tested by either SPFT or PFT. Table 2.4 provides a description of the glass compositions, highlighting the species used to monitor matrix dissolution and the alkalis for which ion exchange rates were determined. These glass compositions include spikes of rhenium and molybdenum as indicators of matrix dissolution (as potential alternatives to boron, as suggested previously [1, 16, 18, 20]) and cesium, which together with sodium, lithium, and potassium, allows for assessment and comparison of the behavior of all of the alkalis in LAW glasses. Rhenium is also a non-radioactive surrogate for technetium and its dissolution behavior, therefore, provides information regarding the long-term immobilization of technetium in LAW glasses.

The recommendations of the above glass compositions for testing [58] were reviewed and approved by WRPS before preparation, characterization, and testing of these glasses.

2.2 Glass Preparation

The three glass compositions selected were prepared from reagent grade or higher purity chemicals according to VSL standard operating procedures. Briefly, an appropriate combination of well-mixed chemicals was melted at 1200ºC for 75 minutes in a platinum-gold crucible. Mixing of the melt was accomplished with a platinum stirrer beginning 15 minutes after the start of melting and continuing for the next 60 minutes, until the end of melting. The melt batch included a rhenium spike targeted at 0.1 wt% Re_2O_7, if all of it were retained in the glass. Since rhenium is subject to significant volatile loss from the glass during melting, excess Re_2O_7 was added to compensate, assuming an average retention of 53.5% based on extensive past testing [61]. This results in the addition of 0.93 g, instead of 0.50 g of Re_2O_7, to each batch targeting 500 g of glass. Spikes of Cs_2O and MoO_3, targeted at 0.15 wt% and 0.10 wt%, respectively, were not over-batched since any volatile losses, which are expected to be much smaller than that for rhenium, have not been as well quantified as that for rhenium.

The as-melted glass samples (before heat treatment) generally showed no visible sulfate layer. Glasses ORLECAP107IX[3] and ORLEC44IX were emerald green in color and AP107WDFLIX was dark brown due to its high Fe_2O_3 content. A portion (~50 to 60 g) of the as-melted glass was set aside and the remainder was subjected to canister centerline cooling (CCC) heat treatment according to the WTP LAW container cooling profile [62] shown in Figure 2.2. After CCC heat treatment, the sample was about 11 cm in diameter at the surface and about 2 cm thick. Glasses AP107WDFLIXCCC and ORLEC44IXCCC remained translucent throughout (brown and emerald green, respectively). On ORLEC44IXCCC, thin dispersed yellow sulfate patches were easily washed off prior to testing. Glass ORLECAP107IXCCC included a crystallization layer of about 2-3 mm in thickness at the platinum crucible wall with a few intrusion zones of 5-6 mm. This lighter-colored crystallized section (near crucible wall) was easily separated from the rest of the glass allowing separate evaluation of the two sections, as described in Section 2.4.

2.3 Glass Compositional Analysis

The primary method used for glass composition analysis was X-ray fluorescence spectroscopy (XRF) on powdered glass samples. A PANalytical Axios^{mAX}-Advanced XRF

[3] "IX" is appended to the parent glass names to distinguish the specific compositions used for the present work.

spectrometer was used for this purpose. The XRF is calibrated over a range of glass compositions using standard reference materials traceable to the National Institute of Standards and Technology (NIST), as well as waste glasses such as the Argonne National Laboratory – Low-Activity Waste Reference Material (ANL-LRM) [63] and the Defense Waste Processing Facility (DWPF) – Environmental Assessment Glass (EA) [64]. Since boron and lithium are not determined by this procedure, it is supplemented by acid digestion followed by solution analysis, as described below.

Glass samples for analysis by direct current plasma atomic emission spectroscopy (DCP-AES) or inductively coupled plasma atomic emission spectroscopy (ICP-AES) analysis are first subjected to microwave-assisted total acid dissolution in Teflon vessels according to VSL standard operating procedures. Twenty milliliters of a 1:5 mixture of concentrated HF:HNO_3 is diluted to 50 ml and used for the dissolution. This procedure is similar to the American Society for Testing and Materials (ASTM) Test Method C1412-99, which also employs a mixture of concentrated HF and HNO_3 in microwave digestion of pulverized glass samples; supplemental use of HCl/H_3BO_3 is not included in the VSL procedure since boron is normally one of the analytes. The solutions resulting from the acid digestion are analyzed by DCP-AES or ICP-AES.

The glass composition analyses were performed on replicate samples, including the as-melted glasses and the core section of the sample subjected to CCC, which were both analyzed separately for composition by XRF, and DCP-AES after total acid digestion. The samples are typically rejected when major oxides, with target concentrations of 3 wt% or more, show relative deviations from the target composition of greater than 10%. The results provided in Table 2.5 show that the glasses are on target for all of the major glass constituents. SO_3 is found to be slightly below target, with a loss of 0.1 to 0.2 wt% SO_3 from target and no significant differences observed between the as-melted glass and the sample subjected to CCC for the two lower sulfate formulations (<0.1 wt% loss), but loss increases in ORLEC44 from 0.1 to 0.2 wt%. Cl is another constituent which shows a loss of ~0.05 to 0.1 wt%.

Rhenium was one of three spikes that were added for the specific purpose of estimating ion-exchange in glass during leaching. Rhenium was over-batched to compensate for volatile loss during melting; evaluation of 363 earlier crucible melts at a target Re_2O_7 concentration of 0.1 wt% showed an average retention of 53.5% [61]. With this compensation, the rhenium content in the three glass samples subjected to CCC varies from 0.126 to 0.130 wt% Re_2O_7. Batching did not include any compensation for volatility of the other two spikes, cesium and molybdenum. The spike of 0.15 wt% Cs_2O in all measured glass samples was found, with minor analytical variability at an average concentration of 0.13 wt%. Molybdenum was batched at 0.1 wt% and was measured at 0.08 wt% MoO_3 on average in all three samples subjected to CCC, indicating a relatively small volatile loss during melting. The measured rhenium, cesium, and molybdenum concentrations (Table 2.4) for each glass were used in normalization of the leaching data presented in Section 4 and the target value was used for the main glass constituents.

2.4 Glass Evaluation and Preparation for Pulse-Flow Testing

In addition to composition analysis, evaluation of the glass samples included scanning electron microscopy (SEM) imaging of cross-sectioned, polished and carbon-coated grains with energy dispersive X-ray spectroscopy (EDS) analysis. These methods were used to verify that samples AP107WDFLIXCCC and ORLEC44IXCC were free of crystallization and, in the case of ORLECAP107IXCCC, to identify the crystalline phases observed in the layer of glass near the crucible wall and to verify that the glass in the center of the crucible was free of secondary phases. Contact with platinum likely catalyzed crystal formation in the laboratory CCC heat treatment but similar crystallization at the full-scale WTP container-melt interface, if present, is expected to be a very small fraction of the total volume of glass in the LAW container. The crystalline layer was, therefore, cut away with a diamond saw.

The glass sample ORLECAP107IXCCC from near the crucible wall contained a sodium sulfate aluminosilicate phase estimated at about 12.87 vol% by SEM in the first few millimeters of glass that was in contact with the crucible wall. The morphology and main constituents identified by EDS indicate the sulfate sodalite lazurite, similar to that previously identified in high sodium and high sulfate glasses such as IDF1B2IXCCC [1]. Composition analysis by EDS of glass free of crystallization at the center of the crucible showed results consistent with the XRF analysis and the target glass composition.

Glass ground from segments from the center area of each CCC heat treated sample were used for the Pulsed-Flow tests (< 0.2 vol% crystals measured in the ground sample ORLECAP107IXCCC). Prior to their use in the leach tests, the glass samples were crushed and sieved to 100-200 mesh (75-149 μm). The ground glass was washed (2 minutes in deionized water and 2 minutes in 99% absolute ethanol) and air-dried to remove fines, which tend to dissolve faster than glass grains during leach tests and, thus, interfere with the test results.

The measured densities of the three glasses are 2.695 $g.cm^{-3}$ for AP107WDFLIXCCC, 2.680 $g.cm^{-3}$ for ORLECAP107IXCCC, and 2.655 $g.cm^{-3}$ for ORLEC44IXCCC.

To simplify discussion in subsequent sections of this report, the three glasses are referred to as AP107WDFL, ORLECAP107, and ORLEC44, and, in some of the data tables these are further shortened to A107, C107 and C44, with the understanding that all of the samples that were tested were collected from the above described batches, CCC heat treated, and free of any crucible-contact crystallized material.

SECTION 3.0
ION-EXCHANGE RATE TESTING

3.1 Pulsed-Flow Test Matrix

The three glasses were subjected to Pulsed-Flow tests as a function of pH, temperature, and time at silicic acid saturation, according to a test matrix similar to that typically used for SPFT testing.

The standard SPFT test matrix on a single glass includes 48 tests that vary temperature, pH, silicic acid concentration, and test time. In the present work, which was focused on the determination of ion exchange rates, only the highest silicic acid concentrations (at each test condition) was used. Similar silicic acid spiking was used for tests at all five values of pH instead of at pH 9 only in the typical SPFT test matrix. In previous SPFT testing, the tests at pH 11 and 12 have employed LiOH/LiCl "buffers." These solutions are not very effective at holding the pH but, more important for the present purpose, they introduce large (and artificial) concentrations of lithium, which can ion exchange with other alkalis (notably sodium) in the glass, thereby complicating data interpretation and preventing the measurement of lithium ion exchange all together. Therefore, alkali-containing buffers were avoided in the present work. Instead, as was successfully used in previous PFT [1], the amine buffer piperidine was used for pH 11; testing at pH 12 was not performed. In addition to the deletion of the pH 12 tests, it was necessary to reduce the number of temperature conditions from four to three due to funding limitations. In this manner, the ion exchange test matrix on a single glass could be completed with 15 tests, according to the matrix described in Table 3.1, which includes:

- Five values of pH (7, 8, 9, 10, 11)
- Three values of temperature (23, 40, 70°C)
- All tests at silicic acid saturation
- All tests measure B, the alkali species Na, K, and Li, Al, and the three spikes Re, Mo, and Cs in solution
- All tests run for sufficient time to adequately define the time dependence (10 to 30 days) and a minimum of 10 samples for each experiment.

3.2 Solution Preparation

Glass leaching experiments at a pH_{RT}[4] range from 7 to 10 were performed in 0.05 M tris(hydroxymethyl)aminomethane (Tris) solutions buffered to the target pH using concentrated HNO_3. Glass leaching experiments at pH_{RT} 11 were performed in piperidine buffered with concentrated HNO_3. A small amount of piperidine was also required to adjust the pH_{RT} 10 solutions. For a 0.05 M piperidine buffer, 4.26 g piperidine (Aldrich, >99.5%, d= 0.862 g/mL, pK_a 11.22) was removed with a syringe from the sealed bottle, added dropwise to a tared plastic bottle containing deionized water and diluted to one liter.

Leaching solutions containing varying amounts of Si were prepared by dissolving analytical grade silicic acid powder ($SiO_2.H_2O$) in 0.05 M Tris or piperidine. Due to the low solubility of amorphous silica in aqueous solutions, Tris stock solutions containing at least 160 ppm [Si] were prepared, heated at 90°C for a period of time, decanted carefully into fresh bottles to avoid transfer of precipitated solids, and analyzed by ICP-AES or DCP-AES in order to determine the concentration of Si. As necessary, the stock solutions were diluted to the target [Si] and buffered to pH_{RT} 7, 8, 9, or 10, as previously described. For the piperidine stock solution, the 2.5 g of silicic acid powder added to one liter of 0.05 M piperidine solution could not be completely dissolved even after a week at 90 °C. After careful decantation and analysis (~750 ppm Si) the solution was diluted with 0.05 M piperidine to the target [Si] and the pH was adjusted from about 11.5 to 11.0 using concentrated nitric acid. The silicic acid (pKa ~ 9.9) brings down the pH of the piperidine solution, so less HNO_3 is needed to adjust the pH to 11. The pH of the piperidine-base 0.05 M stock solution was about 11.5. Concentrated nitric acid (~500 µL) was added to adjust the pH to 11 for one liter of buffer containing silica. Silicic acid also brings down the pH of the 0.05 M Tris solution, to about 9.6, so that about 15 drops of piperidine are needed to adjust the pH to 10.0 at 105 ppm [Si] (~10 drops at 90 ppm [Si] and ~23 drops at 140 ppm [Si]).

The pH_T[5] values of the buffer solutions, heated to the test temperature, were measured using a temperature-compensated pH meter. Determination of pH_T was necessary for the calculation of dissolution rates using Equation (1.1) and the pH dependence of ion exchange in Equations 1.5 and 1.7. The pH values are provided in Table 3.2, showing good agreement with those of solutions used in previous tests [1, 16, 18, 20].

3.3 Description of Pulsed-Flow Experimental Setup

The rationale for flow-through tests such as the SPFT is to achieve steady state with respect to species in solution in order to control the affinity term in the rate law. Frequently, that

[4] Subscript indicates pH values obtained from measurements at room temperature (RT).
[5] Subscript indicates pH values measured at the test temperature *T*.

steady state corresponds to essentially very dilute conditions wherein the affinity term is equal to one. This condition is favored by higher flow rate, but then the concentrations in solution become very small and therefore a practical compromise must be reached. Typical volumetric flow rates employed in SPFT tests on LAW glasses have been in the range of about 7 to 50 µL/min, which corresponds to about 10 to 72 mL/day.

An often simpler approach to flow-through testing is to employ pulsed flow instead of continuous flow, wherein a portion of the leachate solution is replaced by fresh leachant at regular intervals to achieve the same average flow rate. This type of partial replenishment test was developed and employed extensively by VSL beginning in the 1980s for the HLW glass development and testing program and was called the "Pulsed-Flow Test." VSL has hundreds of such tests still in progress that have been running for many decades.

The present tests were designed with a periodic replacement of 50% of the leachate with fresh leachant in a 50-ml stainless steel vessel. The replacements were set at intervals of 1-day at 70 °C and 3-days at 40 °C and 23 °C. The quantity of glass was adjusted so that its surface area would approach the linear flow rate[6], q/S, and residence time values employed in previous SPFT tests on Hanford LAW glasses, as shown in Table 3.1. From each of the 25-ml samples collected, an aliquot of 5 ml was pipetted and reserved for pH measurement, and the remaining 20 ml was sampled for analysis after acidification.

3.4 Sample Analysis

The pH was measured on each sample collected from the flow-tests. The measured pH values were found to remain at the target buffer values with less than 1% relative deviation for all buffers for glass AP107WDFL. With the other two higher waste loading glasses, ORLECAP107 and ORLEC44, the deviation is also less than 1% relative in most experiments, except for the pH_{RT} 7 buffer at 70℃ (+6% relative on average) and at 40℃ (+5%).

Collected samples designated for solution analysis were acidified with a small amount of concentrated HNO_3 and analyzed by DCP-AES for B, Al, Li, K, and Na. Analyses of Mo, Re, and Cs were conducted by inductively coupled plasma – mass spectroscopy (ICP-MS).

A total of 45 pulsed-flow tests were performed yielding, with the buffer blanks, 513 individual samples analyzed for solution chemistry. Among these, five samples were identified as clear outliers evidently resulting from contaminations. At the end of the experiment, the altered glasses were collected, water-washed gently, and air dried. The altered glass samples

[6] The linear flow rate is calculated as the volumetric flow rate divided by the total surface area of glass in the test vessel.

were archived for potential future characterization.

3.5 Data Reduction

To the extent possible, the guidelines for SPFT data analysis in the ASTM standard [65] were adapted for the Pulsed-Flow data, as described in this section. The more substantive changes that are required are described in Sections 3.5.1 and 3.5.2.

For the SPFT, if a glass specimen having a known surface area is contacted by a solution that flows continuously at a known flow rate and at a constant temperature, the concentration of the *i*-th soluble glass component in the effluent solution exiting the reactor vessel can be used to calculate the amount of glass that has dissolved. The flow rate is determined by dividing the mass of solution that is collected for analysis by the duration over which it was collected. The dissolution rate of the glass (g m^{-2} day^{-1}) is then calculated as [65]:

$$(rate) = \frac{\left[C_i - C_i^o\right] \cdot \left(\frac{F}{S^o}\right)}{f_i} \tag{3.1}$$

where:

C_i - is the steady-state concentration of component *i* measured in the effluent solution (g/L)
$C_i°$ - is the background concentration of component *i* in the influent solution as measured in a blank test (g/L)
F - is the solution flow rate (L/day)
$S°$ - is the initial surface area of the glass sample that is exposed to solution (m^2), and
f_i - is the mass fraction of component *i* in the glass (g/g).

Several samples of the effluent solution are collected during the SPFT test to determine the steady-state concentrations of dissolved glass components at a particular solution flow rate.

When testing a crushed glass sample, its surface area ($S°$) is calculated as the product of the specific surface area and the mass of glass (m_g) used in the test. The specific surface area is approximated based on the mesh size of the fraction used in the test and the density of the glass. The particles of glass are presumed to be spherical with diameter (d) equal to the arithmetic average of the openings of the sieves used to prepare the material ($d = 5.625 \times 10^{-5}$ m for the -100 to +200 mesh fraction). The specific surface area (S_p) of a glass having a density ρ is [65]:

$$S_p = 6 \Big/ \rho \cdot d \tag{3.2}$$

thus, $$S^o = S_p \cdot m_g \quad (3.3)$$

The specific areas calculated using this approach are 1.979×10^{-2} $m^2.g^{-1}$ for AP107WDFL (ρ = 2.695 $g.cm^{-3}$), 1.990×10^{-2} $m^2.g^{-1}$ for ORLECAP107 (ρ = 2.680 $g.cm^{-3}$), and 2.009×10^{-2} $m^2.g^{-1}$ for ORLEC44 (ρ = 2.655 $g.cm^{-3}$).

In the SPFT, the volumetric flow rate (F) is calculated by dividing the mass of solution that is collected by the time for its collection and its density (which can be assumed to be 1 g/cm^3 in most cases).

During glass dissolution, the mass and surface area of the glass sample are expected to change over time as material is dissolved. The surface area S_j at time j during a SPFT test is calculated from the following expression [65]:

$$S_j = \frac{3}{\rho r_o} m_0^{1/3} m_j^{2/3} \quad (3.4)$$

where r_o is the radius of the glass particle and m_j is the sample mass at time j. The value of m_j is estimated by the equation [66]:

$$m_j = m_o - \frac{1}{f_i}\left[\sum_{n=1}^{j-1} F_n C_{n,i} \Delta t_n + F_j C_{j,i} \frac{\Delta t_j}{2}\right], \text{ j}\geq1 \quad (3.5)$$

where i is an element representative of the extent of glass dissolution such as boron, which was used for this purpose in the present work. Here it should be noted that Equation (3.5) inherently assumes uniform dissolution during SPFT testing and the absence of any surface alterations such as cracking.

To determine the steady-state concentration (C_i), the measured concentration of the i-th component is plotted as a function of time in order to visually identify the data to be used. Data that precede the attainment of steady-state conditions are excluded before calculating mean and standard deviation of the remainder. The relative standard deviation (the standard deviation divided by the mean) of the calculated steady state concentration must be less than 0.15 for the SPFT test results to be valid [65]. Soluble components monitored in this fashion typically include silicon, aluminum, sodium, and boron. The parameters of Equation (1.1) are typically estimated using normalized dissolution rate (NDR) of boron.

Estimation of K_g. For SPFT data, K_g is estimated from the NDR values obtained at steady state when the glass is leached in the presence of different concentrations of Si and at specific pH and T. To determine the parameter K_g at a given T, NDR values are plotted as a function of the activity of orthosilicic acid ($a[H_4SiO_4]$) present in the effluent solutions at steady state (Equation

(1.1)) and a linear regression on the data is performed. A similar approach was used for the PFT data. Values of $a[H_4SiO_4]$ were determined from the corresponding solution chemistry using the geochemical code PHREEQC. According to Equation (1.1), K_g is given by the value of $a[H_4SiO_4]$ at NDR = 0 [9]. To determine the K_g value at the presumed repository temperature of 15°C, the natural logarithm of the measured K_g values is plotted against the reciprocal of the absolute temperature and a linear regression is performed on the data [9].

Estimation of ion exchange parameters. r_{IEX} and E_{ad} for Na, Li, K, and Cs: Alkali ion exchange rates were obtained by subtracting the normalized PFT dissolution rates of either Mo, Re, or B from the normalized dissolution rate of the alkali and converting the result to moles of the specific alkali per unit glass surface area per unit time (*not* moles of *glass* per unit area per unit time). The activation energy E_{ad} of each alkali evaluated was determined by performing a linear regression of the natural logarithm of the measured r_{IEX} values versus the reciprocal of the absolute temperature. The slope of each regression provides $-E_{ad}/R$ according to Equation (1.3). The results from the regression were then used to extrapolate the r_{IEX} values of each alkali to the presumed repository temperature of 15°C.

The leachant flow in the SPFT is continuous whereas in the PFT it is pulsed and therefore discrete. Consequently, extraction of leach rates from the pulsed flow data requires a different approach from that used for the SPFT data per ASTM C1662. Before describing the pulsed-flow case, it is instructive to describe first the derivation of the rate equation for the continuous case.

3.5.1 Continuous Flow Case

We consider a sample of glass with surface area S in a reactor of volume V that is filled with leachant that flows through the reactor continuously at a constant volumetric flow rate F. The rate of release of species i from the glass at time t is $r_i(t)$ (mass of species i released into the leachant per unit surface area of glass per unit time). The mass of species i in solution in the reactor at time t is $m_i(t)$ and the concentration is $c_i(t) = m_i(t)/V$. That mass increases as a result of release from the glass and decreases as a result of the leachant flow, such that its rate of change is given by:

$$\frac{dm_i(t)}{dt} = r_i(t)S - c_i(t)F \tag{3.6}$$

and therefore:

$$\frac{dc_i(t)}{dt} = r_i(t)\frac{S}{V} - c_i(t)\frac{F}{V} \tag{3.7}$$

At steady state, $dc_i(t)/dt = 0$, so:

$$r_i = c_i(t)\frac{F}{S} \tag{3.8}$$

To obtain the rate of glass dissolution, r_g, we normalize by dividing by f_i, the mass fraction of species i in the glass to obtain:

$$r_g = c_i(t)\frac{F}{Sf_i}, \tag{3.9}$$

which, except for blank subtraction, is exactly the result given in Eq. 3.1 for analysis of SPFT data.

3.5.2 Pulsed-Flow Case

In the PFT, after each time interval Δt, a sample of the leachate of volume ΔV is withdrawn from the vessel for analysis and a volume ΔV of fresh leachant is added to the vessel. Considering the n^{th} and $(n+1)^{th}$ samplings, we denote the concentrations of species i at each point in this process as follows:

$c_{i,n}$ = the concentration of species i at the n^{th} sampling before replacement

$c_{i,n,s}$ = the concentration of species i at the n^{th} sampling after replacement (i.e., at the start of the next leaching interval)

$c_{i,n+1}$ = the concentration of species i at the $(n+1)^{th}$ sampling before replacement (i.e., at the end of that leaching interval).

The mass of species i in the leachant in the vessel after sampling is equal to the mass before sampling minus the mass removed; this quantity divided by the volume gives the concentration at the start of the interval:

$$c_{i,n,s} = (c_{i,n}V - c_{i,n}\Delta V)/V = c_{i,n}\left(1 - \frac{\Delta V}{V}\right) \tag{3.10}$$

Over the interval Δt, the mass of species i added to the solution in the reactor is $r_i S \Delta t$; it is also equal to the change in the concentration multiplied by the leachate volume:

$$(c_{i,n+1} - c_{i,n,s})V = \left[c_{i,n+1} - c_{i,n}\left(1 - \frac{\Delta V}{V}\right)\right]V \tag{3.11}$$

Setting these equal we obtain:

$$r_i(t) = \frac{c_{i,n+1} - c_{i,n}\left[1 - \frac{\Delta V}{V}\right]}{\Delta t \frac{S}{V}} \tag{3.12}$$

As before, the rate of glass dissolution, $r_g(t)$, is obtained through normalization by dividing by f_i, the mass fraction of species *i* in the glass:

$$r_g(t) = \frac{c_{i,n+1} - c_{i,n}\left[1 - \frac{\Delta V}{V}\right]}{\Delta t \frac{S}{V} f_i} \tag{3.13}$$

This is identical to the equation used previously at VSL to extract normalized glass dissolution rates from Pulsed-Flow test data (see, for example [37]).

At steady state, $c_{i,n+1} = c_{i,n}$ and therefore:

$$r_g = c_{i,n} \frac{\Delta V}{\Delta t} \frac{1}{S f_i} = c_{i,n} \frac{F}{S f_i} \ , \tag{3.14}$$

which agrees with the continuous case above (Equation (3.9)).

In the present work, Equation (3.13) was applied to PFT data for each of the alkalis (Li, Na, K, and Cs) and also to the data for the species used to measure release via matrix dissolution (B, Mo, and Re). Note that the concentration values in Equation 3.13 ($c_{i,n}$ and $c_{i,n+1}$) were obtained by first subtracting the background concentrations c_i^o from the corresponding measured concentrations, where:

c_i° = is the background concentration of component *i* in the influent solution as measured in a blank test (Appendix A, Table A0).

Alkali ion exchange rates were then obtained by subtracting the normalized dissolution rates of either Mo, Re, or B from the normalized dissolution rate of the alkali and converting the result to moles of the specific alkali per unit glass surface area per unit time (*not* moles of *glass* per unit

area per unit time). Thus, for alkali R (R = Li, Na, K, Cs) and matrix dissolution indicator M (M = B, Mo, Re), r_{IEX} is given by:

$$r_{IEX,R} = (r_{g,R} - r_{g,M})\frac{f_R}{W_R}, \tag{3.15}$$

where W_R is the atomic mass of R. Since r_g is typically stated in units of g m^{-2} d^{-1} whereas r_{IEX} is typically stated in units of mol m^{-2} s^{-1}, the result in Equation (3.15) is then further divided by the number of seconds per day.

SECTION 4.0
PULSED-FLOW TEST RESULTS

This section provides a discussion of the results from the Pulsed-Flow tests on glasses AP107WDFL, ORLECAP107, and ORLEC44. The results from regression analysis of the data in terms of the model described in Section 1.3 are presented in Section 5.

4.1 General Observations

Effluent solution analytical results for ten successive samples (daily at 70 °C and every 3 days at 40 °C and 23 °C) are provided in Appendix A. The steady-state concentrations of dissolved glass components were calculated as the average of the concentrations of the last few samples in each experiment (samples identified in boldface in Appendix A); they are presented in Tables 4.1 to 4.3 for AP107WDFL, ORLECAP107, and ORLEC44, respectively. The steady-state concentrations were identified visually (see Appendix B) with attention to minimizing the percent relative standard deviation (%RSD) of the dataset averaged, eliminating from the average any negative values if one sample was measured slightly lower than the previous step or due to blank subtraction. The normalized dissolution rate values were calculated according to the data analysis method described in Section 3.5 and accounting for the surface area correction based on boron concentration in the leachates.

Sodium dissolution rates are nearly congruent with those of boron in the acidic range (pH_{RT} values of 7 and 8 are 6.0 and 6.9, respectively, at 70 °C; a pH_{RT} of 7 is 6.6 at 40 °C). Lithium, present in AP107WDFL and ORLEC44, dissolves also nearly congruently to sodium but the data are noisy and closer to the detection limit since the lithium contents are much lower in these two glasses than previously tested (about 1 wt% Li_2O as compared to 2.5 wt% for LAWC22 [1]). Potassium dissolution rates generally remain lower than that of sodium in ORLECAP107 but are near congruent to sodium in ORLEC44. Again, the potassium contents are low (0.5 wt% K_2O), so the data show larger uncertainty than those for ORLEC28 [1], which contains 3.4 wt% K_2O. In many cases, alkali dissolution rates fall below that of boron, such that subtracting the boron dissolution rate from that of the alkali is clearly not a viable method to determine the ion-exchange rate.

The present data show clearly that rhenium and molybdenum are valuable, and perhaps preferable, markers of glass matrix dissolution and for that reason, they were used throughout this data analysis in preference to boron in the estimation of ion-exchange rates (though all are reported). The Na ion-exchange rate was estimated by subtracting from the sodium dissolution rate the dissolution rate of either Re or Mo, in a manner similar to previous data analysis [1, 13-20]. The ion-exchange rate values obtained from subtracting the dissolution rate for Re and Mo

from those for the alkali components are in good agreement with each other. In the rest of the discussion below, the ion-exchange rate values are the average ion exchange rates calculated based on Re and Mo dissolution rates[7], and in the few instances where values based on either one could not be estimated, the value based on only the other is used in the evaluations below. The Na ion-exchange rate was also estimated based on boron dissolution rate but, as noted above, was frequently not measurable because the boron dissolution rate is high at low pH and equal to or greater than the dissolution rates for alkalis.

Plots of Na ion exchange rates calculated using Mo, Re, and B as tracers for bulk glass dissolution as functions of time are presented in Appendix C. From the plots it can be seen that ion exchange rates are highest at the early times and reach steady values at longer times. These steady values of the ion exchange rates (average of the last two to five points, no negative values included) calculated from the average of rates calculated using Mo and Re as tracers are listed in Table 4.4.

Ion exchange rates for Li and K, are also reported. Lithium is a glass modifier added in AP107WDFL and OCRLEC44, where it represents about 10% of the total alkali in the glass; potassium is also present, originating from the LAW, but is relatively low in all three glasses. Potassium concentrations in the leachates are low and often close to that of the blank in AP107WDFL for which potassium normalized dissolution rates and ion exchange rates were often not reportable. The situation is somewhat better for ORLECAP107 and ORLEC44 where the potassium content in the glass is a little higher. Ion exchange rates for both Li and K were evaluated by difference of their normalized dissolution rates from those for Mo and Re and, when possible, from the normalized dissolution rate of B. Li and K ion exchange rates (average of the last two to five points, as for Na described above) calculated from the average of the rates calculated from Mo and Re as tracers, are provided in Table 4.4.

The third spike included in the present study is cesium, which was added to evaluate its leach rate in comparison to the other alkalis. As expected, its leach rate is generally higher than that of Mo and Re and clearly higher in the acidic range where the ion exchange rate is higher. As discussed below, cesium shows an ion exchange rate that is about three orders of magnitude lower than that of sodium, in agreement with previous observations [1, 67].

4.2 AP107WDFL Pulsed-Flow Test Results

AP107WDFL is the glass formulated for LAW AP107 according to the Baseline LAW Glass Correlation [58, 59] whereas the other two glasses are enhanced high waste loading glass formulations. AP107WDFL therefore has a lower waste loading (total of 20.6 mol% alkali

[7] That is, the average of the ion exchange rate using Re-subtraction and the ion exchange rate using Mo-subtraction.

oxides). This glass contains four alkalis (Li, Na, K, and a Cs spike of 0.15 wt%) with sodium representing 89% of the total glass alkali content (18.33 mol% Na_2O), lithium most of the rest (1.97 mol% Li_2O), plus a small amount of K (0.27 mol% K_2O) and Cs (0.03 mol% Cs_2O). The cesium concentration in the leachate was analyzed by ICP-MS along with Mo and Re. K was analyzed by DCP-AES along with all of the other main glass constituents in the leachate. However, the K concentration was too low to yield meaningful ion-exchange data for this glass. Consequently, ORLECAP107 and ORLEC44 were used for that purpose, as described below.

Effluent solution analytical results for AP107WDFL Pulsed-Flow tests at 70 °C, 40 °C, and 23 °C are provided in Appendix A, Tables A1, A2, and A3, respectively, for analyses conducted by DCP-AES, and Tables A10 to A12, respectively, for analyses conducted by ICP-MS. The steady-state dissolution rates of dissolved glass components are collected in Table 4.1 and illustrated as a function of time in Appendix B, Figures B1 to B3, for the three test temperatures. Steady state dissolution rates for B, Li, K, Na, Cs, Mo, and Re are shown in Figures 4.1 to 4.3 where the three glasses are compared at each temperature. It is evident from these plots, which are presented using the same scale for the three glasses, that AP107WDFL, the glass formulated at nominal waste loading, shows much lower dissolution rates than the other two enhanced high waste loading glass formulations.

4.2.1 Time Dependence of Ion-Exchange in AP107WDFL

The time dependence of the sodium ion exchange rates estimated from fourteen of fifteen experiments with glass AP107WDFL fit reasonably well to the $t^{-1/2}$ relationship, as shown in the plots of Figure 4.4. One experiment not shown is at 23 ℃ for pH 11 because too few points were reportable. The fitted data follow the inverse square root of time dependence given in Equation (1.2).

Lithium ion exchange rates show a similar trend, as shown in Figure 4.5; the calculated ion exchange rates for lithium in the figure are based on Mo as the tracer for glass matrix dissolution. In all cases, the decrease of ion exchange rate over time fits well to the $t^{-1/2}$ time dependence.

The cesium leaching rate is two- to ten times lower than that of sodium (see Table 4.1) and in most cases lower than the normalized rate for boron. Therefore, the cesium ion exchange rate could not be estimated based on boron. However, it could be estimated using either Re or Mo as the tracer for matrix dissolution by using results from the late samplings (7 to 10 days at 70 °C, beyond 20 days at 40 °C and 23 °C). The paucity of data did not permit generation of a time dependence plot but were sufficient to compare Cs ion exchange rate values to the rates for other alkalis (Table 4.4).

4.2.2 pH Dependence of Ion Exchange in AP107WDFL

The logarithm of the sodium, lithium, and cesium ion exchange rates (average steady-state values) are plotted as a function of pH_T in Figure 4.6. Unless noted, the ion exchange rate values are based on dissolution rates of Mo and Re; in some of the plots, the dotted lines show the trend if boron is used as the basis, demonstrating how the acidic region biases the ion exchange rate estimation based on boron.

As shown in Figure 4.6, the logarithms of the ion exchange rates of the three alkalis decrease linearly as the pH increases (with fit R^2 values ranging from 0.46 to 0.96), in general accord with the model described in Section 1.3.

It is expected that Li^+ diffuses at a slower rate than Na^+ through the glass because, although it is smaller in size, it possesses a larger field strength [9, 68]. A comparison of the respective Na^+ and Li^+ ion exchange rates for all temperatures and pH conditions used in Pulsed-Flow tests shows on average a factor of 10 between the two rates (Figure 4.7). Since the lithium content in glass AP107WDFL is 10 times lower than the Na content, the lithium ion exchange rate in this glass is evidently similar to that of sodium once adjusted for the respective molar fractions in the glass, as indicated from the near congruence observed in their release rates.

Cs^+ has been reported to exhibit a diffusion coefficient that is 10 times lower than that for Na^+ and to possess a diffusion activation energy that is higher than that of Na^+ by a factor of 2 [67] because heavier cations such as Cs^+ favor stabilization of terminal NBOs [69]. As with Li^+, ion exchange rates for Na^+ and Cs^+ were compared for all temperatures and pH conditions tested in PFT. As shown in the lower part of Figure 4.7, there is on average a factor of 2600 between the two rates; since the cesium content in glass AP107WDFL is 600 times lower than the Na content, the Cs^+ ion exchange rate is about four times lower than the rate for Na^+ once adjusted for the respective molar fractions in the glass.

4.3 ORLECAP107 and ORLEC44 Pulsed-Flow Test Results

The two other glass compositions subjected to Pulsed-Flow testing were selected to represent formulations designed using the Enhanced LAW Glass Correlation. ORLECAP107 is at the high sodium limit (26.24 mol% Na_2O) with a minor amount of potassium (0.39 mol% K_2O). ORLEC44 has combined high limits of sodium and sulfate; this formulation therefore requires addition of lithium and also includes minor amount of potassium (21.18 mol% Na_2O, 2.17 mol% Li_2O and 0.35 mol% K_2O). Both glasses include the same spike of 0.03 mol% Cs_2O as in AP107WDFL. Leachate analytical results for ORLECAP107 and ORLEC44 Pulsed-Flow tests at 70 °C, 40 °C, and 23 °C are collected in Appendix A, Tables A4 to A9 for analyses conducted by DCP-AES and Tables A13 to A18 for analyses conducted by ICP-MS. The steady-state concentrations of dissolved glass components are collected in Tables 4.2 and 4.3 for ORLECAP107 and ORLEC44, respectively, and illustrated in Appendix B for the three test

temperatures. Three samples collected at day 12 in tests on ORLEC44 at 40 °C (pH_{RT} 8, 9 and 10) and two samples at 23 °C tests (pH 7 and 11) appeared to have been contaminated and were eliminated from the dataset. These points do not appear in the figures in Appendix B and were not used in the models described in Section 5.

As expected, the normalized leach rates for all species tested are higher for the two high waste loading glasses than for AP107WDFL, particularly in acidic and near-neutral conditions. As the pH increases and the temperature decreases to 23 °C, the difference decreases but remains clearly visible in Figures 4.1 to 4.3. However, the increase in normalized leach rates is not as strong for Mo, indicating less effect of waste loading on the matrix dissolution of the two glasses ORLECAP107 and ORLEC44. The normalized leach rates of Re were higher, in some tests exceeding that of Cs, which limited the use of rhenium spike to estimate cesium ion exchange.

4.3.1 Time Dependence of Ion Exchange in ORLECAP107 and ORLEC44

The time dependence of the Na ion exchange rate from thirty experiments with glasses ORLECAP107 and ORLEC44 generally fit well the expected $t^{-1/2}$ relationship (Figures 4.8 and 4.9 for ORLECAP107 and ORLEC44, respectively), as was observed with AP107WDFL. At long times, the values tend to stabilize and these limiting values are collected in Table 4.4 for all three glasses.

The lithium concentration is low in ORLEC44 but it still represents 10% of total alkali. ORLECAP107 has no lithium. The potassium concentrations are low in these two glasses, at only ~0.4 mol% K_2O. Evaluation of these ion exchange rates was conducted recognizing that these low concentrations lead to noisy data.

4.3.2 pH Dependence of Ion Exchange in ORLECAP107 and ORLEC44

As shown in Figure 4.10, the logarithms of the ion exchange rates of sodium, potassium, and cesium for ORLECAP107 show similar trends, decreasing linearly as the pH increases, in general accord with the model described in Section 1.3. As can be seen in the figure, the K ion exchange rate is about one to two orders of magnitude lower than that for sodium (between 17 to 317 times lower). Because of its larger size, K^+ is expected to diffuse through the glass at a slower rate than Na^+.

For ORLEC44, as shown in Figure 4.11, the logarithms of the ion exchange rates of sodium, lithium, potassium, and cesium show similar trends, decreasing linearly as the pH increases, in general accord with the model described in Section 1.3. Because of the low K concentration in this glass, there are fewer data above the detection limit for potassium for this glass.

As previously observed for AP107WDFL, the cesium ion exchange rate is orders of magnitude lower than that of sodium in both glasses. Comparison of the Na and Cs ion exchange rates in ORLECAP107 and ORLEC44 to the respective ion exchange rates in AP107WDFL for all temperatures and pH conditions tested in PFT (Figures 4.12) shows that the cesium ion exchange rate is very similar for the two high waste loading glasses and almost one order of magnitude higher than it is in AP107WDFL. The sodium ion exchange rate is on average 16 times larger in ORLECAP107 than in AP107WDFL but only 6 times larger in ORLEC44 than in AP107WDFL. On the one hand, it is not surprising to find the highest sodium ion exchange rate for the glass with the highest sodium content. Cesium release, however, shows a larger deviation from congruence to sodium in ORLEC44 than in ORLECAP107; once adjusted for the respective molar fractions in the glass, the rate is about six times lower than the rate for Na^+ in ORLECAP107 but only 3 times lower than the rate for Na^+ in ORLEC44. However, the Cs^+ ion exchange rates for both of these glasses are higher than that for AP107WDFL, which is the glass with the lowest sodium content, as also is the case for the sodium ion exchanges rates.

4.4 Estimation of K_g for AP107WDFL, ORLECAP107, and ORLEC44

As noted above, determination of K_g was not an objective of the present work and the test matrix was focused instead on ion exchange. However, the available data from the Pulsed-Flow tests were assessed to estimate the K_g parameter for the three new glasses. The results from previous tests [1] showed that the K_g values determined from PFT method showed good agreement with those obtained using the SPFT tests and, therefore, the PFT provides a potential alternative test method for determination of this parameter. As described earlier [1], estimation of the K_g value requires a linear regression of the steady state NDR vs. $a[H_4SiO_4]$. This regression is conducted here using two parallel approaches: using NDR_B and using NDR_{Re}. In view of the limitation in using boron as a matrix dissolution indicator in the acidic region (discussed above), the NDR_B regressions systematically excluded the data at $pH_T = 5.96$ (pH_{RT} 7 at 70 °C). $[H_4SiO_4]$ activities were estimated using the code PHREEQC with solution input descriptions corresponding to the leachates from the tests. The data at pH_{RT} 11 did not comport to the trends expected according to Equation (1.1) and were therefore excluded from this analysis.

The results of regressions at the three experimental temperatures for both NDR_B and NDR_{Re} are given in Figures 4.13, 4.14, and 4.15 for AP107WDFL, ORLECAP107, and ORLEC44, respectively. Plots of the NDR values for boron and rhenium as functions of orthosilicic acid activity and the various fitted equations are given in each figure.

K_g is the value of $a[H_4SiO_4]$ at a dissolution rate of zero (NDR = 0 for Q/K_g equal to one in Equation (1.1)). From the linear fits, six K_g values were calculated for each glass: at three temperatures, each using NDR_B and NDR_{Re}.

Results of the above analysis, given in Table 4.5 and Figure 4.16, provide the data necessary to plot these estimated K_g values as a function of 1/T (K^{-1}) to estimate the value of K_g at the presumed repository temperature of 15ºC, as listed in Table 4.6 and summarized in Table 4.5. As is evident from Table 4.6, the various K_g values are remarkably similar for the three glasses and also to the values obtained previously for the three other glasses subjected to PFT testing [1], which averaged $(1.98 \pm 0.03) \times 10^{-3}$ mol L^{-1}. Furthermore, these values are quite consistent with the values obtained for other LAW glasses, listed in Table 2.1.

SECTION 5.0
MODELING OF PULSED-FLOW TEST DATA

5.1 Data Modeling

The alkali ion exchange rate data obtained from Pulsed-Flow tests for all three glasses were analyzed according to the model described in Section 1.3. It should be noted that whereas the results described in Section 4 were obtained by assessing the variation of the ion exchange rates separately with respect to each of the independent variables (time, temperature, and pH_T), the results in this section were obtained by instead performing regression analysis of the entire data set against the models described in Section 1.3.

The analysis was performed using JMP Pro Version 15.0. For each alkali for each glass, the test matrix (10 time intervals, 5 pH values, and 3 temperatures) provides up to 150 data points for each case. However, this number was reduced somewhat by cases in which the rate subtraction yielded negative values, in addition to five outliers identified earlier due to sample contamination. Whenever possible, which was the vast majority of the cases, the average of the ion exchange rates obtained by subtracting the Re and Mo NDRs from the alkali NDRs were used in the fit; in other cases only one or the other was available, but all non-negative values were used in the model.

Two forms of the model described in Section 1.3 were used: one in which a square-root-of-time dependence was used and another in which a power law in time was used in which the exponent was a fitted parameter (as opposed to being fixed at a value of -½). Thus, the data were analyzed according to Equation (1.6) and also according to Equation (1.8).

Data for three alkalis (Na, Li, Cs) were analyzed for AP107WDFL, three alkalis for ORLECAP107 (Na, K, Cs), and four alkalis for ORLEC44 (Na, Li, K, Cs). Thus, 20 models were developed. As noted in Section 4, models for lithium and potassium are provided even though the concentrations of these species in the glasses are low, particularly for potassium, which leads to noisier and fewer data for modeling and poorer quality models.

Table 5.1 presents the regression statistics, fitted parameters, and uncertainties in the fitted parameters for all alkalis and all three glasses for the square-root-of-time model in Equation (1.6). Predicted versus measured plots for each case are shown in Figures 5.1 – 5.10. Overall, these three-parameter fits of data sets containing between 116 and 148 points are very good. For sodium, the R^2 values are between 0.859 and 0.967; values for cesium are between 0.756 and 0.914. The potassium and lithium values range from 0.785 to 0.861 and 0.763 to 0.913, respectively. The lower values for the lithium and potassium models is due to the low concentrations of these species in the glass and therefore in the leachate, the lower sensitivity of

DCP-AES versus ICP-MS, and trace amounts in the blanks. Similarly, the lower values for cesium likely reflect the greater uncertainty in the data as a result of the very low cesium concentrations in the glass and therefore in the leachates, although this is partially compensated by the higher sensitivity of the measurements by ICP-MS. The activation energies are consistent with the general range found in previous measurements on LAW glasses. However, the values are uniformly lower than the corresponding values obtained in Section 4 from analysis of the temperature dependence of the ion exchange rates at long times. The pH exponent α is reasonably consistent across all of the fits. The mean value across all fits is 0.265; the mean value for sodium is 0.250 and the mean value for cesium is 0.268; the values for potassium and lithium are 0.327 and 0.247, respectively.

Table 5.2 presents the regression statistics, fitted parameters, and uncertainties in the fitted parameters for all alkalis and all three glasses for the power-of-time model in Equation (1.8), where the time exponent is now a fitted parameter instead of being fixed at a value of ½. Predicted versus measured plots for each case are shown in Figures 5.11 – 5.20. Again, overall, these four-parameter fits of data sets containing between 116 and 148 points are very good. For sodium, the R^2 values are between 0.880 and 0.969; values for cesium are between 0.759 and 0.918, while the potassium and lithium values are between 0.769 and 0.920. Again, the lower values for cesium, potassium, and lithium likely reflect the greater uncertainty in the data as a result of the low concentrations of these species in the glass and therefore the leachates. All of the fits with Equation (1.8) are slightly better than those obtained using Equation (1.6); this is still true when comparing the R^2_{adj} which is intended to account for the effect of the difference in the number of fitting parameters. However, the difference is not great. The activation energies are generally very close to those determined from the fits to Equation (1.6) and are consistent with the general range found in previous measurements on LAW glasses; the exceptions are the values for potassium for ORLECAP107, and potassium and cesium for ORLEC44, for which the values from the fits to Equation (1.6) are lower than those from the fits to Equation (1.8). The pH exponent α is reasonably consistent across all of the fits and in good agreement with the results from the fits to Equation (1.6). The mean value across all fits is 0.267; the mean value for sodium is 0.250 and the mean value for cesium is 0.272; the values for potassium and lithium are 0.333 and 0.248, respectively. The additional parameter γ is reasonably consistent across all of the fits with the notable exceptions of potassium and cesium for ORLEC44 for which the values are close to zero and negative, respectively, which is not reasonable. This is likely an indication of datasets that do not adequately define the time dependence in these cases. In both cases, the data sets include a relatively low percentage of cases (56% and 33%, respectively) in which the ion exchange rates could be determined using *both* rhenium and molybdenum, allowing the average to be used; this percentage averaged about 85% for all other datasets. Consequently, the regression results for potassium and cesium for ORLEC44 are shaded and footnoted in Table 5.2. Excluding these two results, the mean value of γ across all fits is 0.376; the mean value for sodium is 0.551 and the mean value for cesium is 0.319; the values for potassium and lithium are 0.169 and 0.465, respectively. Overall, therefore, the present data set suggest that the parameter γ is close to ½ for sodium and lithium but may be slightly smaller than ½ for potassium and cesium. However, the results from similar testing on three other glasses suggested values slightly

larger than ½. Deviations from a value of ½ could be a reflection of departures from simple diffusion behavior such as the effects of concentration and spatially dependent diffusion coefficients, which would not be unlikely in the altered glass reaction zone. However, in view of the very small differences in R^2 values between corresponding fits to Equations (1.6) and (1.8), these apparent departures from a value of ½ may not be significant.

The results for cesium for AP107WDFL are somewhat aberrant in that the activation energy is atypically low and the value of k_{d0} is unusually small. The reason for this is not clear.

Figures 5.21 and 5.22 show predicted versus measured plots for sodium ion exchange for all three glasses for the fits to Equation (1.6) and (1.8), respectively. Figure 5.23 compares the predicted effects of temperature and pH on the sodium ion exchanges rate at 15 °C calculated from the fits to Equation (1.6).

5.2 Activation Energies and Ion Exchange Rates at 15 °C

Table 5.3 and Figure 5.24 compare the values of ion exchange activation energy E_{ad} for Na, Li, K, and Cs obtained from models applied to Pulsed-Flow tests on AP107WDFL, ORLECAP107, and ORLEC44 in the present work. Within the experimental errors, E_{ad} values are very comparable for each glass composition and appear to depend more on the glass composition than the type of alkali; the average values over all alkali types for both models, for a given glass are:

E_{ad} AP107WDFL = 40.0 ± 6.9 kJ mol^{-1},
E_{ad} ORLECAP107 = 58.7 ± 8.7 kJ mol^{-1}, and
E_{ad} ORLEC44 = 58.6 ± 7.1 kJ mol^{-1}.

E_{ad} is higher for the two higher waste loading glasses and lowest for AP107WDFL. A similar observation was made earlier [1], with the lowest E_{ad} for LAWC22, which had the lowest sodium content of the three glasses tested.

The fitted models can be used to calculate the ion exchanges rates at the presumed repository temperature of 15 °C. Table 5.4 lists ion exchange rates for Na, Li, K, and Cs obtained from the two models, extrapolated to 15℃, at 30 days and pH in the range of 7 to 11. For comparison, corresponding values for the three glasses studied in the previous work [1] are listed in Table 5.5.

The observed variation in r_{IEX} (15 °C) in units of mol m^{-2} s^{-1} includes the effect of variations of the concentrations of the various alkalis in the three glasses, which differ significantly. In order to compare the intrinsic ion exchanges rates for each alkali for each glass, it is therefore useful to first normalize r_{IEX} for a given alkali by the molar concentration of that

alkali in the glass. It is convenient to then consider the ratio of the normalized r_{IEX} for sodium to the normalized r_{IEX} for any other alkali. Doing so, we obtain the following average ratios:

Li for AP107WDFL:	0.9
Li for ORLEC44:	1.0
K for ORLECAP107:	1.1
K for ORLEC44:	1.1
Cs for AP107WDFL:	2.7
Cs for ORLECAP107:	4.7
Cs for ORLEC44:	2.7

These trends for the ratios of normalized r_{IEX} (15 °C) values for lithium and cesium are in general agreement with dissolution rates and the results from analysis of data at all temperatures and pH values shown in Figure 4.7 discussed above. For example, the dissolution rate plots in Figures B1 and B2 (Appendix B) demonstrate close congruency between Na and Li, which is in agreement with close ion exchange rates normalized to the glass composition. They are also in qualitative agreement with expectations based on the increasing size of Cs compared to Na and effects of the higher field strength of Li compared to Na. The ratios of normalized r_{IEX} (15 °C) of potassium to sodium are lower than expected given the observed deviation from congruence in dissolution rate but the low fraction of potassium in the glasses results in larger uncertainty in the results for potassium.

With the results from FY19 on three previous glasses [1], we now have six glasses for which ion exchange rates have been estimated using the PFT method. The extrapolated sodium ion exchange rates (r_{IEX} Na (15°C), $pH_{15°C}$ 9) for the FY20 glasses (Table 5.4) and the FY19 glasses (Table 5.5) are compared in Figure 5.25a, which shows a clear trend with sodium content. Regression analysis shows a simple exponential dependence of the sodium ion exchange rate on the Na_2O content of the glass, as shown in Figure 5.25b, with an R^2 of 0.985. Clearly, other glass composition variables will also influence the ion exchange rate but, despite the small dataset, this result suggests that the sodium content is the most important factor for these six glasses. If such a result holds up as more data are added, this could provide a simple means for including the effect of glass composition in the ion exchange model used in the ILAW PA. Data from previous measurements using the SFPT test and boron as the indicator for matrix dissolution, listed in Table 2.1, are also plotted in Figure 5.25b (but were not included in the regression). These data show similar general order of magnitude but considerable scatter and no obvious trend. It is possible that this behavior is a result of the use of boron as an indicator of matrix dissolution in the extraction of the ion exchange rates as compared to the use of rhenium and molybdenum for the PFT data. Consequently, it may be useful to re-test some of these glasses using the present methodology.

SECTION 6.0
COMPARISON OF RESULTS, SUMMARY, AND CONCLUSIONS

The present work builds on the results from FY19 work [1], which collectively addressed the need for:

1) An improved methodology for including ion exchange in the model for ILAW corrosion;

2) An improved method for measuring the relevant ion exchange parameters that is ideally more reliable, efficient, and cost effective than the past approach that employed the SPFT test; and

3) An improved understanding of the variation of ion exchange rates with glass composition.

Thus, this work focused on the alternative ion exchange modeling approach described in Section 1.3 and the use of the Pulsed-Flow test as a potential alternative to the SPFT test for determining ion exchange rate parameters. Ion exchange rates for selected LAW glasses were measured using the Pulsed-Flow test. The test conditions included variations in temperature, pH, and time in order to test the proposed alternative ion exchange model.

The glasses selected for this work were AP107WDFL, ORLECAP107, and ORLEC44. AP107WDFL and ORLECAP107 were selected because they are important to the near-term DFLAW operations since they are designed for the LAW from the likely commissioning tank AP-107. AP107WDFL was formulated using the WTP Baseline LAW Glass Correlation [59] and ORLECAP107 was formulated using the ORP Enhanced LAW Glass Correlation for high waste loading glasses [60]. ORLEC44 was selected because it has the same Na_2O content as LAWA44, but has a much higher SO_3 content; it was also formulated with the Enhanced LAW Glass Correlation [60].

The three selected glasses were fabricated to also include three spikes: Mo and Re as potential alternatives to boron as indicators of glass matrix dissolution and Cs to evaluate its ion exchange rate in comparison to other alkalis. An extensive set of leaching data was collected using the Pulsed-Flow test method, which provides a simpler means of performing flow-through testing.

The data collected were analyzed to extract the various model parameters with particular emphasis on ion exchange. Although not a primary objective of the present work, the available data also permitted estimation of the K_g parameter for the three new glasses.

Overall, the measured ion exchange data are in general accord with expectations based on the proposed ion exchange model described in Section 1.3:

- The measured ion exchanges rates follow the predicted linear dependence on the reciprocal of the square root of time reasonably well.
- The measured ion exchanges rates follow the predicted dependence on pH, with the logarithms of the ion exchange rates decreasing linearly as the pH increases.
- The measured ion exchanges rates follow the predicted Arrhenius dependence on temperature, with the logarithms of the ion exchange rates decreasing linearly with the reciprocal of the absolute temperature.
- Na, Li, K, and Cs all follow the above behavior reasonably well but with rate constants that depend on the alkali in the order Na > Li > K > Cs.

Based on these findings, the alkali ion exchange rate data obtained from Pulsed-Flow tests were subjected to regression analysis to extract the parameters of the model described in Section 1.3. It should be noted that whereas the results described in Section 4 were obtained by assessing the variation of the ion exchange rates separately with respect to each of the independent variables (time, temperature, and pH), the results presented in Section 5 were obtained by performing regression analysis of the entire data set against the models described in Section 1.3. The analysis was performed using JMP Pro Version 15.0.

Two forms of the model described in Section 1.3 were used: one in which a square-root-of-time dependence was used and another in which a power-law-in-time dependence was used in which the exponent was a fitted parameter (as opposed to being fixed at a value of -½). Thus, the data were analyzed according to Equation (1.6) and also according to Equation (1.8). Data for three alkalis (Na, Li, Cs) were analyzed for AP107WDFL, three alkalis for ORLECAP107 (Na, K, Cs), and four alkalis for ORLEC44 (Na, Li, K Cs). Thus, 20 models were developed. Due to the low concentrations of potassium and lithium in these glasses, even though the resulting ion exchange parameters were evaluated, greater uncertainties are expected for these species.

Overall, the three-parameter fits of Equation (1.6) to the data sets containing between 116 and 148 points are very good. For sodium, the R^2 values are between 0.859 and 0.967; values for cesium are between 0.756 and 0.914. The potassium and lithium values range from 0.785 to 0.861 and 0.763 to 0.913, respectively. The lower values for the lithium and potassium models are due to the low concentrations of these species in the glass and therefore in the leachate, the lower sensitivity of DCP-AES versus ICP-MS, and trace amounts in the blanks. Similarly, the lower values for cesium likely reflect the greater uncertainty in the data as a result of the very low cesium concentrations in the glasses and therefore in the leachates, although this is partially compensated by the higher sensitivity of the measurements by ICP-MS. The activation energies are consistent with the general range found in previous measurements on LAW glasses.

However, the values are uniformly lower than the corresponding values obtained in Section 4 from analysis of the temperature dependence of the ion exchange rates at long times. The pH exponent α is reasonably consistent across all of the fits. The mean value across all fits is 0.265; the mean value for sodium is 0.250 and the mean value for cesium is 0.268; the values for potassium and lithium are 0.327 and 0.247, respectively.

Similarly, four-parameter fits of Equation (1.8) to the same data sets are also very good, with slight improvement to the statistics when allowing the additional time parameter γ to vary. For sodium, the R^2 values are between 0.880 and 0.969; values for cesium are between 0.759 and 0.918, while the potassium and lithium values are between 0.769 and 0.920. Again, the lower values for cesium, potassium, and lithium likely reflect the greater uncertainty in the data as a result of the low concentrations of these species in the glass and therefore in the leachates. All of the fits with Equation (1.8) are slightly better than those obtained using Equation (1.6); this is still true when comparing the R^2_{adj} which is intended to account for the effect of the difference in the number of fitting parameters. However, the difference is not great. The activation energies are generally very close to those determined from the fits to Equation (1.6) and are consistent with the general range found in previous measurements on LAW glasses; the exceptions are the values for potassium for ORLECAP107, and potassium and cesium for ORLEC44, for which the values from the fits to Equation (1.6) are lower than those from the fits to Equation (1.8). The pH exponent α is reasonably consistent across all of the fits and in good agreement with the results from the fits to Equation (1.6). The mean value across all fits is 0.267; the mean value for sodium is 0.250 and the mean value for cesium is 0.272; the values for potassium and lithium are 0.333 and 0.248, respectively. The additional parameter γ is reasonably consistent across all of the fits with the notable exceptions of potassium and cesium for ORLEC44 for which the values are close to zero and negative, respectively, which is not reasonable. This is likely an indication of datasets that do not adequately define the time dependence in these cases. In both cases, the data sets include a relatively low percentage of cases (56% and 33%, respectively) in which the ion exchange rates could be determined using *both* rhenium and molybdenum, allowing the average to be used; this percentage averaged about 85% for all other datasets. Excluding these two results, the mean value of γ across all fits is 0.376; the mean value for sodium is 0.551 and the mean value for cesium is 0.319; the values for potassium and lithium are 0.169 and 0.465, respectively. Overall, therefore, the present data set suggest that the parameter γ is close to ½ for sodium and lithium but may be slightly smaller than ½ for potassium and cesium. However, in view of the very small differences in R^2 values between corresponding fits to Equations (1.6) and (1.8), these apparent departures from a value of ½ may not be significant.

As in previous work, attempts were made to estimate the ion exchange rate by subtraction of the normalized boron dissolution rate from that of each of the alkalis; however, positive values were obtained only for sodium. As noted above, this approach assumes that boron is released solely by matrix dissolution whereas its release appears to follow diffusive kinetics. This issue was resolved by including spikes of rhenium and molybdenum, which provided excellent alternative indicators of matrix dissolution with results that were generally in very close agreement with each other. Thus, while parameters were extracted using the conventional boron-

based approach wherever possible, as well as using the Mo- and Re-based approaches, the data indicate that the Mo/Re approach is to be preferred. Unlike boron, molybdate and perrhenate, which are the dominant Mo and Re species in the glass and which are isomorphous (and also isomorphous with sulfate and chromate), are insignificant participants in the glass matrix, instead residing interstitially [70-74]. They are relatively large and therefore diffusive release should be insignificant. Thus, their release relies upon the dissolution of the surrounding glass matrix. Both species form very soluble anions and can be spiked and analyzed reliably at low concentrations such that they do not participate significantly in secondary phase formation, particularly in the case of rhenium. Overall, therefore, we consider these species to be good candidates for alternative markers of matrix dissolution.

SECTION 7.0
QUALITY ASSURANCE

This work was conducted under a quality assurance (QA) program compliant with the applicable criteria of 10 CFR 830.120; the American Society of Mechanical Engineers (ASME) Nuclear Quality Assurance (NQA)-1-2008 including NQA-1a-2009 addenda; and DOE Order 414.1D, Quality Assurance. These QA requirements are implemented through a Quality Assurance Project Plan for WRPS work [75] that is conducted at VSL. Test and procedure requirements by which the testing activities are planned and controlled are also defined in that plan. The program is supported by VSL standard operating procedures were used for this work [76]. This is LAW work and is not subject to the requirements of DOE/RW-0333P, Office of Civilian Waste Management Quality Assurance Requirements and Description (QARD).

SECTION 8.0
REFERENCES

[1] "FY 2019 ILAW Glass Ion Exchange Rate Testing," I.S. Muller, C. Viragh, and I.L. Pegg, Final Report, VSL-19R4620-2, Rev. 0, Vitreous State Laboratory, The Catholic University of America, Washington, DC, 4/27/20.

[2] "FY 2020 ILAW Glass Ion Exchange Rate Testing", I.S. Muller, and I.L. Pegg, VSL-20T4820-1, Rev. 0, Vitreous State Laboratory, The Catholic University of America, Washington DC, 2/11/19.

[3] Request for Off-Site Services (Technical) Statement of Work, "Parameterizing an ILAW Glass Ion Exchange Rate Model to Support the IDF PA," Rev. 0, Requisition #331831, Washington River Protection Solutions, LLC (WRPS), 09/17/19.

[4] "Experimentally Determined Dissolution Kinetics of Na-rich Borosilicate Glasses at Far-From-Equilibrium Conditions: Implications for Transition State Theory," J.P. Icenhower, B.P. McGrail, W.J. Shaw, E.M. Pierce, P. Nachimuthu, D.K. Shuh, E.A. Rodriguez, and J.L. Steele, *Geochimica Cosmochimica Acta,* 72, 2767-2788 (2008).

[5] "Measurement of Kinetic Rate Law Parameters on a Na-Ca-Al Borosilicate Glass for Low-Activity Waste," B.P. McGrail, W.L. Ebert, A.J. Bakel, and D.K. Peeler, *J. Nucl. Mater.* 249, 175-189 (1997).

[6] "Low-Activity Waste Glass Studies: FY 2000 Summary Report," B.P. McGrail, J.P. Icenhower, P.F. Martin, D.R. Rector, H.T. Schaef, E.A. Rodriguez, and J.L. Steele, PNNL-13381, Pacific Northwest National Laboratory, Richland, WA (2000).

[7] "Waste Form Release Data Package for the 2001 Immobilized Low-Activity Waste Performance Assessment," B.P. McGrail, J.P. Icenhower, P.F. Martin, H.T. Schaef, M.J. O'Hara, E.A. Rodriguez, and J.L. Steele, PNNL-13043, Rev. 2, Pacific Northwest National Laboratory, Richland, WA (2001).

[8] "Laboratory Testing of Bulk Vitrified Low-Activity Waste Forms to Support the 2005 Integrated Disposal Facility Performance Assessment," E.M. Pierce, B.P. McGrail, L.M. Bagaasen, E.A. Rodriguez, D.M. Wellman, K.N. Geiszler, S.R. Baum, L.R. Reed, J.V. Crum, and H.T. Schaef, PNNL-15126, Rev. 2, Pacific Northwest National Laboratory, Richland, WA (2005).

[9] "Kinetic Rate Law Parameter Measurements on Borosilicate Waste Glass: Effect of Temperature, pH, and Solution Composition on Alkali Ion Exchange," E.M. Pierce, B.P. McGrail, J.P. Icenhower, E.A. Rodriguez, J.L. Steele, and S.R. Baum, *American Chemical Society Division of Environmental Chemistry*. American Chemical Society, Philadelphia, PA (2004).

[10] "Waste Form Release Data Package for the 2005 Integrated Disposal Facility Performance Assessment," E.M. Pierce, B.P. McGrail, E.A. Rodriguez, H.T. Schaef, K.P. Saripalli, R.J. Serne, K.M. Krupka, P.F. Martin, S.R. Baum, K.N. Geiszler, L.R. Reed, and W.J. Shaw, PNNL-14805, Pacific Northwest National Laboratory, Richland, WA (2004).

[11] "An Experimental Study of the Dissolution Rates of Simulated Aluminoborosilicate Waste Glasses as a Function of pH and Temperature under Dilute Conditions," E.M. Pierce, E.A. Rodriguez, L.J. Calligan, W.J. Shaw, and B.P. McGrail, *Applied Geochemistry,* 23, 2559-2573 (2008).

[12] "A Strategy to Conduct an Analysis of the Long-Term Performance of Low-Activity Waste Glass in a Shallow Subsurface Disposal System at Hanford," J.J. Neeway, E.M. Pierce, V.L. Freedman, J.V. Ryan, and N.P. Qafoku, PNNL-23503, Rev. 0, Pacific Northwest National Laboratory, Richland, WA (2014).

[13] "Immobilized Low-Activity Waste Glass Release Data Package for the Integrated Disposal Facility Performance Assessment," V.L. Freedman, J.V. Ryan, and D.H. Bacon, PNNL-24615, Draft, Pacific Northwest National Laboratory, Richland, WA, August 2015.

[14] "ILAW Glass Testing for Disposal at IDF: Phase 1 Testing," A.E. Papathanassiu, I.S. Muller, M. Brandys, K. Gilbo, A. Barkatt, I. Joseph and I.L. Pegg, Final Report, VSL-11R2270-1, Rev. 0, Vitreous State Laboratory, The Catholic University of America, Washington, DC, 6/6/11.

[15] "A Strategy to Conduct an Analysis of the Long-Term Performance of Low-Activity Waste Glass in a Shallow Subsurface Disposal System at Hanford," B.P. McGrail, W.L. Ebert, D.H. Bacon, and D.M. Strachan, PNNL-11834, Pacific Northwest National Laboratory, Richland, Washington, February 1998.

[16] "FY2016 ILAW Glass Testing for Disposal at IDF" A.E. Papathanassiu, C. Viragh, I.S. Muller, and I.L. Pegg, Final Report, VSL-17R3860-1, Rev. 0, Vitreous State Laboratory, The Catholic University of America, Washington, DC, 7/12/17.

[17] "FY2016 ILAW Glass Corrosion Testing with the Single-Pass Flow-Through Method," J.J. Neeway, B.D. Williams, R.M. Asmussen, I.I. Leavy, B.P. Parruzot, J.R. Stephenson, E.A. Cordova, E.M. McElroy, Final Report, PNNL-26169, RPT-IGTP-013, Rev. 0, Pacific Northwest Laboratory, Richland, WA, April 2017.

[18] "FY2017 ILAW Glass SPFT Testing for Disposal at IDF: Glass IDF21-EC14," C. Viragh, H. Abramowitz, I.S. Muller, A.E. Papathanassiu, and I.L. Pegg, Final Report, VSL-17R4320-2, Rev. 0, Vitreous State Laboratory, The Catholic University of America, Washington DC, 2/27/18.

[19] "FY2017 ILAW Glass Corrosion Testing with the Single-Pass Flow-Through Method," J.J. Neeway et al., Final Report, PNNL-27098, RPT-IGTP-015, Rev. 0.0, Pacific Northwest Laboratory, Richland, WA, February 2018.

[20] "FY2018 ILAW Glass SPFT Testing for Disposal at IDF: Glasses ORLEC46 and ORLEC52," C. Viragh, H. Abramowitz, I.S. Muller, A.E. Papathanassiu, and I.L. Pegg, Final Report, VSL-18R4510-2, Rev. 0, Vitreous State Laboratory, The Catholic University of America, Washington DC, 12/26/18.

[21] "The Activated Complex in Chemical Reactions," H. Eyring, *J. Chem. Phys.* **3**, 107-114 (1935).

[22] "Thermodynamic and Kinetic Constraints on Reaction Rates among Minerals and Aqueous Solutions. I. Theoretical Considerations," P. Åagaard and H.C. Helgeson, *Am. J. Sci.,* 282, 237-285 (1982).

[23] "Letter: Simultaneous Precipitation Kinetics of Kaolinite and Gibbsite at 80°C and pH 3," K.L. Nagy, and A.C. Lasaga, *Geochimica et Cosmochimica Acta* **57**, 4329 – 4335 (1993).

[24] "A General Rate Equation for Nuclear Waste Glass Corrosion," B. Grambow, *Material Research Symposium Proceedings,* 44, 15-27 (1985).

[25] "Kinetic Ion Exchange Salt Effects on Glass Leaching," X. Feng and I.L. Pegg, *Energy, Environment and Information Management*, Eds. H. Wang, S. Chang, and H. Lee, Argonne, IL, p. 7-9, (1992).

[26] "Effects of Salt Solutions on Glass Dissolution," X. Feng and I.L. Pegg, *Phys. Chem. Glasses*, 35, 1 (1994).

[27] "A Glass Dissolution Model for the Effects of S/V on Leachate pH," X. Feng and I.L. Pegg, J. *Non-Cryst. Solids*, 175, 281 (1994).

[28] "Survey of Literature on the Role of Ion Exchange in Glass Corrosion," A.E. Papathanassiu, W. Gong, W. Lutze, and I.L. Pegg, Final Report, VSL-17L4320-1, Rev. 0, Vitreous State Laboratory, The Catholic University of America, Washington DC, 8/2/17.

[29] "A Critical Review of Ion Exchange in Nuclear Waste Glasses to Support the Immobilized Low-Activity Waste Integrated Disposal Facility Rate Model," C.E. Lonergan, PNNL-26594, RPT-IGTP-018, Rev 0.0, Pacific Northwest Laboratory, Richland, WA, August 2017.

[30] "An International Initiative on Long-Term Behavior of High-Level Nuclear Waste Glass," S. Gin, A. Abdelouas, L.J. Criscenti, W.L. Ebert, K. Ferrand, T. Geisler, M.T. Harrison, *et al.*, Mater. Today 16, 243–248 (2013).

[31] "Origin and Consequences of Silicate Glass Passivation by Surface Layers", S. Gin, P. Jollivet, M. Fournier, F. Angeli, P. Frugier, T. Charpentier, Nat. Commun., 6 (2015).

[32] "Characterization of Alteration Phases on HLW Glasses after 15 Years of PCT Leaching," I.S. Muller, S. Ribet, I.L. Pegg, S. Gin, and P. Frugier, *Ceramic Transactions*, Vol. 176 (2005).

[33] "FY2019 Long-Term PCT of ILAW Glasses", I.S. Muller, and I.L. Pegg, VSL-19R4620-1, Rev. 0, Vitreous State Laboratory, The Catholic University of America, Washington, DC, 9/30/19.

[34] "Dissolution and Precipitation Kinetics of Sheet Silicates," K.L. Nagy, *Silicate Mineral Dissolution*. Mineralogical Society of America, Washington, DC (2001).

[35] "Preliminary Results of Durability Testing with Borosilicate Glass Compositions," M. Adel-Hadadi, R. Adiga, Aa. Barkatt, X. Feng, I.L. Pegg, et al., Tech. Info. Center, Office of Sci. and Tech. Info., USDOE, DOE/NE/44139-34, (1988).

[36] "Compositional Effects on Chemical Durability and Viscosity of Nuclear Waste Glasses – Systematic Studies and Structural Thermodynamic Models," X. Feng, Ph.D. Thesis, The Catholic University of America (1988).

[37] "Leach Rate Excursions in Borosilicate Glasses: Effects of Glass and Leachant Composition," Aa. Barkatt, S.A. Olszowka, W. Sousanpour, M.A. Adel-Hadadi, R. Adiga, Al. Barkatt, G.S. Marbury, and S. Li, Mat. Res. Soc. Symp. Proc., 212, 65 (1991).

[38] "Alteration Layers on Glasses After Long-Term Leaching," A.C. Buechele, S.T.- Lai, and I.L. Pegg, *Ceramic Transactions*, Eds. D.K. Peeler and J.C. Marra, vol. 87, p. 423, American Ceramic Society (1998).

[39] "Compositional Effects on the Long-Term Durability of Nuclear Waste Glasses: A Statistical Approach," S. Ribet, I.S. Muller, I.L. Pegg, S. Gin, and P. Frugier, Mat. Res. Soc. Symp. Proc. Vol. 824 (2004).

[40] "The Long-Term Corrosion and Modeling of Two Simulated Belgian Reference High-Level Waste Glasses – Part II," J. Patyn, P. Van Iseghem, and W. Timmermans, Mat. Res. Symp. Soc. Proc., 176, 299 (1990).

[41] "New Insight into the Residual Rate of Borosilicate Glasses: Effect of S/V and Glass Composition", S. Gin, P. Frugier, P. Jollivet, F. Bruguier, E. Curti, Int. J. Appl. Glass Sci., 4 (4), 371-382 (2013).

[42] "Nuclear Glass Durability: New Insight into Alteration Layer Properties," S. Gin, C. Guittonneau, N. Godon, D. Neff, D. Rebiscoul, M. CabieS. Mostefaoui, J. Phys. Chem. C 115 (38), 18696-18706, (2011).

[43] "The Fate of Silicon During Glass Corrosion Under Alkaline Conditions: A Mechanistic and Kinetic Study with the International Simple Glass," S. Gin, P. Jollivet, M. Fournier, C. Berthon, Z. Wang, A. Mitroshkov, Z. Zhu, J. V. Ryan, Geochim. Cosmochim. Acta, 151, 68–85 (2015).

[44] "Resumption of Nuclear Glass Alteration: State of the art," M. Fournier, S. Gin, P. Frugier, J. Nucl. Mater., 448, 348–363 (2014).

[45] "Open Scientific Questions About Nuclear Glass Corrosion," S. Gin, Procedia Materials Science, 163-171 (2014).

[46] "Current Understanding and Remaining Challenges in Modeling Long-Term Degradation of Borosilicate Nuclear Waste Glasses," J.D. Vienna, J.V. Ryan, S. Gin, and Y. Inagaki, Int. J. Appl. Glass Sci., 4, 283–294 (2013).

[47] "Contribution of Atom-Probe Tomography to a Better Understanding of Glass Alteration Mechanisms: Application to a Nuclear Glass Specimen Altered 25 years in a Granitic Environment," S. Gin, J.V. Ryan, D.K. Schreiber, J. Neeway, and M. Cabie, Chem. Geol. 349, 99–109 (2013).

[48] "Effect of Composition on the Short-Term and Long-Term Dissolution Rates of Ten Borosilicate Glasses of Increasing Complexity from 3 to 30 oxides", S. Gin, X. Beaudoux, F. Angeli, C. Jegou, N. Godon, J. Non-Cryst. Solids, 358, 2559–2570 (2012).

[49] "Development of the Vitrification Compositional Envelope to Support Complex-Wide Application of MAWS Technology," I.S. Muller, H. Gan, A.C. Buechele, S.T. Lai, and I.L. Pegg, DOE/CH-9601, September 1996.

[50] "Alteration Phases on High Sodium Waste Glasses after Short- and Long-Term Hydration," A.C. Buechele, S.-T. Lai, and I.L. Pegg, *Ceramic Transactions*, vol. 107, p. 251 (2000).

[51] "FY15 ILAW Glass Testing for Disposal at IDF", I.S. Muller, and I.L. Pegg, VSL-15R3790-1, Rev. 0, Vitreous State Laboratory, The Catholic University of America, Washington, DC, 4/15/16.

[52] "LAW Glass Testing by Long-Perm PCT to Support Disposal at IDF," I.S. Muller, and I.L. Pegg, VSL-17R4320-1, Rev. 0, Vitreous State Laboratory, The Catholic University of America, Washington, DC, 9/28/17.

[53] "Low-Activity Waste Glass Release Calculations for the Integrated Disposal Facility Performance Assessment," R. Arthur, C. Cheng, B. Paris, RPP-CALC-61031, Rev. 0, Intera, Inc. for Washington River Protection Solutions, LLC, Richland, WA, May 2, 2017.

[54] "The Ion Exchange Phase in Corrosion of Nuclear Waste Glasses," M.I. Ojovan, A. Pankov, and W.E. Lee, J. Nucl. Mater., 358, 57-68 (2006).

[55] "SON 68 Nuclear Glass Dissolution Kinetics: Current State of Knowledge and Basis of the New GRAAL Model," P. Frugier, S. Gin, Y. Minet, T. Chave, B. Bonin, N. Godon, J.E. Lartigue, P. Jollivet, A. Ayral, L. De Windt, and G. Santarini, J. Nucl. Materials, 380, 8-21 (2008).

[56] "Application of the GRAAL Model to Leaching Experiments with SON 68 Nuclear Glass in Initially Pure Water," P. Frugier, T. Chave, S. Gin, and J.E. Lartigue, J. Nucl. Materials, 392, 552-567 (2009).

[57] "Interdiffusion of Alkali and Hydronium Ions in Glass: Partial Ionization," R.H. Doremus, J. Non-Cryst. Solids, 48, 431 (1982).

[58] "Selection of ILAW Glasses for FY 2020 Ion Exchange Testing," Vitreous State Laboratory, The Catholic University of America, Washington, DC, 1/3/20.

[59] "Proposed Approach for Development of LAW Glass Formulation Correlation," I.S. Muller, G. Diener, I. Joseph, and I.L. Pegg, Letter Report, VSL-04L4460-1, Rev. 2, Vitreous State Laboratory, The Catholic University of America, Washington, DC, 10/29/04.

[60] "Optimization of Enhanced LAW Correlation Glasses for Processing," I.S. Muller, K.S. Matlack, H. Gan, I.L. Pegg and I. Joseph, Final Report, VSL-19R4460-1, Rev. 0, Vitreous State Laboratory, The Catholic University of America, Washington, DC, 09/30/19.

[61] "FY2018 Long-Term PCT of ILAW Glasses", I.S. Muller, and I.L. Pegg, VSL-18R4510-1, Rev. 0, Vitreous State Laboratory, The Catholic University of America, Washington, DC, 12/19/18.

[62] "LAW Container Centerline Cooling Data" RPP-WTP Memorandum, L. Petkus to C. Musick, CCN# 074181, 10/16/03.

[63] "Round Robin Testing of a Reference Glass for Low-Activity Waste Forms," W.L. Ebert and S.F. Wolf, Department of Energy Report ANL-99/22, Argonne National Laboratory, Argonne, IL (1999).

[64] "Characterization of the Defense Waste Processing Facility (DWPF) Environmental Assessment (EA) Glass Standard Reference Material," C.M. Jantzen, N.E. Bibler, D.C. Beam, C.L. Crawford, and M.A. Pickett, WSRC-TR-92-346, Westinghouse Savannah River Company, Aiken, SC, June, 1993.

[65] "Standard Practice for Measurement of the Glass Dissolution Rate Using the Single-Pass Flow-Through Test Method," ASTM Standard C 1662-10.

[66] "Evaluation of the Single-Pass Flow Through Test to Support a Low-Activity Waste Specification," B.P. McGrail and D.K. Peeler, Final Report, PNNL-10746, Pacific Northwest Laboratory, Richland, WA, 1995.

[67] "Self Diffusion of ^{22}Na and ^{137}Cs in Simulated Nuclear Waste Glass," K. Nonaka. H. Nakajima, S. Mitsui, and J. Echigoya, Mater. Trans, 43, 654-659 (2002).

[68] "Low-Temperature Lithium Diffusion in Simulated High-Level Boroaluminosilicate Nuclear Waste Glasses," J.J. Neeway, S. Kerisit, S. Gin, Z. Wang, Z. Zhu, and J.V. Ryan, J. Non-Cryst. Solids, 405, 83-90 (2014).

[69] ''Probing Alkali Coordination Environments in Alkali Borate Glasses by Multinuclear Magnetic Resonance", V. K. Michaelis, P. M. Aguiar, and S. Kroeker, J. Non-Cryst. Solids, 353, 2582–90 (2007).

[70] "Dissimilar Behavior of Technetium and Rhenium in Borosilicate Waste Glass as Determined by X-Ray Absorption Spectroscopy," W.W. Lukens, D.A. McKeown, A.C. Buechele, I.S. Muller, D.K. Shuh, and I.L. Pegg, Chem. Mater., 19, 559 (2007).

[71] "Tc and Re Behavior in Waste Glass Vapor Hydration Tests," D.A. McKeown, A.C. Buechele, W.W. Lukens, D.K. Shuh, and I.L. Pegg, Environ. Sci. Technol., 41, 431 (2007).

[72] "Raman Studies of Technetium in Borosilicate Waste Glass," D.A. McKeown, A.C. Buechele, W.W. Lukens, I.S. Muller, D.K. Shuh, and I.L. Pegg, Radiochimica Acta, 95, 275 (2007).

[73] "Tc and Re Behavior in Borosilicate Waste Glass Vapor Hydration Tests II," A.C. Buechele, D.A. McKeown, W.W. Lukens, D.K. Shuh, and I.L. Pegg, J. Nuclear Materials, 429, 159 (2012).

[74] "X-ray Absorption and Raman Spectroscopy Studies of Molybdenum Environments in Borosilicate Waste Glasses," D.A. McKeown, H. Gan, and I.L. Pegg, J. Nucl. Mater., 488, 143 (2017).

[75] "Quality Assurance Project Plan for WRPS Support Activities Conducted by VSL," VSL-QAPP-WRPS, Rev. 5, Vitreous State Laboratory, The Catholic University of America, Washington, DC, 9/30/19.

[76] "Master List of Controlled VSL Manuals and Standard Operating Procedures in Use," QA-MLCP, Rev. 173, Vitreous State Laboratory, The Catholic University of America, Washington, DC, 7/31/20.

Table 2.1. Summary of Kinetic Parameters Determined on Various LAW Glasses.

Glass Name	k_0 g-glass m^{-2} d^{-1}	η	E_α kJ mol^{-1}	K_g (15°C)[a] mol L^{-1}	r_{IEX} (15°C)* mol-Na m^{-2} s^{-1}	Source
ORLEC46	2.9×10^{4}	0.39±0.06	58±3	(1.2×10^{-3})	1.4×10^{-10} **	VSL-18R4510-2
ORLEC52	2.0×10^{6}	0.43±0.04	72±4	(5.7×10^{-4})	2.6×10^{-11} **	VSL-18R4510-2
ORLEC28[b]	2.7×10^{6}	0.55±0.02	79±2	(1.3×10^{-4})	2.7×10^{-11} **	PNNL-27098, Rev 0
ORLEC33	3.8×10^{6}	0.56±0.02	81±2	(1.1×10^{-4})	3.3×10^{-11} **	PNNL-27098, Rev 0
ORLEC14	2.7×10^{6}	0.48±0.04	76±2	(6.75×10^{-4})	7.4×10^{-11} **	VSL-17R4320-1, Rev. 0
IDF18-A161	5.9×10^{6}	0.28±0.06	61±6	(2.3×10^{-4})	7.6×10^{-11}	PNNL-26169, Rev 0
ORPLG9	2.5×10^{8}	0.36±0.07	81±7	(log K_g = 100)	5.3×10^{-11}	PNNL-26169, Rev. 0
IDF7-E12	5.7×10^{4}	0.32±0.03	55±5	1.87×10^{-3}	$<1\times10^{-10}$	VSL-17R3860-1, Rev. 0
LAWA44	1.3×10^{4}	0.49±0.08	60±7	1.87×10^{-3} ***	5.3×10^{-11}	PNNL-24615, Rev. 0
LAWB45	1.6×10^{4}	0.34±0.03	53±3	1.79×10^{-3} ***	0	PNNL-24615, Rev. 0
LAWC22[b]	1.0×10^{5}	0.42±0.02	64±2	1.80×10^{-3} ***	1.2×10^{-10}	PNNL-24615, , Rev. 0
					1.28×10^{-11} **	Corrected value
IDF1-B2[b]	4.6×10^{4}	0.49±0.05	64±4	1.70×10^{-3}	3.4×10^{-10}	VSL-11R2270-1, Rev. 0
					6.21×10^{-11} **	Corrected value
LAWABP1	3.4×10^{6}	0.35±0.03	68±3	4.90×10^{-4}	3.4×10^{-11}	PNNL-24615, Rev. 0

***** As-reported values; uncorrected except where indicated (see Section 4.4 of [19]).
** Corrected value, see [29]
*** Corrected value, see [14]
[a] Questionable values are shown in parentheses - Kinetic rate law does not model glass dissolution under saturating conditions.
[b] Glasses evaluated by PFT in FY 2019[1].

Table 2.2. Comparison of Activation Energies and Extrapolated Ion Exchange Rates Previously Determined for Three Glasses by SPFT and Pulsed-Flow Tests [1].

Method	Element	Glass ID	E_{ad} kJ/mol	r_{IEX} (15 °C) mol m^{-2} s^{-1}
			All pH	All pH
SPFT (Mo&Re)[$]	Na	LAWC22	56 ±7 (47)[*]	8.7×10^{-12}
PFT (Mo&Re)	Na	LAWC22	53 ± 7	1.2×10^{-11}
PFT (Mo&Re)	Na	ORLEC28	73 ± 8	4.6×10^{-11}
PFT (Mo&Re)	Na	IDF1B2	55 ± 6	1.1×10^{-10}
SPFT (Mo&Re and B)	Li	LAWC22	46 ± 10	2.7×10^{-12}
PFT (Mo&Re)	Li	LAWC22	37 ± 12	3.7×10^{-12}
PFT (Mo&Re)	K	ORLEC28	78 ± 9	2.5×10^{-12}
SPFT (Mo&Re)	Cs	LAWC22	56 ± 28	3.6×10^{-15}
PFT (Mo&Re)	Cs	LAWC22	50 ± 12	5.4×10^{-15}
PFT (Mo&Re)	Cs	ORLEC28	71 ± 9	1.7×10^{-14}
PFT (Mo&Re)	Cs	IDF1B2	62 ± 8	6.3×10^{-15}

*Lowest pH measurement at 70 °C has been omitted for this value in parentheses
[$] Calculation of ion exchange rates employed the normalized dissolution rates of the elements shown in parentheses to represent the matrix dissolution rates

Table 2.3. Target Compositions (wt%) of Glasses Selected for Ion-Exchange Testing.

Glass ID	AP107WDFL	ORLECAP107	ORLEC44
Al_2O_3	6.10	9.00	7.60
B_2O_3	10.00	11.00	11.00
CaO	3.94	1.95	5.49
Cr_2O_3	0.08	0.34	0.08
Cs_2O	0.15	0.15	0.15
Fe_2O_3	5.50	0.34	0.20
K_2O	0.38	0.54	0.50
Li_2O	0.89	0.00	0.99
MgO	1.48	1.00	1.00
MoO_3	0.10	0.10	0.10
Na_2O	17.20	24.00	20.00
NiO	0.00	0.00	0.01
PbO	0.00	0.00	0.01
SiO_2	45.15	38.59	42.18
SnO_2	0.00	1.02	0.00
TiO_2	1.40	0.34	0.00
V_2O_5	0.00	1.55	2.44
ZnO	3.50	3.00	3.00
ZrO_2	3.00	5.55	3.50
Cl	0.42	0.58	0.20
F	0.04	0.06	0.08
P_2O_5	0.13	0.18	0.12
SO_3	0.44	0.61	1.25
Re_2O_7	0.10	0.10	0.10
Total	100.0	100.0	100.0

Table 2.4. Alkali Content and Species Used to Monitor Matrix Dissolution in Three LAW Glasses.

	Glass ID, wt%	AP107WDFL	ORLECAP107	ORLEC44	Notes
Composition (wt%)	Na_2O	17.20	24.00	20.00	Alkali species undergoing ion exchange
	K_2O	0.38	0.54	0.50	
	Li_2O	0.89	0.00	0.99	
	Cs_2O	0.130*	0.130*	0.130*	
	B_2O_3	10.00	11.00	11.00	Species used to monitor matrix dissolution
	MoO_3	0.080*	0.068*	0.080*	
	Re_2O_7	0.130*	0.126*	0.130*	
Composition (mol%)	Na_2O	18.33	26.24	21.18	Alkali species undergoing ion exchange
	K_2O	0.27	0.39	0.35	
	Li_2O	1.97	0.00	2.17	
	Cs_2O	0.03	0.03	0.03	
	B_2O_3	9.49	10.71	10.37	Species used to monitor matrix dissolution
	MoO_3	0.04	0.04	0.04	
	Re_2O_7	0.02	0.02	0.02	

*Analyzed by XRF

Table 2.5. Target and Analyzed Compositions (wt%) of Glasses Selected for Ion-Exchange Testing.

Glass ID	AP107WDFL	AP107WDFL IX	AP107WDFL IXCCC	ORLECAP107	ORLECAP107 IX	ORLECAP107 IXCCC	ORLEC44	ORLEC44 IX	ORLEC44 IXCCC
	Target	Analyzed*	Analyzed*	Target	Analyzed*	Analyzed*	Target	Analyzed*	Analyzed*
Al_2O_3	6.10	6.63	6.63	9.00	9.30	9.43	7.60	8.02	8.10
B_2O_3	10.00	9.56	9.61	11.00	10.82	10.71	11.00	10.58	10.76
CaO	3.94	4.02	4.08	1.95	2.06	2.00	5.49	5.86	5.66
Cr_2O_3	0.08	0.10	0.09	0.34	0.41	0.43	0.08	0.00	0.00
Cs_2O	0.15	0.14	0.13	0.15	0.13	0.13	0.15	0.12	0.15
Fe_2O_3	5.50	5.82	5.98	0.34	0.40	0.38	0.20	0.27	0.27
K_2O	0.38	0.43	0.42	0.54	0.58	0.56	0.50	0.56	0.55
Li_2O	0.89	0.98	0.96	0.00	0.02	0.02	0.99	1.13	1.13
MgO	1.48	1.51	1.49	1.00	1.00	1.03	1.00	0.96	1.04
MoO_3	0.10	0.07	0.08	0.10	0.08	0.07	0.10	0.09	0.08
Na_2O	17.20	16.31	16.03	24.00	24.25	24.89	20.00	19.16	19.49
NiO	0.00	0.00	0.00	0.00	0.00	0.00	0.01	0.01	0.01
PbO	0.00	0.00	0.00	0.00	0.00	0.00	0.01	0.01	0.01
SiO_2	45.15	45.09	45.04	38.59	38.18	37.70	42.18	42.25	41.98
SnO_2	0.00	0.00	0.00	1.02	0.97	0.99	0.00	0.00	0.00
TiO_2	1.40	1.53	1.53	0.34	0.41	0.39	0.00	0.05	0.04
V_2O_5	0.00	0.00	0.00	1.55	1.60	1.57	2.44	2.65	2.61
ZnO	3.50	3.44	3.47	3.00	2.94	2.87	3.00	2.97	2.97
ZrO_2	3.00	2.95	3.02	5.55	5.32	5.30	3.50	3.44	3.54
Cl	0.42	0.30	0.31	0.58	0.57	0.53	0.20	0.13	0.13
F	0.04	0.04$	0.04$	0.06	0.06$	0.06$	0.08	0.08$	0.08$
P_2O_5	0.13	0.16	0.16	0.18	0.22	0.20	0.12	0.15	0.15
SO_3	0.44	0.38	0.38	0.61	0.57	0.53	1.25	1.10	1.01
Re_2O_7	0.10	0.15	0.13	0.10	0.15	0.13	0.10	0.10	0.13
Total	100.0	99.6	99.6	100.0	100.0	99.9	100.0	99.7	99.9

*Analyzed by XRF except for boron and lithium, which were measured by DCP-AES
$ Target concentration

Table 3.1. Pulsed-Flow Test Matrix.

Temperature [°C]	**Pulsed-Flow Test** (cell volume 50 ml)									
	$[Si]_{in}$	F	pH_{RT}	m_g	S*	S/V	RT	Sampling Interval	Flow	q/S
	[*ppm*]	[*µl/min*]		[*g*]	m^2	m^{-1}	(days)	(days)	cc/day	10^{-8} m/sec
23	35	7	7	3.278	0.065	1306	6.0	3	8.3	0.15
	40	7	8	3.278	0.065	1306	6.0	3	8.3	0.15
	52.5	7	9	3.278	0.065	1306	6.0	3	8.3	0.15
	90	7	10	1.639	0.033	653	6.0	3	8.3	0.30
	230	7	11	1.639	0.033	653	6.0	3	8.3	0.30
40	40	7	7	1.650	0.033	658	6.0	3	8.3	0.29
	45	7	8	1.650	0.033	658	6.0	3	8.3	0.29
	60	7	9	1.650	0.033	658	6.0	3	8.3	0.29
	105	7	10	0.826	0.016	329	6.0	3	8.3	0.59
	270	7	11	0.826	0.016	329	6.0	3	8.3	0.59
70	55	35	7	0.770	0.015	307	2.0	1	25.0	1.89
	60	35	8	0.770	0.015	307	2.0	1	25.0	1.89
	80	35	9	0.770	0.015	307	2.0	1	25.0	1.89
	140	35	10	0.495	0.010	197	2.0	1	25.0	2.93
	360	35	11	0.495	0.010	197	2.0	1	25.0	2.93

* The values listed are calculated using an average glass density of 2.68 g/m^3 for the present three glasses.

Table 3.2. Measured *in Situ* pH (pH_T) of Influent Solutions.

Buffer	$pH_{23°C}$	$pH_{40°C}$	$pH_{70°C}$
Tris – HNO_3	**7.0**	6.6	6.0
Tris – HNO_3	**8.0**	7.6	6.9
Tris – HNO_3	**9.0**	8.6	8.0
Tris – Piperidine – H_4SiO_4	**10.0**	9.6	9.0
Piperidine – HNO_3	**11.0**	10.7	10.0

Table 4.1. Glass Dissolution Rates based on B, Li, K, Na, Cs, Mo, and Re (average of the final few sampling times) from Pulsed-Flow Tests with AP107WDFL at 70 °C, 40 °C, and 23 °C.

Temperature	$[Si]_{in}$	pH_T	NDR_B, g-glass m^{-2} d^{-1}	NDR_{Li}, g-glass m^{-2} d^{-1}	NDR_{Na}, g-glass m^{-2} d^{-1}	NDR_{Mo}, g-glass m^{-2} d^{-1}	NDR_{Cs}, g-glass m^{-2} d^{-1}	NDR_{Re}, g-glass m^{-2} d^{-1}
70°C	55	6.0	0.1094±0.0041	0.1115±0.0027	0.1081±0.0044	0.0031 (value day 9)	0.0643±0.0074	0.0135±0.0018
	60	6.9	0.0377±0.0034	0.0406±0.0079	0.0409±0.005	0.0016±0.0012	0.0163±0.0103	0.0042±0.0048
	80	8.0	0.0104±0.0005	0.0099±0.0014	0.0148±0.0019	0.0046±0.0014	0.0108±0.0027	0.0063±0.0021
	140	9.0	0.0051±0.0017	0.0095±0.0043	0.0115±0.0033	0.0010 (value day 7)	0.0017±0.0005	0.0009±0.0006
	360	10	0.0137±0.0022	0.0096±0.003	0.0101±0.0025	0.0002±0.0002	0.001±0.0006	0.0003±0.0004
40°C	40	6.6	0.0058±0.0002	0.0069±0.0005	0.0059±0.0003	0.0031 (value day 9)	0.0035±0.0008	0.0017±0.0004
	45	7.6	0.0019±0.0001	0.0029±0.0001	0.0025±0.0002	0.0003±0.0002	0.0012±0.0003	0.0008±0.0005
	60	8.6	0.0014±0.0005	0.0015±0.0004	0.0014±0.0001	0.0003±0.0003	0.0007±0.0004	0.0004±0.0003
	105	9.6	0.0008±0.0002	0.0012±0.0001	0.0009±0.0001	0.0010 (value day 7)	0.0003±0.0001	0.0002±0.0001
	270	10.7	0.0017±0.0006	0.0026±0.002	0.002±0.0001	0.0007±0.0003	0.0011±0.0003	0.0009±0.0002
23°C	35	7.0	not reportable	0.0009±0.0002	0.0011±0.00004	0.0001±0.0001	0.0007±0.0001	0.0005±0.0001
	40	8.0	0.0003±0.0002	0.0008±0.0001	0.0007±0.0002	0.0001±0.00004	0.0004±0.0001	0.0003±0.0001
	52.5	9.0	0.0003±0.0001	0.0006±0.0004	0.0006±0.00002	0.0002±0.0001	0.0004±0.0001	0.0003±0.00002
	90	10.0	0.0008±0.0001	0.0030±0.0006	0.0002±0.0001	not reportable	0.0003±0.00001	0.0001±0.00005
	230	11.0	not reportable	0.0009±0.0008	0.0007±0.0001	0.0004±0.0004	0.0004±0.0002	0.0004±0.0003

Notes: In the rate units, "g-glass" represents the mass of glass dissolved as calculated based on the indicated species, as described in Section 3.7. The means and standard deviations listed are calculated from the last two to four time points.

Table 4.2. Glass Dissolution Rates based on B, Li, K, Na, Cs, Mo, and Re (average of the final few sampling times) from Pulsed-Flow Tests with ORLECAP107 at 70 °C, 40 °C, and 23 °C.

Temperature	$[Si]_{in}$	pH_T	NDR_B, g-glass m^{-2} d^{-1}	NDR_{Na}, g-glass m^{-2} d^{-1}	NDR_K, g-glass m^{-2} d^{-1}	NDR_{Mo}, g-glass m^{-2} d^{-1}	NDR_{Cs}, g-glass m^{-2} d^{-1}	NDR_{Re}, g-glass m^{-2} d^{-1}
70°C	55	6.0	0.8597±0.0761	0.9689±0.0392	0.2911±0.0305	0.0151±0.0087	0.1614±0.0252	0.0243±0.006
	60	6.9	0.6174±0.0424	0.6388±0.0527	0.4986±0.0524	0.0079±0.0021	0.0731±0.0241	0.01±0.0051
	80	8.0	0.3245±0.0191	0.2946±0.0094	0.1651±0.0092	0.0024±0.0003	0.0471±0.043	0.0076±0
	140	9.0	0.1947±0.0162	0.1503±0.0039	0.056±0.0132	0.0115±0.009	0.0209±0.0024	0.0073±0.0084
	360	10	0.0826±0.0085	0.0793±0.0024	not reportable	0.0044±0.0022	0.0133±0.0003	0.0044±0.001
40°C	40	6.6	0.0978±0.0084	0.078±0.0058	0.0746±0.0088	0.0008±0.00005	0.0126±0.0002	0.0087±0.0006
	45	7.6	0.0465±0.0039	0.0423±0.0037	0.0311±0.0023	0.0005±0.0001	0.0047±0.0005	0.0036±0.0009
	60	8.6	0.0223±0.0006	0.0186±0.0008	0.007±0.0005	0.0003±0.00005	0.0024±0.0001	0.0029±0.0003
	105	9.6	0.0128±0.0006	0.0118±0.0006	0.0038±0.0028	not reportable	0.0026±0.0016	0.0023±0.002
	270	10.7	0.0013±0.00003	0.0015±0.0002	not reportable	not reportable	0.0007±0.0001	0.0005±0.0001
23°C	35	7.0	0.0111±0.0001	0.0103±0.0007	0.0063±0.0009	0.0003±0.00004	0.0018±0.0002	0.0025±0.0001
	40	8.0	0.0044±0.0007	0.0045±0.0001	0.0029±0.0005	0.0002±0.00002	0.0008±0.00004	0.0009±0.0003
	52.5	9.0	0.0023±0.0004	0.002±0.0001	0.0023±0.0008	0.0001±0.00003	0.0005±0.00004	0.0004±0.0002
	90	10.0	0.0006±0.0004	0.001±0.000004	0.004±0.0013	not reportable	0.0005±0.0002	0.0002±0.0001
	230	11.0	not reportable	0.0006±0.0005	not reportable	not reportable	0.0004±0.0001	0.0001±0.00001

Notes: In the rate units, "g-glass" represents the mass of glass dissolved as calculated based on the indicated species, as described in Section 3.7.
The means and standard deviations listed are calculated from the last two to four time points.

Table 4.3. Glass Dissolution Rates Based on B, Li, K, Na, Cs, Mo, and Re (average of the final few sampling times) from Pulsed-Flow Tests with ORLEC44 at 70 °C, 40 °C, and 23 °C.

Temperature	$[Si]_{in}$	pH_T	NDR_B, g-glass m^{-2} d^{-1}	NDR_{Li}, g-glass m^{-2} d^{-1}	NDR_{Na}, g-glass m^{-2} d^{-1}	NDR_K, g-glass m^{-2} d^{-1}	NDR_{Mo}, g-glass m^{-2} d^{-1}	NDR_{Cs}, g-glass m^{-2} d^{-1}	NDR_{Re}, g-glass m^{-2} d^{-1}
70°C	55	6.0	0.7747±0.0592	0.9424±0.075	0.6737±0.0384	0.8235±0.0132	0.0206±0.0322	0.2207±0.0486	0.0505±0.0118
	60	6.9	0.4113±0.0399	0.4711±0.0464	0.4012±0.0383	0.4231±0.0345	0.0073±0.0008	0.1388±0.0049	0.0377±0.0083
	80	8.0	0.1147±0.0083	0.1085±0.0129	0.1111±0.0082	0.0844±0.0096	0.0039±0.0005	0.0479±0.0051	0.0364±0.0033
	140	9.0	0.0784±0.008	0.076±0.0042	0.0779±0.0049	0.0852±0.0053	0.0041±0.0011	0.0269±0.0013	0.0353±0.0076
	360	10.0	0.0143±0.0013	0.0131±0.0022	0.0168±0.0016	not reportable	0.0010±0.0002	0.007±0.0005	0.0025±0.0004
40°C	40	6.6	0.0878±0.0016	0.0905±0.0025	0.073±0.0043	0.0656±0.0115	0.0031±0.0004	0.0188±0.0018	0.0341±0.0008
	45	7.6	0.0265±0.0013	0.0275±0.0026	0.0244±0.0003	0.0242±0.0021	0.0010±0.0002	0.0092±0.0009	0.0142±0.0014
	60	8.6	0.0081±0.0005	0.006±0.0003	0.0066±0.0001	0.004±0.0007	0.0004±0.00002	0.0038±0.0004	0.0055±0.0006
	105	9.6	0.0029±0.0004	0.0024±0.0009	0.0032±0.0001	not reportable	not reportable	0.0023±0.0001	0.0022±0.0001
	270	10.7	0.0019±0.0003	0.0045±0.0009	0.0018±0.0001	not reportable	0.0004±0.0001	0.0013±0.0002	0.0008±0.0001
23°C	35	7.0	0.0128±0.0003	0.0125±0.0003	0.0107±0.0005	0.0074±0.0008	0.0012±0.0001	0.0025±0.0002	0.0063±0.0007
	40	8.0	0.0026±0.0001	0.0029±0.0002	0.0029±0.0002	0.0029±0.0009	0.0005±0.0001	0.0011±0.0002	0.0017±0.0001
	52.5	9.0	0.0009±0.0004	0.0011±0.0002	0.0016±0.00005	0.0021±0.0003	0.0003±0.0001	0.0007±0.0001	0.0009±0.0001
	90	10.0	0.0011±0.0005	0.0014±0.0007	0.0010±0.00001	not reportable	not reportable	0.0006±0.0002	0.0004±0.0001
	230	11.0	0.0010±0.0002	0.0016±0.0001	0.0006±0.0002	not reportable	0.0008±0.0005	0.0013±0.0001	0.0008±0.0002

Notes: In the rate units, "g-glass" represents the mass of glass dissolved as calculated based on the indicated species, as described in Section 3.7.
The means and standard deviations listed are calculated from the last two to four time points.

Table 4.4. Alkali Ion Exchange Rates (in mol m^{-2} s^{-1})[(a)] from Pulsed-Flow Tests Performed on AP107WDFL, ORLECAP107, and ORLEC44 (average of the final few sampling times).

Glass ID			AP107WDFL			ORLECAP107			ORLEC44			
pH_{RT}	pH_T	$[Si]_{in}$	$r_{IEX\ Na}$, mol m^{-2} s^{-1}	$r_{IEX\ Li}$, mol m^{-2} s^{-1}	$r_{IEX\ Cs}$, [(b)] mol m^{-2} s^{-1}	$r_{IEX\ Na}$, mol m^{-2} s^{-1}	$r_{IEX\ K}$, mol m^{-2} s^{-1}	$r_{IEX\ Cs}$, [(b)] mol m^{-2} s^{-1}	$r_{IEX\ Na}$, mol m^{-2} s^{-1}	$r_{IEX\ Li}$, mol m^{-2} s^{-1}	$r_{IEX\ K}$, mol m^{-2} s^{-1}	$r_{IEX\ Cs}$, [(b)] mol m^{-2} s^{-1}
70°C Experiments												
7	6.0	55	6.43E-09	6.79E-10	6.13E-12	7.68E-08	3.62E-10	1.55E-11	4.77E-08	6.60E-09	9.68E-10	1.59E-11
8	6.9	60	2.41E-09	2.53E-10	9.21E-13	5.40E-08	6.56E-10	6.94E-12	2.65E-08	3.07E-09	4.63E-10	1.24E-11
9	8.0	80	8.50E-10	5.70E-11	3.24E-13	2.60E-08	2.13E-10	6.10E-12	6.99E-09	6.95E-10	8.09E-11	3.24E-12
10	9.0	140	7.63E-10	5.92E-11	1.76E-13	1.35E-08	4.26E-11	1.95E-12	4.29E-09	4.24E-10	6.86E-11	2.24E-12
11	10.0	360	6.71E-10	6.50E-11	6.11E-14	6.83E-09	4.66E-12	8.61E-13	1.19E-09	8.18E-11	not reportable	5.81E-13
40°C Experiments												
7	6.6	40	3.27E-10	3.97E-11	2.81E-13	6.56E-09	9.11E-11	1.25E-12	4.41E-09	5.85E-10	6.37E-11	1.72E-12
8	7.6	45	1.26E-10	1.59E-11	7.56E-14	3.43E-09	3.86E-11	4.56E-13	1.26E-09	1.38E-10	2.04E-11	8.74E-13
9	8.6	60	7.04E-11	4.17E-12	3.56E-14	1.53E-09	7.21E-12	2.23E-13	2.57E-10	2.41E-11	4.47E-12	3.62E-13
10	9.6	105	5.58E-11	8.15E-12	3.08E-14	1.02E-09	4.57E-12	2.09E-13	1.46E-10	2.03E-11	not reportable	2.27E-13
11	10.7	270	8.32E-11	4.92E-12	2.89E-14	1.39E-10	not reportable	7.44E-14	9.85E-11	2.69E-11	not reportable	1.17E-13
23°C Experiments												
7	7.0	35	5.14E-11	3.34E-12	4.04E-14	7.65E-10	6.19E-12	1.60E-13	4.92E-10	6.40E-11	5.06E-12	1.41E-13
8	8.0	40	3.19E-11	4.16E-12	2.22E-14	3.22E-10	3.44E-12	6.00E-14	1.30E-10	1.68E-11	2.63E-12	6.23E-14
9	9.0	52.5	2.26E-11	3.31E-12	1.53E-14	1.72E-10	2.82E-12	4.42E-14	7.13E-11	6.03E-12	1.90E-12	3.83E-14
10	10.0	90	1.95E-11	2.04E-11	2.16E-14	8.59E-11	5.15E-12	4.45E-14	5.98E-11	5.40E-12	not reportable	5.20E-14
11	11.0	230	not reportable	2.80E-12	7.87E-15	5.19E-11	not reportable	2.98E-14	not reportable	4.37E-12	3.18E-12	6.64E-14

[(a)] "mol" in the r_{iex} units refers to moles of the indicated alkali element released by ion exchange.
[(b)] At 40°C, $r_{IEX\ Cs}$ was calculated by difference to Mo when the Re data were not reportable.

Table 4.5. Regression Results to Obtain K_g from Pulsed-Flow Test Data for AP107WDFL, ORLECAP107, and ORLEC44.

-	Temperature	NDR element	K_g (mol L^{-1})
AP107WDFLCC	**70°C Linear fit**	B	3.41×10^{-3}
		Re	3.50×10^{-3}
	40°C Linear fit	B	1.99×10^{-3}
		Re	1.99×10^{-3}
	23°C Linear fit	B	1.92×10^{-3}
		Re	2.05×10^{-3}
	15°C extrapolation	B	1.57×10^{-3}
		Re	1.66×10^{-3}
AP107WDFL average 15 ℃ K_g = 1.62 x 10^{-3}			
ORLECAP107CC	**70°C Linear fit**	B	3.66×10^{-3}
		Re	3.91×10^{-3}
	40°C Linear fit	B	1.99×10^{-3}
		Re	2.10×10^{-3}
	23°C Linear fit	B	1.71×10^{-3}
		Re	1.69×10^{-3}
	15°C extrapolation	B	1.37×10^{-3}
		Re	1.36×10^{-3}
ORLECAP107 average 15 ℃ K_g = 1.37 x 10^{-3}			
ORLEC44IXCC	**70°C Linear fit**	B	3.49×10^{-3}
		Re	5.19×10^{-3}
	40°C Linear fit	B	1.90×10^{-3}
		Re	1.94×10^{-3}
	23°C Linear fit	B	1.60×10^{-3}
		Re	1.65×10^{-3}
	15°C extrapolation	B	1.29×10^{-3}
		Re	1.16×10^{-3}
ORLEC44 average 15 ℃ K_g = 1.22 x 10^{-3}			

Table 4.6. Values of the Parameter K_g (mol L^{-1}) at 15 °C for Glasses AP107WDFL, ORLECAP107, and ORLEC44 from Pulsed-Flow Tests.

Basis	AP107WDFL	ORLECAP107	ORLEC44
Based on NDR_B	1.57×10^{-3}	1.37×10^{-3}	1.29×10^{-3}
Based on NDR_{Re}	1.66×10^{-3}	1.36×10^{-3}	1.16×10^{-3}
Average	1.62×10^{-3}	1.37×10^{-3}	1.22×10^{-3}

Table 5.1. Summary of Regression Statistics and Model Parameters; Uncertainties in Parentheses.

Glass ID	AP107 WDFL	AP107 WDFL	AP107 WDFL	ORLEC AP107	ORLEC AP107	ORLEC AP107	ORLEC44	ORLEC44	ORLEC44	ORLEC44
Element	**Na**	Li	Cs	**Na**	K	Cs	**Na**	Li	K	Cs
R^2	0.859	0.763	0.756	0.967	0.785	0.914	0.939	0.913	0.861	0.851
R^2_{Adj}	0.857	0.760	0.752	0.967	0.782	0.913	0.938	0.912	0.858	0.849
Root Mean Square Error	0.291	0.365	0.385	0.178	0.423	0.263	0.229	0.293	0.374	0.362
Mean of Response ($Log_{10}\ r_{IEX}$)	-9.603	-10.545	-13.039	-8.597	-10.635	-12.367	-8.984	-9.960	-10.721	-12.314
Number of Observations	148	139	140	147	127	136	140	138	116	132
Model Terms:	$Log\ (r_{IEX}) = A + (B/T) + C\times pH - (1/2)*log(t)$									
A (Intercept)	0.02 (0.4)	-1.6 (0.52)	-5.2 (0.54)	4.8 (0.25)	-0.14 (0.63)	-0.92 (0.37)	3.01 (0.32)	2.32 (0.41)	1.88 (0.57)	-0.56 (0.52)
B (1/Temp, K)	-2524.0 (130.9)	-2364.5 (169.2)	-1570.1 (177)	-3316.8 (80.1)	-2292.5 (203.1)	-2808.8 (122.8)	-2771.3 (104.6)	-2740 (134.6)	-3029.4 (191.3)	-2829.5 (173.7)
C (pH)	-0.136 (0.017)	-0.12 (0.022)	-0.283 (0.023)	-0.286 (0.01)	-0.340 (0.028)	-0.245 (0.016)	-0.329 (0.014)	-0.375 (0.017)	-0.315 (0.027)	-0.277 (0.022)
Parameters in Equation 1.6:										
Log (k_{d0}, mol $m^{-2}\ s^{-1/2}$)	2.79 (0.4)	1.17 (0.52)	-2.43 (0.54)	7.57 (0.245)	2.63 (0.633)	1.84 (0.371)	5.78 (0.32)	5.09 (0.41)	4.65 (0.57)	2.21 (0.52)
E_{ad}, kJ	48.3 (2.5)	45.3 (3.2)	30.1 (3.4)	63.5 (1.5)	43.9 (3.9)	53.8 (2.4)	53.1 (2.0)	52.5 (3.7)	58.0 (3.7)	54.2 (3.3)
α	0.136 (0.017)	0.120 (0.022)	0.283 (0.023)	0.286 (0.01)	0.340 (0.028	0.245 (0.016)	0.329 (0.014)	0.375 (0.017)	0.315 (0.027)	0.277 (0.022)

Table 5.2. Summary of Regression Statistics and Model Parameters; Uncertainties in Parentheses.

Glass ID	**AP107 WDFL**	**AP107 WDFL**	**AP107 WDFL**	**ORLEC AP107**	**ORLEC AP107**	**ORLEC AP107**	**ORLEC44**	**ORLEC44**	**ORLEC44**	**ORLEC44**
Element	**Na**	Li	Cs	**Na**	K	Cs	**Na**	Li	K	Cs
R^2	0.880	0.769	0.759	0.969	0.796	0.918	0.939	0.920	0.885	0.897
R^2_{Adj}	0.877	0.764	0.754	0.968	0.791	0.916	0.938	0.918	0.882	0.894
Root Mean Square Error	0.269	0.361	0.384	0.174	0.414	0.258	0.229	0.283	0.341	0.302
Mean of Response (Log_{10} r_{IEX})	-9.603	-10.545	-13.039	-8.597	-10.635	-12.367	-8.984	-9.960	-10.721	-12.314
Number of Observations	148	139	140	147	127	136	140	138	116	132
Model Terms: Log (r_{IEX}) = A + (B/T) + C× pH + D*log(t)										
A (Intercept)	-0.85 (0.41)	-2.02 (0.57)	-4.74 (0.64)	5.14 (0.27)	0.89 (0.74)	-0.35 (0.43)	3.18 (0.35)	2.96 (0.44)	3.11 (0.58)	1.54 (0.52)
B (1/Temp, K)	-2140.6 (143.7)	-2174.1 (196.2)	-1762.4 (226.5)	-3461.4 (94.7)	-2707.8 (256.5)	-3049.9 (154.5)	-2844.7 (123.1)	-3016.2 (154.4)	-3557.2 (205.1)	-3709.1 (186.4)
C (pH)	-0.135 (0.015)	-0.120 (0.021)	-0.284 (0.023)	-0.286 (0.01)	-0.346 (0.027)	-0.247 (0.015)	-0.329 (0.014)	-0.376 (0.017)	-0.320 (0.025)	-0.283 (0.019)
D (log(t))	-0.849 (0.07)	-0.677 (0.095)	-0.345 (0.115)	-0.373 (0.047)	-0.169 (0.129)	-0.294 (0.083)	-0.432 (0.06)	-0.254 (0.074)	-0.01 (0.1)	0.215 (0.095)
Parameters in Equation 1.8:										
Log (k_{d0}, mol m^{-2} $s^{(\gamma-1)}$)	3.64 (0.54)	1.62 (0.73)	-2.74 (0.85)	7.28 (0.36)	7.28 (0.36)	1.4 (0.59)	5.61 (0.46)	4.51 (0.58)	3.46 (0.76)	0.78 (0.7)
E_{ad}, kJ	41.0 (2.8)	41.6 (3.8)	33.7 (4.3)	66.3 (1.8)	66.3 (1.8)	58.4 (3)	54.5 (2.4)	57.7 (3)	68.1 (3.9)	71.0 (3.6)
α	0.135 (0.015)	0.120 (0.021)	0.284 (0.023)	0.286 (0.01)	0.346 (0.027)	0.247 (0.015)	0.329 (0.014)	0.376 (0.017)	0.320 (0.025)	0.283 (0.019)
γ	0.849 (0.07)	0.677 (0.095)	0.345 (0.115)	0.373 (0.047)	0.169 (0.129)	0.294 (0.083)	0.432 (0.06)	0.254 (0.074)	0.01 (0.1)	-0.215 (0.095)

Note: Results for ORLEC44 shaded in gray are less reliable since only 56% and 33% (for K and Cs, respectively) of the dataset have ion exchange values based on *both* Re *and* Mo such that the averages could be used. See text.

Table 5.3. Comparison of Activation Energies Determined for Na, K, Li, and Cs for Glasses AP107WDFL, ORLECAP107 and ORLEC44.

Element	Glass ID	E_{ad} kJ/mol	
		Equation 1.6	Equation 1.8
Na	AP107WDFL	48.3	41.0
Na	ORLECAP107	63.5	66.3
Na	ORLEC44	53.1	54.5
Li	AP107WDFL	45.3	41.6
Li	ORLEC44	52.5	57.7
K	ORLECAP107	43.9	66.3
K	ORLEC44	58.0	68.1
Cs	AP107WDFL	30.1	33.7
Cs	ORLECAP107	53.8	58.4
Cs	ORLEC44	54.2	71.0

Table 5.4. Comparison of Extrapolated Ion Exchange Rates Determined for Na, K, Li, and Cs for Glasses AP107WDFL, ORLECAP107 and ORLEC44.

IEX Rate at 15 ℃ and 30 days from Eq. 1.6 (mol m^{-2} s^{-1})										
Glass ID	**AP107 WDFL**	**AP107 WDFL**	**AP107 WDFL**	**ORLEC AP107**	**ORLEC AP107**	**ORLEC AP107**	**ORLEC44**	**ORLEC44**	**ORLEC44**	**ORLEC44**
pH_T	Na	Li	Cs	Na	K	Cs	Na	Li	K	Cs
7	3.73E-11	4.13E-12	4.27E-14	3.49E-10	6.15E-12	7.42E-14	2.21E-10	2.76E-11	2.62E-12	8.67E-14
8	2.73E-11	3.13E-12	2.22E-14	1.81E-10	2.81E-12	4.23E-14	1.03E-10	1.16E-11	1.27E-12	4.58E-14
9	2.00E-11	2.38E-12	1.16E-14	9.37E-11	1.29E-12	2.41E-14	4.84E-11	4.91E-12	6.13E-13	2.42E-14
10	1.46E-11	1.80E-12	6.03E-15	4.86E-11	5.89E-13	1.37E-14	2.27E-11	2.07E-12	2.97E-13	1.28E-14
11	1.07E-11	1.37E-12	3.14E-15	2.52E-11	2.70E-13	7.79E-15	1.06E-11	8.74E-13	1.44E-13	6.76E-15
IEX Rate at 15 ℃ and 30 days from Eq. 1.8 (mol m-2 s-1)										
Glass ID	**AP107 WDFL**	**AP107 WDFL**	**AP107 WDFL**	**ORLEC AP107**	**ORLEC AP107**	**ORLEC AP107**	**ORLEC44**	**ORLEC44**	**ORLEC44**	**ORLEC44**
pH_T	Na	Li	Cs	Na	K	Cs	Na	Li	K	Cs
7	3.26E-11	3.85E-12	4.41E-14	3.65E-10	6.59E-12	7.83E-14	2.27E-10	3.02E-11	3.20E-12	9.93E-14
8	2.39E-11	2.92E-12	2.29E-14	1.89E-10	2.97E-12	4.43E-14	1.06E-10	1.27E-11	1.53E-12	5.17E-14
9	1.75E-11	2.21E-12	1.19E-14	9.75E-11	1.34E-12	2.51E-14	4.98E-11	5.34E-12	7.33E-13	2.70E-14
10	1.29E-11	1.68E-12	6.19E-15	5.04E-11	6.06E-13	1.42E-14	2.33E-11	2.25E-12	3.51E-13	1.40E-14
11	9.42E-12	1.27E-12	3.22E-15	2.61E-11	2.73E-13	8.03E-15	1.09E-11	9.46E-13	1.68E-13	7.32E-15

Table 5.5. Extrapolated Sodium Ion Exchange Rates Determined from Model Parameters in [1], for Glasses IDF1B2, ORLEC28 and LAWC22 (15 ℃, 30 days, pH_T 9).

Model	IDF1B2	ORLEC28	LAWC22
Eq. 1.6	1.50E-10	7.30E-11	1.28E-11
Eq. 1.8	1.45E-10	7.20E-11	1.20E-11

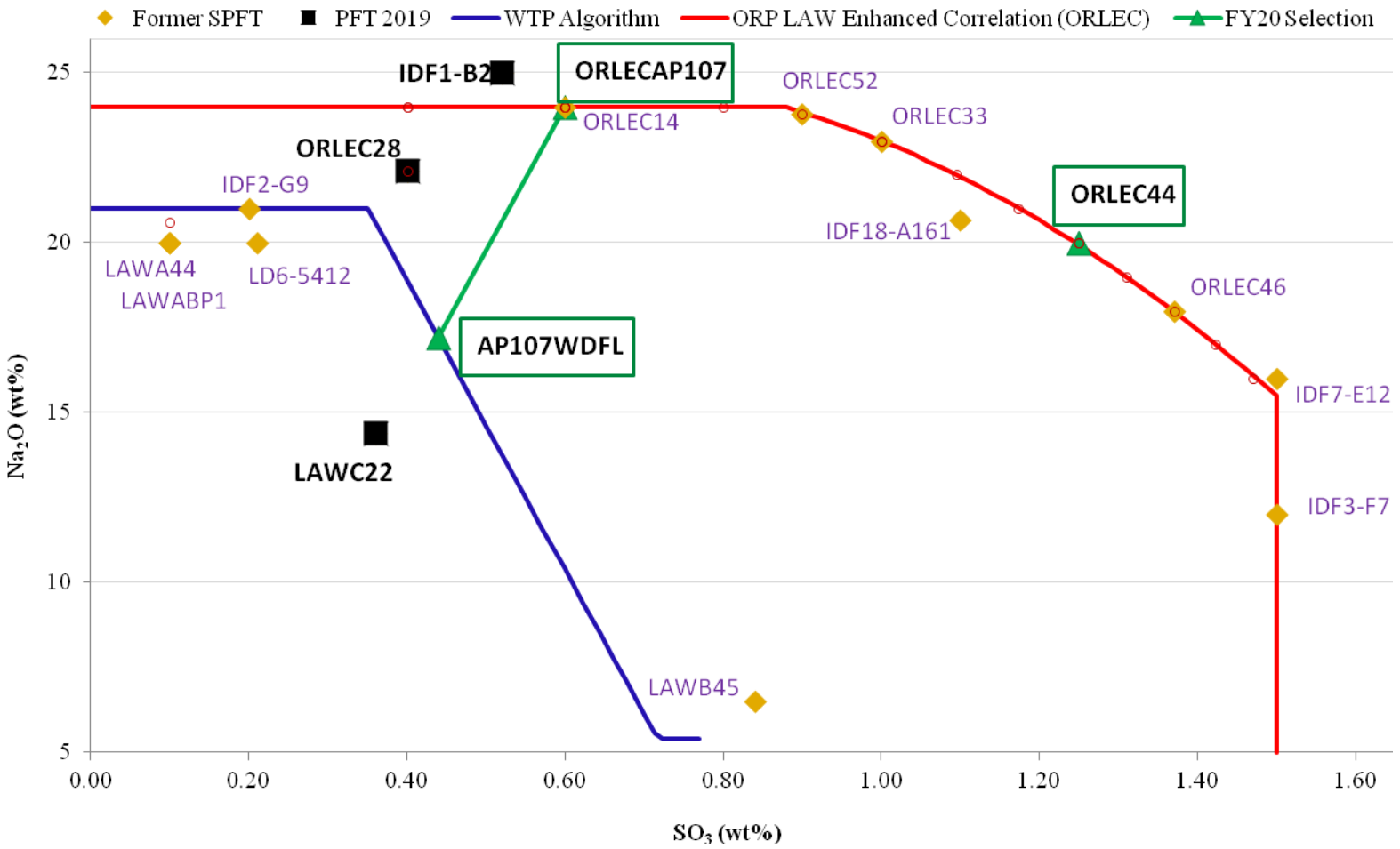

Figure 2.1. Na_2O and SO_3 concentrations for the IDF glasses previously tested by SPFT (purple diamonds) and by PFT (black squares) compared to the three FY20 glasses recommended for ion exchange testing by PFT (green triangles); the line from AP107WDFL to ORLECAP107 shows the waste loading increase from 20.5 to 28.6 wt%.

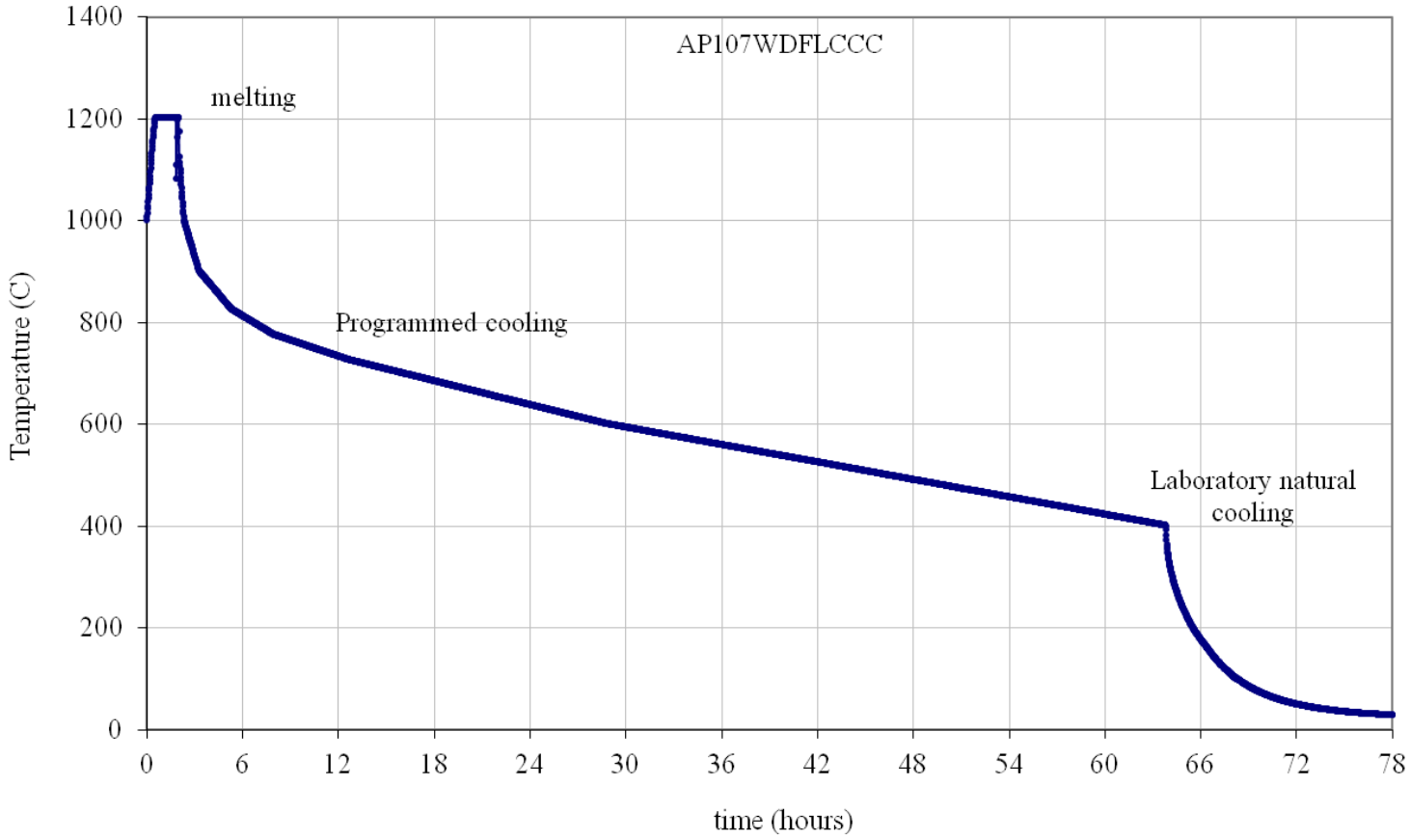

Figure 2.2. CCC profile recorded in the preparation of AP107WDFLCCC.

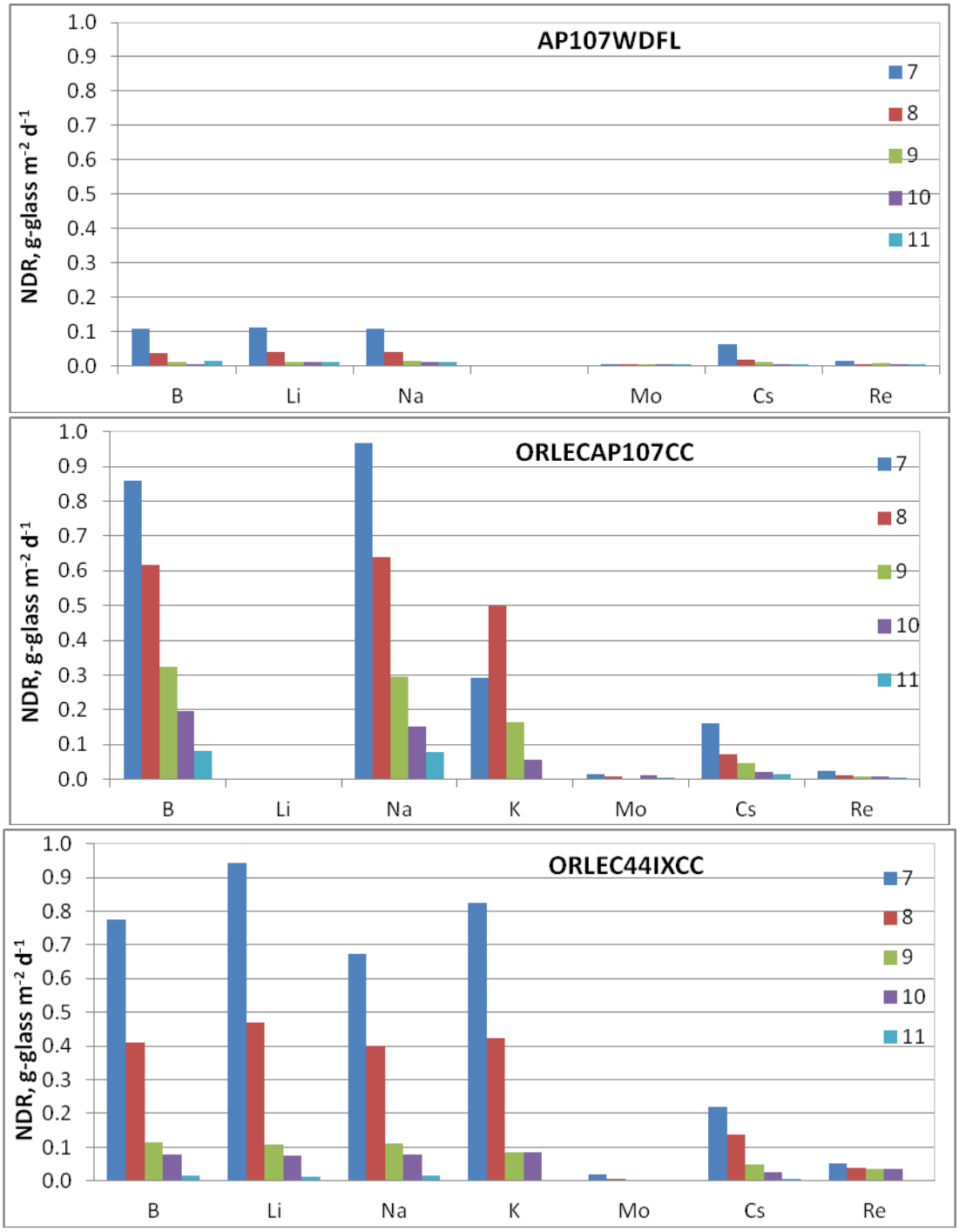

Figure 4.1. Dissolution rates of B, Li, K, Na, Cs, Mo, and Re from Pulsed-Flow tests for the three glasses at 70 °C and five pH values (labels show pH_{RT}).

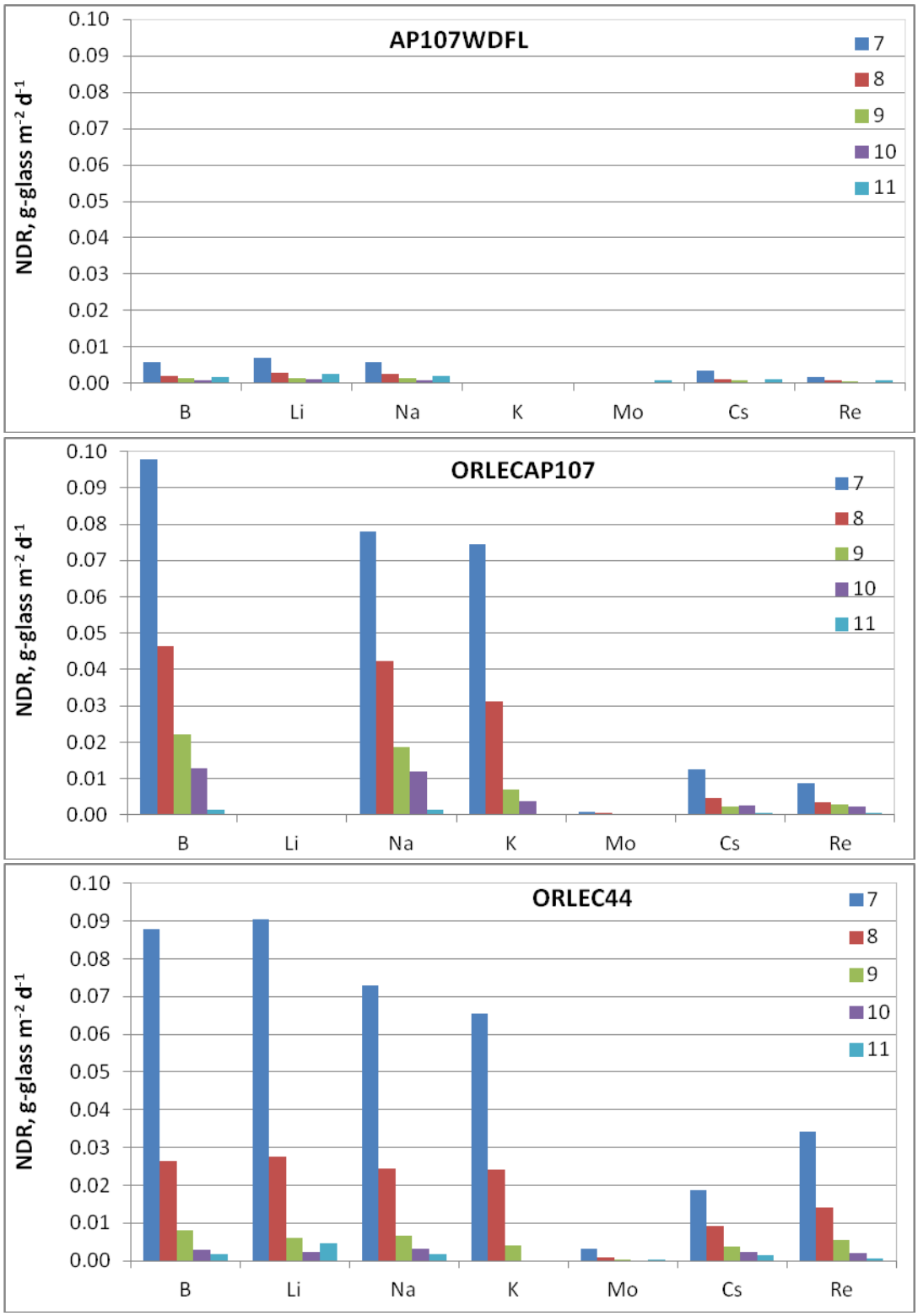

Figure 4.2. Dissolution rates of B, Li, K, Na, Cs, Mo, and Re from Pulsed-Flow tests for the three glasses at 40 °C and five pH values (labels show pH_{RT}).

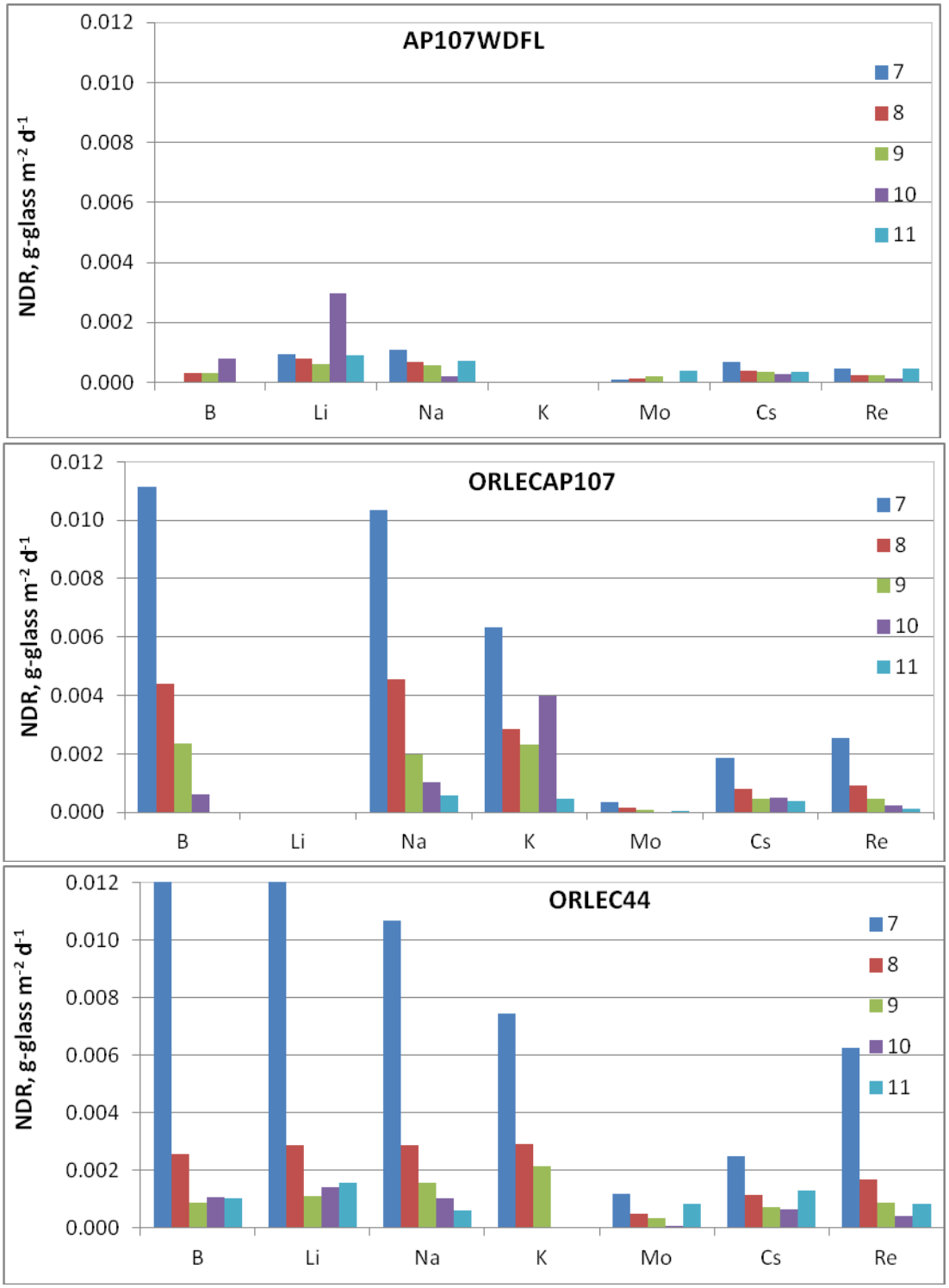

Figure 4.3. Dissolution rates of B, Li, K, Na, Cs, Mo, and Re from Pulsed-Flow tests for the three glasses at 23 °C and five pH values (labels show pH_{RT}).

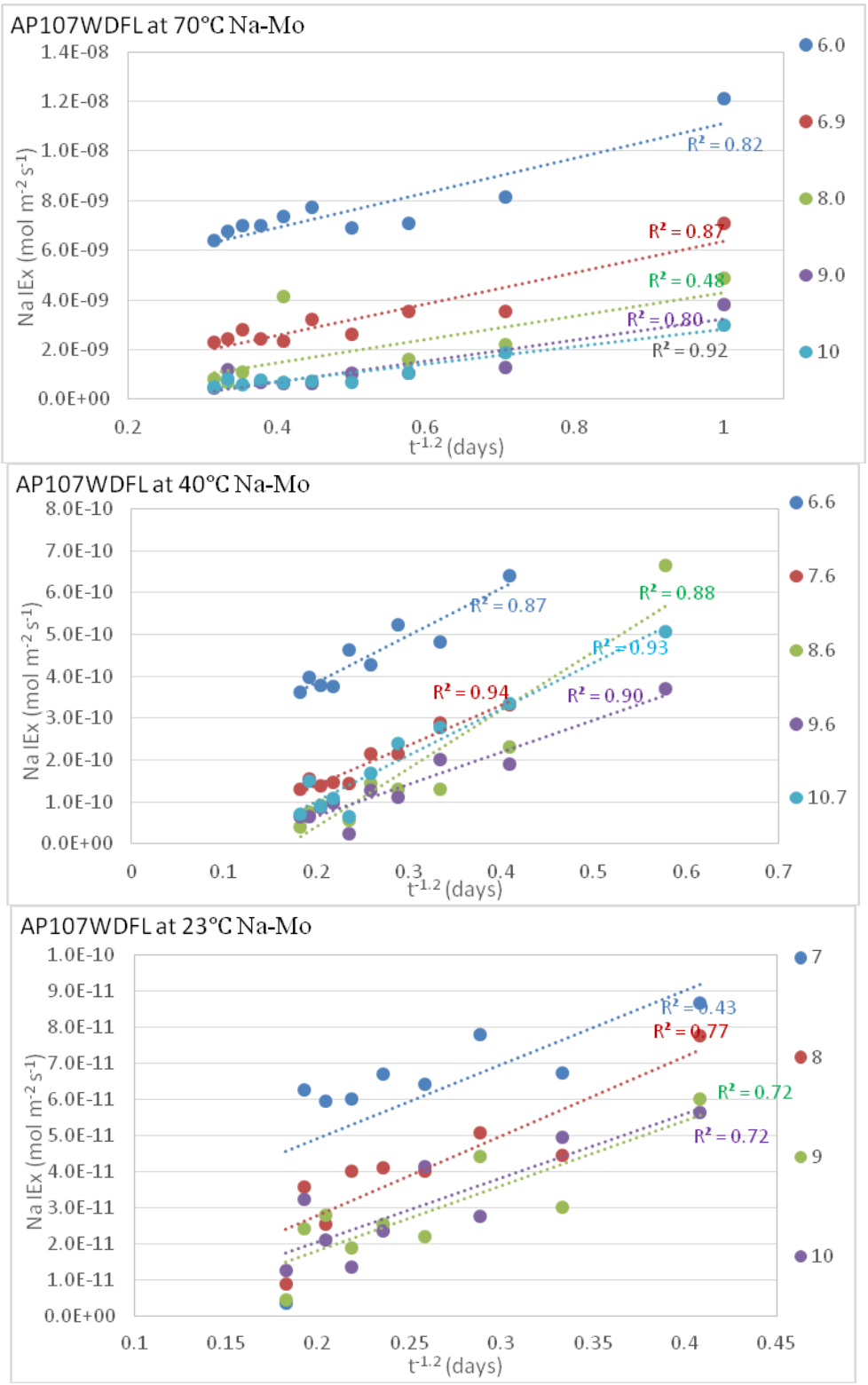

Figure 4.4. Plots of sodium ion exchange rate as a function of square root of time (in days) from Pulsed-Flow tests conducted at 70 °C, 40 °C, and 23 °C with AP107WDFL.

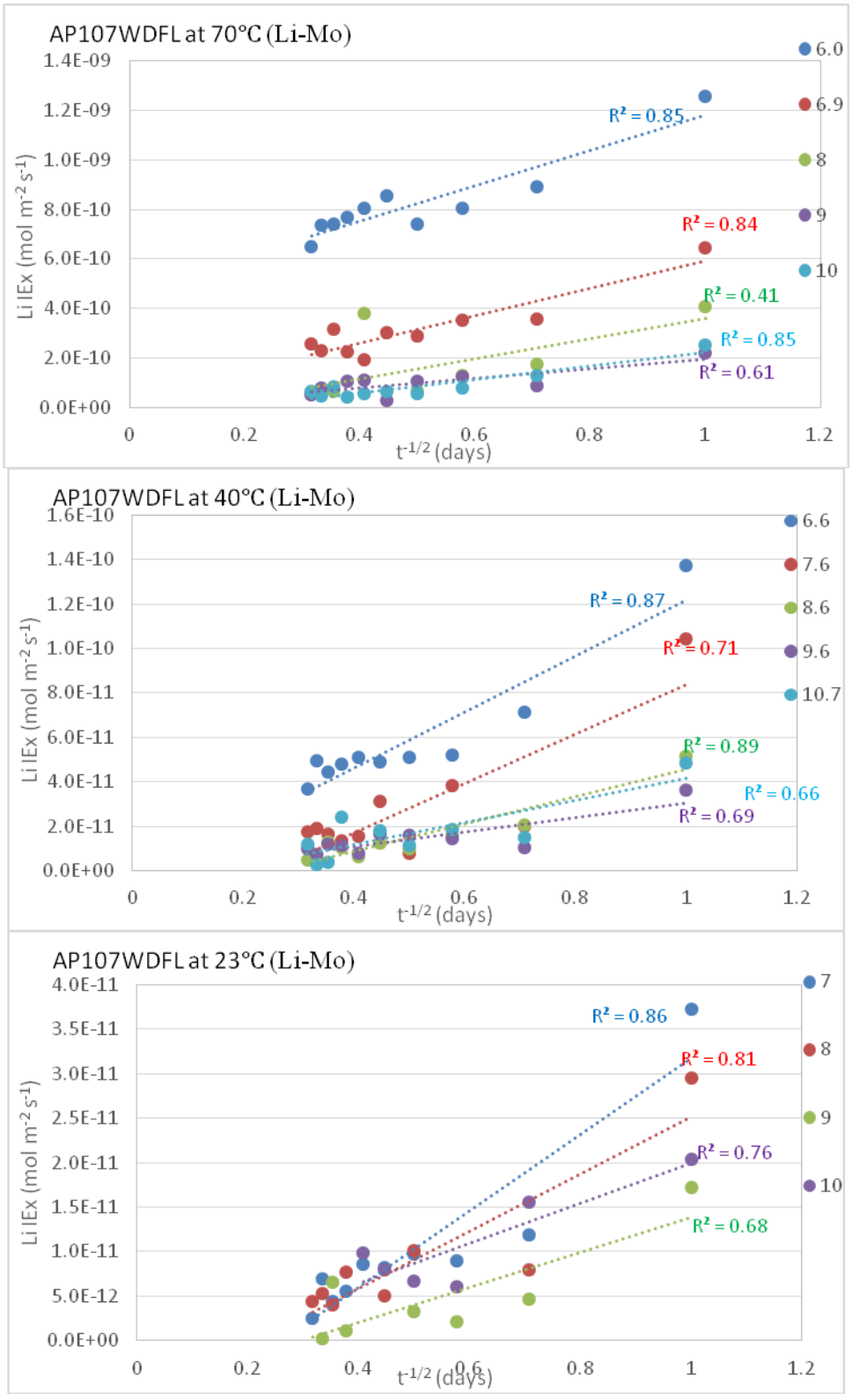

Figure 4.5. Plots of lithium ion exchange rate as a function of square root of time from Pulsed-Flow tests conducted at 70 °C, 40 °C, and 23 °C with AP107WDFL.

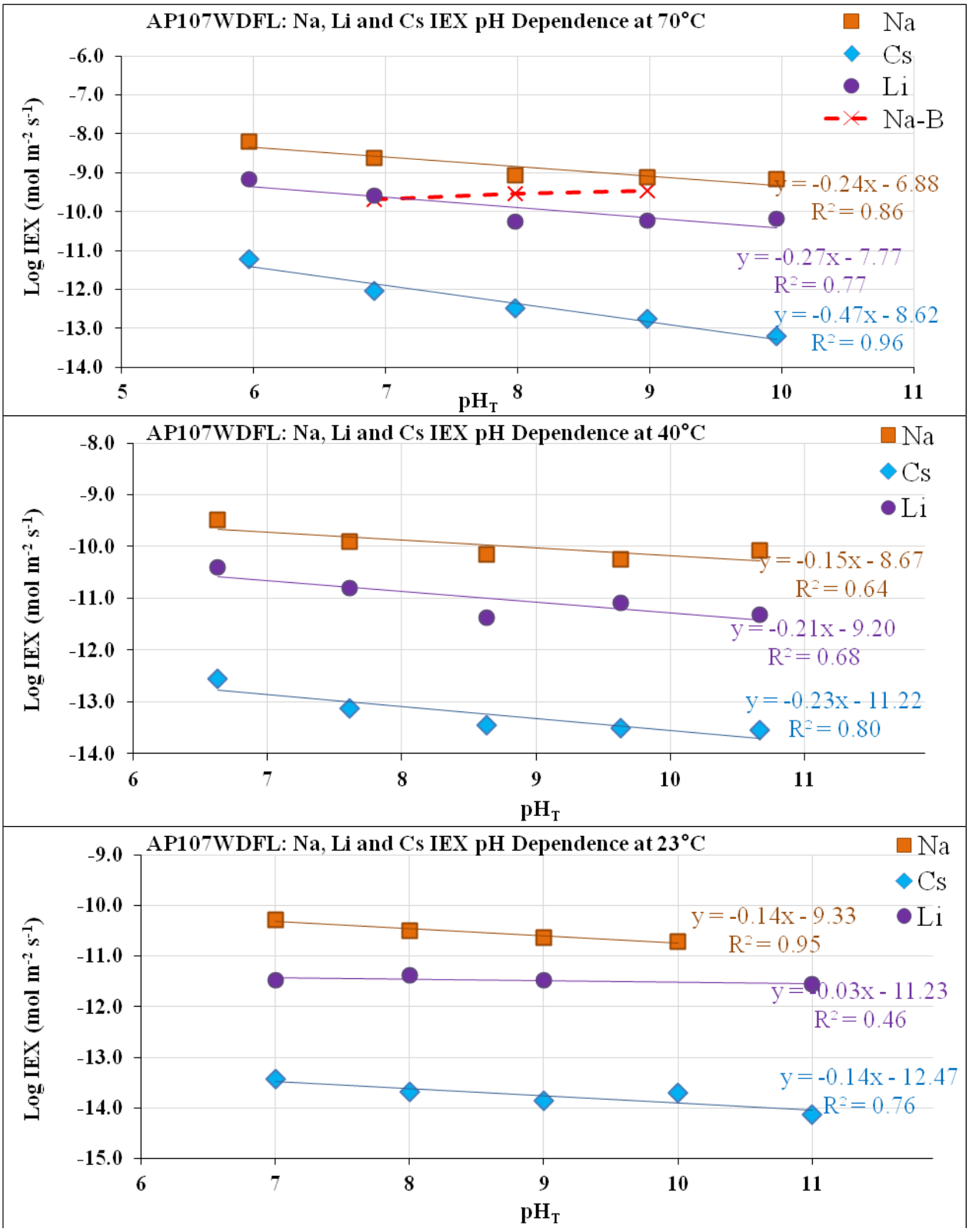

Figure 4.6. Plots of sodium, lithium, and cesium ion exchange rates as a function of pH for AP107WDFL.

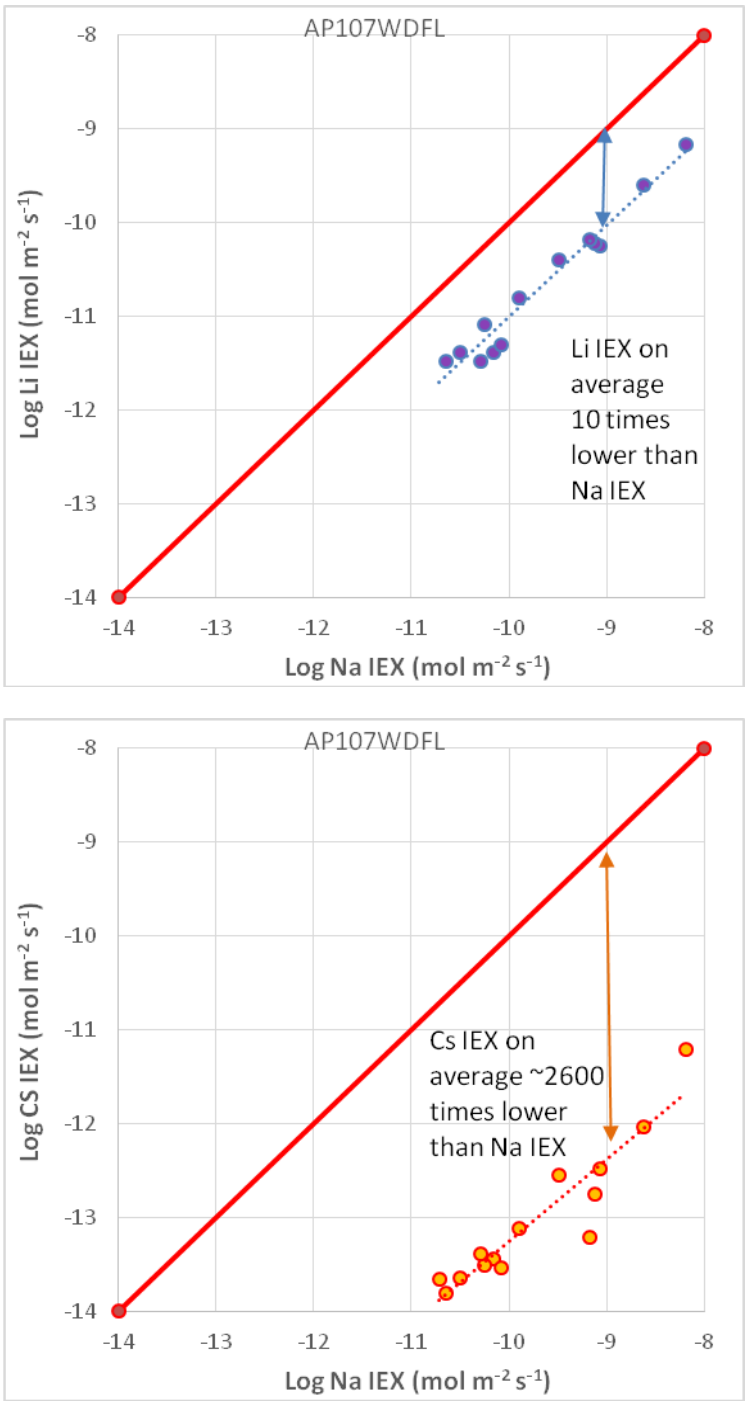

Figure 4.7. Plots of lithium (top) and cesium (bottom) ion exchange rates as a function of sodium ion exchange rate at all pH and temperature values for AP107WDFL. The red line denotes equality of the alkali ion exchange rates; the Li data fall ~1 log units below Na and the Cs data fall ~3 log units below Na.

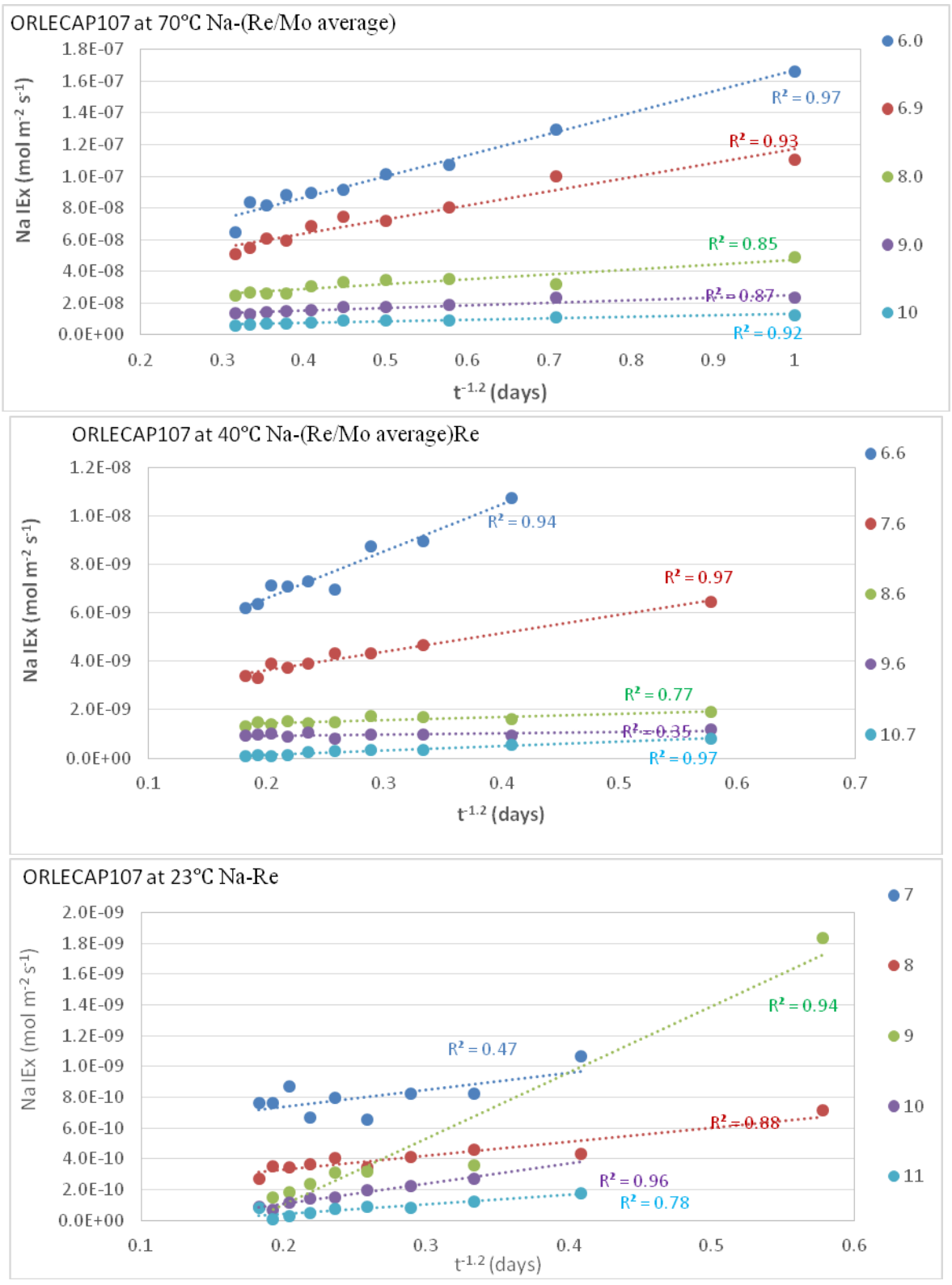

Figure 4.8. Plots of sodium ion exchange rates as a function of square root of time from Pulsed-Flow tests conducted at 70 °C, 40 °C, and 23 °C with ORLECAP107.

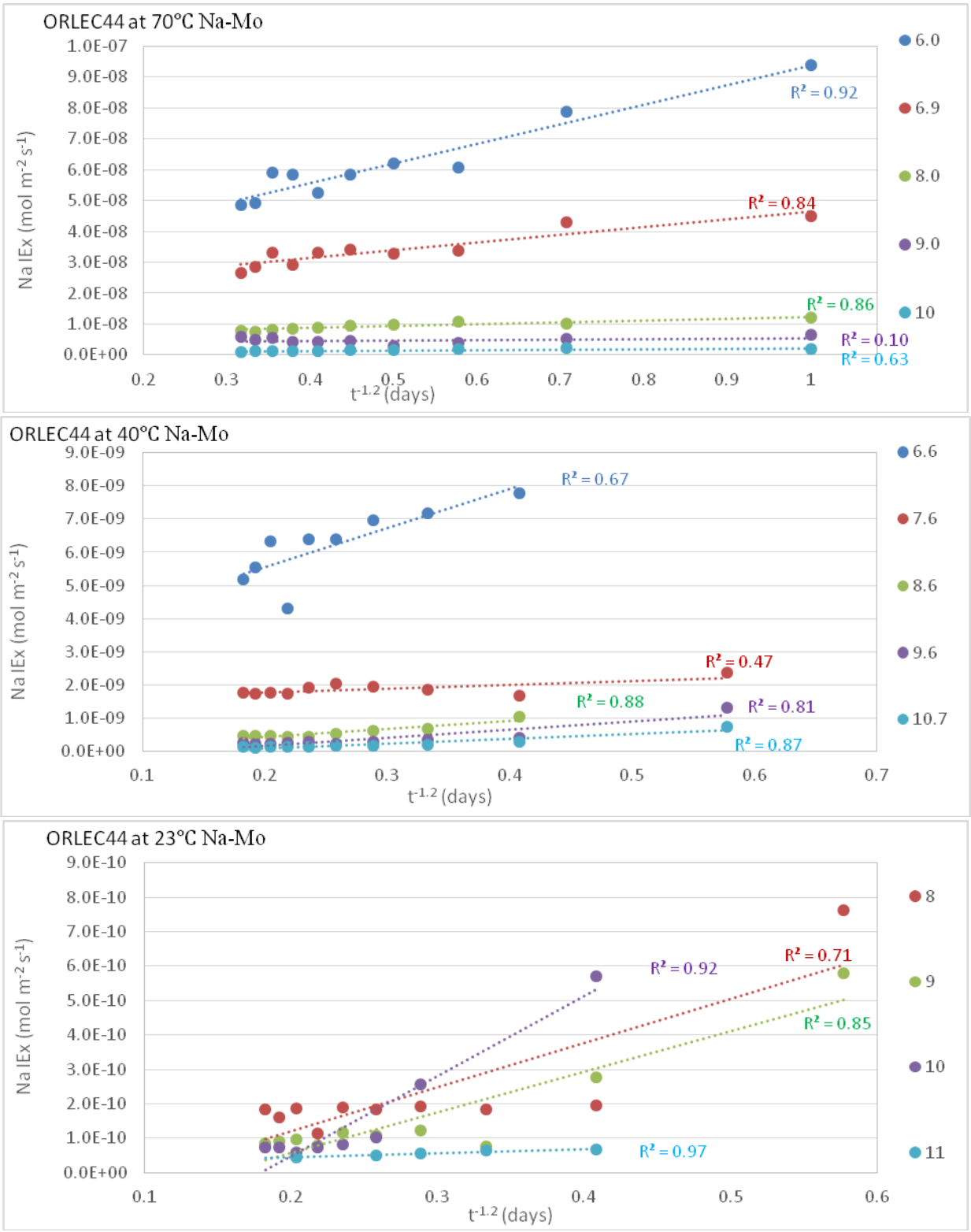

Figure 4.9. Plots of sodium ion exchange rates as a function of square root of time from Pulsed-Flow tests conducted at 70 °C, 40 °C, and 23 °C with ORLEC44.

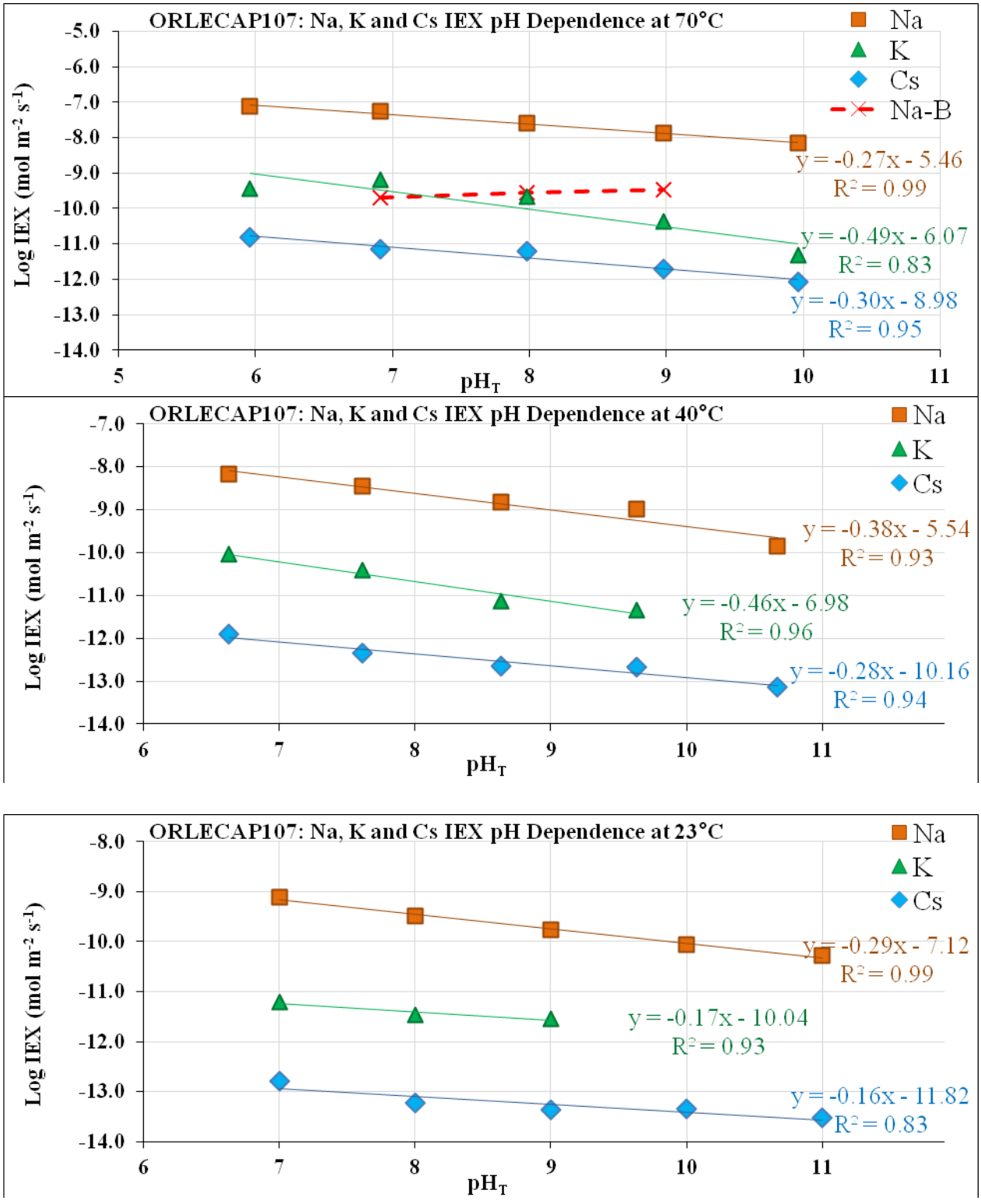

Figure 4.10. Plots of sodium, potassium, and cesium ion exchange rates as a function of pH for ORLECAP107.

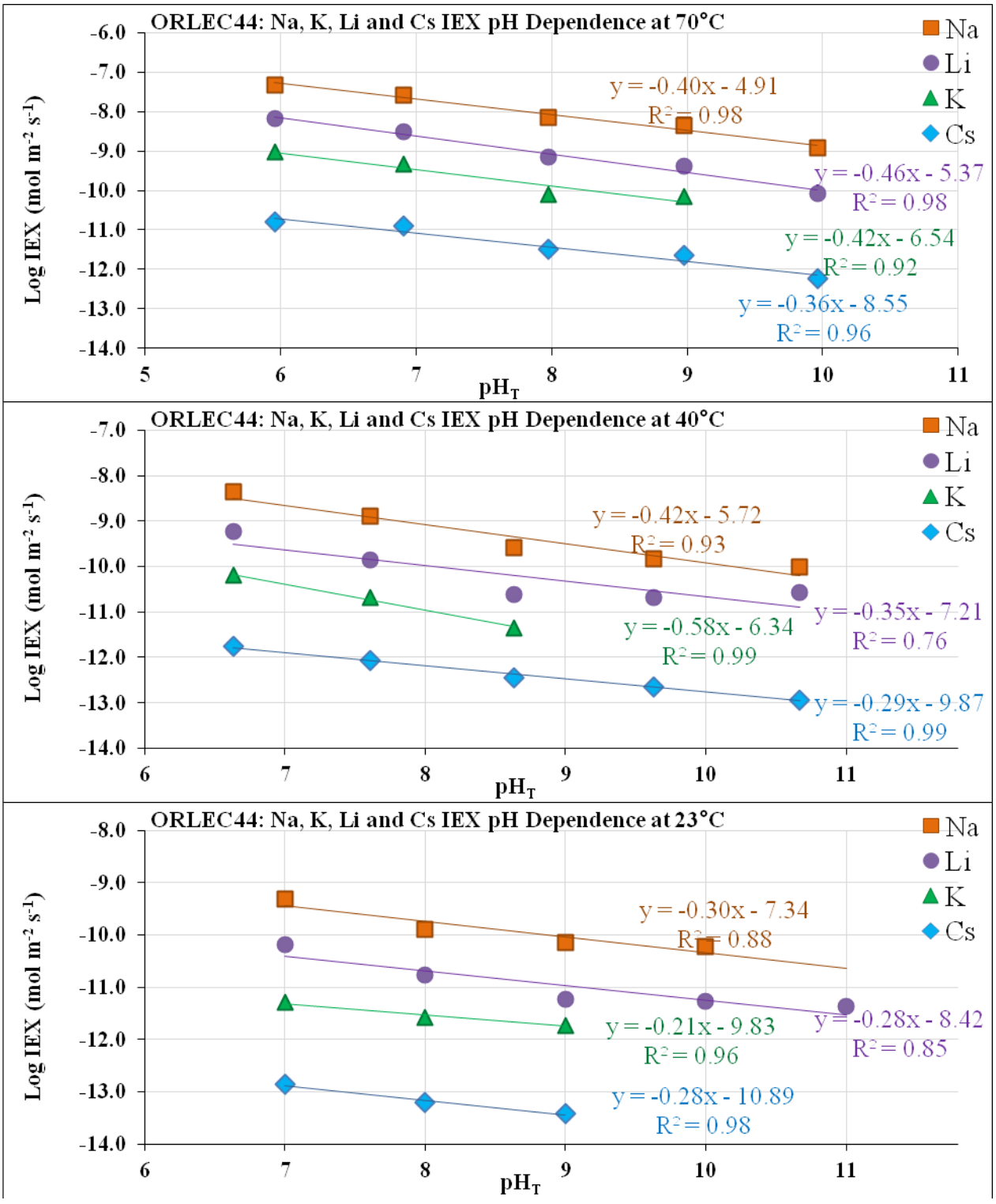

Figure 4.11. Plots of sodium, lithium, potassium and cesium ion exchange rates as a function of pH for ORLEC44.

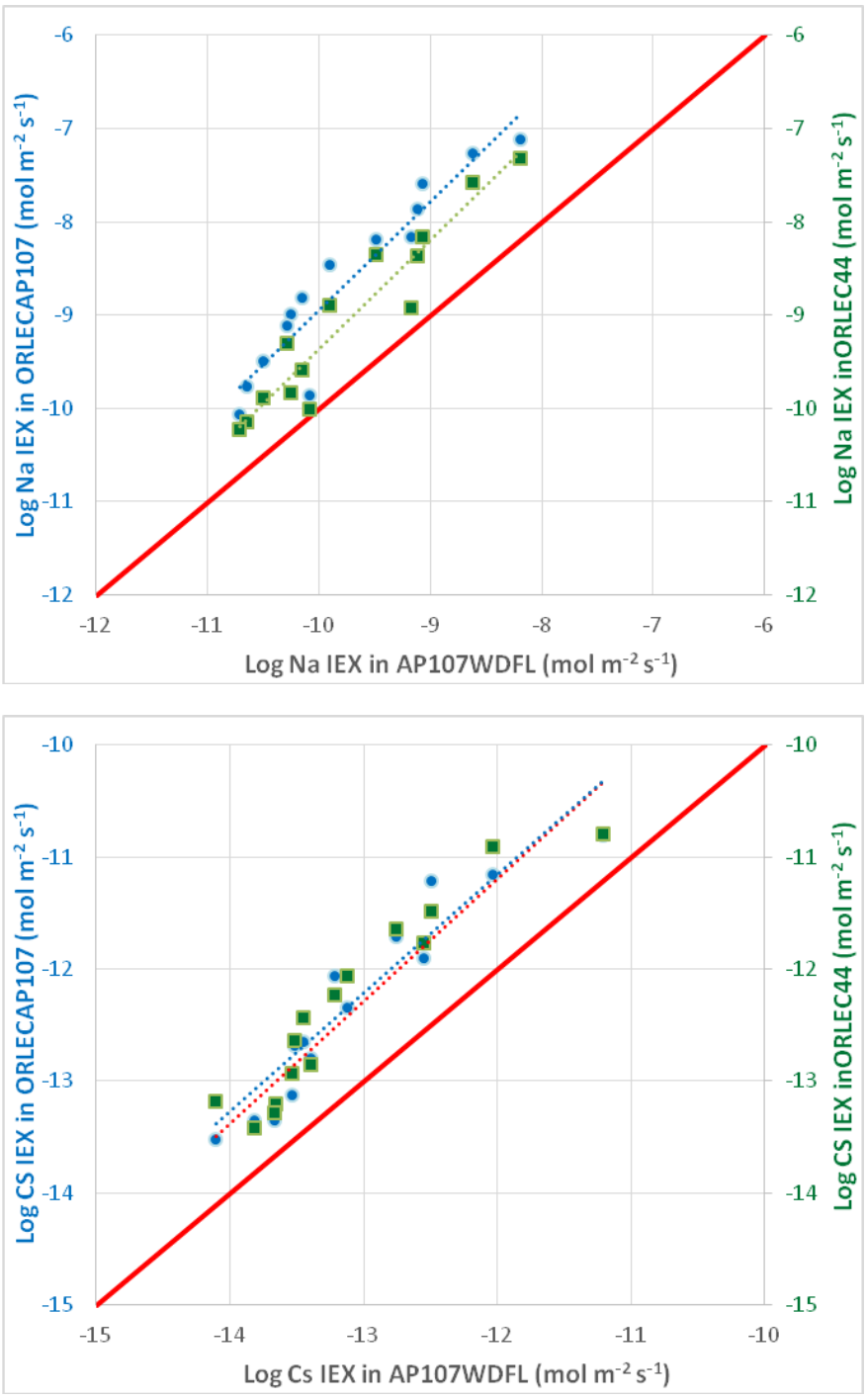

Figure 4.12. Plots of sodium ion exchange rate (top) and cesium ion exchange rate (bottom) for ORLECAP107 and ORLEC44 as a function of the respective ion exchange rate of AP107WDFL at all pH and temperature values. The red line denotes equality of the alkali ion exchange rates; the Cs data fall ~3.5 to 4 log units below that of Na.

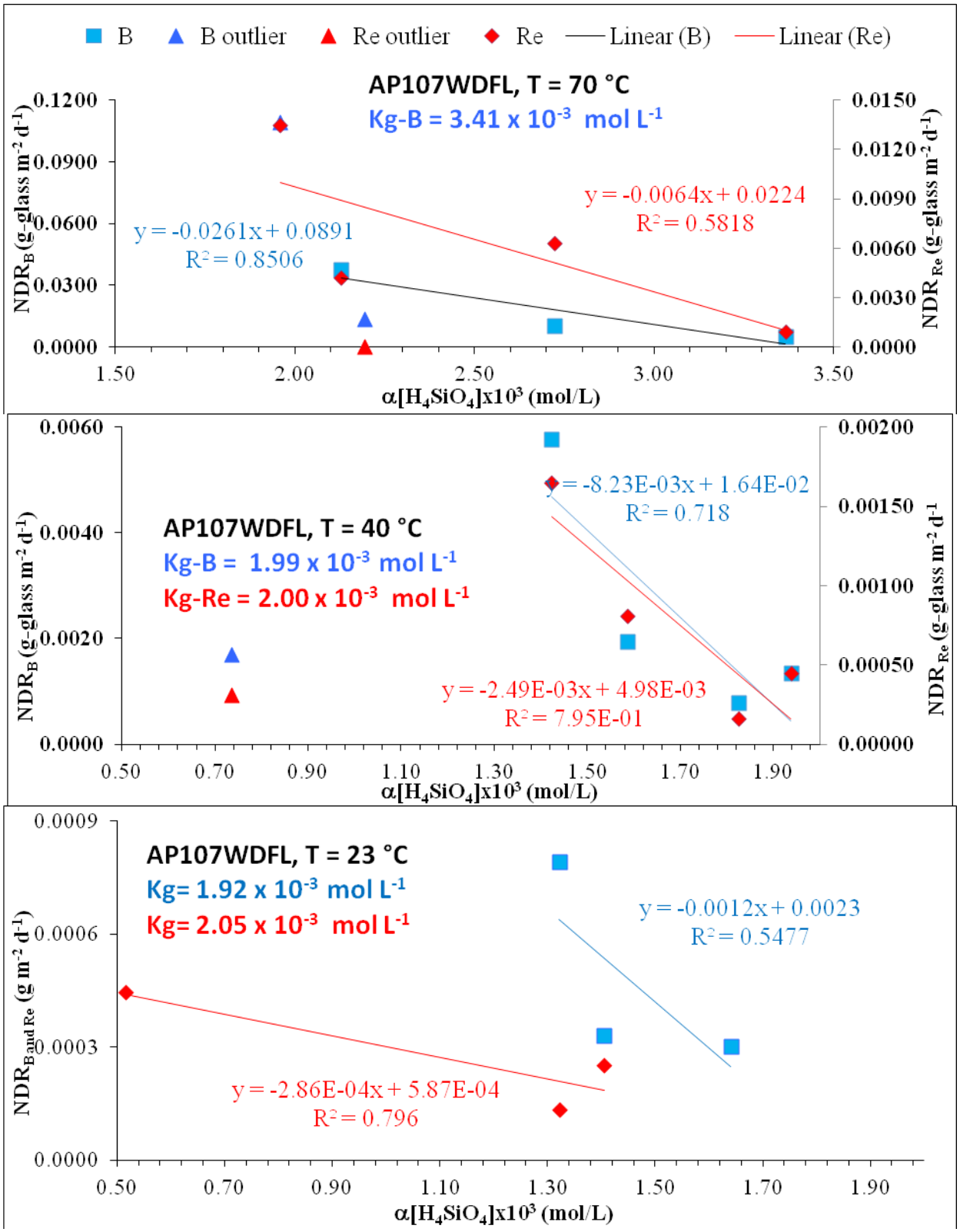

Figure 4.13. Linear regressions of boron and rhenium steady state NDR as a function of [H_4SiO_4] to assess K_g for AP107WDFL.

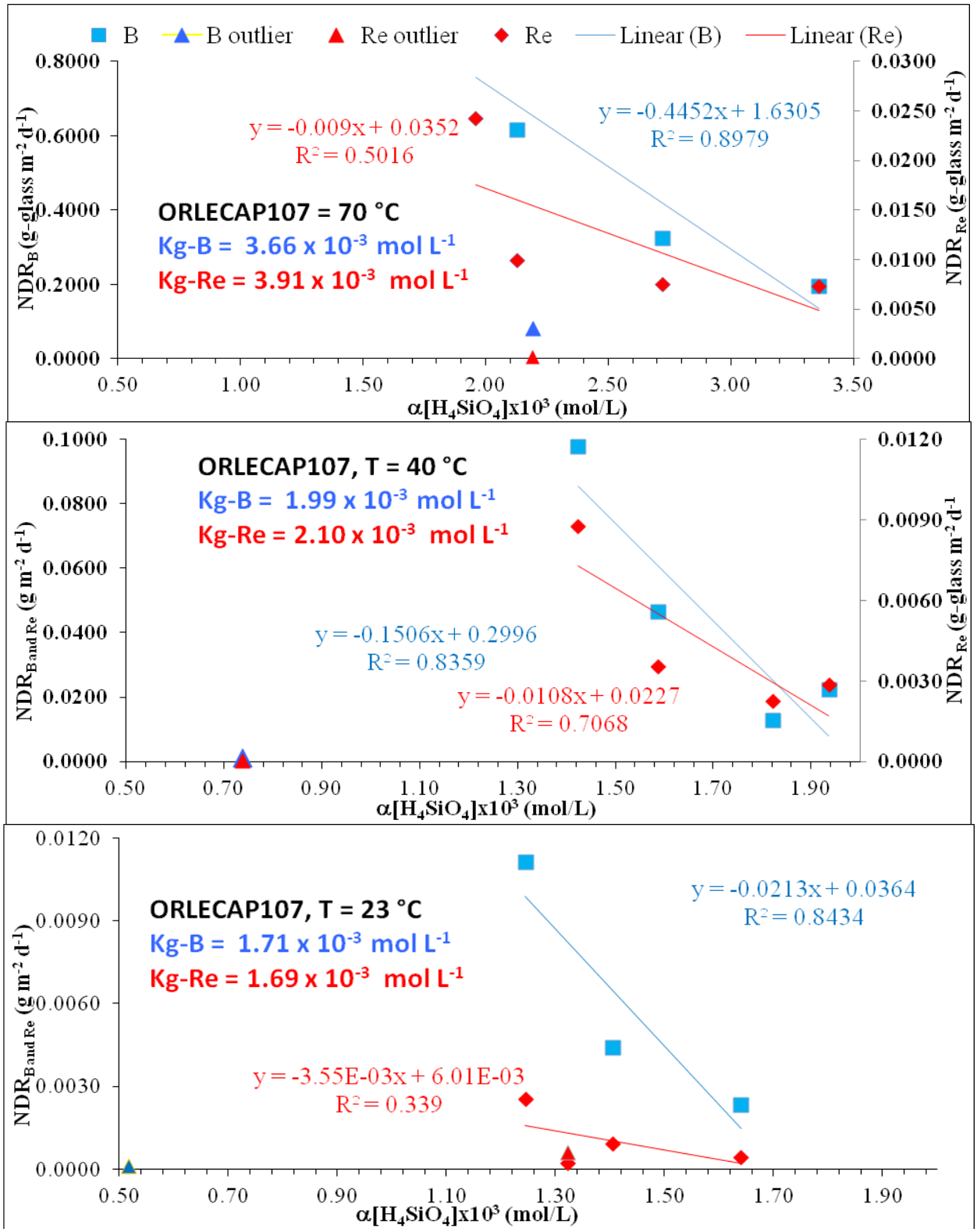

Figure 4.14. Linear regressions of boron and rhenium steady state NDR as a function of [H_4SiO_4] to assess K_g for ORLECAP107.

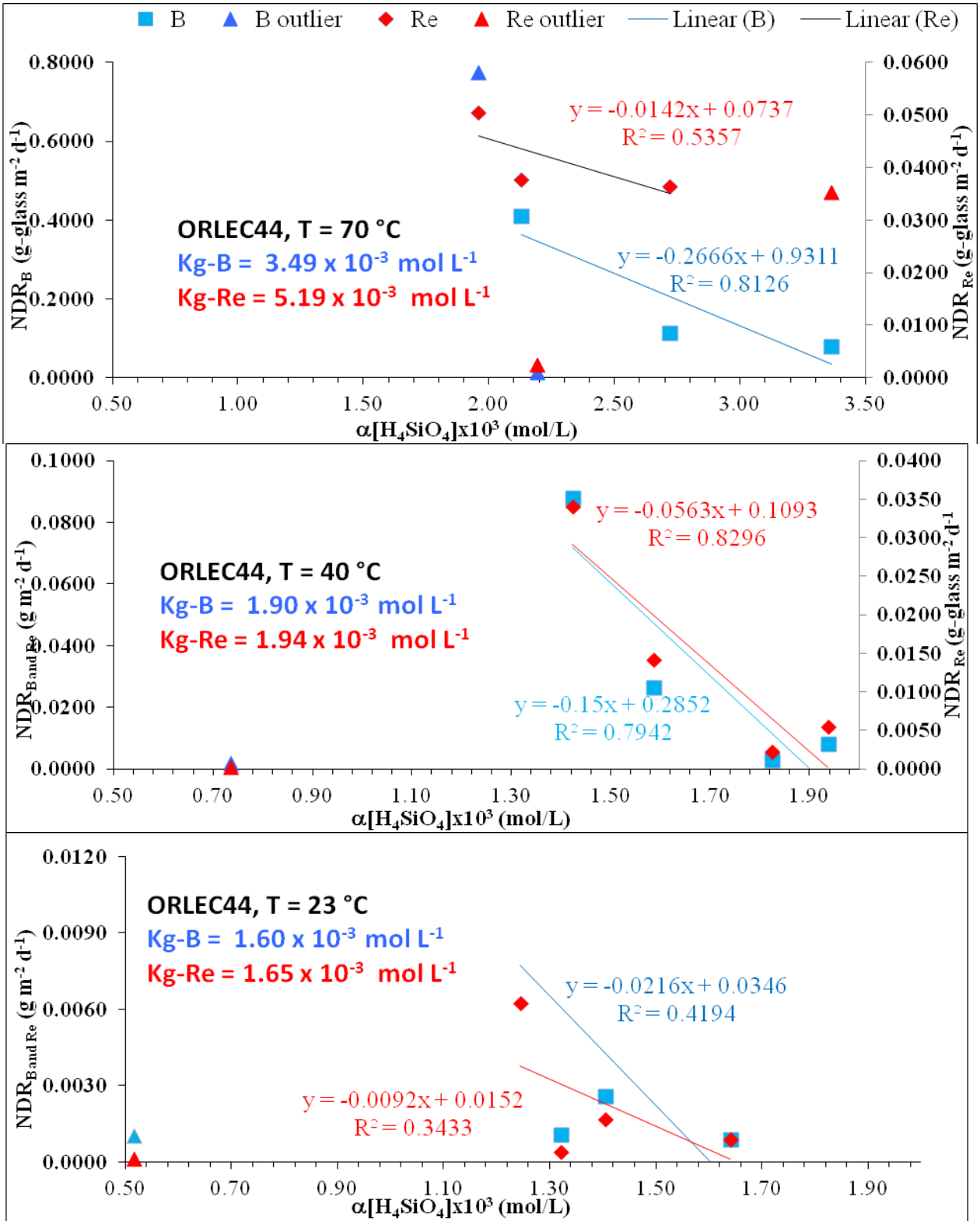

Figure 4.15. Linear regressions of boron and rhenium steady state NDR as a function of [H_4SiO_4] to assess K_g for ORLEC44.

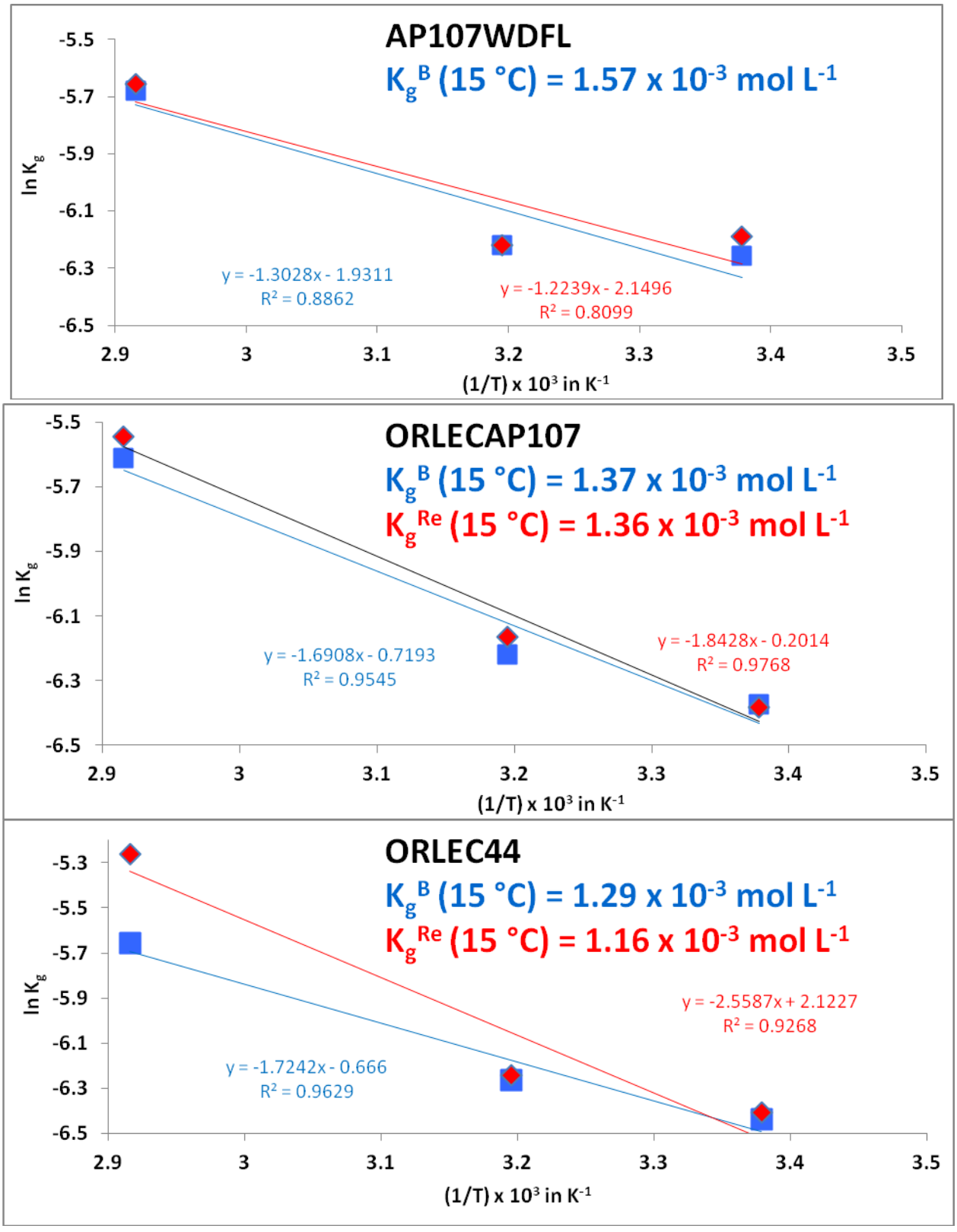

Figure 4.16. Ln K_g values for AP107WDFL, ORLECAP107, and ORLEC44 obtained from linear regression as a function of 1/T (K^{-1}) to estimate K_g at 15°C.

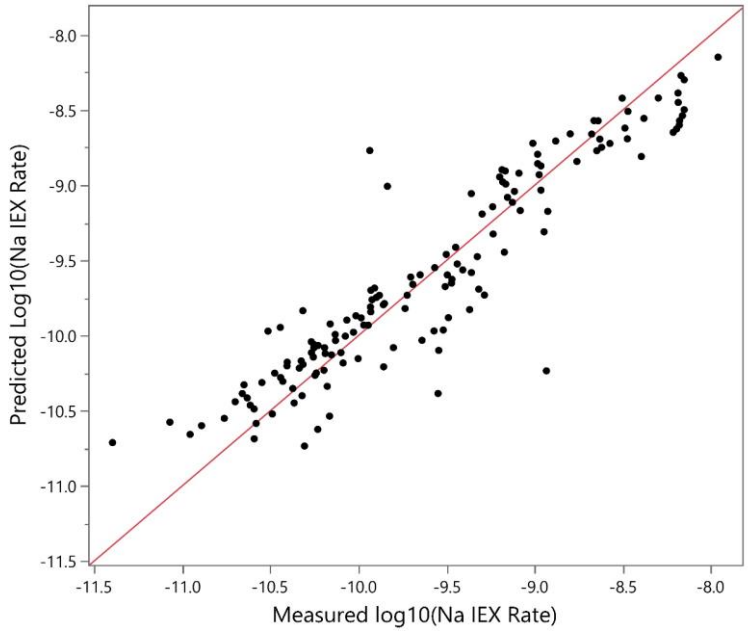

Figure 5.1. Predicted vs. measured plot for sodium ion exchange rate for AP107WDFL (Equation 1.6).

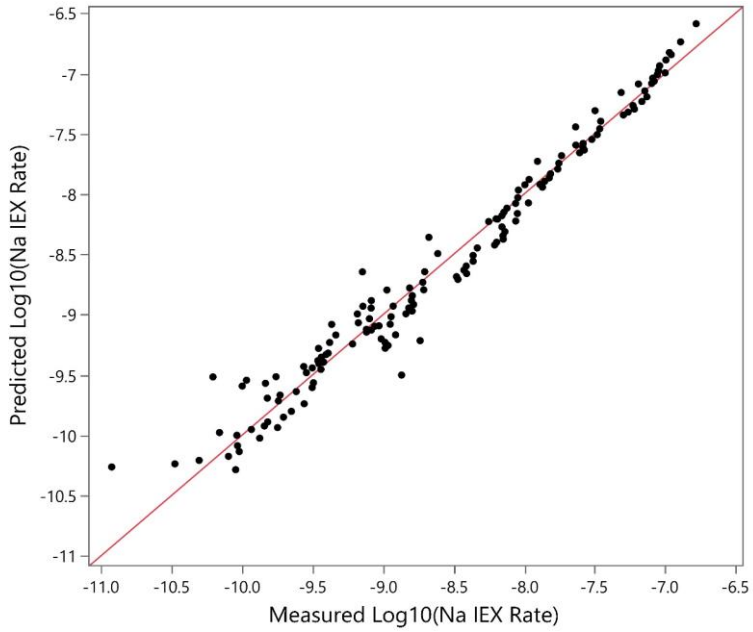

Figure 5.2. Predicted vs. measured plot for sodium ion exchange rate for ORLECAP107 (Equation 1.6).

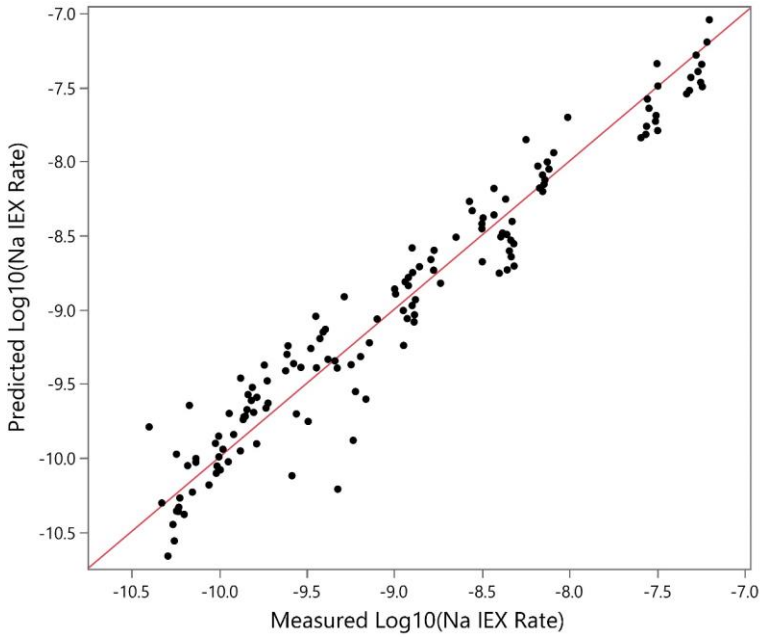

Figure 5.3. Predicted vs. measured plot for sodium ion exchange rate for ORLEC44 (Equation 1.6).

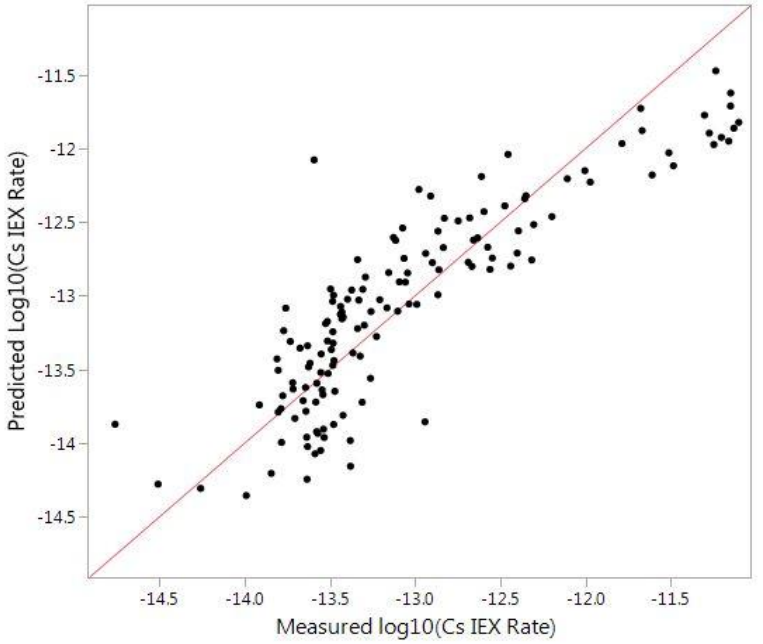

Figure 5.4. Predicted vs. measured plot for cesium ion exchange rate for AP107WDFL (Equation 1.6).

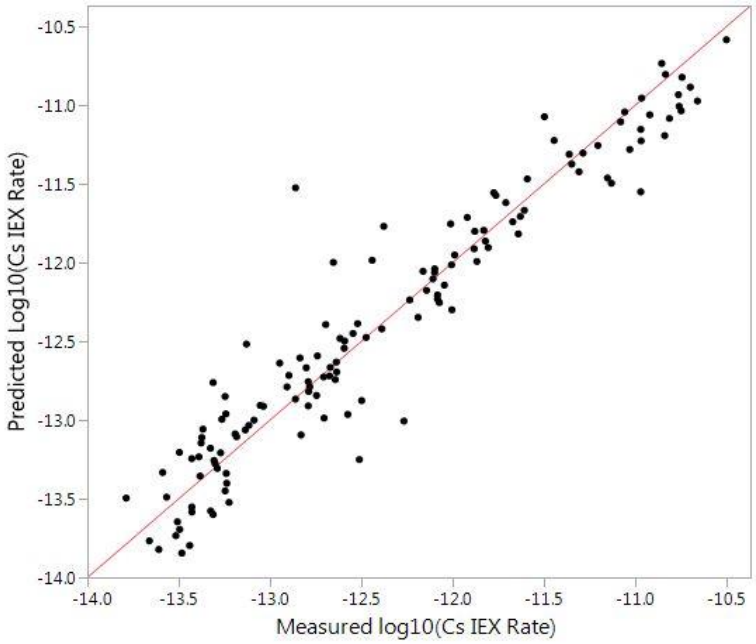

Figure 5.5. Predicted vs. measured plot for cesium ion exchange rate for ORLECAP107 (Equation 1.6).

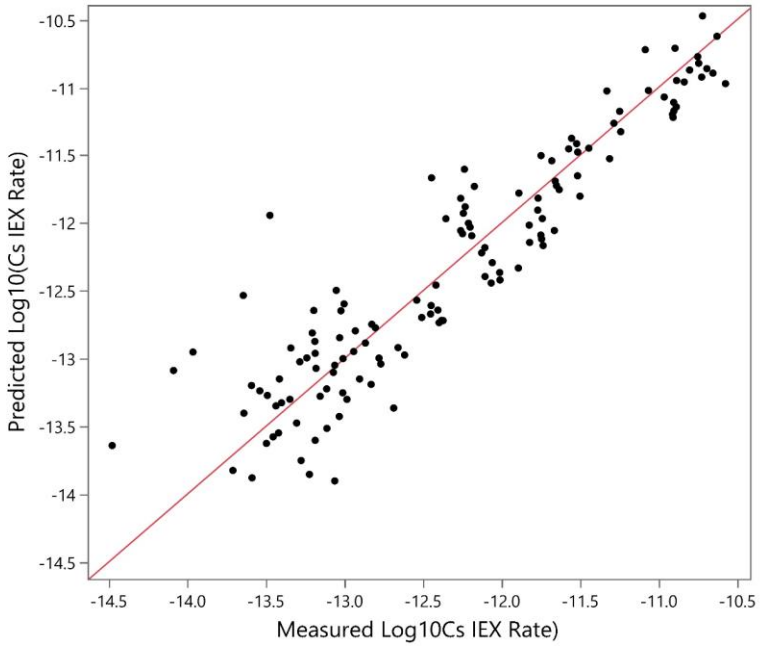

Figure 5.6. Predicted vs. measured plot for cesium ion exchange rate for ORLEC44 (Equation 1.6).

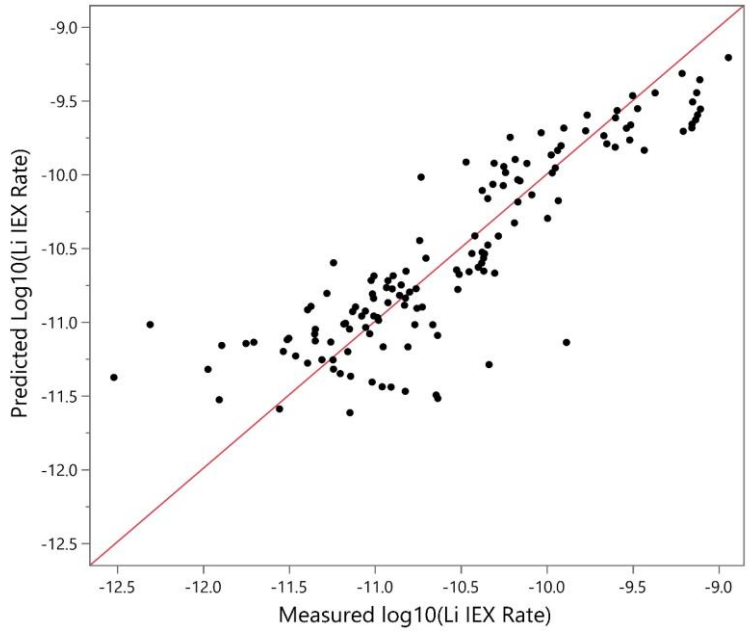

Figure 5.7. Predicted vs. measured plot for lithium ion exchange rate for AP107WDFL (Equation 1.6).

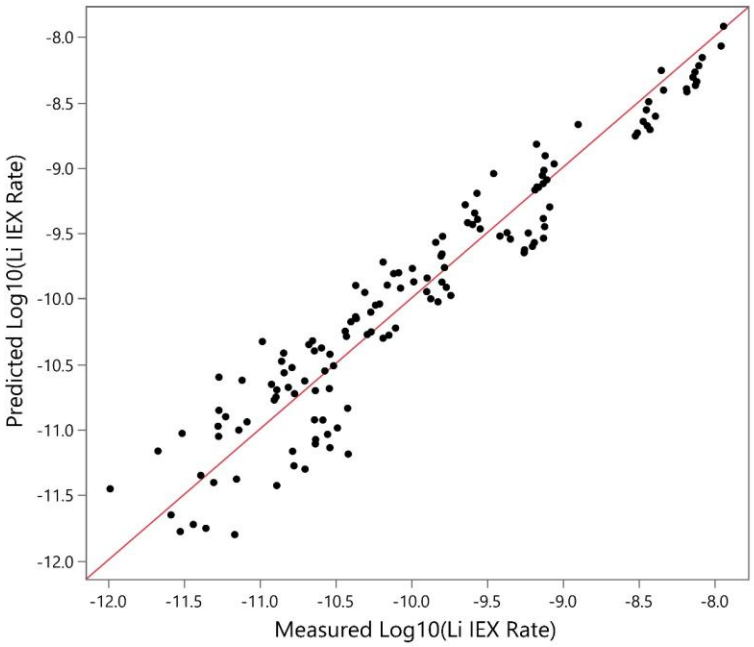

Figure 5.8. Predicted vs. measured plot for lithium ion exchange rate for ORLEC44 (Equation 1.6).

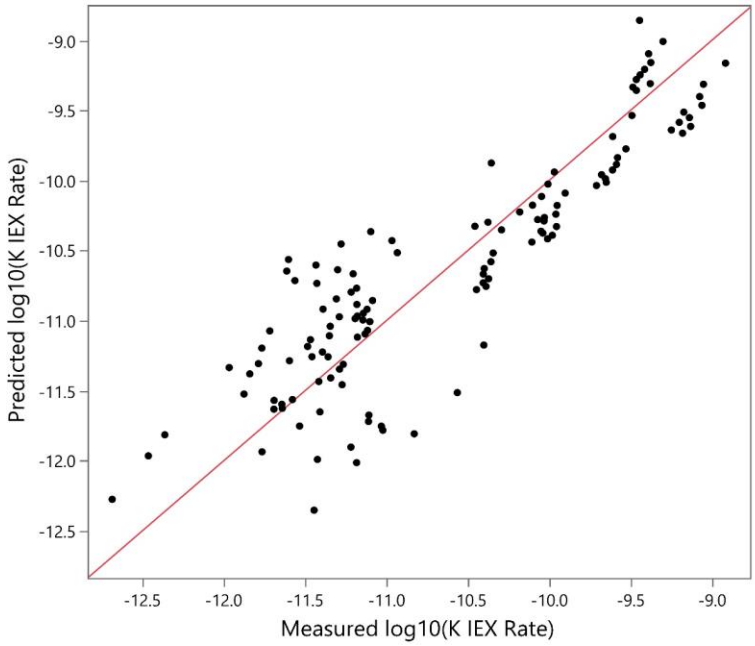

Figure 5.9. Predicted vs. measured plot for potassium ion exchange rate for ORLECAP107 (Equation 1.6).

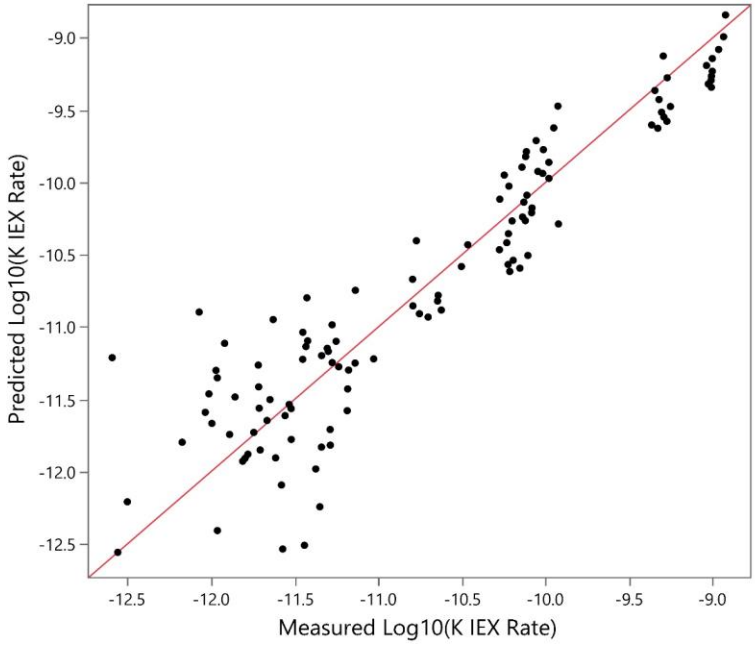

Figure 5.10. Predicted vs. measured plot for potassium ion exchange rate for ORLEC44 (Equation 1.6).

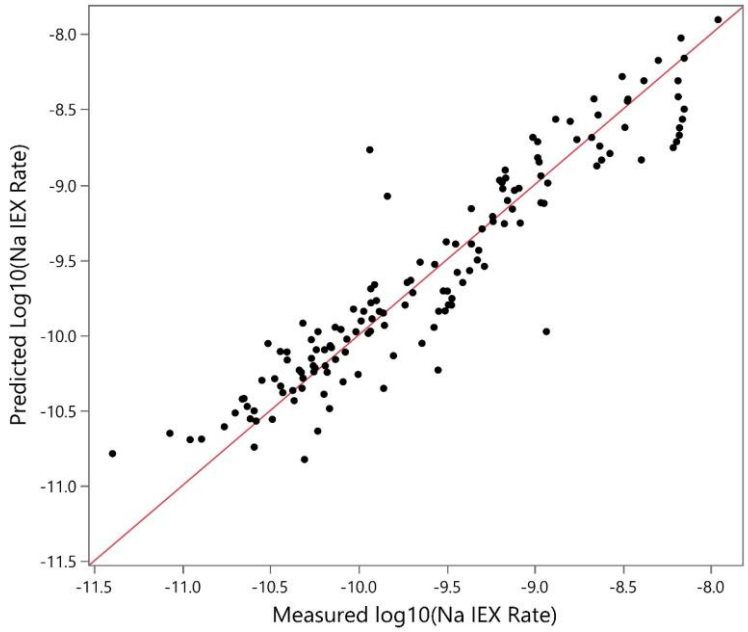

Figure 5.11. Predicted vs. measured plot for sodium ion exchange rate for AP107WDFL (Equation 1.8).

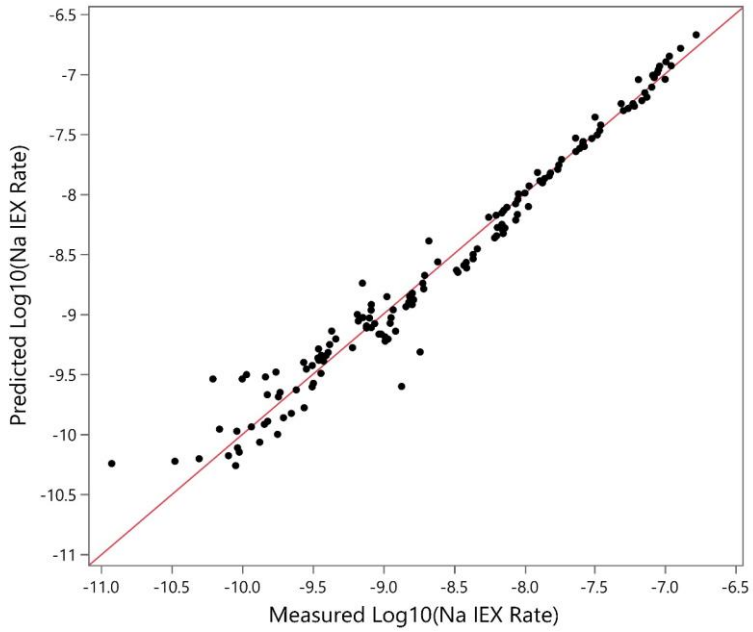

Figure 5.12. Predicted vs. measured plot for sodium ion exchange rate for ORLECAP107 (Equation 1.8).

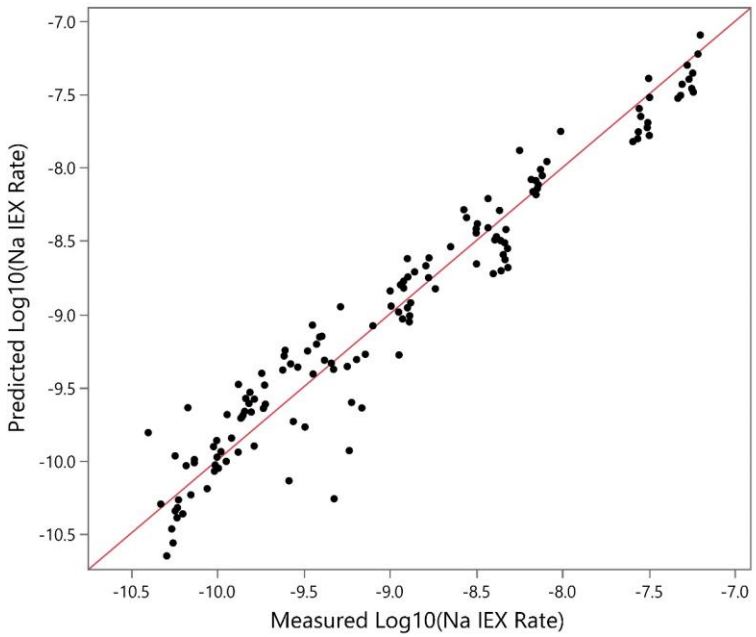

Figure 5.13. Predicted vs. measured plot for sodium ion exchange rate for ORLEC44 (Equation 1.8).

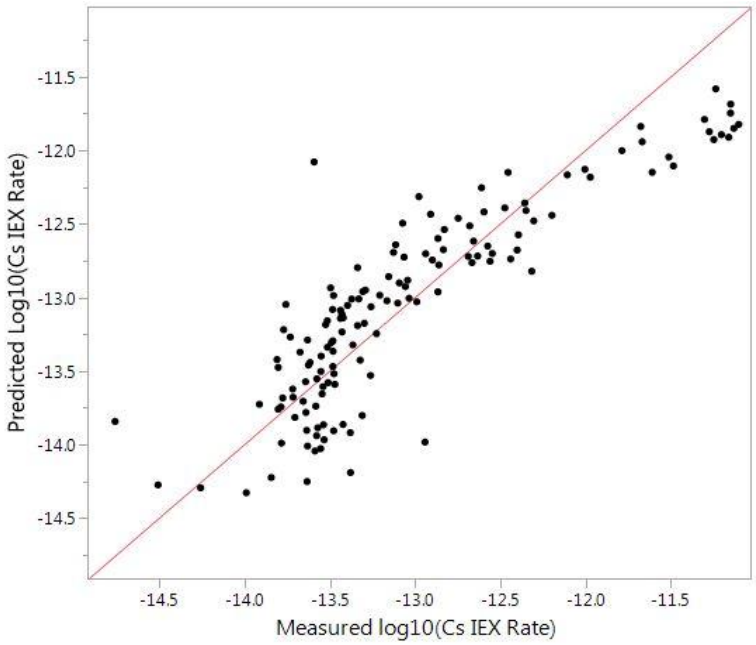

Figure 5.14. Predicted vs. measured plot for cesium ion exchange rate for AP107WDFL (Equation 1.8).

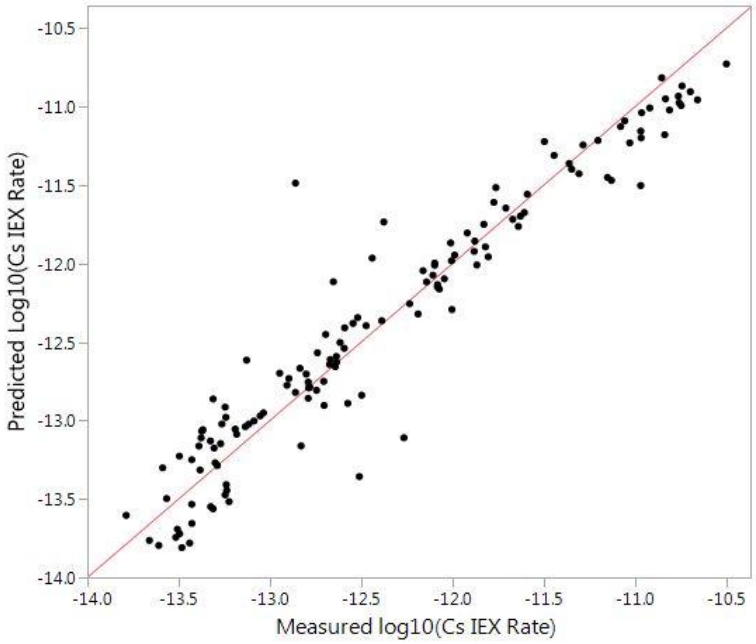

Figure 5.15. Predicted vs. measured plot for cesium ion exchange rate for ORLECAP107 (Equation 1.8).

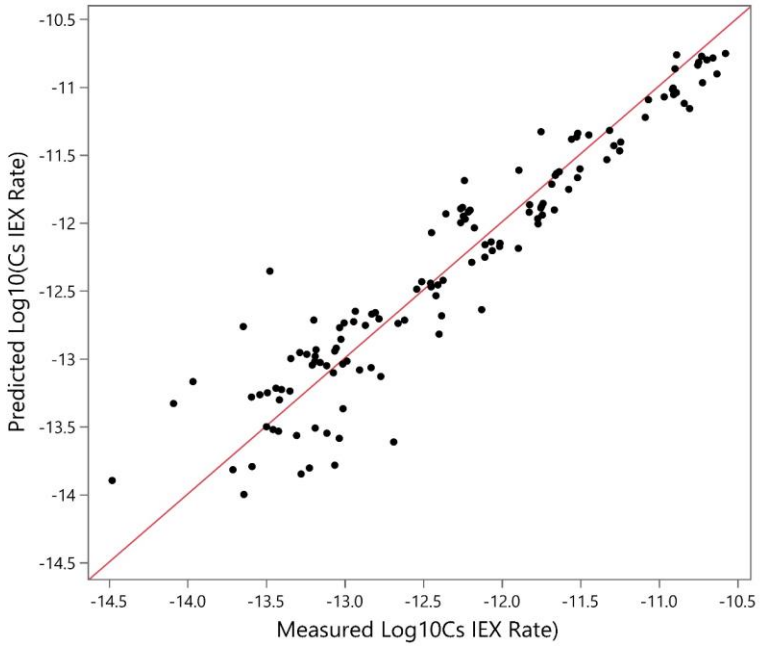

Figure 5.16. Predicted vs. measured plot for cesium ion exchange rate for ORLEC44 (Equation 1.8).

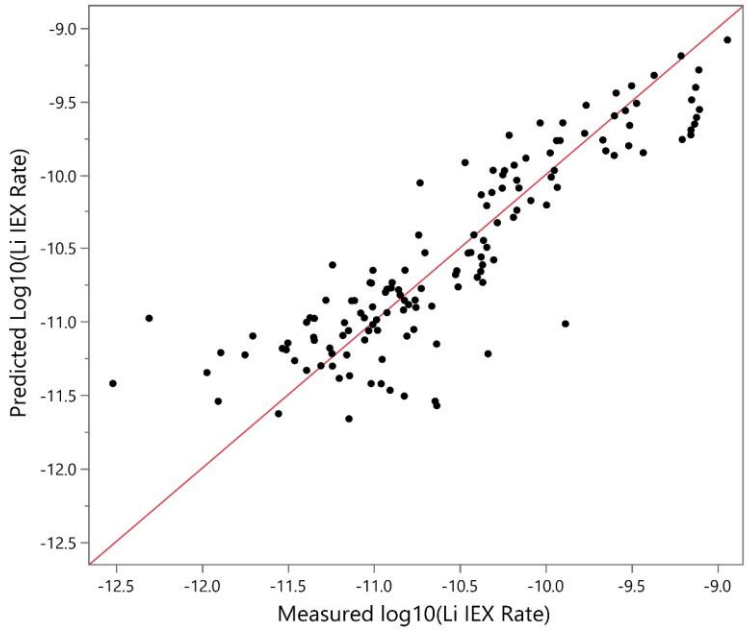

Figure 5.17. Predicted vs. measured plot for lithium ion exchange rate for AP107WDFL (Equation 1.8).

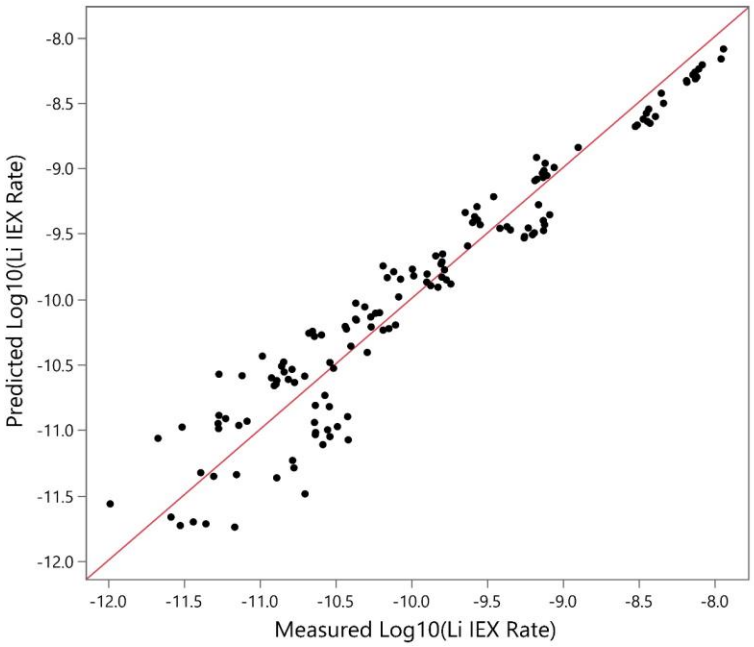

Figure 5.18. Predicted vs. measured plot for lithium ion exchange rate for ORLEC44 (Equation 1.8).

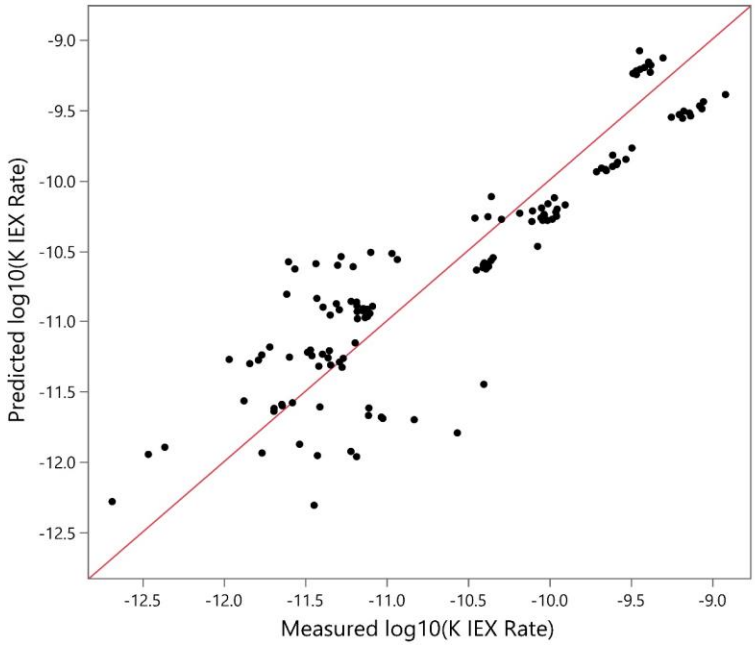

Figure 5.19. Predicted vs. measured plot for potassium ion exchange rate for ORLECAP107 (Equation 1.8).

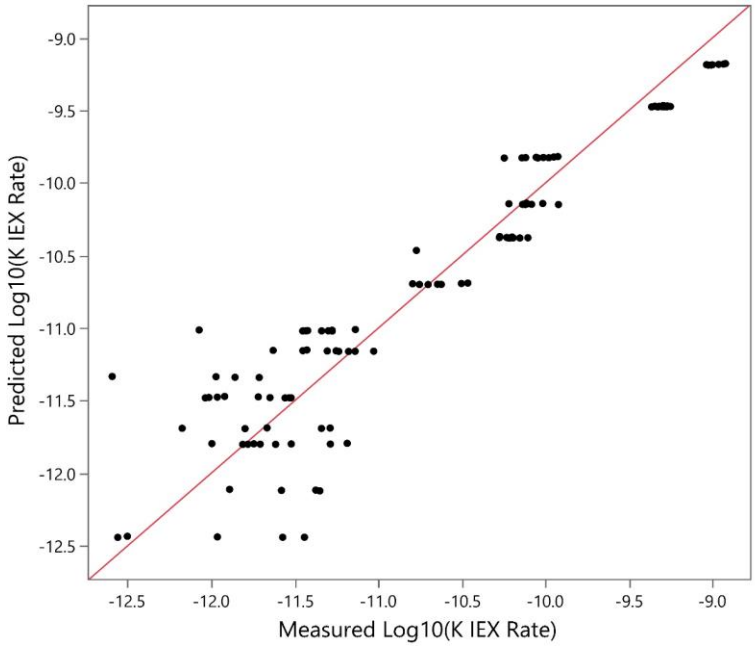

Figure 5.20. Predicted vs. measured plot for potassium ion exchange rate for ORLEC44 (Equation 1.8).

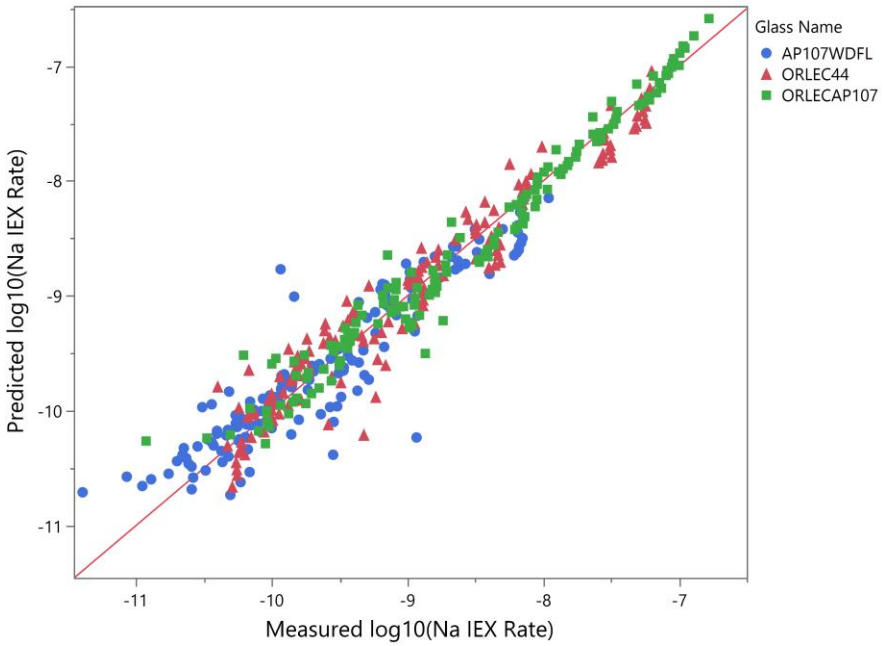

Figure 5.21. Predicted vs. measured plot for sodium ion exchange rate for all three glasses using models given by Equation 1.6.

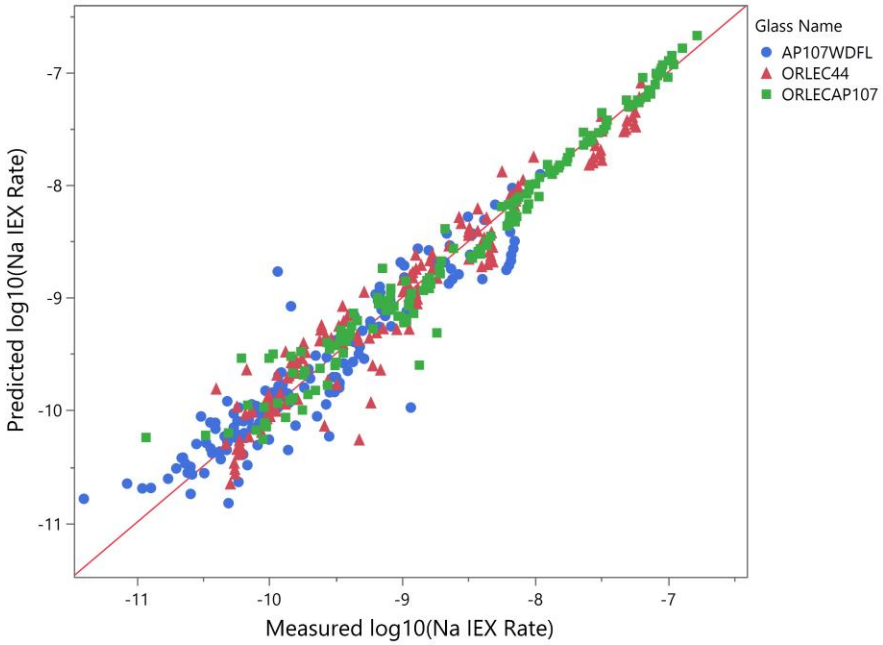

Figure 5.22. Predicted vs. measured plot for sodium ion exchange rate for all three glasses using models given by Equation 1.8.

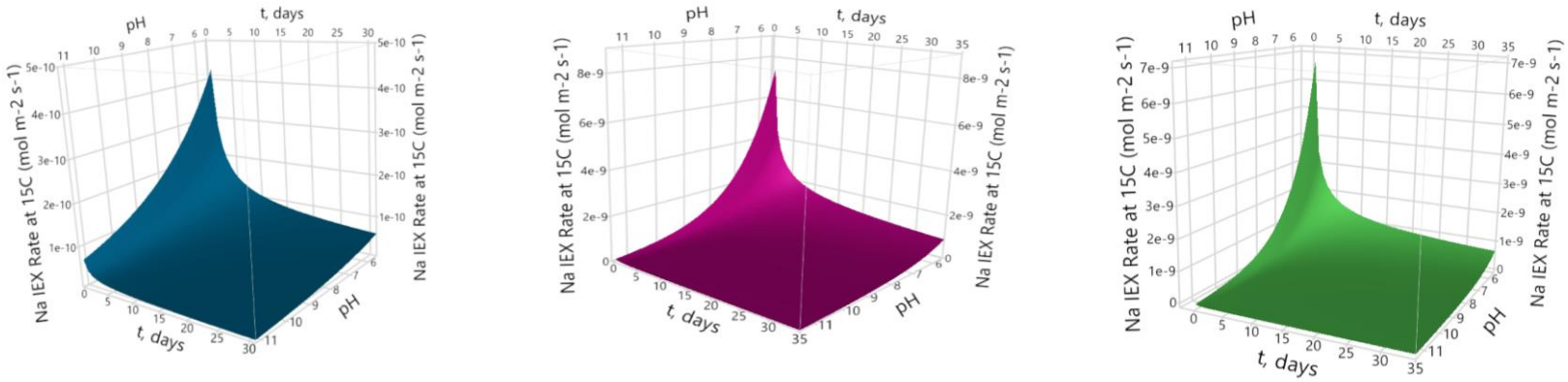

AP107WDFL **ORLECAP107** **ORLEC44**

Figure 5.23. Predicted sodium ion exchange rate at 15°C as a function of pH and time for the three glasses (using Equation 1.6).

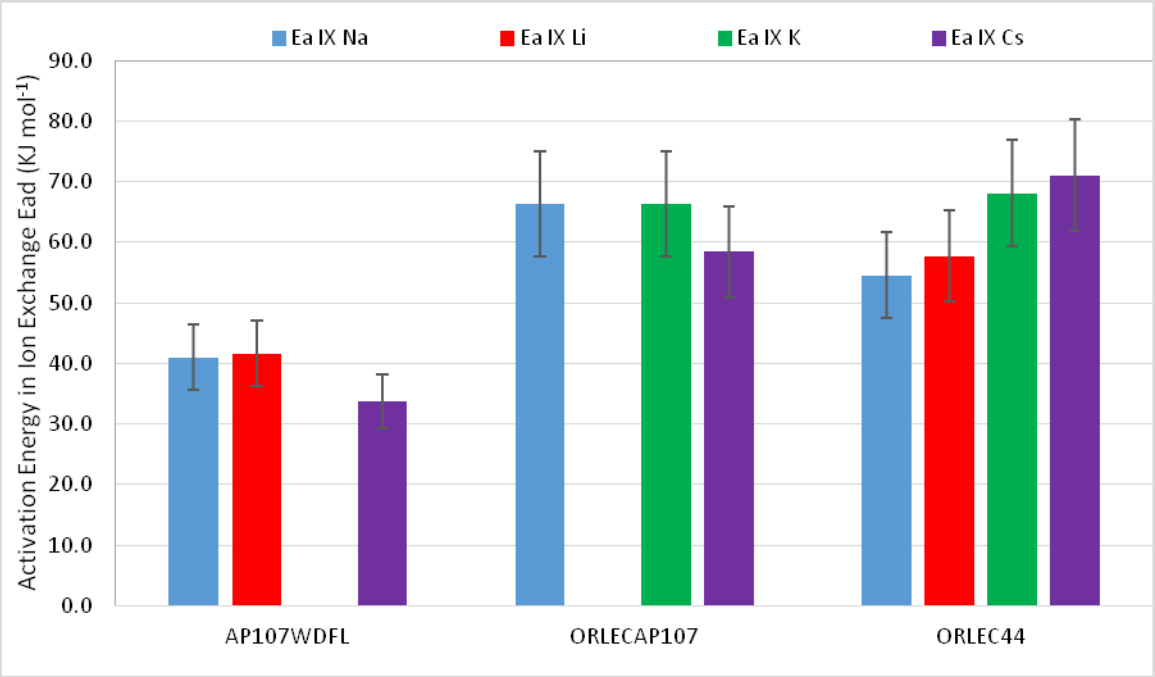

Figure 5.24. Plots of ion exchange activation energy E_{ad} for the various alkalis for AP107WDFL, ORLECAP107, and ORLEC44

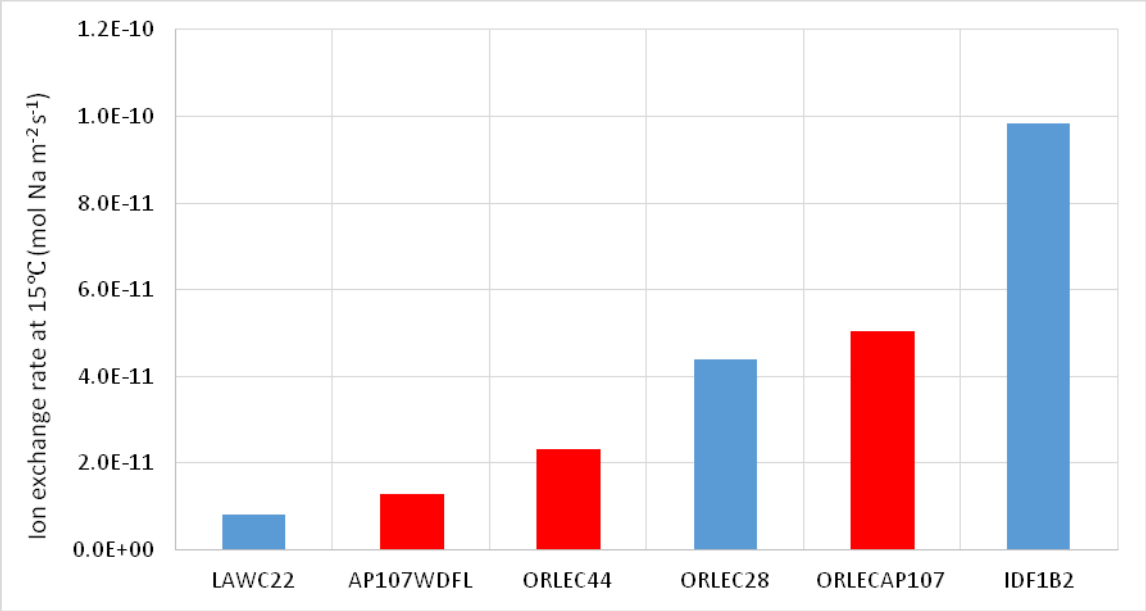

Figure 5.25a. Plot of sodium ion exchange rates at 15 °C for six glasses tested by Pulsed-Flow tests. The sodium content in the glasses increases from left to right. Red bars are from the FY19 work [1], blue bars are from the present work.

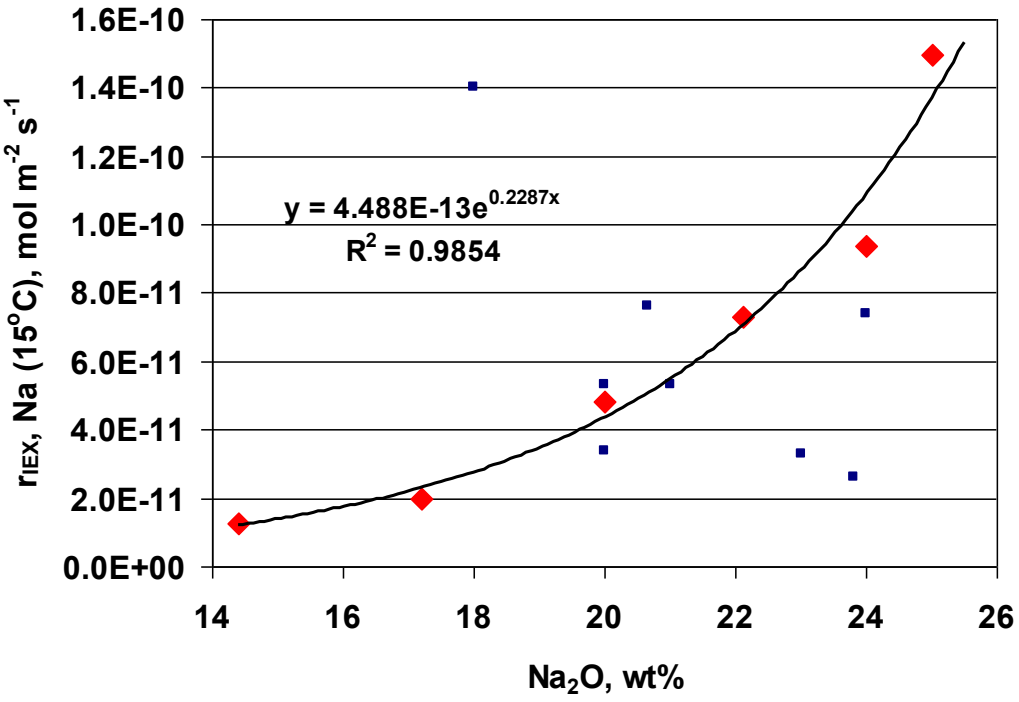

Figure 5.25b. Plot of sodium ion exchange rates at 15 °C versus Na_2O content for six glasses tested by Pulsed-Flow tests (red diamonds) and fitted regression line. Data from SPFT tests (Table 2.1) are also shown (blue squares) but these were not included in the fit.

APPENDIX A

PULSED-FLOW TEST DATA FOR LAW GLASSES AP107WDFL, ORLECAP107 and ORLEC44

Table A0. DCP-AES and ICPMS concentration analyses (ppm) for the fifteen buffers.

For test Temperature °C.	Sample ID	Inf [Si] ppm	pH 23°C	pH_T	[B][a] ppm	[Li][a] ppm	[Na] ppm	[K] ppm	[Al] ppm	[Mo] ppm	[Cs] ppm	[Re] ppm
70	BLKA1	55	7	6.0	0.0034	0.0035	0.3524	0.1015	0.0200	0.00020	0.000008	0.000005
	BLKB1	60	8	6.9	0.0034	0.0065	0.3837	0.0458	0.0383	0.00019	0.000009	0.000006
	BLKC1	80	9	8.0	0.0034	0.0081	0.4544	0.0559	0.0485	0.00019	0.000018	0.000011
	BLKD1	140	10	9.0	0.0034	0.0086	0.2948	0.0380	0.0517	0.00017	0.000007	0.000005
	BLKE1	360	11	10	0.0034	0.0035	1.0743	0.0623	0.0753	0.00007	0.000023	0.000016
40	Blank A2	40	8	6.6	0.0034	0.0035	0.1108	0.0275	0.0176	0.00094	0.000013	0.000005
	Blank B2	45	8	7.6	0.0034	0.0035	0.1120	0.0180	0.0191	0.00048	0.000017	0.000005
	Blank C2	60	8	8.6	0.0034	0.0035	0.1235	0.0364	0.0228	0.00038	0.000020	0.000016
	Blank D2	105	8	9.6	0.0034	0.0035	0.2566	0.0381	0.0487	0.00042	0.000015	0.000013
	Blank E2	270	8	10.7	0.0034	0.0035	0.7213	0.0331	0.0518	0.00037	0.000062	0.000026
23	BLKA3	35	9	7.0	0.0034	0.0035	0.1406	0.0434	0.0154	0.00084	0.000049	0.000042
	BLKB3	40	9	8.0	0.0034	0.0035	0.1355	0.0376	0.0190	0.00042	0.000010	0.000020
	BLKC3	52.5	9	9.0	0.0034	0.0035	0.1235	0.0200	0.0208	0.00020	0.000014	0.000004
	BLKD3	90	9	10.0	0.0034	0.0035	0.1944	0.0255	0.0449	0.00048	0.000005	0.000001
	BLKE3	230	9	11.0	0.0034	0.0035	0.9431	0.0586	0.0798	0.00019	0.000005	0.000003

[a] Detection limits for [B] = 0.0034 ppm and [Li] = 0.0035 used when none detectable in the blanks.

Table A1. DCP-AES Analysis Results from Dissolution of Glass AP107WDFL at 70 °C: leachate concentration (ppm) and NDR_i (g m^{-2} d^{-1}).

Exp.	Sample ID	Inf [Si] ppm	T °C	Flow Rate, m^3/d	Time, days	pH 23°C	Glass Mass g	SA m^2	[B] ppm	B Rate g_{glass} m^{-2} d^{-1}	[Li] ppm	Li Rate g_{glass} m^{-2} d^{-1}	[Na] ppm	Na Rate g_{glass} m^{-2} d^{-1}	[K] ppm	K Rate g_{glass} m^{-2} d^{-1}	[Al] ppm	Al Rate g_{glass} m^{-2} d^{-1}
1	A107IX70-1D1	55	70	2.50E-05	1	7	0.77	0.01523	2.134	0.2253	0.3252	0.2543	10.4640	0.2602	0.3966	0.3073	0.0580	0.0039
	A107IX70-1D2	55	70	2.50E-05	2	7	0.77	0.01520	2.371	0.1379	0.3424	0.1409	10.7620	0.1380	0.4100	0.1678	0.0419	0.0003
	A107IX70-1D3	55	70	2.50E-05	3	7	0.77	0.01518	2.352	0.1235	0.3343	0.1280	10.2510	0.1212	0.4159	0.1674	0.0459	0.0015
	A107IX70-1D4	55	70	2.50E-05	4	7	0.77	0.01515	2.380	0.1278	0.3385	0.1347	10.4770	0.1338	0.4285	0.1777	0.2095	0.0180
	A107IX70-1D5	55	70	2.50E-05	5	7	0.77	0.01513	2.287	0.1165	0.3163	0.1156	9.7261	0.1117	0.4186	0.1610	0.0498	-0.0066
	A107IX70-1D6	55	70	2.50E-05	6	7	0.77	0.01510	2.179	0.1102	0.3124	0.1215	9.6401	0.1193	0.4134	0.1610	0.0490	0.0015
	A107IX70-1D7	55	70	2.50E-05	7	7	0.77	0.01508	2.150	**0.1131**	0.3014	**0.1145**	9.2778	**0.1112**	0.4007	**0.1507**	0.0503	0.0016
	A107IX70-1D8	55	70	2.50E-05	8	7	0.77	0.01506	2.115	**0.1110**	0.2894	**0.1095**	9.0760	**0.1109**	0.4255	**0.1836**	0.0528	**0.0018**
	A107IX70-1D9	55	70	2.50E-05	9	7	0.77	0.01504	2.086	**0.1099**	0.2846	**0.1105**	8.8832	**0.1086**	0.4348	**0.1806**	0.0524	**0.0017**
	A107IX70-1D10	55	70	2.50E-05	10	7	0.77	0.01501	2.010	**0.1036**	0.2650	0.0970	8.5178	**0.1018**	0.4142	**0.1543**	0.0481	**0.0012**
2	A107IX70-2D1	60	70	2.50E-05	1	8	0.77	0.01523	0.947	0.0998	0.1876	0.1431	6.5845	0.1595	0.1579	0.1167	0.1205	0.0084
	A107IX70-2D2	60	70	2.50E-05	2	8	0.77	0.01522	0.965	0.0518	0.1699	0.0588	5.8813	0.0617	0.1779	0.0792	0.0958	0.0017
	A107IX70-2D3	60	70	2.50E-05	3	8	0.77	0.01521	0.972	0.0516	0.1534	0.0528	5.3242	0.0564	0.1758	0.0667	0.1002	0.0034
	A107IX70-2D4	60	70	2.50E-05	4	8	0.77	0.01520	0.900	0.0437	0.1425	0.0507	4.7854	0.0498	0.1908	0.0834	0.0970	0.0028
	A107IX70-2D5	60	70	2.50E-05	5	8	0.77	0.01519	0.870	0.0443	0.1245	0.0408	4.3950	0.0467	0.1998	0.0851	0.0948	0.0028
	A107IX70-2D6	60	70	2.50E-05	6	8	0.77	0.01518	0.825	0.0411	0.1080	0.0349	4.0612	0.0431	0.1580	0.0368	0.0940	0.0028
	A107IX70-2D7	60	70	2.50E-05	7	8	0.77	0.01518	0.801	0.0410	0.0989	0.0342	3.7516	0.0395	0.1582	**0.0588**	0.0864	0.0021
	A107IX70-2D8	60	70	2.50E-05	8	8	0.77	0.01517	0.791	**0.0412**	0.1132	**0.0492**	3.8734	**0.0466**	0.1889	0.0909	0.0921	**0.0030**
	A107IX70-2D9	60	70	2.50E-05	9	8	0.77	0.01516	0.750	**0.0375**	0.1009	**0.0338**	3.6228	**0.0386**	0.1752	**0.0605**	0.0834	**0.0019**
	A107IX70-2D10	60	70	2.50E-05	10	8	0.77	0.01515	0.700	**0.0344**	0.1010	**0.0388**	3.4510	**0.0374**	0.1923	0.0856	0.0808	**0.0020**
3	A107IX70-3D1	80	70	2.50E-05	1	9	0.77	0.01524	0.481	0.0505	0.1158	0.0851	4.3939	0.1013	0.0857	0.0310	0.0972	0.0049
	A107IX70-3D2	80	70	2.50E-05	2	9	0.77	0.01523	0.407	0.0174	0.0929	0.0262	3.7872	0.0351	0.0696	-0.0013	0.1055	0.0033
	A107IX70-3D3	80	70	2.50E-05	3	9	0.77	0.01523	0.332	0.0134	0.0700	0.0172	3.0411	0.0237	0.0710	0.0086	0.0934	0.0017
	A107IX70-3D4	80	70	2.50E-05	4	9	0.77	0.01522	0.333	0.0175	0.0614	0.0195	2.7504	0.0258	0.0712	0.0081	0.1320	0.0062
	A107IX70-3D5	80	70	2.50E-05	5	9	0.77	0.01522	0.288	0.0126	0.0501	0.0139	2.2854	0.0176	0.0661	0.0026	0.0895	-0.0001
	A107IX70-3D6	80	70	2.50E-05	6	9	0.77	0.01522	0.599	0.0480	0.0831	0.0445	3.4519	0.0536	0.0999	0.0405	0.4577	0.0396
	A107IX70-3D7	80	70	2.50E-05	7	9	0.77	0.01521	0.262	-0.0041	0.0399	-0.0027	1.8851	-0.0018	0.0629	-0.0157	0.0852	-0.0171
	A107IX70-3D8	80	70	2.50E-05	8	9	0.77	0.01521	0.237	**0.0110**	0.0338	**0.0096**	1.8272	**0.0169**	0.0657	**0.0066**	0.0802	**0.0014**
	A107IX70-3D9	80	70	2.50E-05	9	9	0.77	0.01521	0.216	**0.0101**	0.0331	**0.0114**	1.6992	**0.0144**	0.0721	**0.0118**	0.0758	**0.0012**
	A107IX70-3D10	80	70	2.50E-05	10	9	0.77	0.01520	0.204	**0.0100**	0.0293	**0.0087**	1.5870	**0.0131**	0.0659	**0.0020**	0.0763	**0.0014**
4	A107IX70-4D1	140	70	2.50E-05	1	10	0.50	0.00979	0.247	0.0400	0.0515	0.0527	2.3023	0.0803	0.0376	-0.0006	0.1253	0.0116
	A107IX70-4D2	140	70	2.50E-05	2	10	0.50	0.00979	0.174	0.0081	0.0427	0.0187	1.9414	0.0257	0.0369	-0.0015	0.1085	0.0032
	A107IX70-4D3	140	70	2.50E-05	3	10	0.50	0.00979	0.140	0.0083	0.0374	0.0176	1.5209	0.0161	0.0384	0.0016	0.0995	0.0031
	A107IX70-4D4	140	70	2.50E-05	4	10	0.50	0.00979	0.122	0.0084	0.0337	0.0163	1.3357	0.0171	0.0327	-0.0088	0.0979	0.0035
	A107IX70-4D5	140	70	2.50E-05	5	10	0.50	0.00979	0.099	**0.0059**	0.0260	0.0090	1.1812	0.0146	0.1164	0.1314	0.0915	0.0026
	A107IX70-4D6	140	70	2.50E-05	6	10	0.50	0.00979	0.089	**0.0063**	0.0301	0.0189	1.0492	0.0125	0.1188	0.0674	0.0891	0.0028
	A107IX70-4D7	140	70	2.50E-05	7	10	0.50	0.00979	0.066	**0.0032**	0.0306	0.0169	0.9598	**0.0115**	0.1155	**0.0601**	0.0819	**0.0018**
	A107IX70-4D8	140	70	2.50E-05	8	10	0.50	0.00979	0.096	0.0101	0.0288	**0.0144**	0.9754	**0.0139**	0.1233	**0.0754**	0.1228	0.0089
	A107IX70-4D9	140	70	2.50E-05	9	10	0.50	0.00978	0.097	0.0077	0.0217	**0.0069**	0.9761	**0.0137**	0.1170	**0.0590**	0.1034	**0.0026**
	A107IX70-4D10	140	70	2.50E-05	10	10	0.50	0.00978	0.062	0.0020	0.0184	**0.0071**	0.8064	**0.0068**	0.1168	**0.0637**	0.0772	0.0000
5	A107IX70-5D1	360	70	2.50E-05	1	11	0.50	0.00979	0.283	0.0459	0.0484	0.0552	2.706	0.0653	0.0444	-0.0096	0.1080	0.0052
	A107IX70-5D2	360	70	2.50E-05	2	11	0.50	0.00979	0.255	0.0183	0.0362	0.0125	2.457	0.0227	0.0469	-0.0035	0.1073	0.0025
	A107IX70-5D3	360	70	2.50E-05	3	11	0.50	0.00979	0.287	0.0260	0.0291	0.0114	2.184	0.0167	0.0441	-0.0057	0.0985	0.0011
	A107IX70-5D4	360	70	2.50E-05	4	11	0.50	0.00979	0.276	0.0216	0.0242	0.0097	1.928	0.0120	0.0539	0.0004	0.0864	-0.0001
	A107IX70-5D5	360	70	2.50E-05	5	11	0.50	0.00978	0.286	0.0241	0.0227	0.0109	1.824	0.0129	0.0343	-0.0129	0.0897	0.0014
	A107IX70-5D6	360	70	2.50E-05	6	11	0.50	0.00978	0.090	-0.0090	0.0201	0.0086	1.734	0.0114	0.0167	-0.0171	0.1873	0.0166
	A107IX70-5D7	360	70	2.50E-05	7	11	0.50	0.00978	0.159	0.0185	0.0162	0.0054	1.676	0.0109	0.0139	-0.0138	0.0831	-0.0076
	A107IX70-5D8	360	70	2.50E-05	8	11	0.50	0.00978	0.169	**0.0144**	0.0200	**0.0124**	1.612	**0.0095**	0.0443	0.0033	0.0745	-0.0007
	A107IX70-5D9	360	70	2.50E-05	9	11	0.50	0.00978	0.180	**0.0155**	0.0171	**0.0065**	1.663	**0.0128**	0.0319	-0.0116	0.0967	0.0035
	A107IX70-5D10	360	70	2.50E-05	10	11	0.50	0.00977	0.160	**0.0113**	0.0184	**0.0100**	1.566	**0.0079**	0.0374	-0.0052	0.0781	-0.0013

Table A2. DCP-AES Analysis Results from Dissolution of Glass AP107WDFL at 40 °C.

Exp.	Sample ID	Inf [Si] ppm	T °C	Flow Rate, m^3/d	Time, days	pH 23°C	Glass Mass g	SA m^2	[B] ppm	B Rate $g_{glass}\ m^{-2}\ d^{-1}$	[Li] ppm	Li Rate $g_{glass}\ m^{-2}\ d^{-1}$	[Na] ppm	Na Rate $g_{glass}\ m^{-2}\ d^{-1}$	[K] ppm	K Rate $g_{glass}\ m^{-2}\ d^{-1}$	[Al] ppm	Al Rate $g_{glass}\ m^{-2}\ d^{-1}$
1	A107IX40-1D1	40	40	8.33E-06	3	7	1.65	0.03265	1.141	0.0187	0.2260	0.0274	7.3135	0.0288	0.1692	0.0229	0.0507	0.0005
	A107IX40-1D2	40	40	8.33E-06	6	7	1.65	0.03263	1.145	0.0094	0.1961	0.0100	6.1143	0.0096	0.1838	0.0138	0.0491	0.0002
	A107IX40-1D3	40	40	8.33E-06	9	7	1.65	0.03262	1.063	0.0080	0.1712	0.0088	5.3017	0.0088	0.1436	0.0062	0.0482	0.0002
	A107IX40-1D4	40	40	8.33E-06	12	7	1.65	0.03261	0.966	0.0071	0.1468	0.0073	4.7193	0.0081	0.1733	0.0142	0.0415	0.0001
	A107IX40-1D5	40	40	8.33E-06	15	7	1.65	0.03260	0.896	0.0068	0.1343	0.0073	4.1167	0.0068	0.1505	0.0081	0.0408	0.0002
	A107IX40-1D6	40	40	8.33E-06	18	7	1.65	0.03259	0.888	0.0072	0.1310	0.0076	3.9792	0.0075	0.1464	0.0093	0.0381	0.0001
	A107IX40-1D7	40	40	8.33E-06	21	7	1.65	0.03258	0.808	**0.0060**	0.1243	**0.0070**	3.5199	**0.0059**	0.1526	**0.0106**	0.0440	0.0003
	A107IX40-1D8	40	40	8.33E-06	24	7	1.65	0.03258	0.756	**0.0058**	0.1151	**0.0063**	3.2560	**0.0058**	0.1530	**0.0102**	0.0443	**0.0002**
	A107IX40-1D9	40	40	8.33E-06	27	7	1.65	0.03257	0.734	**0.0058**	0.1188	**0.0073**	3.2604	**0.0063**	0.1597	**0.0113**	0.0440	**0.0002**
	A107IX40-1D10	40	40	8.33E-06	30	7	1.65	0.03256	0.701	**0.0055**	0.1042	0.0053	3.0890	**0.0056**	0.1792	0.0139	0.0444	**0.0002**
2	A107IX40-2D1	45	40	8.33E-06	3	8	1.65	0.03265	0.699	0.0114	0.1610	0.0194	5.6514	0.0222	0.1519	0.0217	0.1052	0.0014
	A107IX40-2D2	45	40	8.33E-06	6	8	1.65	0.03264	0.537	0.0030	0.1114	0.0036	4.3396	0.0058	0.1333	0.0078	0.1087	0.0007
	A107IX40-2D3	45	40	8.33E-06	9	8	1.65	0.03264	0.357	0.0014	0.1035	0.0057	3.3594	0.0045	0.1099	0.0055	0.0929	0.0005
	A107IX40-2D4	45	40	8.33E-06	12	8	1.65	0.03263	0.354	0.0029	0.0682	0.0018	2.7477	0.0041	0.1133	0.0080	0.0905	0.0005
	A107IX40-2D5	45	40	8.33E-06	15	8	1.65	0.03263	0.328	0.0025	0.0721	0.0045	2.2479	0.0033	0.1201	0.0088	0.0887	0.0005
	A107IX40-2D6	45	40	8.33E-06	18	8	1.65	0.03263	0.316	0.0025	0.0647	0.0033	2.0007	0.0033	0.1380	0.0112	0.0883	0.0005
	A107IX40-2D7	45	40	8.33E-06	21	8	1.65	0.03262	0.264	0.0017	0.0515	0.0021	1.6696	0.0025	0.1117	0.0055	0.0807	0.0004
	A107IX40-2D8	45	40	8.33E-06	24	8	1.65	0.03262	0.257	**0.0020**	0.0506	**0.0028**	1.5451	**0.0026**	0.1169	**0.0084**	0.0787	**0.0005**
	A107IX40-2D9	45	40	8.33E-06	27	8	1.65	0.03262	0.249	**0.0020**	0.0508	**0.0029**	1.4734	**0.0026**	0.1283	**0.0099**	0.0800	**0.0005**
	A107IX40-2D10	45	40	8.33E-06	30	8	1.65	0.03262	0.238	**0.0018**	0.0501	**0.0028**	1.3711	**0.0023**	0.1348	**0.0100**	0.0725	**0.0004**
3	A107IX40-3D1	60	40	8.33E-06	3	9	1.65	0.03265	0.506	0.0083	0.1084	0.0129	4.0580	0.0157	0.0597	0.0038	0.0890	0.0010
	A107IX40-3D2	60	40	8.33E-06	6	9	1.65	0.03265	0.418	0.0027	0.0830	0.0033	3.0735	0.0039	0.0449	-0.0005	0.0809	0.0004
	A107IX40-3D3	60	40	8.33E-06	9	9	1.65	0.03264	0.274	0.0010	0.0690	0.0032	2.3170	0.0029	0.0422	0.0002	0.0734	0.0003
	A107IX40-3D4	60	40	8.33E-06	12	9	1.65	0.03264	0.248	0.0018	0.0511	0.0018	1.8213	0.0024	0.0428	0.0006	0.0668	0.0003
	A107IX40-3D5	60	40	8.33E-06	15	9	1.65	0.03264	0.213	**0.0014**	0.0394	0.0015	1.4585	0.0019	0.0424	0.0005	0.0612	0.0003
	A107IX40-3D6	60	40	8.33E-06	18	9	1.65	0.03263	0.188	**0.0013**	0.0367	**0.0019**	1.2559	0.0019	0.0308	-0.0014	0.0482	0.0001
	A107IX40-3D7	60	40	8.33E-06	21	9	1.65	0.03263	0.166	**0.0012**	0.0332	**0.0016**	1.1115	0.0017	0.0255	-0.0013	0.0581	**0.0004**
	A107IX40-3D8	60	40	8.33E-06	24	9	1.65	0.03263	0.117	0.0005	0.0336	**0.0019**	0.9844	**0.0015**	0.0228	-0.0013	0.0565	**0.0003**
	A107IX40-3D9	60	40	8.33E-06	27	9	1.65	0.03263	0.151	**0.0015**	0.0266	**0.0010**	0.9150	**0.0014**	0.0219	-0.0012	0.0529	**0.0002**
	A107IX40-3D10	60	40	8.33E-06	30	9	1.65	0.03263	0.113	0.0006	0.0258	**0.0013**	0.8431	**0.0013**	0.0342	0.0008	0.0524	**0.0002**
4	A107IX40-4D1	105	40	8.33E-06	3	10	0.83	0.01635	0.206	0.0066	0.0548	0.0126	1.8951	0.0131	0.0372	-0.0003	0.1029	0.0017
	A107IX40-4D2	105	40	8.33E-06	6	10	0.83	0.01634	0.179	0.0025	0.0387	0.0024	1.5583	0.0039	0.0320	-0.0018	0.0877	0.0004
	A107IX40-4D3	105	40	8.33E-06	9	10	0.83	0.01634	0.121	0.0010	0.0276	0.0016	1.2339	0.0026	0.0511	0.0052	0.0693	0.0000
	A107IX40-4D4	105	40	8.33E-06	12	10	0.83	0.01634	0.115	0.0017	0.0251	0.0024	0.9673	0.0018	0.0358	-0.0028	0.0623	0.0001
	A107IX40-4D5	105	40	8.33E-06	15	10	0.83	0.01634	0.072	0.0004	0.0217	0.0018	0.7902	0.0014	0.0264	-0.0034	0.0579	0.0001
	A107IX40-4D6	105	40	8.33E-06	18	10	0.83	0.01634	0.061	0.0008	0.0224	0.0024	0.7226	0.0016	0.0255	-0.0022	0.0512	-0.0001
	A107IX40-4D7	105	40	8.33E-06	21	10	0.83	0.01634	0.062	**0.0010**	0.0180	0.0013	0.6302	0.0011	0.0295	-0.0008	0.0538	0.0001
	A107IX40-4D8	105	40	8.33E-06	24	10	0.83	0.01634	0.058	**0.0008**	0.0161	**0.0013**	0.5614	**0.0009**	0.0301	-0.0012	0.0461	-0.0002
	A107IX40-4D9	105	40	8.33E-06	27	10	0.83	0.01634	0.047	**0.0005**	0.0140	**0.0010**	0.5271	**0.0009**	0.0236	-0.0034	0.0462	0.0000
	A107IX40-4D10	105	40	8.33E-06	30	10	0.83	0.01634	0.016	-0.0003	0.0138	**0.0012**	0.4956	**0.0008**	0.0237	-0.0023	0.0456	-0.0001
5	A107IX40-5D1	270	40	8.33E-06	3	11	0.83	0.01634	0.263	0.0085	0.0533	0.0122	2.353	0.0130	0.0545	0.0069	0.1815	0.0041
	A107IX40-5D2	270	40	8.33E-06	6	11	0.83	0.01634	0.303	0.0056	0.0408	0.0031	2.298	0.0061	0.0492	0.0018	0.2017	0.0027
	A107IX40-5D3	270	40	8.33E-06	9	11	0.83	0.01634	0.298	0.0048	0.0360	0.0034	2.136	0.0050	0.0546	0.0044	0.2011	0.0023
	A107IX40-5D4	270	40	8.33E-06	12	11	0.83	0.01634	0.252	0.0033	0.0295	0.0024	1.988	0.0045	0.0515	0.0025	0.1830	0.0018
	A107IX40-5D5	270	40	8.33E-06	15	11	0.83	0.01633	0.206	0.0026	0.0281	0.0029	1.709	0.0028	0.0427	0.0001	0.1364	0.0006
	A107IX40-5D6	270	40	8.33E-06	18	11	0.83	0.01633	0.135	0.0010	0.0230	0.0018	1.594	0.0030	0.0490	0.0036	0.1295	0.0011
	A107IX40-5D7	270	40	8.33E-06	21	11	0.83	0.01633	0.124	**0.0018**	0.0293	**0.0039**	1.423	0.0021	0.0719	0.0100	0.1190	**0.0009**
	A107IX40-5D8	270	40	8.33E-06	24	11	0.83	0.01633	0.136	**0.0024**	0.0214	**0.0012**	1.329	**0.0021**	0.0503	-0.0007	0.1093	**0.0008**
	A107IX40-5D9	270	40	8.33E-06	27	11	0.83	0.01633	0.099	**0.0010**	0.0123	0.0000	1.258	**0.0019**	0.0700	**0.0091**	0.0881	**0.0002**
	A107IX40-5D10	270	40	8.33E-06	30	11	0.83	0.01633	0.102	**0.0017**	0.0189	**0.0027**	1.250	**0.0021**	0.0735	**0.0071**	0.1073	**0.0012**

Table A3. DCP-AES Analysis Results from Dissolution of Glass AP107WDFL at 23 °C.

Exp.	Sample ID	Inf [Si] ppm	T °C	Flow Rate, m^3/d	Time, days	pH 23°C	Glass Mass g	SA m^2	[B] ppm	B Rate $g_{-glass}\ m^{-2}\ d^{-1}$	[Li] ppm	Li Rate $g_{-glass}\ m^{-2}\ d^{-1}$	[Na] ppm	Na Rate $g_{-glass}\ m^{-2}\ d^{-1}$	[K] ppm	K Rate $g_{-glass}\ m^{-2}\ d^{-1}$	[Al] ppm	Al Rate $g_{-glass}\ m^{-2}\ d^{-1}$
1	A107IX23-1D1	35	23	8.33E-06	3	7	3.28	0.06487	0.678	0.0056	0.1536	0.0093	5.9169	0.0116	0.1009	0.0047	0.0379	0.0002
	A107IX23-1D2	35	23	8.33E-06	6	7	3.28	0.06486	0.508	0.0014	0.1136	0.0022	4.3130	0.0026	0.0671	-0.0004	0.0331	0.0001
	A107IX23-1D3	35	23	8.33E-06	9	7	3.28	0.06486	0.020	-0.0020	0.0850	0.0016	3.3097	0.0022	0.0580	0.0002	0.0284	0.0000
	A107IX23-1D4	35	23	8.33E-06	12	7	3.28	0.06486	<DL	-	0.0712	0.0017	2.5159	0.0016	0.0662	0.0013	0.0301	0.0001
	A107IX23-1D5	35	23	8.33E-06	15	7	3.28	0.06486	<DL	-	0.0593	0.0014	1.9314	0.0012	0.0687	0.0011	0.0316	0.0001
	A107IX23-1D6	35	23	8.33E-06	18	7	3.28	0.06486	<DL	-	0.0541	0.0014	1.7134	0.0014	0.0587	0.0002	0.0273	0.0000
	A107IX23-1D7	35	23	8.33E-06	21	7	3.28	0.06486	<DL	-	0.0441	**0.0009**	1.4926	0.0011	0.0531	0.0002	0.0307	0.0001
	A107IX23-1D8	35	23	8.33E-06	24	7	3.28	0.06486	<DL	-	0.0350	**0.0007**	1.3606	**0.0011**	0.0372	**-0.0009**	0.0275	**0.0000**
	A107IX23-1D9	35	23	8.33E-06	27	7	3.28	0.06486	<DL	-	0.0382	**0.0012**	1.2967	**0.0011**	0.0488	**0.0007**	0.0267	**0.0000**
	A107IX23-1D10	35	23	8.33E-06	30	7	3.28	0.06486	<DL	-	0.0284	0.0005	1.2333	**0.0010**	0.0518	**0.0005**	0.0285	**0.0001**
2	A107IX23-2D3	40	23	8.33E-06	3	8	3.28	0.06487	0.570	0.0047	0.1310	0.0079	5.1548	0.0101	0.0943	0.0046	0.0673	0.0004
	A107IX23-2D4	40	23	8.33E-06	6	8	3.28	0.06486	0.204	-0.0007	0.0939	0.0017	3.6517	0.0020	0.0781	0.0010	0.0531	0.0001
	A107IX23-2D5	40	23	8.33E-06	9	8	3.28	0.06486	0.248	0.0012	0.0564	0.0005	2.6206	0.0015	0.0707	0.0010	0.0514	0.0001
	A107IX23-2D6	40	23	8.33E-06	12	8	3.28	0.06486	0.193	0.0006	0.0566	0.0016	2.0616	0.0014	0.0732	0.0016	0.0490	0.0001
	A107IX23-2D7	40	23	8.33E-06	15	8	3.28	0.06486	0.153	0.0005	0.0457	0.0010	1.5600	0.0009	0.0593	0.0003	0.0465	0.0001
	A107IX23-2D8	40	23	8.33E-06	18	8	3.28	0.06486	0.116	0.0003	0.0228	-0.0001	1.3612	0.0010	0.0487	0.0000	0.0480	0.0001
	A107IX23-2D9	40	23	8.33E-06	21	8	3.28	0.06485	0.077	0.0001	0.0343	0.0013	1.1542	0.0008	0.0469	**0.0003**	0.0402	0.0001
	A107IX23-2D10	40	23	8.33E-06	24	8	3.28	0.06485	0.063	**0.0002**	0.0311	**0.0008**	1.0483	**0.0008**	0.0560	0.0011	0.0432	**0.0001**
	A107IX23-2D11	40	23	8.33E-06	27	8	3.28	0.06485	0.098	**0.0005**	0.0320	**0.0009**	0.9743	**0.0008**	0.0505	**0.0003**	0.0531	**0.0002**
	A107IX23-2D12	40	23	8.33E-06	30	8	3.28	0.06485	0.083	**0.0003**	0.0297	**0.0007**	0.8009	**0.0005**	0.0559	0.0010	0.0515	**0.0001**
3	A107IX23-3D1	52	23	8.33E-06	3	9	3.28	0.06487	0.395	0.0032	0.0896	0.0053	3.7477	0.0073	0.0466	0.0022	0.0644	0.0003
	A107IX23-3D2	52	23	8.33E-06	6	9	3.28	0.06487	0.265	0.0005	0.0611	0.0009	2.6724	0.0015	0.0433	0.0008	0.0513	0.0001
	A107IX23-3D3	52	23	8.33E-06	9	9	3.28	0.06486	0.155	0.0002	0.0443	0.0007	1.9282	0.0011	0.0127	-0.0015	0.0541	0.0001
	A107IX23-3D4	52	23	8.33E-06	12	9	3.28	0.06486	0.128	0.0004	0.0325	0.0005	1.5155	0.0010	0.0241	0.0006	0.0489	0.0001
	A107IX23-3D5	52	23	8.33E-06	15	9	3.28	0.06486	0.115	0.0004	0.0181	0.0000	1.2169	0.0008	0.0016	-0.0017	0.0484	0.0001
	A107IX23-3D6	52	23	8.33E-06	18	9	3.28	0.06486	0.073	0.0001	0.0116	0.0001	1.0764	0.0008	0.0032	-0.0006	0.0440	0.0001
	A107IX23-3D7	52	23	8.33E-06	21	9	3.28	0.06486	0.077	**0.0003**	0.0139	**0.0004**	0.8867	0.0006	0.0146	0.0002	0.0422	**0.0001**
	A107IX23-3D8	52	23	8.33E-06	24	9	3.28	0.06486	<DL	-	0.0271	**0.0011**	0.7949	**0.0006**	0.0605	**0.0035**	0.0550	**0.0002**
	A107IX23-3D9	52	23	8.33E-06	27	9	3.28	0.06486	0.017	**0.0004**	0.0207	**0.0003**	0.7574	**0.0006**	0.0305	**-0.0008**	0.0439	**0.0000**
	A107IX23-3D10	52	23	8.33E-06	30	9	3.28	0.06486	0.035	**0.0002**	0.0063	-0.0004	0.7221	**0.0006**	0.0161	**-0.0007**	0.0409	**0.0001**
4	A107IX23-4D1	90	23	8.33E-06	3	10	1.64	0.03243	0.231	0.0038	0.0482	0.0055	1.8870	0.0068	0.0364	0.0018	0.0837	0.0006
	A107IX23-4D2	90	23	8.33E-06	6	10	1.64	0.03243	0.152	0.0006	0.0459	0.0025	1.3154	0.0011	0.0226	-0.0014	0.0663	0.0000
	A107IX23-4D3	90	23	8.33E-06	9	10	1.64	0.03243	0.109	0.0005	0.0305	0.0007	0.9829	0.0009	0.0326	0.0014	0.0635	0.0001
	A107IX23-4D4	90	23	8.33E-06	12	10	1.64	0.03243	0.076	0.0003	0.0239	0.0009	0.7789	0.0008	0.0385	0.0015	0.0544	0.0000
	A107IX23-4D5	90	23	8.33E-06	15	10	1.64	0.03243	0.052	0.0002	0.0220	0.0010	0.6448	0.0006	0.0280	-0.0007	0.0628	0.0002
	A107IX23-4D6	90	23	8.33E-06	18	10	1.64	0.03243	0.004	-0.0004	0.0254	0.0016	0.5573	0.0006	0.0288	0.0003	0.0563	0.0000
	A107IX23-4D7	90	23	8.33E-06	21	10	1.64	0.03243	0.056	0.0009	0.0280	0.0017	0.4686	0.0004	0.0442	0.0028	0.0642	0.0002
	A107IX23-4D8	90	23	8.33E-06	24	10	1.64	0.03243	0.068	**0.0006**	0.0341	**0.0023**	0.4171	**0.0003**	0.0329	-0.0003	0.0701	**0.0002**
	A107IX23-4D9	90	23	8.33E-06	27	10	1.64	0.03243	0.087	**0.0009**	0.0458	**0.0033**	0.3447	**0.0002**	0.0497	**0.0033**	0.0730	**0.0002**
	A107IX23-4D10	90	23	8.33E-06	30	10	1.64	0.03243	0.099	**0.0009**	0.0510	**0.0033**	0.2894	**0.0001**	0.0605	**0.0037**	0.0749	**0.0003**
5	A107IX23-5D9	230	23	8.33E-06	3	11	1.64	0.03243	1.710	0.0283	0.2707	0.0331	8.950	0.0322	0.2580	0.0325	2.0787	0.0318
	A107IX23-5D8	230	23	8.33E-06	6	11	1.64	0.03241	1.563	0.0117	0.2428	0.0131	7.620	0.0108	0.2366	0.0128	1.8716	0.0126
	A107IX23-5D1	230	23	8.33E-06	9	11	1.64	0.03240	0.290	-0.0082	0.0373	-0.0106	2.280	-0.0081	0.0597	-0.0143	0.1271	-0.0135
	A107IX23-5D2	230	23	8.33E-06	12	11	1.64	0.03240	0.153	0.0001	0.0310	0.0013	1.804	0.0008	0.0747	0.0025	0.1224	0.0003
	A107IX23-5D3	230	23	8.33E-06	15	11	1.64	0.03240	0.093	0.0002	0.0146	-0.0003	1.597	0.0009	0.0688	0.0004	0.1222	0.0003
	A107IX23-5D4	230	23	8.33E-06	18	11	1.64	0.03239	0.033	-0.0003	0.0083	-0.0001	1.469	0.0008	0.0710	0.0012	0.1284	0.0004
	A107IX23-5D5	230	23	8.33E-06	21	11	1.64	0.03239	<DL	-	0.0077	**0.0002**	1.440	0.0009	0.0691	0.0007	0.1305	0.0004
	A107IX23-5D6	230	23	8.33E-06	24	11	1.64	0.03239	0.090	0.0016	0.0113	**0.0007**	1.366	**0.0007**	0.0895	**0.0042**	0.1370	**0.0005**
	A107IX23-5D7	230	23	8.33E-06	27	11	1.64	0.03239	<DL	-	0.0214	**0.0017**	1.319	**0.0007**	0.0972	**0.0038**	0.1286	**0.0003**
	A107IX23-5D10	230	23	8.33E-06	30	11	1.64	0.03240	0.059	0.0020	0.0108	-0.0002	1.341	**0.0008**	0.0897	**0.0019**	0.1212	**0.0003**

Table A4. DCP-AES Analysis Results from Dissolution of Glass ORLECAP107 at 70 °C.

Exp.	Sample ID	Inf [Si] ppm	T °C	Flow Rate, m^3/d	Time, days	pH 23°C	Glass Mass g	SA m^2	[B] ppm	B Rate $g_{glass}\ m^{-2}\ d^{-1}$	[Na] ppm	Na Rate $g_{glass}\ m^{-2}\ d^{-1}$	[K] ppm	K Rate $g_{glass}\ m^{-2}\ d^{-1}$	[Al] ppm	Al Rate $g_{glass}\ m^{-2}\ d^{-1}$
1	C107IX70-1D1	55	70	2.50E-05	1	7	0.77	0.01520	25.812	2.4856	120.500	2.2199	2.6909	0.6337	0.1285	0.0075
	C107IX70-1D2	55	70	2.50E-05	2	7	0.77	0.01493	28.901	1.5680	140.120	1.4989	3.1376	0.4338	0.1459	0.0050
	C107IX70-1D3	55	70	2.50E-05	3	7	0.77	0.01465	27.150	1.2684	134.830	1.2378	2.9963	0.3495	0.1344	0.0037
	C107IX70-1D4	55	70	2.50E-05	4	7	0.77	0.01439	25.991	1.2629	128.010	1.1791	2.9518	0.3627	0.1419	0.0047
	C107IX70-1D5	55	70	2.50E-05	5	7	0.77	0.01414	23.729	1.1111	117.200	1.0530	2.7460	0.3208	0.1398	0.0044
	C107IX70-1D6	55	70	2.50E-05	6	7	0.77	0.01391	21.146	0.9765	110.280	1.0397	2.5838	0.3102	0.1388	**0.0044**
	C107IX70-1D7	55	70	2.50E-05	7	7	0.77	0.01370	20.142	1.0222	104.660	**1.0114**	2.3923	**0.2850**	0.1362	**0.0044**
	C107IX70-1D8	55	70	2.50E-05	8	7	0.77	0.01350	18.804	**0.9468**	97.420	**0.9343**	2.4654	**0.3358**	0.1509	**0.0057**
	C107IX70-1D9	55	70	2.50E-05	9	7	0.77	0.01331	16.921	**0.8265**	94.443	**0.9609**	2.2584	**0.2724**	0.3004	0.0169
	C107IX70-1D10	55	70	2.50E-05	10	7	0.77	0.01314	15.698	**0.8059**	81.817	0.7354	2.1377	**0.2711**	0.1448	-0.0012
2	C107IX70-2D1	60	70	2.50E-05	1	8	0.77	0.01524	17.533	1.6838	80.058	1.4682	1.6149	1.1490	0.1705	0.0091
	C107IX70-2D2	60	70	2.50E-05	2	8	0.77	0.01505	20.456	1.1365	102.750	1.1664	1.7969	0.7165	0.1637	0.0041
	C107IX70-2D3	60	70	2.50E-05	3	8	0.77	0.01486	19.568	0.9201	99.772	0.9111	1.7820	0.6464	0.1511	0.0035
	C107IX70-2D4	60	70	2.50E-05	4	8	0.77	0.01467	18.629	0.8825	93.070	0.8231	1.8011	0.6750	0.1539	0.0042
	C107IX70-2D5	60	70	2.50E-05	5	8	0.77	0.01449	17.483	0.8251	90.970	0.8575	1.6159	0.5333	0.2246	0.0093
	C107IX70-2D6	60	70	2.50E-05	6	8	0.77	0.01432	16.910	0.8350	85.735	0.7858	1.5599	0.5683	0.1328	0.0001
	C107IX70-2D7	60	70	2.50E-05	7	8	0.77	0.01416	14.558	**0.6308**	77.191	**0.6770**	1.4251	**0.4905**	0.1319	**0.0034**
	C107IX70-2D8	60	70	2.50E-05	8	8	0.77	0.01401	13.608	**0.6609**	72.931	**0.6841**	1.4444	**0.5645**	0.1334	**0.0036**
	C107IX70-2D9	60	70	2.50E-05	9	8	0.77	0.01388	12.667	**0.6181**	67.444	**0.6228**	1.2884	**0.4368**	0.1327	**0.0035**
	C107IX70-2D10	60	70	2.50E-05	10	8	0.77	0.01376	11.596	**0.5598**	61.901	**0.5713**	1.2868	**0.5027**	0.1300	**0.0034**
3	C107IX70-3D1	80	70	2.50E-05	1	9	0.77	0.01528	8.398	0.8040	37.386	0.6786	0.5704	0.3756	0.1766	0.0088
	C107IX70-3D2	80	70	2.50E-05	2	9	0.77	0.01520	9.462	0.5068	40.626	0.4011	0.6264	0.2300	0.1458	0.0023
	C107IX70-3D3	80	70	2.50E-05	3	9	0.77	0.01510	9.812	0.4923	42.160	0.4020	0.6591	0.2349	0.1287	0.0022
	C107IX70-3D4	80	70	2.50E-05	4	9	0.77	0.01501	9.678	0.4653	42.306	0.3929	0.6364	0.2074	0.1174	0.0020
	C107IX70-3D5	80	70	2.50E-05	5	9	0.77	0.01491	9.357	0.4433	41.646	0.3816	0.6234	0.2074	0.1096	0.0019
	C107IX70-3D6	80	70	2.50E-05	6	9	0.77	0.01482	8.515	0.3786	39.415	0.3479	0.5985	0.1948	0.0974	0.0013
	C107IX70-3D7	80	70	2.50E-05	7	9	0.77	0.01474	8.006	0.3720	35.709	**0.3004**	0.5457	**0.1654**	0.0954	0.0016
	C107IX70-3D8	80	70	2.50E-05	8	9	0.77	0.01467	7.384	**0.3372**	33.388	**0.2930**	0.5226	**0.1687**	0.0866	0.0011
	C107IX70-3D9	80	70	2.50E-05	9	9	0.77	0.01460	7.021	**0.3337**	32.670	**0.3030**	0.5168	**0.1739**	0.0870	**0.0014**
	C107IX70-3D10	80	70	2.50E-05	10	9	0.77	0.01453	6.516	**0.3026**	31.151	**0.2820**	0.4846	**0.1523**	0.0873	**0.0014**
4	C107IX70-4D1	140	70	2.50E-05	1	10	0.50	0.00984	3.048	0.4530	13.326	0.3720	0.1363	0.1116	0.1293	0.0083
	C107IX70-4D2	140	70	2.50E-05	2	10	0.50	0.00980	4.072	0.3803	16.744	0.2846	0.1742	0.0991	0.1185	0.0030
	C107IX70-4D3	140	70	2.50E-05	3	10	0.50	0.00976	3.777	0.2608	15.860	0.2111	0.1695	0.0725	0.1124	0.0029
	C107IX70-4D4	140	70	2.50E-05	4	10	0.50	0.00973	3.695	0.2715	15.413	0.2118	0.1687	0.0745	0.0971	0.0016
	C107IX70-4D5	140	70	2.50E-05	5	10	0.50	0.00969	3.562	0.2587	14.888	0.2038	0.1552	0.0598	0.0937	0.0021
	C107IX70-4D6	140	70	2.50E-05	6	10	0.50	0.00966	3.284	0.2275	13.773	0.1797	0.1638	0.0776	0.0903	0.0019
	C107IX70-4D7	140	70	2.50E-05	7	10	0.50	0.00963	3.075	0.2177	13.012	0.1744	0.1329	0.0371	0.0854	0.0016
	C107IX70-4D8	140	70	2.50E-05	8	10	0.50	0.00960	2.939	**0.2134**	12.626	0.1747	0.1239	0.0447	0.2067	**0.0151**
	C107IX70-4D9	140	70	2.50E-05	9	10	0.50	0.00957	2.691	**0.1865**	11.676	**0.1530**	0.1209	**0.0466**	0.1253	**-0.0004**
	C107IX70-4D10	140	70	2.50E-05	10	10	0.50	0.00954	2.549	**0.1843**	11.001	**0.1476**	0.1353	**0.0653**	0.0813	**-0.0008**
5	C107IX70-5D1	360	70	2.50E-05	1	11	0.50	0.00984	1.400	0.2076	8.796	0.2202	0.1057	0.0164	0.1148	0.0042
	C107IX70-5D2	360	70	2.50E-05	2	11	0.50	0.00983	1.717	0.1512	9.429	0.1284	0.1067	0.0086	0.1077	0.0014
	C107IX70-5D3	360	70	2.50E-05	3	11	0.50	0.00981	1.678	0.1219	8.950	0.1058	0.1058	0.0081	0.0939	0.0003
	C107IX70-5D4	360	70	2.50E-05	4	11	0.50	0.00980	1.656	0.1218	8.642	0.1041	0.1156	0.0120	0.0913	0.0007
	C107IX70-5D5	360	70	2.50E-05	5	11	0.50	0.00978	1.557	0.1088	8.308	0.0990	0.0987	0.0037	0.0875	0.0004
	C107IX70-5D6	360	70	2.50E-05	6	11	0.50	0.00977	1.401	0.0930	7.650	0.0851	0.0898	0.0036	0.0819	0.0001
	C107IX70-5D7	360	70	2.50E-05	7	11	0.50	0.00975	1.265	**0.0845**	7.130	**0.0797**	0.0847	0.0033	0.0855	0.0007
	C107IX70-5D8	360	70	2.50E-05	8	11	0.50	0.00974	1.234	**0.0900**	6.930	**0.0815**	0.0958	0.0085	0.1037	**0.0025**
	C107IX70-5D9	360	70	2.50E-05	9	11	0.50	0.00973	1.106	**0.0734**	6.660	**0.0767**	0.0760	-0.0011	0.1154	**0.0028**
	C107IX70-5D10	360	70	2.50E-05	10	11	0.50	0.00972	0.997	0.0666	6.050	0.0631	0.0757	0.0025	0.0733	-0.0024

Table A5. DCP-AES Analysis Results from Dissolution of Glass ORLECAP107 at 40 °C.

Exp.	Sample ID	Inf [Si] ppm	T °C	Flow Rate, m^3/d	Time, days	pH 23°C	Glass Mass g	SA m^2	[B] ppm	B Rate $g_{glass}\ m^{-2}\ d^{-1}$	[Na] ppm	Na Rate $g_{glass}\ m^{-2}\ d^{-1}$	[K] ppm	K Rate $g_{glass}\ m^{-2}\ d^{-1}$	[Al] ppm	Al Rate $g_{glass}\ m^{-2}\ d^{-1}$
1	C107IX40-1D1	40	40	8.33E-06	3	7	1.65	0.03278	12.412	0.1847	55.5380	0.1583	1.1373	0.1259	0.2026	0.0020
	C107IX40-1D2	40	40	8.33E-06	6	7	1.65	0.03264	16.398	0.1523	74.2670	0.1332	1.5285	0.1078	0.1353	0.0003
	C107IX40-1D3	40	40	8.33E-06	9	7	1.65	0.03247	16.950	0.1315	74.6510	0.1080	1.5843	0.0924	0.1400	0.0007
	C107IX40-1D4	40	40	8.33E-06	12	7	1.65	0.03231	16.834	0.1262	73.5300	0.1047	1.5884	0.0901	0.1473	0.0007
	C107IX40-1D5	40	40	8.33E-06	15	7	1.65	0.03215	15.908	0.1137	65.3690	0.0831	1.4591	0.0753	0.1489	0.0007
	C107IX40-1D6	40	40	8.33E-06	18	7	1.65	0.03199	15.797	0.1196	63.4430	0.0898	1.5311	0.0916	0.2237	0.0015
	C107IX40-1D7	40	40	8.33E-06	21	7	1.65	0.03184	14.573	0.1022	60.6110	0.0848	1.4021	**0.0727**	0.2032	0.0009
	C107IX40-1D8	40	40	8.33E-06	24	7	1.65	0.03170	13.462	**0.0950**	58.9820	**0.0845**	1.4301	**0.0839**	0.2097	**0.0011**
	C107IX40-1D9	40	40	8.33E-06	27	7	1.65	0.03157	13.670	**0.1072**	55.1920	**0.0760**	1.3933	**0.0783**	0.1165	**0.0000**
	C107IX40-1D10	40	40	8.33E-06	30	7	1.65	0.03144	12.704	**0.0911**	52.3220	**0.0734**	1.2457	**0.0633**	0.1099	**0.0005**
2	C107IX40-2D1	45	40	8.33E-06	3	8	1.65	0.03280	7.890	0.1173	32.0690	0.0912	0.7490	0.0829	1.9911	0.0210
	C107IX40-2D2	45	40	8.33E-06	6	8	1.65	0.03273	6.167	0.0331	30.6290	0.0416	0.5101	0.0144	0.1304	-0.0093
	C107IX40-2D3	45	40	8.33E-06	9	8	1.65	0.03266	7.547	0.0666	35.4940	0.0577	0.6130	0.0397	0.1263	0.0006
	C107IX40-2D4	45	40	8.33E-06	12	8	1.65	0.03259	8.253	0.0670	36.7140	0.0543	0.6555	0.0388	0.1386	0.0007
	C107IX40-2D5	45	40	8.33E-06	15	8	1.65	0.03251	8.230	0.0616	36.8020	0.0530	0.6376	0.0344	0.1244	0.0005
	C107IX40-2D6	45	40	8.33E-06	18	8	1.65	0.03243	8.018	0.0587	34.6590	0.0468	0.6152	0.0330	0.1141	0.0005
	C107IX40-2D7	45	40	8.33E-06	21	8	1.65	0.03235	7.586	0.0539	32.8270	**0.0447**	0.6201	0.0349	0.7084	0.0069
	C107IX40-2D8	45	40	8.33E-06	24	8	1.65	0.03228	7.166	**0.0510**	32.4240	**0.0463**	0.5980	**0.0321**	0.5201	**0.0017**
	C107IX40-2D9	45	40	8.33E-06	27	8	1.65	0.03221	6.507	**0.0443**	29.6380	**0.0389**	0.5906	**0.0326**	0.4458	**0.0019**
	C107IX40-2D10	45	40	8.33E-06	30	8	1.65	0.03215	6.166	**0.0442**	28.4240	**0.0394**	0.5505	**0.0285**	0.4084	**0.0019**
3	C107IX40-3D1	60	40	8.33E-06	3	9	1.65	0.03282	2.791	0.0414	16.7000	0.0473	0.1568	0.0136	0.1287	0.0011
	C107IX40-3D2	60	40	8.33E-06	6	9	1.65	0.03279	3.735	0.0348	17.9460	0.0272	0.1861	0.0102	0.1297	0.0006
	C107IX40-3D3	60	40	8.33E-06	9	9	1.65	0.03275	3.936	0.0308	17.5560	0.0244	0.1920	0.0092	0.1172	0.0004
	C107IX40-3D4	60	40	8.33E-06	12	9	1.65	0.03271	4.014	0.0305	17.4320	0.0246	0.1903	0.0087	0.1084	0.0004
	C107IX40-3D5	60	40	8.33E-06	15	9	1.65	0.03268	3.677	0.0249	15.6630	0.0197	0.1724	0.0067	0.0957	0.0003
	C107IX40-3D6	60	40	8.33E-06	18	9	1.65	0.03264	3.649	0.0270	14.8030	0.0198	0.1753	0.0081	0.0870	0.0003
	C107IX40-3D7	60	40	8.33E-06	21	9	1.65	0.03261	3.378	0.0232	14.4510	0.0201	0.1506	0.0051	0.0800	0.0002
	C107IX40-3D8	60	40	8.33E-06	24	9	1.65	0.03257	3.384	0.0254	13.8290	**0.0188**	0.1595	**0.0075**	0.0789	**0.0003**
	C107IX40-3D9	60	40	8.33E-06	27	9	1.65	0.03254	3.153	**0.0219**	13.6990	**0.0193**	0.1592	**0.0070**	0.0754	**0.0002**
	C107IX40-3D10	60	40	8.33E-06	30	9	1.65	0.03251	3.092	**0.0227**	13.0660	**0.0177**	0.1547	**0.0065**	0.0687	**0.0002**
4	C107IX40-4D1	105	40	8.33E-06	3	10	0.83	0.01643	0.958	0.0284	6.6063	0.0362	0.0890	0.0115	0.1309	0.0018
	C107IX40-4D2	105	40	8.33E-06	6	10	0.83	0.01642	1.026	0.0162	6.4143	0.0170	0.0841	0.0047	0.1046	0.0003
	C107IX40-4D3	105	40	8.33E-06	9	10	0.83	0.01641	1.040	0.0156	5.7970	0.0140	0.0656	0.0010	0.0891	0.0003
	C107IX40-4D4	105	40	8.33E-06	12	10	0.83	0.01640	1.057	0.0159	5.4871	0.0140	0.0732	0.0048	0.0780	0.0002
	C107IX40-4D5	105	40	8.33E-06	15	10	0.83	0.01639	1.113	0.0174	5.6938	0.0161	0.0915	0.0081	0.3153	0.0054
	C107IX40-4D6	105	40	8.33E-06	18	10	0.83	0.01638	1.023	0.0138	5.0816	**0.0120**	0.0745	**0.0022**	0.0608	-0.0026
	C107IX40-4D7	105	40	8.33E-06	21	10	0.83	0.01637	0.950	**0.0130**	4.7606	**0.0120**	0.0661	**0.0022**	0.0649	**0.0002**
	C107IX40-4D8	105	40	8.33E-06	24	10	0.83	0.01636	1.105	0.0187	5.3624	0.0163	0.0884	**0.0083**	0.2406	0.0039
	C107IX40-4D9	105	40	8.33E-06	27	10	0.83	0.01635	0.963	**0.0122**	4.7144	**0.0109**	0.0706	**0.0017**	0.0563	-0.0019
	C107IX40-4D10	105	40	8.33E-06	30	10	0.83	0.01634	0.929	**0.0133**	4.6472	**0.0124**	0.0758	**0.0049**	0.0574	**0.0001**
5	C107IX40-5D1	270	40	8.33E-06	3	11	0.83	0.01644	0.477	0.0141	5.1131	0.0250	0.0741	0.0093	0.1273	0.0016
	C107IX40-5D2	270	40	8.33E-06	6	11	0.83	0.01643	0.379	0.0041	4.2500	0.0076	0.0538	0.0001	0.1166	0.0006
	C107IX40-5D3	270	40	8.33E-06	9	11	0.83	0.01643	0.282	0.0027	3.4523	0.0055	0.0552	0.0027	0.1043	0.0004
	C107IX40-5D4	270	40	8.33E-06	12	11	0.83	0.01643	0.258	0.0034	2.9066	0.0047	0.0529	0.0020	0.1003	0.0004
	C107IX40-5D5	270	40	8.33E-06	15	11	0.83	0.01642	0.241	0.0033	2.4973	0.0039	0.0397	-0.0007	0.1016	0.0005
	C107IX40-5D6	270	40	8.33E-06	18	11	0.83	0.01642	0.227	0.0031	2.2573	0.0037	0.0644	0.0063	0.0993	0.0004
	C107IX40-5D7	270	40	8.33E-06	21	11	0.83	0.01642	0.209	0.0028	1.8728	0.0022	0.0807	0.0072	0.1000	0.0005
	C107IX40-5D8	270	40	8.33E-06	24	11	0.83	0.01642	0.106	0.0000	1.5650	**0.0015**	0.0899	0.0075	0.1035	**0.0005**
	C107IX40-5D9	270	40	8.33E-06	27	11	0.83	0.01642	0.098	**0.0013**	1.4496	**0.0017**	0.1112	0.0113	0.1110	**0.0006**
	C107IX40-5D10	270	40	8.33E-06	30	11	0.83	0.01642	0.095	**0.0013**	1.3143	**0.0013**	0.0429	-0.0066	0.1009	**0.0004**

Table A6. DCP-AES Analysis Results from Dissolution of Glass ORLECAP107 at 23 °C.

Exp.	Sample ID	Inf [Si] ppm	T °C	Flow Rate, m^3/d	Time, days	pH 23°C	Glass Mass g	SA m^2	[B] ppm	B Rate $g_{glass}\ m^{-2}\ d^{-1}$	[Na] ppm	Na Rate $g_{glass}\ m^{-2}\ d^{-1}$	[K] ppm	K Rate $g_{glass}\ m^{-2}\ d^{-1}$	[Al] ppm	Al Rate $g_{glass}\ m^{-2}\ d^{-1}$
1	C107IX23-1D1	35	23	8.33E-06	3	7	3.28	0.06522	2.146	0.0160	17.9380	**0.0255**	0.2246	0.0103	0.0591	0.0002
	C107IX23-1D2	35	23	8.33E-06	6	7	3.28	0.06520	2.943	0.0140	19.0860	0.0144	0.2107	0.0044	0.0623	0.0001
	C107IX23-1D3	35	23	8.33E-06	9	7	3.28	0.06517	2.871	0.0105	17.3320	0.0111	0.2093	0.0047	0.0642	0.0001
	C107IX23-1D4	35	23	8.33E-06	12	7	3.28	0.06514	2.990	0.0116	16.4320	0.0111	0.2393	0.0065	0.0524	0.0001
	C107IX23-1D5	35	23	8.33E-06	15	7	3.28	0.06511	2.799	0.0098	14.2100	0.0085	0.2269	0.0049	0.0480	0.0001
	C107IX23-1D6	35	23	8.33E-06	18	7	3.28	0.06509	2.932	0.0115	14.4180	0.0104	0.2478	0.0064	0.0458	0.0001
	C107IX23-1D7	35	23	8.33E-06	21	7	3.28	0.06506	2.992	0.0114	13.3690	0.0088	0.2224	0.0044	0.0453	0.0001
	C107IX23-1D8	35	23	8.33E-06	24	7	3.28	0.06503	2.976	**0.0111**	14.5300	**0.0112**	0.2535	**0.0069**	0.0469	**0.0001**
	C107IX23-1D9	35	23	8.33E-06	27	7	3.28	0.06500	2.962	**0.0111**	14.2490	**0.0100**	0.2413	**0.0053**	0.0486	**0.0001**
	C107IX23-1D10	35	23	8.33E-06	30	7	3.28	0.06497	2.981	**0.0113**	14.0470	**0.0099**	0.2603	**0.0068**	0.0444	**0.0001**
2	C107IX23-2D3	40	23	8.33E-06	3	8	3.28	0.06523	1.675	0.0125	15.8360	0.0225	0.1738	0.0078	0.0935	0.0004
	C107IX23-2D4	40	23	8.33E-06	6	8	3.28	0.06521	1.472	0.0047	12.1820	0.0060	0.2115	0.0060	0.0873	0.0002
	C107IX23-2D5	40	23	8.33E-06	9	8	3.28	0.06520	1.346	0.0046	10.5620	0.0063	0.1704	0.0026	0.1867	0.0007
	C107IX23-2D6	40	23	8.33E-06	12	8	3.28	0.06518	1.227	0.0041	8.9671	0.0052	0.1585	0.0031	0.0731	-0.0002
	C107IX23-2D7	40	23	8.33E-06	15	8	3.28	0.06517	1.157	0.0041	7.6834	0.0045	0.1519	0.0031	0.0649	0.0001
	C107IX23-2D8	40	23	8.33E-06	18	8	3.28	0.06516	1.245	0.0050	7.5612	0.0052	0.1603	0.0037	0.0613	0.0001
	C107IX23-2D9	40	23	8.33E-06	21	8	3.28	0.06515	1.122	**0.0037**	7.0670	**0.0046**	0.1546	**0.0032**	0.0614	0.0001
	C107IX23-2D10	40	23	8.33E-06	24	8	3.28	0.06514	1.253	**0.0052**	6.7186	**0.0045**	0.1406	**0.0025**	0.0538	**0.0001**
	C107IX23-2D11	40	23	8.33E-06	27	8	3.28	0.06513	1.201	**0.0043**	6.5731	**0.0045**	0.1713	0.0047	0.0612	**0.0001**
	C107IX23-2D12	40	23	8.33E-06	30	8	3.28	0.06512	0.718	0.0009	5.6973	0.0034	0.1242	0.0011	0.0536	**0.0001**
3	C107IX23-3D7	52	23	8.33E-06	3	9	3.28	0.06520	7.503	0.0561	40.8780	0.0585	1.2092	0.0678	10.8960	0.0583
	C107IX23-3D8	52	23	8.33E-06	6	9	3.28	0.06514	4.023	0.0020	21.1340	0.0009	0.6069	-0.0004	5.5685	0.0006
	C107IX23-3D5	52	23	8.33E-06	9	9	3.28	0.06512	1.399	-0.0046	10.0250	-0.0009	0.2027	-0.0063	1.4813	-0.0071
	C107IX23-3D1	52	23	8.33E-06	12	9	3.28	0.06510	1.204	0.0038	12.7390	0.0110	0.1163	0.0003	0.0994	-0.0035
	C107IX23-3D2	52	23	8.33E-06	15	9	3.28	0.06509	0.835	0.0017	9.0730	0.0038	0.0896	0.0012	0.4061	0.0019
	C107IX23-3D3	52	23	8.33E-06	18	9	3.28	0.06509	0.700	0.0021	7.3837	0.0040	0.0986	0.0025	0.0736	-0.0008
	C107IX23-3D4	52	23	8.33E-06	21	9	3.28	0.06508	0.569	0.0016	5.8891	0.0031	0.0958	**0.0021**	0.0705	0.0001
	C107IX23-3D6	52	23	8.33E-06	24	9	3.28	0.06508	0.221	-0.0005	4.4035	**0.0020**	0.0870	**0.0017**	0.0611	0.0001
	C107IX23-3D9	52	23	8.33E-06	27	9	3.28	0.06507	0.457	**0.0026**	3.6097	**0.0019**	0.1092	**0.0032**	0.0487	**0.0000**
	C107IX23-3D10	52	23	8.33E-06	30	9	3.28	0.06507	0.508	**0.0021**	3.5257	0.0024	0.1736	0.0062	0.0536	**0.0001**
4	C107IX23-4D8	90	23	8.33E-06	3	10	1.64	0.03260	4.307	0.0644	20.4850	0.0583	0.5835	0.0637	5.5186	0.0587
	C107IX23-4D1	90	23	8.33E-06	6	10	1.64	0.03257	0.567	-0.0238	5.8956	-0.0128	0.0587	-0.0281	0.0938	-0.0289
	C107IX23-4D2	90	23	8.33E-06	9	10	1.64	0.03257	0.342	0.0008	4.1539	0.0032	0.0624	0.0023	0.0793	0.0001
	C107IX23-4D3	90	23	8.33E-06	12	10	1.64	0.03257	0.227	0.0008	3.0937	0.0026	0.0481	0.0005	0.0689	0.0001
	C107IX23-4D4	90	23	8.33E-06	15	10	1.64	0.03256	0.184	0.0010	2.4279	0.0023	0.0322	-0.0005	0.0582	0.0000
	C107IX23-4D5	90	23	8.33E-06	18	10	1.64	0.03256	0.209	0.0017	2.2647	0.0027	0.0778	0.0056	0.1447	0.0010
	C107IX23-4D6	90	23	8.33E-06	21	10	1.64	0.03256	0.138	**0.0005**	1.6728	0.0013	0.0601	0.0010	0.0665	-0.0003
	C107IX23-4D7	90	23	8.33E-06	24	10	1.64	0.03256	0.144	**0.0011**	1.3941	0.0013	0.0453	0.0003	0.0622	**0.0001**
	C107IX23-4D9	90	23	8.33E-06	27	10	1.64	0.03256	0.094	**0.0003**	1.1452	**0.0010**	0.0623	**0.0031**	0.0637	**0.0001**
	C107IX23-4D10	90	23	8.33E-06	30	10	1.64	0.03256	<DL	-	1.0226	**0.0010**	0.0869	**0.0049**	0.0660	**0.0001**
5	C107IX23-5D1	230	23	8.33E-06	3	11	1.64	0.03261	0.478	0.0071	5.2622	0.0124	0.0386	-0.0023	0.1403	0.0006
	C107IX23-5D2	230	23	8.33E-06	6	11	1.64	0.03261	0.238	0.0000	3.8611	0.0022	0.0448	-0.0004	0.1115	0.0000
	C107IX23-5D3	230	23	8.33E-06	9	11	1.64	0.03261	0.221	0.0015	2.9631	0.0016	0.0421	-0.0011	0.1091	0.0001
	C107IX23-5D4	230	23	8.33E-06	12	11	1.64	0.03261	0.089	-0.0003	2.3455	0.0011	0.0147	-0.0041	0.1011	0.0001
	C107IX23-5D5	230	23	8.33E-06	15	11	1.64	0.03261	<DL	-	2.0679	0.0012	0.0336	-0.0004	0.0992	0.0001
	C107IX23-5D6	230	23	8.33E-06	18	11	1.64	0.03261	0.088	0.0017	1.8607	0.0010	0.0326	-0.0015	0.1001	0.0001
	C107IX23-5D7	230	23	8.33E-06	21	11	1.64	0.03261	<DL	-	1.6279	0.0006	0.0478	0.0003	0.0935	0.0000
	C107IX23-5D8	230	23	8.33E-06	24	11	1.64	0.03261	0.077	0.0022	1.4574	**0.0005**	0.0429	-0.0012	0.1095	**0.0002**
	C107IX23-5D9	230	23	8.33E-06	27	11	1.64	0.03261	0.040	0.0000	1.2680	**0.0002**	0.0348	**-0.0018**	0.1012	**0.0001**
	C107IX23-5D10	230	23	8.33E-06	30	11	1.64	0.03261	<DL	-	1.4834	**0.0011**	0.0711	**0.0028**	0.0999	**0.0001**

Table A7. DCP-AES Analysis Results from Dissolution of Glass ORLEC44 at 70 °C.

Exp.	Sample ID	Inf [Si] ppm	T °C	Flow Rate, m^3/d	Time, days	pH 23°C	Glass Mass g	SA m^2	[B] ppm	B Rate $g_{glass}\ m^{-2}\ d^{-1}$	[Li] ppm	Li Rate $g_{glass}\ m^{-2}\ d^{-1}$	[Na] ppm	Na Rate $g_{glass}\ m^{-2}\ d^{-1}$	[K] ppm	K Rate $g_{glass}\ m^{-2}\ d^{-1}$	[Al] ppm	Al Rate $g_{glass}\ m^{-2}\ d^{-1}$
1	C44IX70-1D1	55	70	2.50E-05	1	7	0.77	0.01537	19.055	1.8138	3.3672	2.3678	77.8980	1.6996	2.4322	1.8270	0.0981	0.0063
	C44IX70-1D2	55	70	2.50E-05	2	7	0.77	0.01517	23.000	1.3000	4.2161	1.8058	91.5780	1.1653	2.8915	1.2909	0.1017	0.0035
	C44IX70-1D3	55	70	2.50E-05	3	7	0.77	0.01495	21.500	0.9792	3.8370	1.2507	84.3220	0.8648	2.7835	1.0378	0.0986	0.0031
	C44IX70-1D4	55	70	2.50E-05	4	7	0.77	0.01474	19.812	0.8998	3.4816	1.1464	80.4630	0.8716	2.5614	0.9149	0.0920	0.0028
	C44IX70-1D5	55	70	2.50E-05	5	7	0.77	0.01455	18.539	0.8685	3.1785	1.0684	75.5920	0.8150	2.3380	0.8339	0.0876	0.0027
	C44IX70-1D6	55	70	2.50E-05	6	7	0.77	0.01437	16.874	**0.7746**	2.9328	1.0108	68.8450	0.7241	2.2572	0.8703	0.0899	0.0031
	C44IX70-1D7	55	70	2.50E-05	7	7	0.77	0.01420	16.443	**0.8253**	2.8576	1.0592	68.5330	0.8054	2.1807	0.8500	0.0854	0.0027
	C44IX70-1D8	55	70	2.50E-05	8	7	0.77	0.01403	16.198	**0.8320**	2.7627	**1.0276**	68.2210	0.8113	2.1175	**0.8387**	0.2027	**0.0133**
	C44IX70-1D9	55	70	2.50E-05	9	7	0.77	0.01387	15.255	**0.7552**	2.5528	**0.9129**	63.1270	**0.7008**	2.0475	**0.8152**	0.4601	**0.0313**
	C44IX70-1D10	55	70	2.50E-05	10	7	0.77	0.01371	14.062	**0.6865**	2.4018	**0.8867**	58.0560	**0.6466**	2.0037	**0.8165**	0.0786	**-0.0146**
2	C44IX70-2D1	60	70	2.50E-05	1	8	0.77	0.01542	9.518	0.9031	1.4695	1.0267	39.8820	0.8631	1.1338	0.8502	0.1322	0.00756
	C44IX70-2D2	60	70	2.50E-05	2	8	0.77	0.01532	12.037	0.6954	1.8761	0.8042	48.5960	0.6262	1.3917	0.6310	0.1310	0.00371
	C44IX70-2D3	60	70	2.50E-05	3	8	0.77	0.01520	11.020	0.4814	1.7641	0.5858	45.8700	0.4739	1.3075	0.4667	0.1189	0.00280
	C44IX70-2D4	60	70	2.50E-05	4	8	0.77	0.01509	10.651	0.4984	1.6484	0.5471	43.7570	0.4605	1.2615	0.4669	0.1169	0.00315
	C44IX70-2D5	60	70	2.50E-05	5	8	0.77	0.01499	10.291	0.4847	1.6438	0.5894	43.0480	0.4716	1.2826	0.5056	0.1196	0.00348
	C44IX70-2D6	60	70	2.50E-05	6	8	0.77	0.01489	9.816	0.4590	1.4918	**0.4845**	41.7580	0.4536	1.2066	**0.4390**	0.1095	**0.00255**
	C44IX70-2D7	60	70	2.50E-05	7	8	0.77	0.01479	9.313	**0.4356**	1.4395	**0.5050**	38.6080	**0.3994**	1.1724	**0.4449**	0.1091	**0.00295**
	C44IX70-2D8	60	70	2.50E-05	8	8	0.77	0.01470	9.162	**0.4484**	1.4297	**0.5202**	39.2620	**0.4530**	1.1671	**0.4574**	0.1110	**0.00315**
	C44IX70-2D9	60	70	2.50E-05	9	8	0.77	0.01461	8.599	**0.4024**	1.3021	**0.4325**	36.7920	**0.3913**	1.0619	**0.3756**	0.1048	**0.00257**
	C44IX70-2D10	60	70	2.50E-05	10	8	0.77	0.01453	7.865	**0.3590**	1.2088	**0.4130**	34.1510	**0.3609**	1.0342	**0.3984**	0.0951	**0.00202**
3	C44IX70-3D1	80	70	2.50E-05	1	9	0.77	0.01545	2.587	0.2446	0.3780	0.2590	13.2690	0.2242	0.2984	0.1891	0.0994	0.0041
	C44IX70-3D2	80	70	2.50E-05	2	9	0.77	0.01543	3.213	0.1820	0.4495	0.1799	14.5320	0.1675	0.3332	0.1219	0.0997	0.0021
	C44IX70-3D3	80	70	2.50E-05	3	9	0.77	0.01540	3.109	0.1426	0.4283	0.1403	14.2870	0.1487	0.3364	0.1110	0.0980	0.0019
	C44IX70-3D4	80	70	2.50E-05	4	9	0.77	0.01537	3.103	0.1473	0.4383	0.1550	13.7640	0.1402	0.3473	0.1186	0.0970	0.0019
	C44IX70-3D5	80	70	2.50E-05	5	9	0.77	0.01534	3.012	0.1393	0.4067	0.1295	13.1700	0.1332	0.3192	0.0924	0.0861	0.0011
	C44IX70-3D6	80	70	2.50E-05	6	9	0.77	0.01531	2.811	0.1247	0.3833	0.1244	12.3540	0.1220	0.3312	0.1131	0.0818	**0.0012**
	C44IX70-3D7	80	70	2.50E-05	7	9	0.77	0.01528	2.655	**0.1195**	0.3729	0.1255	11.8220	0.1195	0.2963	**0.0810**	0.0800	**0.0012**
	C44IX70-3D8	80	70	2.50E-05	8	9	0.77	0.01525	2.575	**0.1196**	0.3547	**0.1165**	11.3400	**0.1149**	0.2925	**0.0919**	0.0785	**0.0012**
	C44IX70-3D9	80	70	2.50E-05	9	9	0.77	0.01523	2.512	**0.1175**	0.3436	**0.1152**	11.1780	**0.1168**	0.2655	**0.0722**	0.1930	0.0106
	C44IX70-3D10	80	70	2.50E-05	10	9	0.77	0.01520	2.321	**0.1024**	0.3074	**0.0936**	10.4050	**0.1017**	0.2772	**0.0923**	0.0688	-0.0043
4	C44IX70-4D1	140	70	2.50E-05	1	10	0.50	0.00994	0.861	0.1263	0.1396	0.1427	5.6274	0.1852	0.1691	0.1591	0.1765	0.0156
	C44IX70-4D2	140	70	2.50E-05	2	10	0.50	0.00993	0.833	0.0591	0.1266	0.0572	5.0624	0.0713	0.1856	0.0995	0.1086	-0.0007
	C44IX70-4D3	140	70	2.50E-05	3	10	0.50	0.00992	0.775	0.0526	0.1130	0.0495	4.3158	0.0556	0.1683	0.0687	0.1002	0.0025
	C44IX70-4D4	140	70	2.50E-05	4	10	0.50	0.00991	1.018	0.0929	0.1456	0.0925	5.1119	0.0954	0.2026	0.1209	0.4119	0.0421
	C44IX70-4D5	140	70	2.50E-05	5	10	0.50	0.00991	0.786	0.0406	0.1092	0.0351	3.9431	0.0422	0.1690	0.0592	0.0905	-0.0177
	C44IX70-4D6	140	70	2.50E-05	6	10	0.50	0.00990	0.841	0.0660	0.1076	0.0532	3.9483	0.0623	0.1752	0.0873	0.0868	**0.0020**
	C44IX70-4D7	140	70	2.50E-05	7	10	0.50	0.00989	0.885	0.0686	0.1090	0.0557	3.9019	0.0607	0.1766	**0.0853**	0.0815	**0.0015**
	C44IX70-4D8	140	70	2.50E-05	8	10	0.50	0.00988	0.978	**0.0791**	0.1292	**0.0771**	4.3368	**0.0763**	0.1728	**0.0799**	0.0808	**0.0018**
	C44IX70-4D9	140	70	2.50E-05	9	10	0.50	0.00987	1.070	**0.0859**	0.1415	**0.0796**	4.7584	**0.0834**	0.1794	**0.0904**	0.1478	0.0103
	C44IX70-4D10	140	70	2.50E-05	10	10	0.50	0.00986	1.009	**0.0700**	0.1401	**0.0714**	4.6935	**0.0741**	0.1980	0.1092	0.0752	-0.0031
5	C44IX70-5D1	360	70	2.50E-05	1	11	0.50	0.00994	0.509	0.0744	0.0950	0.0997	4.5673	0.1184	0.0440	-0.0221	0.1208	0.0057
	C44IX70-5D2	360	70	2.50E-05	2	11	0.50	0.00994	0.449	0.0284	0.0756	0.0287	3.9926	0.0397	0.0367	-0.0200	0.1054	0.0009
	C44IX70-5D3	360	70	2.50E-05	3	11	0.50	0.00993	0.408	0.0269	0.0630	0.0256	3.3360	0.0272	0.0398	-0.0118	0.0993	0.0011
	C44IX70-5D4	360	70	2.50E-05	4	11	0.50	0.00993	0.352	0.0215	0.0457	0.0135	2.9897	0.0266	0.0664	0.0187	0.0879	0.0001
	C44IX70-5D5	360	70	2.50E-05	5	11	0.50	0.00993	0.342	0.0243	0.0398	0.0166	2.6742	0.0218	0.0351	-0.0355	0.0849	0.0004
	C44IX70-5D6	360	70	2.50E-05	6	11	0.50	0.00992	0.347	0.0257	0.0389	0.0188	2.6341	0.0258	0.0288	-0.0241	0.1236	0.0054
	C44IX70-5D7	360	70	2.50E-05	7	11	0.50	0.00992	0.297	0.0179	0.0371	0.0174	2.3484	0.0168	0.0331	-0.0152	0.0817	-0.0022
	C44IX70-5D8	360	70	2.50E-05	8	11	0.50	0.00992	0.253	**0.0152**	0.0344	**0.0154**	2.2168	**0.0172**	0.0439	-0.0046	0.0791	**0.0001**
	C44IX70-5D9	360	70	2.50E-05	9	11	0.50	0.00991	0.132	0.0006	0.0292	**0.0111**	2.1798	**0.0182**	0.0173	-0.0435	0.0795	**0.0003**
	C44IX70-5D10	360	70	2.50E-05	10	11	0.50	0.00991	0.158	**0.0133**	0.0280	**0.0127**	2.0672	**0.0150**	0.0192	-0.0251	0.0815	**0.0005**

Table A8. DCP-AES Analysis Results from Dissolution of Glass ORLEC44 at 40 °C.

Exp.	Sample ID	Inf [Si] ppm	T °C	Flow Rate, m^3/d	Time, days	pH 23°C	Glass Mass g	SA m^2	[B] ppm	B Rate $g_{glass}\ m^{-2}\ d^{-1}$	[Li] ppm	Li Rate $g_{glass}\ m^{-2}\ d^{-1}$	[Na] ppm	Na Rate $g_{glass}\ m^{-2}\ d^{-1}$	[K] ppm	K Rate $g_{glass}\ m^{-2}\ d^{-1}$	[Al] ppm	Al Rate $g_{glass}\ m^{-2}\ d^{-1}$
1	C44IX40-1D1	40	40	8.33E-06	3	7	1.65	0.03309	11.064	0.1631	1.6123	0.1754	42.0480	0.1423	1.0782	0.1275	0.0807	0.0008
	C44IX40-1D2	40	40	8.33E-06	6	7	1.65	0.03296	15.961	0.1544	2.2844	0.1616	55.4170	0.1170	1.4146	0.1050	0.0875	0.0005
	C44IX40-1D3	40	40	8.33E-06	9	7	1.65	0.03280	16.621	0.1285	2.4816	0.1471	59.2690	0.1079	1.5176	0.0976	0.0842	0.0004
	C44IX40-1D4	40	40	8.33E-06	12	7	1.65	0.03264	16.217	0.1182	2.4714	0.1358	58.9070	0.1006	1.4522	0.0837	0.0832	0.0004
	C44IX40-1D5	40	40	8.33E-06	15	7	1.65	0.03248	15.077	0.1046	2.2128	0.1083	55.9380	0.0914	1.3340	0.0735	0.0827	0.0004
	C44IX40-1D6	40	40	8.33E-06	18	7	1.65	0.03233	15.654	0.1225	2.2397	0.1263	54.0630	0.0905	1.4176	0.0916	0.1065	0.0007
	C44IX40-1D7	40	40	8.33E-06	21	7	1.65	0.03217	15.922	0.1227	2.3821	0.1413	55.3100	0.0985	1.5869	0.1079	3.1884	0.0403
	C44IX40-1D8	40	40	8.33E-06	24	7	1.65	0.03202	13.652	**0.0867**	1.9701	**0.0876**	47.4690	**0.0693**	1.2298	**0.0530**	0.1797	-0.0184
	C44IX40-1D9	40	40	8.33E-06	27	7	1.65	0.03189	12.689	**0.0897**	1.8004	**0.0920**	45.8370	**0.0776**	1.2279	**0.0755**	0.1736	0.0010
	C44IX40-1D10	40	40	8.33E-06	30	7	1.65	0.03177	12.011	**0.0870**	1.7114	**0.0919**	43.3500	**0.0720**	1.1684	**0.0684**	0.0782	-0.0002
2	C44IX40-2D1	45	40	8.33E-06	3	8	1.65	0.03313	3.811	0.0561	0.5458	0.0591	16.2760	0.0548	0.4373	0.0509	0.0967	0.00097
	C44IX40-2D2	45	40	8.33E-06	6	8	1.65	0.03309	4.294	0.0352	0.6333	0.0391	16.4750	0.0281	0.4838	0.0311	0.1000	0.00053
	C44IX40-2D3	45	40	8.33E-06	9	8	1.65	0.03304	4.413	0.0334	0.6663	0.0380	16.6150	0.0283	0.4911	0.0292	0.0934	0.00042
	C44IX40-2D4	45	40	8.33E-06	12	8	1.65	0.03298	8.090	*outlier*	1.0834	*outlier*	31.0140	*outlier*	0.9905	*outlier*	4.0849	*outlier*
	C44IX40-2D5	45	40	8.33E-06	15	8	1.65	0.03292	4.200	0.0295	0.6128	0.0305	16.3440	0.0272	0.4840	0.0280	0.0779	0.00027
	C44IX40-2D6	45	40	8.33E-06	18	8	1.65	0.03288	4.181	0.0308	0.6086	0.0330	16.2800	0.0275	0.4871	0.0288	0.1023	0.00068
	C44IX40-2D7	45	40	8.33E-06	21	8	1.65	0.03284	3.839	**0.0260**	0.5404	**0.0257**	15.2600	**0.0242**	0.4335	0.0221	0.0752	0.00018
	C44IX40-2D8	45	40	8.33E-06	24	8	1.65	0.03280	3.791	**0.0278**	0.5564	**0.0313**	14.9210	**0.0248**	0.4429	**0.0266**	0.0677	**0.00026**
	C44IX40-2D9	45	40	8.33E-06	27	8	1.65	0.03277	3.735	**0.0274**	0.5170	**0.0261**	14.6040	**0.0243**	0.4158	**0.0227**	0.0663	**0.00029**
	C44IX40-2D10	45	40	8.33E-06	30	8	1.65	0.03273	3.549	**0.0250**	0.5039	**0.0269**	14.4830	**0.0244**	0.4059	**0.0232**	0.0672	**0.00031**
3	C44IX40-3D1	60	40	8.33E-06	3	9	1.65	0.03314	1.718	0.0253	0.1874	0.0200	5.9213	0.0164	0.1630	0.0153	0.5533	0.0066
	C44IX40-3D2	60	40	8.33E-06	6	9	1.65	0.03312	1.748	0.0131	0.2699	0.0190	9.5334	0.0221	0.1743	0.0090	0.0898	-0.0025
	C44IX40-3D3	60	40	8.33E-06	9	9	1.65	0.03310	1.695	0.0121	0.2460	0.0119	8.2254	0.0115	0.1606	0.0067	0.0813	0.0003
	C44IX40-3D4	60	40	8.33E-06	12	9	1.65	0.03306	6.533	*outlier*	1.0299	*outlier*	27.7200	*outlier*	0.8612	*outlier*	6.0159	*outlier*
	C44IX40-3D5	60	40	8.33E-06	15	9	1.65	0.03302	1.326	0.0070	0.2032	0.0086	6.5903	0.0082	0.1334	0.0043	0.0711	0.0002
	C44IX40-3D6	60	40	8.33E-06	18	9	1.65	0.03301	1.286	0.0092	0.1479	0.0049	5.0363	0.0057	0.1092	0.0030	0.0947	0.0006
	C44IX40-3D7	60	40	8.33E-06	21	9	1.65	0.03300	1.305	0.0098	0.1299	**0.0059**	4.2692	0.0057	0.1075	0.0042	0.0536	-0.0001
	C44IX40-3D8	60	40	8.33E-06	24	9	1.65	0.03299	1.212	**0.0082**	0.1191	**0.0057**	4.1113	**0.0065**	0.1059	**0.0041**	0.0534	**0.0002**
	C44IX40-3D9	60	40	8.33E-06	27	9	1.65	0.03297	1.183	**0.0085**	0.1168	**0.0061**	4.0651	**0.0066**	0.0978	**0.0032**	0.0481	**0.0001**
	C44IX40-3D10	60	40	8.33E-06	30	9	1.65	0.03296	1.101	**0.0075**	0.1183	**0.0064**	4.0171	**0.0066**	0.1055	**0.0047**	0.0482	**0.0002**
4	C44IX40-4D1	105	40	8.33E-06	3	10	0.83	0.01659	0.544	0.0159	0.0917	0.0192	4.2180	0.0276	0.0690	0.0075	0.1182	0.0017
	C44IX40-4D2	105	40	8.33E-06	6	10	0.83	0.01658	0.482	0.0061	0.0758	0.0061	3.2900	0.0071	0.0610	0.0018	0.0891	0.0001
	C44IX40-4D3	105	40	8.33E-06	9	10	0.83	0.01658	0.384	0.0042	0.0614	0.0047	2.5648	0.0054	0.0560	0.0016	0.0742	0.0001
	C44IX40-4D4	105	40	8.33E-06	12	10	0.83	0.01657	1.561	*outlier*	0.2316	*outlier*	7.3933	*outlier*	0.2018	*outlier*	1.5206	*outlier*
	C44IX40-4D5	105	40	8.33E-06	15	10	0.83	0.01656	0.271	0.0023	0.0383	0.0013	1.7744	0.0025	0.0422	-0.0012	0.0642	0.0001
	C44IX40-4D6	105	40	8.33E-06	18	10	0.83	0.01656	0.249	0.0033	0.0300	-0.0191	1.5617	0.0037	0.0358	-0.0010	0.0563	0.0000
	C44IX40-4D7	105	40	8.33E-06	21	10	0.83	0.01656	0.215	**0.0026**	0.0301	0.0029	1.4524	0.0037	0.0423	0.0013	0.0527	0.0000
	C44IX40-4D8	105	40	8.33E-06	24	10	0.83	0.01656	0.225	**0.0034**	0.0318	0.0033	1.3184	**0.0031**	0.0393	-0.0002	0.0509	0.0000
	C44IX40-4D9	105	40	8.33E-06	27	10	0.83	0.01655	0.222	**0.0032**	0.0256	**0.0017**	1.2414	**0.0031**	0.0384	-0.0001	0.0485	0.0000
	C44IX40-4D10	105	40	8.33E-06	30	10	0.83	0.01655	0.200	**0.0026**	0.0285	**0.0030**	1.2256	**0.0032**	0.0505	0.0030	0.0502	0.0000
5	C44IX40-5D1	270	40	8.33E-06	3	11	0.83	0.01659	0.595	0.0174	0.0928	0.0194	4.3953	0.0249	0.0721	0.0094	0.1948	0.0036
	C44IX40-5D2	270	40	8.33E-06	6	11	0.83	0.01658	0.562	0.0077	0.0882	0.0087	3.7431	0.0080	0.0599	0.0018	0.1850	0.0015
	C44IX40-5D3	270	40	8.33E-06	9	11	0.83	0.01658	0.439	0.0046	0.0757	0.0065	2.9831	0.0051	0.0639	0.0042	0.1640	0.0011
	C44IX40-5D4	270	40	8.33E-06	12	11	0.83	0.01658	0.359	0.0040	0.0664	0.0058	2.4026	0.0037	0.0721	0.0057	0.1422	0.0009
	C44IX40-5D5	270	40	8.33E-06	15	11	0.83	0.01657	0.334	0.0045	0.0576	0.0049	2.0051	0.0030	0.0446	-0.0019	0.1203	0.0006
	C44IX40-5D6	270	40	8.33E-06	18	11	0.83	0.01657	0.323	0.0046	0.0504	0.0043	1.7450	0.0026	0.0462	0.0018	0.1137	0.0007
	C44IX40-5D7	270	40	8.33E-06	21	11	0.83	0.01657	0.211	**0.0014**	0.0442	**0.0037**	1.5557	0.0022	0.0578	0.0044	0.0999	0.0004
	C44IX40-5D8	270	40	8.33E-06	24	11	0.83	0.01656	0.172	**0.0019**	0.0440	**0.0044**	1.4146	**0.0019**	0.0436	-0.0004	0.0862	**0.0003**
	C44IX40-5D9	270	40	8.33E-06	27	11	0.83	0.01656	0.168	**0.0024**	0.0272	0.0008	1.3379	**0.0018**	0.0392	0.0002	0.0858	**0.0004**
	C44IX40-5D10	270	40	8.33E-06	30	11	0.83	0.01656	0.105	0.0006	0.0405	**0.0055**	1.2824	**0.0017**	0.0432	0.0017	0.0759	**0.0002**

Table A9. DCP-AES Analysis Results from Dissolution of Glass ORLEC44 at 23 °C.

Exp.	Sample ID	Inf [Si] ppm	T °C	Flow Rate, m^3/d	Time, days	pH 23°C	Glass Mass g	SA m^2	[B] ppm	B Rate $g_{glass}\ m^{-2}\ d^{-1}$	[Li] ppm	Li Rate $g_{glass}\ m^{-2}\ d^{-1}$	[Na] ppm	Na Rate $g_{glass}\ m^{-2}\ d^{-1}$	[K] ppm	K Rate $g_{glass}\ m^{-2}\ d^{-1}$	[Al] ppm	Al Rate $g_{glass}\ m^{-2}\ d^{-1}$
1	C44IX23-1D1	35	23	8.33E-06	3	7	3.28	0.0658	2.622	0.0194	0.4022	0.0218	14.5450	0.0246	0.2445	0.0123	0.0310	0.0001
	C44IX23-1D2	35	23	8.33E-06	6	7	3.28	0.0658	2.808	0.0111	0.4183	0.0118	13.2550	0.0101	0.2308	0.0053	0.0327	0.0001
	C44IX23-1D3	35	23	8.33E-06	9	7	3.28	0.0658	2.860	0.0108	0.4326	0.0122	12.2260	0.0094	0.2498	0.0069	0.0310	0.0000
	C44IX23-1D4	35	23	8.33E-06	12	7	3.28	0.0658	2.826	0.0103	0.4259	0.0114	11.6470	0.0093	0.2526	0.0065	0.0341	0.0001
	C44IX23-1D5	35	23	8.33E-06	15	7	3.28	0.0657	2.857	0.0107	0.4212	0.0113	11.1130	0.0089	0.2522	0.0064	0.0317	0.0000
	C44IX23-1D6	35	23	8.33E-06	18	7	3.28	0.0657	7.281	outlier	1.1646	outlier	30.2060	outlier	0.9067	outlier	5.6774	outlier
	C44IX23-1D7	35	23	8.33E-06	21	7	3.28	0.0656	2.994	0.0116	0.4147	0.0111	11.0920	0.0094	0.2525	0.0141	0.0309	0.0001
	C44IX23-1D8	35	23	8.33E-06	24	7	3.28	0.0656	3.209	**0.0127**	0.4304	**0.0122**	12.1280	0.0112	0.2711	**0.0075**	0.0310	**0.0000**
	C44IX23-1D9	35	23	8.33E-06	27	7	3.28	0.0656	3.378	**0.0132**	0.4500	**0.0128**	12.5760	**0.0110**	0.2901	**0.0081**	0.0328	**0.0001**
	C44IX23-1D10	35	23	8.33E-06	30	7	3.28	0.0655	3.379	**0.0126**	0.4556	**0.0126**	12.3940	**0.0103**	0.2751	**0.0066**	0.0311	**0.0000**
2	C44IX23-2D1	40	23	8.33E-06	3	8	3.28	0.0658	1.423	0.0105	0.2296	0.0124	9.9755	0.0168	0.1703	0.0081	0.0395	0.00013
	C44IX23-2D2	40	23	8.33E-06	6	8	3.28	0.0658	1.249	0.0040	0.1877	0.0039	7.9594	0.0050	0.1708	0.0041	0.0426	0.00008
	C44IX23-2D3	40	23	8.33E-06	9	8	3.28	0.0658	1.054	0.0032	0.1663	0.0039	6.2464	0.0038	0.1510	0.0029	0.0428	0.00008
	C44IX23-2D4	40	23	8.33E-06	12	8	3.28	0.0658	0.919	0.0029	0.1389	0.0030	5.0635	0.0032	0.1383	0.0027	0.0450	0.00009
	C44IX23-2D5	40	23	8.33E-06	15	8	3.28	0.0658	0.817	0.0026	0.1287	0.0032	4.3349	0.0030	0.1092	0.0013	0.0475	0.00010
	C44IX23-2D6	40	23	8.33E-06	18	8	3.28	0.0658	0.730	0.0024	0.1200	0.0030	4.0441	0.0031	0.1204	0.0029	0.0428	0.00006
	C44IX23-2D7	40	23	8.33E-06	21	8	3.28	0.0658	0.721	**0.0026**	0.0989	0.0020	3.4025	0.0022	0.1398	0.0037	0.0453	0.00009
	C44IX23-2D8	40	23	8.33E-06	24	8	3.28	0.0658	0.709	**0.0026**	0.1196	0.0038	3.5678	**0.0031**	0.1473	**0.0036**	0.0399	**0.00005**
	C44IX23-2D9	40	23	8.33E-06	27	8	3.28	0.0658	0.698	**0.0025**	0.1110	**0.0027**	3.4103	**0.0027**	0.1233	**0.0019**	0.0435	**0.00009**
	C44IX23-2D10	40	23	8.33E-06	30	8	3.28	0.0658	0.770	0.0031	0.1128	**0.0030**	3.4495	**0.0029**	0.1338	**0.0033**	0.0426	**0.00007**
3	C44IX23-3D1	52	23	8.33E-06	3	9	3.28	0.0658	0.885	0.0065	0.1571	0.0084	7.9114	0.0129	0.1870	0.0102	0.1144	0.0006
	C44IX23-3D2	52	23	8.33E-06	6	9	3.28	0.0658	0.646	0.0015	0.1206	0.0022	5.6815	0.0028	0.1761	0.0044	0.0988	0.0002
	C44IX23-3D3	52	23	8.33E-06	9	9	3.28	0.0658	0.574	0.0018	0.0899	0.0015	4.6019	0.0029	0.1503	0.0032	0.0755	0.0001
	C44IX23-3D4	52	23	8.33E-06	12	9	3.28	0.0658	0.482	0.0014	0.0728	0.0014	3.5641	0.0020	0.1209	0.0022	0.0649	0.0001
	C44IX23-3D5	52	23	8.33E-06	15	9	3.28	0.0658	0.424	0.0013	0.0642	0.0014	2.9694	0.0019	0.1211	0.0031	0.0582	0.0001
	C44IX23-3D6	52	23	8.33E-06	18	9	3.28	0.0658	0.359	0.0011	0.0600	0.0014	2.5758	0.0018	0.1449	0.0045	0.0548	0.0001
	C44IX23-3D7	52	23	8.33E-06	21	9	3.28	0.0658	0.354	0.0013	0.0597	0.0015	2.2834	0.0016	0.1221	0.0024	0.0500	0.0001
	C44IX23-3D8	52	23	8.33E-06	24	9	3.28	0.0658	0.341	**0.0012**	0.0626	0.0017	2.2157	**0.0017**	0.1052	**0.0021**	0.0470	**0.0001**
	C44IX23-3D9	52	23	8.33E-06	27	9	3.28	0.0658	0.310	**0.0010**	0.0502	**0.0009**	2.0633	**0.0015**	0.1038	**0.0025**	0.0455	**0.0001**
	C44IX23-3D10	52	23	8.33E-06	30	9	3.28	0.0658	0.214	**0.0004**	0.0502	**0.0013**	1.9474	**0.0015**	0.0918	**0.0018**	0.0377	**0.0000**
4	C44IX23-4D1	90	23	8.33E-06	3	10	1.64	0.0329	0.422	0.0062	0.0714	0.0074	3.6190	0.0118	0.0668	0.0050	0.0823	0.0005
	C44IX23-4D2	90	23	8.33E-06	6	10	1.64	0.0329	0.285	0.0011	0.0524	0.0016	2.4764	0.0019	0.0007	-0.0055	0.0668	0.0000
	C44IX23-4D3	90	23	8.33E-06	9	10	1.64	0.0329	0.231	0.0013	0.0324	0.0005	1.8657	0.0018	0.0274	0.0017	0.0590	0.0000
	C44IX23-4D4	90	23	8.33E-06	12	10	1.64	0.0329	0.200	0.0012	0.0203	0.0003	1.5486	0.0018	0.0085	-0.0022	0.0569	0.0001
	C44IX23-4D5	90	23	8.33E-06	15	10	1.64	0.0329	0.212	0.0016	0.0343	0.0025	1.2185	0.0012	0.0365	0.0024	0.0595	0.0001
	C44IX23-4D6	90	23	8.33E-06	18	10	1.64	0.0329	0.167	0.0009	0.0183	-0.0001	1.0820	0.0013	0.0264	-0.0006	0.0478	-0.0001
	C44IX23-4D7	90	23	8.33E-06	21	10	1.64	0.0329	0.169	0.0012	0.0205	0.0011	0.9752	0.0012	0.0264	0.0001	0.0658	0.0002
	C44IX23-4D8	90	23	8.33E-06	24	10	1.64	0.0329	0.154	**0.0010**	0.0227	0.0012	0.8870	**0.0010**	0.0224	-0.0004	0.0355	-0.0003
	C44IX23-4D9	90	23	8.33E-06	27	10	1.64	0.0329	0.119	**0.0006**	0.0215	**0.0009**	0.8439	**0.0010**	0.0102	-0.0017	0.0466	**0.0001**
	C44IX23-4D10	90	23	8.33E-06	30	10	1.64	0.0329	0.169	**0.0016**	0.0296	**0.0019**	0.8144	**0.0010**	0.0489	0.0038	0.0619	**0.0002**
5	C44IX23-5D1	230	23	8.33E-06	3	11	1.64	0.0329	0.596	0.0088	0.0910	0.0096	4.8550	0.0133	0.0895	0.0038	0.4880	0.0051
	C44IX23-5D2	230	23	8.33E-06	6	11	1.64	0.0329	0.289	-0.0002	0.0435	-0.0004	3.0072	0.0004	0.0728	-0.0002	0.1375	-0.0018
	C44IX23-5D3	230	23	8.33E-06	9	11	1.64	0.0329	0.242	0.0014	0.0257	0.0002	2.4857	0.0017	0.0634	-0.0003	0.1274	0.0002
	C44IX23-5D4	230	23	8.33E-06	12	11	1.64	0.0329	1.109	outlier	0.1614	outlier	6.1226	outlier	0.1533	outlier	1.2108	outlier
	C44IX23-5D5	230	23	8.33E-06	15	11	1.64	0.0329	0.211	0.0013	0.0217	0.0008	2.0590	0.0012	0.0718	0.0013	0.1279	0.0003
	C44IX23-5D6	230	23	8.33E-06	18	11	1.64	0.0329	0.214	0.0016	0.0076	-0.0005	1.9898	0.0017	0.0405	-0.0030	0.1183	0.0002
	C44IX23-5D7	230	23	8.33E-06	21	11	1.64	0.0329	0.207	0.0015	0.0214	0.0017	1.7984	0.0011	0.0588	0.0011	0.1176	0.0002
	C44IX23-5D8	230	23	8.33E-06	24	11	1.64	0.0329	0.184	**0.0012**	0.0235	0.0012	1.7559	0.0013	0.0879	0.0036	0.1182	**0.0002**
	C44IX23-5D9	230	23	8.33E-06	27	11	1.64	0.0329	0.156	**0.0009**	0.0282	**0.0016**	1.5676	**0.0007**	0.1010	0.0034	0.1164	**0.0002**
	C44IX23-5D10	230	23	8.33E-06	30	11	1.64	0.0329	<DL	-	0.0298	**0.0015**	1.3933	**0.0005**	0.0867	0.0008	0.1152	**0.0002**

Table A10. ICP-MS Analysis Results from Dissolution of Glass AP107WDFL at 70 °C.

Exp.	Sample ID	Inf [Si] ppm	T °C	Flow Rate, m^3/d	Time, days	pH 23°C	Glass Mass g	SA m^2	[Mo] ppm	Mo Rate $g_{glass}\ m^{-2}\ d^{-1}$	[Cs] ppm	Cs Rate $g_{glass}\ m^{-2}\ d^{-1}$	[Re] ppm	Re Rate $g_{glass}\ m^{-2}\ d^{-1}$
1	A107IX70-1D1	55	70	2.50E-05	1	7	0.77	0.01523	0.01181	0.0715	0.05360	0.1435	0.0326	0.1072
	A107IX70-1D2	55	70	2.50E-05	2	7	0.77	0.01520	0.00784	0.0113	0.06203	0.0945	0.0300	0.0451
	A107IX70-1D3	55	70	2.50E-05	3	7	0.77	0.01518	0.00581	0.0111	0.06304	0.0860	0.0237	0.0288
	A107IX70-1D4	55	70	2.50E-05	4	7	0.77	0.01515	0.00729	0.0265	0.06081	0.0788	0.0234	0.0381
	A107IX70-1D5	55	70	2.50E-05	5	7	0.77	0.01513	0.00231	-0.0089	0.05853	0.0758	0.0156	0.0128
	A107IX70-1D6	55	70	2.50E-05	6	7	0.77	0.01510	0.00195	0.0043	0.05937	0.0813	0.0138	0.0200
	A107IX70-1D7	55	70	2.50E-05	7	7	0.77	0.01508	0.00146	0.0024	0.05096	**0.0575**	0.0110	**0.0135**
	A107IX70-1D8	55	70	2.50E-05	8	7	0.77	0.01506	0.00111	0.0018	0.05001	**0.0664**	0.0097	**0.0142**
	A107IX70-1D9	55	70	2.50E-05	9	7	0.77	0.01504	0.00116	**0.0032**	0.05220	**0.0738**	0.0095	**0.0154**
	A107IX70-1D10	55	70	2.50E-05	10	7	0.77	0.01501	0.00106	0.0024	0.04800	**0.0595**	0.0081	**0.0110**
2	A107IX70-2D1	60	70	2.50E-05	1	8	0.77	0.01523	0.00814	0.0489	0.02760	0.0738	0.0181	0.0594
	A107IX70-2D2	60	70	2.50E-05	2	8	0.77	0.01522	0.00523	0.0066	0.02609	0.0329	0.0149	0.0191
	A107IX70-2D3	60	70	2.50E-05	3	8	0.77	0.01521	0.00291	0.0012	0.02016	0.0191	0.0094	0.0063
	A107IX70-2D4	60	70	2.50E-05	4	8	0.77	0.01520	0.00297	0.0087	0.02610	0.0430	0.0107	0.0196
	A107IX70-2D5	60	70	2.50E-05	5	8	0.77	0.01519	0.00104	-0.0033	0.01146	-0.0043	0.0040	-0.0045
	A107IX70-2D6	60	70	2.50E-05	6	8	0.77	0.01518	0.00168	0.0066	0.02100	0.0410	0.0063	0.0142
	A107IX70-2D7	60	70	2.50E-05	7	8	0.77	0.01518	0.00119	0.0016	0.01506	0.0122	0.0045	0.0044
	A107IX70-2D8	60	70	2.50E-05	8	8	0.77	0.01517	0.00116	**0.0029**	0.01796	**0.0280**	0.0044	**0.0072**
	A107IX70-2D9	60	70	2.50E-05	9	8	0.77	0.01516	0.00075	**0.0005**	0.01218	**0.0086**	0.0029	**0.0021**
	A107IX70-2D10	60	70	2.50E-05	10	8	0.77	0.01515	0.00072	**0.0015**	0.01070	**0.0124**	0.0025	**0.0034**
3	A107IX70-3D1	80	70	2.50E-05	1	9	0.77	0.01524	0.00433	0.0254	0.00897	0.0239	0.0063	0.0207
	A107IX70-3D2	80	70	2.50E-05	2	9	0.77	0.01523	0.00233	0.0004	0.00581	0.0035	0.0038	0.0020
	A107IX70-3D3	80	70	2.50E-05	3	9	0.77	0.01523	0.00101	-0.0015	0.00289	-0.0001	0.0017	-0.0006
	A107IX70-3D4	80	70	2.50E-05	4	9	0.77	0.01522	0.00226	0.0102	0.00694	0.0147	0.0042	0.0110
	A107IX70-3D5	80	70	2.50E-05	5	9	0.77	0.01522	0.00444	0.0198	0.01054	0.0189	0.0069	0.0158
	A107IX70-3D6	80	70	2.50E-05	6	9	0.77	0.01522	0.00059	-0.0106	0.00220	-0.0083	0.0012	-0.0075
	A107IX70-3D7	80	70	2.50E-05	7	9	0.77	0.01521	0.00131	**0.0056**	0.00584	**0.0127**	0.0030	**0.0079**
	A107IX70-3D8	80	70	2.50E-05	8	9	0.77	0.01521	0.00072	-0.0002	0.00357	0.0017	0.0016	0.0003
	A107IX70-3D9	80	70	2.50E-05	9	9	0.77	0.01521	0.00104	**0.0036**	0.00510	**0.0089**	0.0023	**0.0048**
	A107IX70-3D10	80	70	2.50E-05	10	9	0.77	0.01520	0.00069	0.0005	0.00303	0.0013	0.0013	0.0005
4	A107IX70-4D1	140	70	2.50E-05	1	10	0.50	0.00979	0.00233	0.0207	0.00274	0.0114	0.0020	0.0102
	A107IX70-4D2	140	70	2.50E-05	2	10	0.50	0.00979	0.00183	0.0055	0.00296	0.0066	0.0020	0.0050
	A107IX70-4D3	140	70	2.50E-05	3	10	0.50	0.00979	0.00093	-0.0007	0.00178	0.0012	0.0011	0.0006
	A107IX70-4D4	140	70	2.50E-05	4	10	0.50	0.00979	0.00063	0.0007	0.00128	0.0016	0.0008	0.0010
	A107IX70-4D5	140	70	2.50E-05	5	10	0.50	0.00979	0.00090	0.0048	0.00177	0.0047	0.0010	0.0033
	A107IX70-4D6	140	70	2.50E-05	6	10	0.50	0.00979	0.00080	0.0026	0.00177	0.0037	0.0010	0.0026
	A107IX70-4D7	140	70	2.50E-05	7	10	0.50	0.00979	0.00060	**0.0011**	0.00138	**0.0021**	0.0008	**0.0014**
	A107IX70-4D8	140	70	2.50E-05	8	10	0.50	0.00979	0.00226	0.0180	0.00378	0.0128	0.0027	0.0117
	A107IX70-4D9	140	70	2.50E-05	9	10	0.50	0.00978	0.00073	-0.0046	0.00159	-0.0013	0.0010	-0.0020
	A107IX70-4D10	140	70	2.50E-05	10	10	0.50	0.00978	0.00041	-0.0004	0.00112	**0.0013**	0.0006	**0.0005**
5	A107IX70-5D1	360	70	2.50E-05	1	11	0.50	0.00979	0.00199	0.0184	0.00237	0.0098	0.0015	0.0076
	A107IX70-5D2	360	70	2.50E-05	2	11	0.50	0.00979	0.00034	-0.0066	0.00070	-0.0021	0.0004	-0.0021
	A107IX70-5D3	360	70	2.50E-05	3	11	0.50	0.00979	0.00020	-0.0001	0.00062	0.0011	0.0003	0.0005
	A107IX70-5D4	360	70	2.50E-05	4	11	0.50	0.00979	0.00028	0.0014	0.00083	0.0021	0.0004	0.0012
	A107IX70-5D5	360	70	2.50E-05	5	11	0.50	0.00978	0.00030	0.0012	0.00077	0.0014	0.0003	0.0007
	A107IX70-5D6	360	70	2.50E-05	6	11	0.50	0.00978	0.00023	0.0004	0.00059	0.0008	0.0003	0.0006
	A107IX70-5D7	360	70	2.50E-05	7	11	0.50	0.00978	0.00003	-0.0011	0.00023	-0.0003	0.0001	-0.0004
	A107IX70-5D8	360	70	2.50E-05	8	11	0.50	0.00978	0.00008	**0.0003**	0.00048	**0.0015**	0.0002	**0.0007**
	A107IX70-5D9	360	70	2.50E-05	9	11	0.50	0.00978	0.00002	-0.0002	0.00024	0.0000	0.0001	**0.0000**
	A107IX70-5D10	360	70	2.50E-05	10	11	0.50	0.00977	0.00002	**0.0001**	0.00028	**0.0006**	0.0001	**0.0001**

Table A11. ICP-MS Analysis Results from Dissolution of Glass AP107WDFL at 40 °C.

Exp.	Sample ID	Inf [Si] ppm	T °C	Flow Rate, m^3/d	Time, days	pH 23°C	Glass Mass g	SA m^2	[Mo] ppm	Mo Rate $g_{glass}\ m^{-2}\ d^{-1}$	[Cs] ppm	Cs Rate $g_{glass}\ m^{-2}\ d^{-1}$	[Re] ppm	Re Rate $g_{glass}\ m^{-2}\ d^{-1}$
1	A107IX40-1D1	40	40	8.33E-06	3	7	1.65	0.03265	0.00865	0.0074	0.02778	0.0116	0.0262	0.0134
	A107IX40-1D2	40	40	8.33E-06	6	7	1.65	0.03263	0.00439	-0.0004	0.01994	0.0025	0.0160	0.0015
	A107IX40-1D3	40	40	8.33E-06	9	7	1.65	0.03262	0.00396	0.0012	0.02675	0.0070	0.0182	0.0052
	A107IX40-1D4	40	40	8.33E-06	12	7	1.65	0.03261	0.00235	-0.0001	0.02001	0.0028	0.0121	0.0015
	A107IX40-1D5	40	40	8.33E-06	15	7	1.65	0.03260	0.00180	0.0002	0.01876	0.0036	0.0103	0.0022
	A107IX40-1D6	40	40	8.33E-06	18	7	1.65	0.03259	0.00163	0.0002	0.02162	0.0051	0.0101	0.0025
	A107IX40-1D7	40	40	8.33E-06	21	7	1.65	0.03258	0.00132	0.0000	0.01941	**0.0036**	0.0086	**0.0018**
	A107IX40-1D8	40	40	8.33E-06	24	7	1.65	0.03258	0.00098	-0.0001	0.01548	**0.0024**	0.0065	**0.0011**
	A107IX40-1D9	40	40	8.33E-06	27	7	1.65	0.03257	0.00107	**0.0001**	0.01844	**0.0045**	0.0072	**0.0020**
	A107IX40-1D10	40	40	8.33E-06	30	7	1.65	0.03256	0.00098	0.0000	0.01729	**0.0034**	0.0068	**0.0016**
2	A107IX40-2D1	45	40	8.33E-06	3	8	1.65	0.03265	0.00481	0.0041	0.01165	0.0048	0.0100	0.0051
	A107IX40-2D2	45	40	8.33E-06	6	8	1.65	0.03264	0.00331	0.0006	0.00908	0.0014	0.0074	0.0012
	A107IX40-2D3	45	40	8.33E-06	9	8	1.65	0.03264	0.00195	0.0001	0.00689	0.0010	0.0048	0.0006
	A107IX40-2D4	45	40	8.33E-06	12	8	1.65	0.03263	0.00192	0.0007	0.00760	0.0017	0.0049	0.0013
	A107IX40-2D5	45	40	8.33E-06	15	8	1.65	0.03263	0.00110	-0.0001	0.00477	0.0004	0.0030	0.0003
	A107IX40-2D6	45	40	8.33E-06	18	8	1.65	0.03263	0.00189	0.0011	0.00893	0.0027	0.0051	0.0018
	A107IX40-2D7	45	40	8.33E-06	21	8	1.65	0.03262	0.00138	0.0002	0.00684	**0.0010**	0.0038	0.0006
	A107IX40-2D8	45	40	8.33E-06	24	8	1.65	0.03262	0.00142	**0.0005**	0.00732	**0.0016**	0.0040	**0.0011**
	A107IX40-2D9	45	40	8.33E-06	27	8	1.65	0.03262	0.00111	**0.0002**	0.00615	**0.0010**	0.0032	**0.0006**
	A107IX40-2D10	45	40	8.33E-06	30	8	1.65	0.03262	0.00107	**0.0003**	0.00605	**0.0012**	0.0030	**0.0007**
3	A107IX40-3D1	60	40	8.33E-06	3	9	1.65	0.03265	0.00597	0.0054	0.01153	0.0048	0.0102	0.0052
	A107IX40-3D2	60	40	8.33E-06	6	9	1.65	0.03265	0.00349	0.0003	0.00758	0.0007	0.0062	0.0006
	A107IX40-3D3	60	40	8.33E-06	9	9	1.65	0.03264	0.00280	0.0008	0.00689	0.0013	0.0052	0.0011
	A107IX40-3D4	60	40	8.33E-06	12	9	1.65	0.03264	0.00196	0.0004	0.00517	0.0007	0.0036	0.0005
	A107IX40-3D5	60	40	8.33E-06	15	9	1.65	0.03264	0.00083	-0.0003	0.00248	0.0000	0.0016	-0.0001
	A107IX40-3D6	60	40	8.33E-06	18	9	1.65	0.03263	0.00164	0.0010	0.00524	0.0017	0.0032	0.0012
	A107IX40-3D7	60	40	8.33E-06	21	9	1.65	0.03263	0.00113	**0.0001**	0.00348	0.0004	0.0021	**0.0002**
	A107IX40-3D8	60	40	8.33E-06	24	9	1.65	0.03263	0.00077	0.0000	0.00259	**0.0003**	0.0015	**0.0002**
	A107IX40-3D9	60	40	8.33E-06	27	9	1.65	0.03263	0.00085	**0.0003**	0.00291	**0.0007**	0.0017	**0.0005**
	A107IX40-3D10	60	40	8.33E-06	30	9	1.65	0.03263	0.00129	**0.0007**	0.00420	**0.0011**	0.0025	**0.0008**
4	A107IX40-4D1	105	40	8.33E-06	3	10	0.83	0.01635	0.00426	0.0073	0.00584	0.0048	0.0051	0.0052
	A107IX40-4D2	105	40	8.33E-06	6	10	0.83	0.01634	0.00279	0.0009	0.00439	0.0012	0.0035	0.0010
	A107IX40-4D3	105	40	8.33E-06	9	10	0.83	0.01634	0.00133	-0.0005	0.00243	0.0002	0.0018	0.0000
	A107IX40-4D4	105	40	8.33E-06	12	10	0.83	0.01634	0.00089	0.0000	0.00178	0.0005	0.0012	0.0003
	A107IX40-4D5	105	40	8.33E-06	15	10	0.83	0.01634	0.00036	-0.0006	0.00080	-0.0001	0.0005	-0.0001
	A107IX40-4D6	105	40	8.33E-06	18	10	0.83	0.01634	0.00103	0.0012	0.00236	0.0016	0.0012	0.0010
	A107IX40-4D7	105	40	8.33E-06	21	10	0.83	0.01634	0.00051	-0.0004	0.00126	0.0001	0.0007	0.0000
	A107IX40-4D8	105	40	8.33E-06	24	10	0.83	0.01634	0.00026	-0.0004	0.00064	0.0000	0.0003	0.0000
	A107IX40-4D9	105	40	8.33E-06	27	10	0.83	0.01634	0.00031	-0.0001	0.00080	**0.0004**	0.0004	**0.0002**
	A107IX40-4D10	105	40	8.33E-06	30	10	0.83	0.01634	0.00027	-0.0002	0.00068	**0.00023**	0.0003	**0.0001**
5	A107IX40-5D1	270	40	8.33E-06	3	11	0.83	0.01634	0.00307	0.0052	0.00501	0.0041	0.0047	0.0048
	A107IX40-5D2	270	40	8.33E-06	6	11	0.83	0.01634	0.00217	0.0009	0.00380	0.0010	0.0036	0.0012
	A107IX40-5D3	270	40	8.33E-06	9	11	0.83	0.01634	0.00163	0.0007	0.00308	0.0009	0.0027	0.0010
	A107IX40-5D4	270	40	8.33E-06	12	11	0.83	0.01634	0.00138	0.0007	0.00294	0.0011	0.0024	0.0011
	A107IX40-5D5	270	40	8.33E-06	15	11	0.83	0.01633	0.00099	0.0002	0.00219	0.0006	0.0017	0.0005
	A107IX40-5D6	270	40	8.33E-06	18	11	0.83	0.01633	0.00174	0.0020	0.00361	0.0020	0.0029	0.0020
	A107IX40-5D7	270	40	8.33E-06	21	11	0.83	0.01633	0.00127	**0.0004**	0.00288	**0.0008**	0.0022	**0.0007**
	A107IX40-5D8	270	40	8.33E-06	24	11	0.83	0.01633	0.00117	**0.0007**	0.00274	**0.0010**	0.0020	**0.0009**
	A107IX40-5D9	270	40	8.33E-06	27	11	0.83	0.01633	0.00053	-0.0005	0.00133	-0.0001	0.0009	-0.0001
	A107IX40-5D10	270	40	8.33E-06	30	11	0.83	0.01633	0.00097	**0.0010**	0.00250	**0.0015**	0.0016	**0.0012**

Table A12. ICP-MS Analysis Results from Dissolution of Glass AP107WDFL at 23 °C.

Exp.	Sample ID	Inf [Si] ppm	T °C	Flow Rate, m^3/d	Time, days	pH 23°C	Glass Mass g	SA m^2	[Mo] ppm	Mo Rate $g_{glass}\ m^{-2}\ d^{-1}$	[Cs] ppm	Cs Rate $g_{glass}\ m^{-2}\ d^{-1}$	[Re] ppm	Re Rate $g_{glass}\ m^{-2}\ d^{-1}$
1	A107IX23-1D1	35	23	8.33E-06	3	7	3.28	0.06487	0.00883	0.0039	0.01325	0.0028	0.0172	0.0044
	A107IX23-1D2	35	23	8.33E-06	6	7	3.28	0.06486	0.00573	0.0004	0.01099	0.0009	0.0128	0.0011
	A107IX23-1D3	35	23	8.33E-06	9	7	3.28	0.06486	0.00397	0.0003	0.00985	0.0009	0.0091	0.0007
	A107IX23-1D4	35	23	8.33E-06	12	7	3.28	0.06486	0.00290	0.0002	0.00885	0.0008	0.0071	0.0006
	A107IX23-1D5	35	23	8.33E-06	15	7	3.28	0.06486	0.00222	0.0002	0.00786	0.0007	0.0058	0.0006
	A107IX23-1D6	35	23	8.33E-06	18	7	3.28	0.06486	0.00184	0.0002	0.00735	0.0007	0.0052	0.0006
	A107IX23-1D7	35	23	8.33E-06	21	7	3.28	0.06486	0.00163	0.0001	0.00680	**0.0006**	0.0044	**0.0004**
	A107IX23-1D8	35	23	8.33E-06	24	7	3.28	0.06486	0.00135	**0.0001**	0.00589	**0.0005**	0.0038	**0.0004**
	A107IX23-1D9	35	23	8.33E-06	27	7	3.28	0.06486	0.00143	**0.0002**	0.00694	**0.0008**	0.0041	**0.0006**
	A107IX23-1D10	35	23	8.33E-06	30	7	3.28	0.06486	0.00137	**0.0001**	0.00688	**0.0007**	0.0038	**0.0005**
2	A107IX23-2D3	40	23	8.33E-06	3	8	3.28	0.06487	0.00786	0.0036	0.01179	0.0025	0.0129	0.0033
	A107IX23-2D4	40	23	8.33E-06	6	8	3.28	0.06486	0.00517	0.0005	0.01026	0.0009	0.0090	0.0006
	A107IX23-2D5	40	23	8.33E-06	9	8	3.28	0.06486	0.00364	0.0004	0.00920	0.0009	0.0072	0.0007
	A107IX23-2D6	40	23	8.33E-06	12	8	3.28	0.06486	0.00238	0.0002	0.00731	0.0006	0.0051	0.0004
	A107IX23-2D7	40	23	8.33E-06	15	8	3.28	0.06486	0.00189	0.0002	0.00610	0.0005	0.0041	0.0004
	A107IX23-2D8	40	23	8.33E-06	18	8	3.28	0.06486	0.00166	0.0002	0.00581	0.0006	0.0036	0.0004
	A107IX23-2D9	40	23	8.33E-06	21	8	3.28	0.06485	0.00144	0.0002	0.00502	0.0004	0.0033	0.0004
	A107IX23-2D10	40	23	8.33E-06	24	8	3.28	0.06485	0.00128	**0.0002**	0.00478	**0.0005**	0.0030	**0.0003**
	A107IX23-2D11	40	23	8.33E-06	27	8	3.28	0.06485	0.00115	**0.0001**	0.00436	**0.0004**	0.0024	**0.0002**
	A107IX23-2D12	40	23	8.33E-06	30	8	3.28	0.06485	0.00099	**0.0001**	0.00358	**0.0003**	0.0020	**0.0002**
3	A107IX23-3D1	52	23	8.33E-06	3	9	3.28	0.06487	0.00606	0.0028	0.00726	0.0015	0.0091	0.0023
	A107IX23-3D2	52	23	8.33E-06	6	9	3.28	0.06487	0.00360	0.0002	0.00629	0.0006	0.0055	0.0003
	A107IX23-3D3	52	23	8.33E-06	9	9	3.28	0.06486	0.00281	0.0004	0.00670	0.0007	0.0046	0.0005
	A107IX23-3D4	52	23	8.33E-06	12	9	3.28	0.06486	0.00161	0.0001	0.00470	0.0003	0.0029	0.0002
	A107IX23-3D5	52	23	8.33E-06	15	9	3.28	0.06486	0.00159	0.0003	0.00534	0.0006	0.0030	0.0004
	A107IX23-3D6	52	23	8.33E-06	18	9	3.28	0.06486	0.00117	0.0001	0.00417	0.0003	0.0022	0.0002
	A107IX23-3D7	52	23	8.33E-06	21	9	3.28	0.06486	0.00117	0.0002	0.00420	0.0004	0.0020	**0.0002**
	A107IX23-3D8	52	23	8.33E-06	24	9	3.28	0.06486	0.00107	**0.0002**	0.00370	**0.0003**	0.0020	**0.0002**
	A107IX23-3D9	52	23	8.33E-06	27	9	3.28	0.06486	0.00127	**0.0003**	0.00396	**0.0004**	0.0021	**0.0003**
	A107IX23-3D10	52	23	8.33E-06	30	9	3.28	0.06486	0.00101	**0.0001**	0.00359	**0.0003**	0.0020	**0.0002**
4	A107IX23-4D1	90	23	8.33E-06	3	10	1.64	0.03243	0.00314	0.0026	0.00385	0.0016	0.0042	0.0022
	A107IX23-4D2	90	23	8.33E-06	6	10	1.64	0.03243	0.00202	0.0002	0.00351	0.0007	0.0025	0.0002
	A107IX23-4D3	90	23	8.33E-06	9	10	1.64	0.03243	0.00108	-0.0002	0.00232	0.0002	0.0011	-0.0001
	A107IX23-4D4	90	23	8.33E-06	12	10	1.64	0.03243	0.00066	-0.0001	0.00195	0.0003	0.0009	0.0002
	A107IX23-4D5	90	23	8.33E-06	15	10	1.64	0.03243	0.00043	-0.0001	0.00148	0.0002	0.0006	0.0001
	A107IX23-4D6	90	23	8.33E-06	18	10	1.64	0.03243	0.00059	0.0001	0.00177	0.0004	0.0006	0.0002
	A107IX23-4D7	90	23	8.33E-06	21	10	1.64	0.03243	0.00025	-0.0003	0.00094	0.0000	0.0003	0.0000
	A107IX23-4D8	90	23	8.33E-06	24	10	1.64	0.03243	0.00035	0.0000	0.00117	**0.0003**	0.0005	**0.0002**
	A107IX23-4D9	90	23	8.33E-06	27	10	1.64	0.03243	0.00036	-0.0001	0.00127	**0.0003**	0.0004	**0.0001**
	A107IX23-4D10	90	23	8.33E-06	30	10	1.64	0.03243	0.00016	-0.0002	0.00062	-0.00001	0.0002	0.0000
5	A107IX23-5D9	230	23	8.33E-06	3	11	1.64	0.03243	0.01672	0.0159	0.03195	0.0134	0.0240	0.0123
	A107IX23-5D8	230	23	8.33E-06	6	11	1.64	0.03241	0.01531	0.0066	0.03041	0.0061	0.0239	0.0061
	A107IX23-5D1	230	23	8.33E-06	9	11	1.64	0.03240	0.00271	-0.0049	0.00262	-0.0053	0.0039	-0.0041
	A107IX23-5D2	230	23	8.33E-06	12	11	1.64	0.03240	0.00114	-0.0003	0.00155	0.0001	0.0014	-0.0003
	A107IX23-5D3	230	23	8.33E-06	15	11	1.64	0.03240	0.00172	0.0010	0.00227	0.0006	0.0017	0.0005
	A107IX23-5D4	230	23	8.33E-06	18	11	1.64	0.03239	0.00067	-0.0003	0.00138	0.0001	0.0009	0.0000
	A107IX23-5D5	230	23	8.33E-06	21	11	1.64	0.03239	0.00151	0.0010	0.00260	0.0008	0.0020	**0.0008**
	A107IX23-5D6	230	23	8.33E-06	24	11	1.64	0.03239	0.00117	**0.0003**	0.00215	**0.0004**	0.0015	**0.0003**
	A107IX23-5D7	230	23	8.33E-06	27	11	1.64	0.03239	0.00149	**0.0008**	0.00244	**0.0006**	0.0019	**0.0006**
	A107IX23-5D10	230	23	8.33E-06	30	11	1.64	0.03240	0.00088	**0.0000**	0.00164	**0.0002**	0.0012	**0.0001**

Table A13. ICP-MS Analysis Results from Dissolution of Glass ORLECAP107 at 70 °C.

Exp.	Sample ID	Inf [Si] ppm	T °C	Flow Rate, m^3/d	Time, days	pH 23°C	Glass Mass g	SA m^2	[Mo] ppm	Mo Rate $g_{-glass}\ m^{-2}\ d^{-1}$	[Cs] ppm	Cs Rate $g_{-glass}\ m^{-2}\ d^{-1}$	[Re] ppm	Re Rate $g_{-glass}\ m^{-2}\ d^{-1}$
1	C107IX70-1D1	55	70	2.50E-05	1	7	0.77	0.01520	0.01757	0.1261	0.15764	0.4229	0.1767	0.6001
	C107IX70-1D2	55	70	2.50E-05	2	7	0.77	0.01493	0.01059	0.0126	0.14754	0.1877	0.1174	0.1005
	C107IX70-1D3	55	70	2.50E-05	3	7	0.77	0.01465	0.00734	0.0146	0.14972	0.2113	0.0783	0.0689
	C107IX70-1D4	55	70	2.50E-05	4	7	0.77	0.01439	0.00619	0.0186	0.15740	0.2339	0.0594	0.0728
	C107IX70-1D5	55	70	2.50E-05	5	7	0.77	0.01414	0.00496	0.0138	0.14531	0.1921	0.0424	0.0462
	C107IX70-1D6	55	70	2.50E-05	6	7	0.77	0.01391	0.00489	0.0183	0.15557	0.2431	0.0362	0.0558
	C107IX70-1D7	55	70	2.50E-05	7	7	0.77	0.01370	0.00444	0.0153	0.14168	0.1902	0.0282	0.0380
	C107IX70-1D8	55	70	2.50E-05	8	7	0.77	0.01350	0.00408	**0.0144**	0.13330	**0.1887**	0.0213	**0.0273**
	C107IX70-1D9	55	70	2.50E-05	9	7	0.77	0.01331	0.00505	**0.0241**	0.11202	**0.1390**	0.0179	**0.0282**
	C107IX70-1D10	55	70	2.50E-05	10	7	0.77	0.01314	0.00344	**0.0068**	0.10643	**0.1564**	0.0134	**0.0173**
2	C107IX70-2D1	60	70	2.50E-05	1	8	0.77	0.01524	0.01510	0.1079	0.09179	0.2456	0.1054	0.3570
	C107IX70-2D2	60	70	2.50E-05	2	8	0.77	0.01505	0.01018	0.0186	0.10121	0.1498	0.0753	0.0773
	C107IX70-2D3	60	70	2.50E-05	3	8	0.77	0.01486	0.00553	0.0025	0.08525	0.0951	0.0443	0.0232
	C107IX70-2D4	60	70	2.50E-05	4	8	0.77	0.01467	0.00468	0.0137	0.07796	0.0982	0.0297	0.0265
	C107IX70-2D5	60	70	2.50E-05	5	8	0.77	0.01449	0.00414	0.0130	0.08440	0.1278	0.0265	0.0415
	C107IX70-2D6	60	70	2.50E-05	6	8	0.77	0.01432	0.00332	0.0089	0.09733	0.1570	0.0222	0.0324
	C107IX70-2D7	60	70	2.50E-05	7	8	0.77	0.01416	0.00291	**0.0090**	0.08915	0.1166	0.0172	0.0222
	C107IX70-2D8	60	70	2.50E-05	8	8	0.77	0.01401	0.00225	**0.0055**	0.06707	**0.0655**	0.0108	**0.0081**
	C107IX70-2D9	60	70	2.50E-05	9	8	0.77	0.01388	0.00237	**0.0091**	0.06762	**0.1001**	0.0096	**0.0158**
	C107IX70-2D10	60	70	2.50E-05	10	8	0.77	0.01376	0.00183	0.0045	0.05198	**0.0538**	0.0064	**0.0060**
3	C107IX70-3D1	80	70	2.50E-05	1	9	0.77	0.01528	0.01022	0.0724	0.03834	0.1023	0.0572	0.1932
	C107IX70-3D2	80	70	2.50E-05	2	9	0.77	0.01520	0.00729	0.0151	0.04858	0.0789	0.0507	0.0752
	C107IX70-3D3	80	70	2.50E-05	3	9	0.77	0.01510	0.00397	0.0017	0.04377	0.0526	0.0317	0.0218
	C107IX70-3D4	80	70	2.50E-05	4	9	0.77	0.01501	0.00235	0.0020	0.04073	0.0512	0.0205	0.0160
	C107IX70-3D5	80	70	2.50E-05	5	9	0.77	0.01491	0.00181	0.0040	0.04177	0.0585	0.0162	0.0206
	C107IX70-3D6	80	70	2.50E-05	6	9	0.77	0.01482	0.00152	0.0038	0.04870	**0.0765**	0.0129	0.0167
	C107IX70-3D7	80	70	2.50E-05	7	9	0.77	0.01474	0.00120	0.0026	0.05217	**0.0769**	0.0099	0.0121
	C107IX70-3D8	80	70	2.50E-05	8	9	0.77	0.01467	0.00082	0.0009	0.02690	**0.0022**	0.0058	0.0029
	C107IX70-3D9	80	70	2.50E-05	9	9	0.77	0.01460	0.00079	**0.0022**	0.05125	**0.1056**	0.0050	**0.0076**
	C107IX70-3D10	80	70	2.50E-05	10	9	0.77	0.01453	0.00084	**0.0026**	0.03321	**0.0213**	0.0046	**0.0075**
4	C107IX70-4D1	140	70	2.50E-05	1	10	0.50	0.00984	0.00716	0.0784	0.01458	0.0604	0.0281	0.1474
	C107IX70-4D2	140	70	2.50E-05	2	10	0.50	0.00980	0.00469	0.0115	0.01586	0.0356	0.0213	0.0384
	C107IX70-4D3	140	70	2.50E-05	3	10	0.50	0.00976	0.00235	-0.0010	0.01289	0.0207	0.0127	0.0109
	C107IX70-4D4	140	70	2.50E-05	4	10	0.50	0.00973	0.00204	0.0088	0.01443	0.0334	0.0104	0.0213
	C107IX70-4D5	140	70	2.50E-05	5	10	0.50	0.00969	0.00139	0.0033	0.01515	0.0334	0.0084	0.0171
	C107IX70-4D6	140	70	2.50E-05	6	10	0.50	0.00966	0.00113	0.0040	0.01455	0.0294	0.0062	0.0107
	C107IX70-4D7	140	70	2.50E-05	7	10	0.50	0.00963	0.00082	**0.0020**	0.01330	0.0255	0.0048	0.0089
	C107IX70-4D8	140	70	2.50E-05	8	10	0.50	0.00960	0.00224	**0.0200**	0.01192	**0.0224**	0.0055	**0.0169**
	C107IX70-4D9	140	70	2.50E-05	9	10	0.50	0.00957	0.00229	**0.0125**	0.01118	**0.0222**	0.0035	**0.0041**
	C107IX70-4D10	140	70	2.50E-05	10	10	0.50	0.00954	0.00056	-0.0078	0.00982	**0.0181**	0.0020	**0.0010**
5	C107IX70-5D1	360	70	2.50E-05	1	11	0.50	0.00984	0.00698	0.0775	0.01095	0.0453	0.0162	0.0849
	C107IX70-5D2	360	70	2.50E-05	2	11	0.50	0.00983	0.00375	0.0026	0.01001	0.0187	0.0105	0.0124
	C107IX70-5D3	360	70	2.50E-05	3	11	0.50	0.00981	0.00213	0.0024	0.00901	0.0166	0.0064	0.0059
	C107IX70-5D4	360	70	2.50E-05	4	11	0.50	0.00980	0.00130	0.0023	0.00871	0.0174	0.0040	0.0042
	C107IX70-5D5	360	70	2.50E-05	5	11	0.50	0.00978	0.00076	0.0008	0.00777	0.0141	0.0025	0.0029
	C107IX70-5D6	360	70	2.50E-05	6	11	0.50	0.00977	0.00046	0.0005	0.00640	0.0104	0.0015	0.0011
	C107IX70-5D7	360	70	2.50E-05	7	11	0.50	0.00975	0.00020	-0.0007	0.00392	0.0029	0.0007	-0.0003
	C107IX70-5D8	360	70	2.50E-05	8	11	0.50	0.00974	0.00048	**0.0039**	0.00511	**0.0131**	0.0011	**0.0037**
	C107IX70-5D9	360	70	2.50E-05	9	11	0.50	0.00973	0.00087	**0.0068**	0.00578	**0.0134**	0.0015	**0.0051**
	C107IX70-5D10	360	70	2.50E-05	10	11	0.50	0.00972	0.00068	**0.0024**	0.00480	0.0079	0.0005	-0.0015

Table A14. ICP-MS Analysis Results from Dissolution of Glass ORLECAP107 at 40 °C.

Exp.	Sample ID	Inf [Si] ppm	T °C	Flow Rate, m^3/d	Time, days	pH 23°C	Glass Mass g	SA m^2	[Mo] ppm	Mo Rate $g_{-glass}\ m^{-2}\ d^{-1}$	[Cs] ppm	Cs Rate $g_{-glass}\ m^{-2}\ d^{-1}$	[Re] ppm	Re Rate $g_{-glass}\ m^{-2}\ d^{-1}$
1	C107IX40-1D1	40	40	8.33E-06	3	7	1.65	0.03278	0.01735	0.0184	0.06646	0.0276	0.1363	0.0715
	C107IX40-1D2	40	40	8.33E-06	6	7	1.65	0.03264	0.01195	0.0024	0.07449	0.0172	0.1140	0.0242
	C107IX40-1D3	40	40	8.33E-06	9	7	1.65	0.03247	0.00781	0.0012	0.07044	0.0139	0.0846	0.0146
	C107IX40-1D4	40	40	8.33E-06	12	7	1.65	0.03231	0.00568	0.0012	0.06807	0.0138	0.0677	0.0135
	C107IX40-1D5	40	40	8.33E-06	15	7	1.65	0.03215	0.00458	0.0011	0.06418	0.0127	0.0520	0.0097
	C107IX40-1D6	40	40	8.33E-06	18	7	1.65	0.03199	0.00430	0.0014	0.07148	0.0167	0.0543	0.0152
	C107IX40-1D7	40	40	8.33E-06	21	7	1.65	0.03184	0.00364	0.0009	0.06487	0.0124	0.0465	0.0104
	C107IX40-1D8	40	40	8.33E-06	24	7	1.65	0.03170	0.00327	**0.0009**	0.06246	**0.0129**	0.0405	**0.0093**
	C107IX40-1D9	40	40	8.33E-06	27	7	1.65	0.03157	0.00306	**0.0009**	0.06033	**0.0125**	0.0363	**0.0087**
	C107IX40-1D10	40	40	8.33E-06	30	7	1.65	0.03144	0.00287	**0.0008**	0.05888	**0.0124**	0.0331	**0.0082**
2	C107IX40-2D1	45	40	8.33E-06	3	8	1.65	0.03280	0.01692	0.0184	0.05088	0.0211	0.0373	0.0196
	C107IX40-2D2	45	40	8.33E-06	6	8	1.65	0.03273	0.01425	0.0062	0.03453	0.0038	0.0756	0.0299
	C107IX40-2D3	45	40	8.33E-06	9	8	1.65	0.03266	0.00883	0.0016	0.03436	0.0071	0.0564	0.0098
	C107IX40-2D4	45	40	8.33E-06	12	8	1.65	0.03259	0.00619	0.0017	0.05349	0.0151	0.0470	0.0099
	C107IX40-2D5	45	40	8.33E-06	15	8	1.65	0.03251	0.00430	0.0011	0.04387	0.0072	0.0382	0.0078
	C107IX40-2D6	45	40	8.33E-06	18	8	1.65	0.03243	0.00314	0.0009	0.03676	0.0062	0.0302	0.0059
	C107IX40-2D7	45	40	8.33E-06	21	8	1.65	0.03235	0.00245	0.0007	0.02925	**0.0046**	0.0249	0.0052
	C107IX40-2D8	45	40	8.33E-06	24	8	1.65	0.03228	0.00197	**0.0006**	0.02712	**0.0053**	0.0211	**0.0046**
	C107IX40-2D9	45	40	8.33E-06	27	8	1.65	0.03221	0.00168	**0.0005**	0.02544	**0.0050**	0.0165	**0.0032**
	C107IX40-2D10	45	40	8.33E-06	30	8	1.65	0.03215	0.00141	**0.0004**	0.02226	**0.0040**	0.0136	**0.0029**
3	C107IX40-3D1	60	40	8.33E-06	3	9	1.65	0.03282	0.01287	0.0140	0.01713	0.0071	0.0496	0.0260
	C107IX40-3D2	60	40	8.33E-06	6	9	1.65	0.03279	0.00799	0.0015	0.01684	0.0034	0.0419	0.0090
	C107IX40-3D3	60	40	8.33E-06	9	9	1.65	0.03275	0.00477	0.0007	0.01546	0.0029	0.0311	0.0053
	C107IX40-3D4	60	40	8.33E-06	12	9	1.65	0.03271	0.00311	0.0006	0.01493	0.0030	0.0256	0.0053
	C107IX40-3D5	60	40	8.33E-06	15	9	1.65	0.03268	0.00200	0.0003	0.01228	0.0020	0.0189	0.0032
	C107IX40-3D6	60	40	8.33E-06	18	9	1.65	0.03264	0.00157	0.0004	0.01237	0.0026	0.0168	0.0039
	C107IX40-3D7	60	40	8.33E-06	21	9	1.65	0.03261	0.00126	0.0003	0.01177	0.0023	0.0143	0.0031
	C107IX40-3D8	60	40	8.33E-06	24	9	1.65	0.03257	0.00113	**0.0004**	0.01196	**0.0025**	0.0133	**0.0032**
	C107IX40-3D9	60	40	8.33E-06	27	9	1.65	0.03254	0.00100	**0.0003**	0.01138	**0.0023**	0.0116	**0.0026**
	C107IX40-3D10	60	40	8.33E-06	30	9	1.65	0.03251	0.00093	**0.0003**	0.01146	**0.0024**	0.0111	**0.0028**
4	C107IX40-4D1	105	40	8.33E-06	3	10	0.83	0.01643	0.00721	0.0152	0.00772	0.0064	0.0218	0.0228
	C107IX40-4D2	105	40	8.33E-06	6	10	0.83	0.01642	0.00441	0.0013	0.00674	0.0024	0.0170	0.0065
	C107IX40-4D3	105	40	8.33E-06	9	10	0.83	0.01641	0.00230	-0.0003	0.00528	0.0016	0.0113	0.0029
	C107IX40-4D4	105	40	8.33E-06	12	10	0.83	0.01640	0.00142	0.0001	0.00468	0.0017	0.0085	0.0030
	C107IX40-4D5	105	40	8.33E-06	15	10	0.83	0.01639	0.00399	0.0069	0.00924	0.0057	0.0109	0.0070
	C107IX40-4D6	105	40	8.33E-06	18	10	0.83	0.01638	0.00068	-0.0034	0.00410	-0.0004	0.0055	0.0001
	C107IX40-4D7	105	40	8.33E-06	21	10	0.83	0.01637	0.00060	0.0001	0.00401	**0.0016**	0.0049	**0.0022**
	C107IX40-4D8	105	40	8.33E-06	24	10	0.83	0.01636	0.00266	0.0048	0.00745	**0.0045**	0.0071	**0.0049**
	C107IX40-4D9	105	40	8.33E-06	27	10	0.83	0.01635	0.00041	-0.0025	0.00368	0.0000	0.0037	**0.0001**
	C107IX40-4D10	105	40	8.33E-06	30	10	0.83	0.01634	0.00038	-0.0001	0.00398	**0.0018**	0.0036	**0.0018**
5	C107IX40-5D1	270	40	8.33E-06	3	11	0.83	0.01644	0.00631	0.0133	0.00538	0.0044	0.0152	0.0159
	C107IX40-5D2	270	40	8.33E-06	6	11	0.83	0.01643	0.00343	0.0002	0.00399	0.0010	0.0090	0.0015
	C107IX40-5D3	270	40	8.33E-06	9	11	0.83	0.01643	0.00220	0.0007	0.00348	0.0012	0.0060	0.0016
	C107IX40-5D4	270	40	8.33E-06	12	11	0.83	0.01643	0.00135	0.0001	0.00283	0.0009	0.0038	0.0008
	C107IX40-5D5	270	40	8.33E-06	15	11	0.83	0.01642	0.00090	0.0001	0.00231	0.0007	0.0026	0.0007
	C107IX40-5D6	270	40	8.33E-06	18	11	0.83	0.01642	0.00074	0.0002	0.00231	0.0009	0.0021	0.0008
	C107IX40-5D7	270	40	8.33E-06	21	11	0.83	0.01642	0.00054	0.0000	0.00205	**0.0007**	0.0015	**0.0005**
	C107IX40-5D8	270	40	8.33E-06	24	11	0.83	0.01642	0.00047	0.0000	0.00210	**0.0008**	0.0014	**0.0006**
	C107IX40-5D9	270	40	8.33E-06	27	11	0.83	0.01642	0.00038	-0.0001	0.00171	**0.0005**	0.0010	**0.0003**
	C107IX40-5D10	270	40	8.33E-06	30	11	0.83	0.01642	0.00036	0.0000	0.00171	**0.0007**	0.0009	**0.0004**

Table A15. ICP-MS Analysis Results from Dissolution of Glass ORLECAP107 at 23 °C.

Exp.	Sample ID	Inf [Si] ppm	T °C	Flow Rate, m^3/d	Time, days	pH 23°C	Glass Mass g	SA m^2	[Mo] ppm	Mo Rate $g_{-glass}\ m^{-2}\ d^{-1}$	[Cs] ppm	Cs Rate $g_{-glass}\ m^{-2}\ d^{-1}$	[Re] ppm	Re Rate $g_{-glass}\ m^{-2}\ d^{-1}$
1	C107IX23-1D1	35	23	8.33E-06	3	7	3.28	0.06522	0.02662	0.0145	0.02135	0.0044	0.0783	0.0207
	C107IX23-1D2	35	23	8.33E-06	6	7	3.28	0.06520	0.01611	0.0013	0.02048	0.0020	0.0534	0.0038
	C107IX23-1D3	35	23	8.33E-06	9	7	3.28	0.06517	0.00928	0.0005	0.01901	0.0018	0.0393	0.0033
	C107IX23-1D4	35	23	8.33E-06	12	7	3.28	0.06514	0.00610	0.0006	0.01943	0.0021	0.0318	0.0032
	C107IX23-1D5	35	23	8.33E-06	15	7	3.28	0.06511	0.00386	0.0002	0.01648	0.0014	0.0241	0.0022
	C107IX23-1D6	35	23	8.33E-06	18	7	3.28	0.06509	0.00298	0.0004	0.01726	0.0019	0.0221	0.0026
	C107IX23-1D7	35	23	8.33E-06	21	7	3.28	0.06506	0.00239	0.0003	0.01552	0.0014	0.0201	0.0024
	C107IX23-1D8	35	23	8.33E-06	24	7	3.28	0.06503	0.00229	**0.0004**	0.01692	**0.0019**	0.0198	**0.0026**
	C107IX23-1D9	35	23	8.33E-06	27	7	3.28	0.06500	0.00211	**0.0003**	0.01802	**0.0020**	0.0198	**0.0026**
	C107IX23-1D10	35	23	8.33E-06	30	7	3.28	0.06497	0.00207	**0.0003**	0.01682	**0.0016**	0.0190	**0.0024**
2	C107IX23-2D3	40	23	8.33E-06	3	8	3.28	0.06523	0.02373	0.0131	0.01714	0.0036	0.0603	0.0159
	C107IX23-2D4	40	23	8.33E-06	6	8	3.28	0.06521	0.01340	0.0007	0.01435	0.0012	0.0365	0.0017
	C107IX23-2D5	40	23	8.33E-06	9	8	3.28	0.06520	0.00827	0.0008	0.01343	0.0013	0.0243	0.0016
	C107IX23-2D6	40	23	8.33E-06	12	8	3.28	0.06518	0.00437	0.0000	0.01090	0.0009	0.0162	0.0011
	C107IX23-2D7	40	23	8.33E-06	15	8	3.28	0.06517	0.00267	0.0002	0.00877	0.0007	0.0122	0.0011
	C107IX23-2D8	40	23	8.33E-06	18	8	3.28	0.06516	0.00182	0.0002	0.00881	0.0009	0.0109	0.0013
	C107IX23-2D9	40	23	8.33E-06	21	8	3.28	0.06515	0.00141	**0.0002**	0.00863	0.0009	0.0091	0.0010
	C107IX23-2D10	40	23	8.33E-06	24	8	3.28	0.06514	0.00118	**0.0002**	0.00833	**0.0008**	0.0088	**0.0011**
	C107IX23-2D11	40	23	8.33E-06	27	8	3.28	0.06513	0.00112	**0.0002**	0.00793	**0.0008**	0.0084	**0.0011**
	C107IX23-2D12	40	23	8.33E-06	30	8	3.28	0.06512	0.00084	0.0000	0.00605	0.0004	0.0065	**0.0006**
3	C107IX23-3D7	52	23	8.33E-06	3	9	3.28	0.06520	0.05121	0.0288	0.10601	0.0221	0.1794	0.0473
	C107IX23-3D8	52	23	8.33E-06	6	9	3.28	0.06514	0.04613	0.0115	0.08510	0.0067	0.0958	0.0016
	C107IX23-3D5	52	23	8.33E-06	9	9	3.28	0.06512	0.01412	-0.0051	0.02572	-0.0035	0.0301	-0.0047
	C107IX23-3D1	52	23	8.33E-06	12	9	3.28	0.06510	0.02545	0.0103	0.01305	0.0000	0.0580	0.0113
	C107IX23-3D2	52	23	8.33E-06	15	9	3.28	0.06509	0.01274	0.0000	0.00906	0.0005	0.0309	0.0005
	C107IX23-3D3	52	23	8.33E-06	18	9	3.28	0.06509	0.00699	0.0003	0.00762	0.0006	0.0182	0.0007
	C107IX23-3D4	52	23	8.33E-06	21	9	3.28	0.06508	0.00382	0.0001	0.00668	0.0006	0.0115	0.0006
	C107IX23-3D6	52	23	8.33E-06	24	9	3.28	0.06508	0.00143	-0.0003	0.00539	**0.0004**	0.0066	**0.0002**
	C107IX23-3D9	52	23	8.33E-06	27	9	3.28	0.06507	0.00090	**0.0000**	0.00508	**0.0005**	0.0050	**0.0005**
	C107IX23-3D10	52	23	8.33E-06	30	9	3.28	0.06507	0.00070	**0.0001**	0.00483	**0.0005**	0.0050	**0.0007**
4	C107IX23-4D8	90	23	8.33E-06	3	10	1.64	0.03260	0.03045	0.0338	0.05304	0.0221	0.0995	0.0525
	C107IX23-4D1	90	23	8.33E-06	6	10	1.64	0.03257	0.01317	-0.0026	0.00693	-0.0082	0.0288	-0.0111
	C107IX23-4D2	90	23	8.33E-06	9	10	1.64	0.03257	0.00676	-0.0001	0.00504	0.0007	0.0150	0.0003
	C107IX23-4D3	90	23	8.33E-06	12	10	1.64	0.03257	0.00372	0.0001	0.00419	0.0007	0.0079	0.0002
	C107IX23-4D4	90	23	8.33E-06	15	10	1.64	0.03256	0.00199	-0.0001	0.00354	0.0006	0.0044	0.0003
	C107IX23-4D5	90	23	8.33E-06	18	10	1.64	0.03256	0.00224	0.0011	0.00490	0.0013	0.0041	0.0010
	C107IX23-4D6	90	23	8.33E-06	21	10	1.64	0.03256	0.00082	-0.0006	0.00301	0.0002	0.0019	0.0000
	C107IX23-4D7	90	23	8.33E-06	24	10	1.64	0.03256	0.00055	-0.0001	0.00241	**0.0004**	0.0013	**0.0002**
	C107IX23-4D9	90	23	8.33E-06	27	10	1.64	0.03256	0.00066	0.0002	0.00284	**0.0007**	0.0012	**0.0003**
	C107IX23-4D10	90	23	8.33E-06	30	10	1.64	0.03256	0.00040	-0.0002	0.00251	**0.0005**	0.0010	**0.0002**
5	C107IX23-5D1	230	23	8.33E-06	3	11	1.64	0.03261	0.01166	0.0129	0.00530	0.0022	0.0266	0.0140
	C107IX23-5D2	230	23	8.33E-06	6	11	1.64	0.03261	0.00611	0.0002	0.00348	0.0003	0.0136	0.0002
	C107IX23-5D3	230	23	8.33E-06	9	11	1.64	0.03261	0.00319	0.0000	0.00290	0.0005	0.0072	0.0002
	C107IX23-5D4	230	23	8.33E-06	12	11	1.64	0.03261	0.00170	0.0000	0.00238	0.0004	0.0040	0.0002
	C107IX23-5D5	230	23	8.33E-06	15	11	1.64	0.03261	0.00105	0.0001	0.00228	0.0005	0.0023	0.0002
	C107IX23-5D6	230	23	8.33E-06	18	11	1.64	0.03261	0.00071	0.00010	0.00214	0.0004	0.0015	0.00015
	C107IX23-5D7	230	23	8.33E-06	21	11	1.64	0.03261	0.00052	0.00007	0.00180	0.0003	0.0010	**0.00012**
	C107IX23-5D8	230	23	8.33E-06	24	11	1.64	0.03261	0.00041	0.00007	0.00201	**0.0005**	0.0008	0.00017
	C107IX23-5D9	230	23	8.33E-06	27	11	1.64	0.03261	0.00031	**0.00001**	0.00171	**0.0003**	0.0006	**0.00012**
	C107IX23-5D10	230	23	8.33E-06	30	11	1.64	0.03261	0.00028	**0.00003**	0.00180	**0.0004**	0.0006	**0.00013**

Table A16. ICP-MS Analysis Results from Dissolution of Glass ORLEC44 at 70 °C.

Exp.	Sample ID	Inf [Si] ppm	T °C	Flow Rate, m^3/d	Time, days	pH 23°C	Glass Mass g	SA m^2	[Mo] ppm	Mo Rate $g_{-glass}\ m^{-2}\ d^{-1}$	[Cs] ppm	Cs Rate $g_{-glass}\ m^{-2}\ d^{-1}$	[Re] ppm	Re Rate $g_{-glass}\ m^{-2}\ d^{-1}$
1	C44IX70-1D1	55	70	2.50E-05	1	7	0.77	0.01537	0.07272	0.4422	0.23403	0.6207	0.3904	1.2703
	C44IX70-1D2	55	70	2.50E-05	2	7	0.77	0.01517	0.05439	0.1109	0.24032	0.3315	0.3717	0.5823
	C44IX70-1D3	55	70	2.50E-05	3	7	0.77	0.01495	0.03588	0.0538	0.22112	0.2754	0.2631	0.2585
	C44IX70-1D4	55	70	2.50E-05	4	7	0.77	0.01474	0.02432	0.0399	0.20981	0.2746	0.1835	0.1762
	C44IX70-1D5	55	70	2.50E-05	5	7	0.77	0.01455	0.01720	0.0319	0.19677	0.2575	0.1340	0.1454
	C44IX70-1D6	55	70	2.50E-05	6	7	0.77	0.01437	0.01229	**0.0234**	0.18704	0.2516	0.0955	0.0994
	C44IX70-1D7	55	70	2.50E-05	7	7	0.77	0.01420	0.00958	**0.0221**	0.18444	0.2611	0.0713	0.0829
	C44IX70-1D8	55	70	2.50E-05	8	7	0.77	0.01403	0.00830	**0.0228**	0.16737	**0.2184**	0.0528	0.0613
	C44IX70-1D9	55	70	2.50E-05	9	7	0.77	0.01387	0.01066	**0.0433**	0.14259	**0.1732**	0.0427	**0.0588**
	C44IX70-1D10	55	70	2.50E-05	10	7	0.77	0.01371	0.00511	**-0.0021**	0.16224	**0.2704**	0.0329	**0.0421**
2	C44IX70-2D1	60	70	2.50E-05	1	8	0.77	0.01542	0.04335	0.2624	0.12841	0.3395	0.1899	0.6161
	C44IX70-2D2	60	70	2.50E-05	2	8	0.77	0.01532	0.02994	0.0500	0.13871	0.1983	0.2002	0.3436
	C44IX70-2D3	60	70	2.50E-05	3	8	0.77	0.01520	0.01849	0.0211	0.12836	0.1583	0.1547	0.1798
	C44IX70-2D4	60	70	2.50E-05	4	8	0.77	0.01509	0.01260	0.0202	0.12347	0.1601	0.1190	0.1381
	C44IX70-2D5	60	70	2.50E-05	5	8	0.77	0.01499	0.00859	0.0137	0.11850	0.1544	0.0868	0.0910
	C44IX70-2D6	60	70	2.50E-05	6	8	0.77	0.01489	0.00619	0.0113	0.11582	0.1549	0.0624	0.0640
	C44IX70-2D7	60	70	2.50E-05	7	8	0.77	0.01479	0.00482	0.0104	0.11303	0.1519	0.0460	0.0499
	C44IX70-2D8	60	70	2.50E-05	8	8	0.77	0.01470	0.00376	**0.0080**	0.10799	**0.1428**	0.0354	**0.0423**
	C44IX70-2D9	60	70	2.50E-05	9	8	0.77	0.01461	0.00314	**0.0075**	0.10432	**0.1404**	0.0302	**0.0427**
	C44IX70-2D10	60	70	2.50E-05	10	8	0.77	0.01453	0.00265	**0.0064**	0.09967	**0.1333**	0.0233	**0.0282**
3	C44IX70-3D1	80	70	2.50E-05	1	9	0.77	0.01545	0.01037	0.0618	0.04006	0.1057	0.0383	0.1240
	C44IX70-3D2	80	70	2.50E-05	2	9	0.77	0.01543	0.01039	0.0310	0.05181	0.0840	0.0662	0.1525
	C44IX70-3D3	80	70	2.50E-05	3	9	0.77	0.01540	0.00621	0.0056	0.04643	0.0543	0.0558	0.0738
	C44IX70-3D4	80	70	2.50E-05	4	9	0.77	0.01537	0.00447	0.0077	0.04642	0.0616	0.0501	0.0722
	C44IX70-3D5	80	70	2.50E-05	5	9	0.77	0.01534	0.00311	0.0047	0.04459	0.0568	0.0424	0.0566
	C44IX70-3D6	80	70	2.50E-05	6	9	0.77	0.01531	0.00255	0.0055	0.04337	0.0561	0.0366	0.0503
	C44IX70-3D7	80	70	2.50E-05	7	9	0.77	0.01528	0.00207	**0.0043**	0.04267	0.0560	0.0306	**0.0403**
	C44IX70-3D8	80	70	2.50E-05	8	9	0.77	0.01525	0.00170	**0.0035**	0.03913	**0.0475**	0.0257	**0.0343**
	C44IX70-3D9	80	70	2.50E-05	9	9	0.77	0.01523	0.00382	0.0177	0.03563	**0.0430**	0.0235	**0.0348**
	C44IX70-3D10	80	70	2.50E-05	10	9	0.77	0.01520	0.00122	-0.0049	0.03761	**0.0531**	0.0177	0.0196
4	C44IX70-4D1	140	70	2.50E-05	1	10	0.50	0.00994	0.01073	0.0996	0.01808	0.0742	0.0186	0.0937
	C44IX70-4D2	140	70	2.50E-05	2	10	0.50	0.00993	0.00578	0.0031	0.01592	0.0282	0.0172	0.0400
	C44IX70-4D3	140	70	2.50E-05	3	10	0.50	0.00992	0.00353	0.0052	0.01400	0.0248	0.0154	0.0340
	C44IX70-4D4	140	70	2.50E-05	4	10	0.50	0.00991	0.00775	0.0557	0.02243	0.0634	0.0196	0.0603
	C44IX70-4D5	140	70	2.50E-05	5	10	0.50	0.00991	0.00177	-0.0207	0.01314	0.0079	0.0135	0.0187
	C44IX70-4D6	140	70	2.50E-05	6	10	0.50	0.00990	0.00152	**0.0052**	0.01285	0.0259	0.0136	0.0344
	C44IX70-4D7	140	70	2.50E-05	7	10	0.50	0.00989	0.00118	**0.0031**	0.01227	0.0241	0.0134	0.0333
	C44IX70-4D8	140	70	2.50E-05	8	10	0.50	0.00988	0.00108	**0.0039**	0.01237	**0.0257**	0.0141	**0.0375**
	C44IX70-4D9	140	70	2.50E-05	9	10	0.50	0.00987	0.00234	0.0163	0.01306	**0.0284**	0.0153	**0.0416**
	C44IX70-4D10	140	70	2.50E-05	10	10	0.50	0.00986	0.00095	-0.0029	0.01298	**0.0267**	0.0129	**0.0269**
5	C44IX70-5D1	360	70	2.50E-05	1	11	0.50	0.00994	0.00995	0.0932	0.01040	0.0426	0.0088	0.0441
	C44IX70-5D2	360	70	2.50E-05	2	11	0.50	0.00994	0.00594	0.0088	0.00908	0.0158	0.0064	0.0103
	C44IX70-5D3	360	70	2.50E-05	3	11	0.50	0.00993	0.00326	0.0024	0.00692	0.0097	0.0046	0.0067
	C44IX70-5D4	360	70	2.50E-05	4	11	0.50	0.00993	0.00207	0.0039	0.00603	0.0104	0.0035	0.0060
	C44IX70-5D5	360	70	2.50E-05	5	11	0.50	0.00993	0.00127	0.0019	0.00511	0.0085	0.0026	0.0044
	C44IX70-5D6	360	70	2.50E-05	6	11	0.50	0.00992	0.00161	0.0089	0.00570	0.0129	0.0030	0.0085
	C44IX70-5D7	360	70	2.50E-05	7	11	0.50	0.00992	0.00086	0.0002	0.00443	**0.0064**	0.0017	0.0011
	C44IX70-5D8	360	70	2.50E-05	8	11	0.50	0.00992	0.00055	**0.0008**	0.00410	**0.0076**	0.0014	**0.0027**
	C44IX70-5D9	360	70	2.50E-05	9	11	0.50	0.00991	0.00044	**0.0012**	0.00380	**0.0071**	0.0013	**0.0027**
	C44IX70-5D10	360	70	2.50E-05	10	11	0.50	0.00991	0.00036	**0.0010**	0.00358	**0.0068**	0.0010	**0.0021**

Table A17. ICP-MS Analysis Results from Dissolution of Glass ORLEC44 at 40 °C.

Exp.	Sample ID	Inf [Si] ppm	T °C	Flow Rate, m^3/d	Time, days	pH 23°C	Glass Mass g	SA m^2	[Mo] ppm	Mo Rate $g_{-glass}\ m^{-2}\ d^{-1}$	[Cs] ppm	Cs Rate $g_{-glass}\ m^{-2}\ d^{-1}$	[Re] ppm	Re Rate $g_{-glass}\ m^{-2}\ d^{-1}$
1	C44IX40-1D1	40	40	8.33E-06	3	7	1.65	0.03309	0.04673	0.0432	0.11346	0.0466	0.2490	0.1255
	C44IX40-1D2	40	40	8.33E-06	6	7	1.65	0.03296	0.03720	0.0127	0.12639	0.0287	0.3125	0.0951
	C44IX40-1D3	40	40	8.33E-06	9	7	1.65	0.03280	0.03152	0.0119	0.13032	0.0278	0.3257	0.0862
	C44IX40-1D4	40	40	8.33E-06	12	7	1.65	0.03264	0.02374	0.0072	0.12331	0.0242	0.2897	0.0648
	C44IX40-1D5	40	40	8.33E-06	15	7	1.65	0.03248	0.01841	0.0058	0.10918	0.0199	0.2521	0.0551
	C44IX40-1D6	40	40	8.33E-06	18	7	1.65	0.03233	0.01483	0.0050	0.11481	0.0253	0.2250	0.0511
	C44IX40-1D7	40	40	8.33E-06	21	7	1.65	0.03217	0.05000	0.0409	0.19362	0.0575	0.2492	0.0709
	C44IX40-1D8	40	40	8.33E-06	24	7	1.65	0.03202	0.00975	-0.0153	0.10046	0.0015	0.1713	0.0243
	C44IX40-1D9	40	40	8.33E-06	27	7	1.65	0.03189	0.00874	**0.0033**	0.09134	**0.0175**	0.1498	**0.0335**
	C44IX40-1D10	40	40	8.33E-06	30	7	1.65	0.03177	0.00771	**0.0028**	0.09257	**0.0201**	0.1409	**0.0347**
2	C44IX40-2D1	45	40	8.33E-06	3	8	1.65	0.03313	0.02488	0.0230	0.05688	0.0233	0.1046	0.0526
	C44IX40-2D2	45	40	8.33E-06	6	8	1.65	0.03309	0.01857	0.0056	0.05673	0.0116	0.1142	0.0312
	C44IX40-2D3	45	40	8.33E-06	9	8	1.65	0.03304	0.01332	0.0036	0.05491	0.0109	0.1141	0.0287
	C44IX40-2D4	45	40	8.33E-06	12	8	1.65	0.03298	0.06957	outlier	0.18286	outlier	0.1821	outlier
	C44IX40-2D5	45	40	8.33E-06	15	8	1.65	0.03292	0.00690	0.0000	0.04727	0.0082	0.0945	0.0190
	C44IX40-2D6	45	40	8.33E-06	18	8	1.65	0.03288	0.00553	0.0018	0.05690	0.0137	0.0853	0.0193
	C44IX40-2D7	45	40	8.33E-06	21	8	1.65	0.03284	0.00413	0.0011	0.05306	0.0102	0.0761	0.0170
	C44IX40-2D8	45	40	8.33E-06	24	8	1.65	0.03280	0.00353	**0.0012**	0.04708	**0.0085**	0.0643	**0.0134**
	C44IX40-2D9	45	40	8.33E-06	27	8	1.65	0.03277	0.00305	**0.0010**	0.04803	**0.0102**	0.0632	**0.0158**
	C44IX40-2D10	45	40	8.33E-06	30	8	1.65	0.03273	0.00261	**0.0008**	0.04532	**0.0088**	0.0578	**0.0133**
3	C44IX40-3D1	60	40	8.33E-06	3	9	1.65	0.03314	0.01037	0.0094	0.04006	0.0164	0.0383	0.0193
	C44IX40-3D2	60	40	8.33E-06	6	9	1.65	0.03312	0.01423	0.0084	0.03555	0.0064	0.0476	0.0143
	C44IX40-3D3	60	40	8.33E-06	9	9	1.65	0.03310	0.00986	0.0024	0.03237	0.0060	0.0439	0.0101
	C44IX40-3D4	60	40	8.33E-06	12	9	1.65	0.03306	0.09240	outlier	0.20692	outlier	0.1534	outlier
	C44IX40-3D5	60	40	8.33E-06	15	9	1.65	0.03302	0.00637	0.0012	0.02563	0.0039	0.0344	0.0063
	C44IX40-3D6	60	40	8.33E-06	18	9	1.65	0.03301	0.00332	0.0000	0.02081	0.0033	0.0270	**0.0049**
	C44IX40-3D7	60	40	8.33E-06	21	9	1.65	0.03300	0.00200	0.0001	0.01969	**0.0038**	0.0250	**0.0058**
	C44IX40-3D8	60	40	8.33E-06	24	9	1.65	0.03299	0.00162	**0.0004**	0.01888	**0.0037**	0.0234	**0.0055**
	C44IX40-3D9	60	40	8.33E-06	27	9	1.65	0.03297	0.00140	**0.0004**	0.01740	**0.0033**	0.0216	**0.0050**
	C44IX40-3D10	60	40	8.33E-06	30	9	1.65	0.03296	0.00129	**0.0004**	0.01926	**0.0044**	0.0233	**0.0063**
4	C44IX40-4D1	105	40	8.33E-06	3	10	0.83	0.01659	0.00576	0.0101	0.01329	0.0109	0.0147	0.0148
	C44IX40-4D2	105	40	8.33E-06	6	10	0.83	0.01658	0.00395	0.0016	0.00970	0.0025	0.0104	0.0030
	C44IX40-4D3	105	40	8.33E-06	9	10	0.83	0.01658	0.00255	0.0007	0.01026	0.0044	0.0101	0.0050
	C44IX40-4D4	105	40	8.33E-06	12	10	0.83	0.01657	0.02371	outlier	0.04787	outlier	0.0391	outlier
	C44IX40-4D5	105	40	8.33E-06	15	10	0.83	0.01656	0.00131	-0.0003	0.00653	0.0011	0.0060	0.0009
	C44IX40-4D6	105	40	8.33E-06	18	10	0.83	0.01656	0.00093	0.0001	0.00623	**0.0024**	0.0052	**0.0022**
	C44IX40-4D7	105	40	8.33E-06	21	10	0.83	0.01656	0.00077	0.0002	0.00582	**0.0022**	0.0048	**0.0022**
	C44IX40-4D8	105	40	8.33E-06	24	10	0.83	0.01656	0.00061	**0.00003**	0.00548	**0.0021**	0.0044	**0.0020**
	C44IX40-4D9	105	40	8.33E-06	27	10	0.83	0.01655	0.00054	**0.00004**	0.00554	**0.0023**	0.0045	**0.0023**
	C44IX40-4D10	105	40	8.33E-06	30	10	0.83	0.01655	0.00048	**0.00000**	0.00636	0.0029	0.0050	0.0028
5	C44IX40-5D1	270	40	8.33E-06	3	11	0.83	0.01659	0.00835	0.0150	0.01639	0.0134	0.0162	0.0162
	C44IX40-5D2	270	40	8.33E-06	6	11	0.83	0.01658	0.00672	0.0044	0.01199	0.0031	0.0110	0.0030
	C44IX40-5D3	270	40	8.33E-06	9	11	0.83	0.01658	0.00486	0.0025	0.01222	0.0051	0.0100	0.0045
	C44IX40-5D4	270	40	8.33E-06	12	11	0.83	0.01658	0.00346	0.0016	0.00901	0.0023	0.0065	0.0015
	C44IX40-5D5	270	40	8.33E-06	15	11	0.83	0.01657	0.00235	0.0008	0.00749	0.0024	0.0049	0.0016
	C44IX40-5D6	270	40	8.33E-06	18	11	0.83	0.01657	0.00183	0.0009	0.00701	0.0026	0.0041	0.0016
	C44IX40-5D7	270	40	8.33E-06	21	11	0.83	0.01657	0.00140	**0.0006**	0.00527	**0.0014**	0.0028	**0.0008**
	C44IX40-5D8	270	40	8.33E-06	24	11	0.83	0.01656	0.00105	**0.0003**	0.00450	**0.0015**	0.0022	**0.0008**
	C44IX40-5D9	270	40	8.33E-06	27	11	0.83	0.01656	0.00089	**0.0003**	0.00368	**0.0011**	0.0017	**0.0006**
	C44IX40-5D10	270	40	8.33E-06	30	11	0.83	0.01656	0.00067	0.0001	0.00360	**0.0014**	0.0017	**0.0008**

Table A18. ICP-MS Analysis Results from Dissolution of Glass ORLEC44 at 23 °C.

Exp.	Sample ID	Inf [Si] ppm	T °C	Flow Rate, m^3/d	Time, days	pH 23°C	Glass Mass g	SA m^2	[Mo] ppm	Mo Rate $g_{-glass}\ m^{-2}\ d^{-1}$	[Cs] ppm	Cs Rate $g_{-glass}\ m^{-2}\ d^{-1}$	[Re] ppm	Re Rate $g_{-glass}\ m^{-2}\ d^{-1}$
1	C44IX23-1D1	35	23	8.33E-06	3	7	3.28	0.0658	0.02030	0.0092	0.02173	0.0045	0.0501	0.0127
	C44IX23-1D2	35	23	8.33E-06	6	7	3.28	0.0658	0.01771	0.0034	0.02356	0.0026	0.0536	0.0072
	C44IX23-1D3	35	23	8.33E-06	9	7	3.28	0.0658	0.01338	0.0019	0.02227	0.0022	0.0508	0.0061
	C44IX23-1D4	35	23	8.33E-06	12	7	3.28	0.0658	0.01118	0.0019	0.02501	0.0029	0.0516	0.0066
	C44IX23-1D5	35	23	8.33E-06	15	7	3.28	0.0657	0.01095	0.0023	0.02677	0.0029	0.0607	0.0089
	C44IX23-1D6	35	23	8.33E-06	18	7	3.28	0.0657	0.01490	outlier	0.18659	outlier	0.1622	outlier
	C44IX23-1D7	35	23	8.33E-06	21	7	3.28	0.0656	0.00745	0.0007	0.02234	0.0046	0.0484	0.0123
	C44IX23-1D8	35	23	8.33E-06	24	7	3.28	0.0656	0.00761	0.0017	0.02588	0.0030	0.0570	0.0083
	C44IX23-1D9	35	23	8.33E-06	27	7	3.28	0.0656	0.00660	**0.0011**	0.02553	**0.0026**	0.0511	**0.0057**
	C44IX23-1D10	35	23	8.33E-06	30	7	3.28	0.0655	0.00634	**0.0013**	0.02409	**0.0023**	0.0522	**0.0068**
2	C44IX23-2D1	40	23	8.33E-06	3	8	3.28	0.0658	0.01426	0.0066	0.01603	0.0033	0.0302	0.0077
	C44IX23-2D2	40	23	8.33E-06	6	8	3.28	0.0658	0.01224	0.0023	0.01586	0.0016	0.0259	0.0027
	C44IX23-2D3	40	23	8.33E-06	9	8	3.28	0.0658	0.00905	0.0013	0.01700	0.0019	0.0234	0.0027
	C44IX23-2D4	40	23	8.33E-06	12	8	3.28	0.0658	0.00602	0.0006	0.01439	0.0012	0.0182	0.0016
	C44IX23-2D5	40	23	8.33E-06	15	8	3.28	0.0658	0.00430	0.0005	0.01174	0.0009	0.0150	0.0015
	C44IX23-2D6	40	23	8.33E-06	18	8	3.28	0.0658	0.00348	0.0005	0.01138	0.0011	0.0136	0.0016
	C44IX23-2D7	40	23	8.33E-06	21	8	3.28	0.0658	0.00342	0.0007	0.01167	0.0012	0.0146	0.0020
	C44IX23-2D8	40	23	8.33E-06	24	8	3.28	0.0658	0.00312	**0.0006**	0.01095	**0.0011**	0.0140	**0.0017**
	C44IX23-2D9	40	23	8.33E-06	27	8	3.28	0.0658	0.00284	**0.0005**	0.01187	**0.0013**	0.0139	**0.0018**
	C44IX23-2D10	40	23	8.33E-06	30	8	3.28	0.0658	0.00246	**0.0004**	0.01081	**0.0010**	0.0134	**0.0016**
3	C44IX23-3D1	52	23	8.33E-06	3	9	3.28	0.0658	0.01106	0.0052	0.01135	0.0023	0.0181	0.0046
	C44IX23-3D2	52	23	8.33E-06	6	9	3.28	0.0658	0.00377	-0.0009	0.00593	0.0001	0.0057	-0.0008
	C44IX23-3D3	52	23	8.33E-06	9	9	3.28	0.0658	0.00597	0.0019	0.01251	0.0020	0.0141	0.0028
	C44IX23-3D4	52	23	8.33E-06	12	9	3.28	0.0658	0.00397	0.0004	0.01003	0.0008	0.0110	0.0010
	C44IX23-3D5	52	23	8.33E-06	15	9	3.28	0.0658	0.00305	0.0005	0.00840	0.0007	0.0088	0.0008
	C44IX23-3D6	52	23	8.33E-06	18	9	3.28	0.0658	0.00200	0.0002	0.00637	0.0004	0.0064	0.0005
	C44IX23-3D7	52	23	8.33E-06	21	9	3.28	0.0658	0.00223	0.0005	0.00726	0.0008	0.0076	0.0011
	C44IX23-3D8	52	23	8.33E-06	24	9	3.28	0.0658	0.00214	**0.0004**	0.00779	**0.0009**	0.0079	**0.0010**
	C44IX23-3D9	52	23	8.33E-06	27	9	3.28	0.0658	0.00179	**0.0003**	0.00713	**0.0007**	0.0070	**0.0008**
	C44IX23-3D10	52	23	8.33E-06	30	9	3.28	0.0658	0.00165	**0.0003**	0.00674	**0.0007**	0.0068	**0.0008**
4	C44IX23-4D1	90	23	8.33E-06	3	10	1.64	0.0329	0.00486	0.0042	0.00658	0.0027	0.0075	0.0038
	C44IX23-4D2	90	23	8.33E-06	6	10	1.64	0.0329	0.00820	0.0052	0.01144	0.0034	0.0159	0.0062
	C44IX23-4D3	90	23	8.33E-06	9	10	1.64	0.0329	0.00261	-0.0016	0.00629	0.0002	0.0045	-0.0017
	C44IX23-4D4	90	23	8.33E-06	12	10	1.64	0.0329	0.00197	0.0004	0.00669	0.0015	0.0038	0.0008
	C44IX23-4D5	90	23	8.33E-06	15	10	1.64	0.0329	0.00132	0.0001	0.00505	0.0007	0.0027	0.0004
	C44IX23-4D6	90	23	8.33E-06	18	10	1.64	0.0329	0.00123	0.0003	0.00544	0.0012	0.0026	0.0007
	C44IX23-4D7	90	23	8.33E-06	21	10	1.64	0.0329	0.00123	0.0004	0.00484	0.0009	0.0027	0.0007
	C44IX23-4D8	90	23	8.33E-06	24	10	1.64	0.0329	0.00092	**0.0001**	0.00380	**0.0006**	0.0022	**0.0004**
	C44IX23-4D9	90	23	8.33E-06	27	10	1.64	0.0329	0.00077	**0.0001**	0.00403	**0.0009**	0.0020	**0.0005**
	C44IX23-4D10	90	23	8.33E-06	30	10	1.64	0.0329	0.00065	**0.0000**	0.00312	**0.0005**	0.0016	**0.0003**
5	C44IX23-5D1	230	23	8.33E-06	3	11	1.64	0.0329	0.00740	0.0068	0.01709	0.0071	0.0140	0.0071
	C44IX23-5D2	230	23	8.33E-06	6	11	1.64	0.0329	0.00350	-0.0003	0.00568	-0.0012	0.0059	-0.0005
	C44IX23-5D3	230	23	8.33E-06	9	11	1.64	0.0329	0.00303	0.0011	0.00509	0.0009	0.0047	0.0009
	C44IX23-5D4	230	23	8.33E-06	12	11	1.64	0.0329	0.00821	outlier	0.04346	outlier	0.0234	outlier
	C44IX23-5D5	230	23	8.33E-06	15	11	1.64	0.0329	0.00200	0.0004	0.00479	0.0009	0.0033	0.0005
	C44IX23-5D6	230	23	8.33E-06	18	11	1.64	0.0329	0.00361	0.0024	0.00633	0.0016	0.0050	0.0017
	C44IX23-5D7	230	23	8.33E-06	21	11	1.64	0.0329	0.00336	0.0014	0.00636	0.0013	0.0047	0.0011
	C44IX23-5D8	230	23	8.33E-06	24	11	1.64	0.0329	0.00236	**0.0006**	0.00606	**0.0012**	0.0038	**0.0007**
	C44IX23-5D9	230	23	8.33E-06	27	11	1.64	0.0329	0.00269	**0.0013**	0.00622	**0.0013**	0.0040	**0.0011**
	C44IX23-5D10	230	23	8.33E-06	30	11	1.64	0.0329	0.00204	**0.0006**	0.00659	**0.0014**	0.0033	**0.0007**

APPENDIX B

PLOTS OF PULSED-FLOW TEST DATA

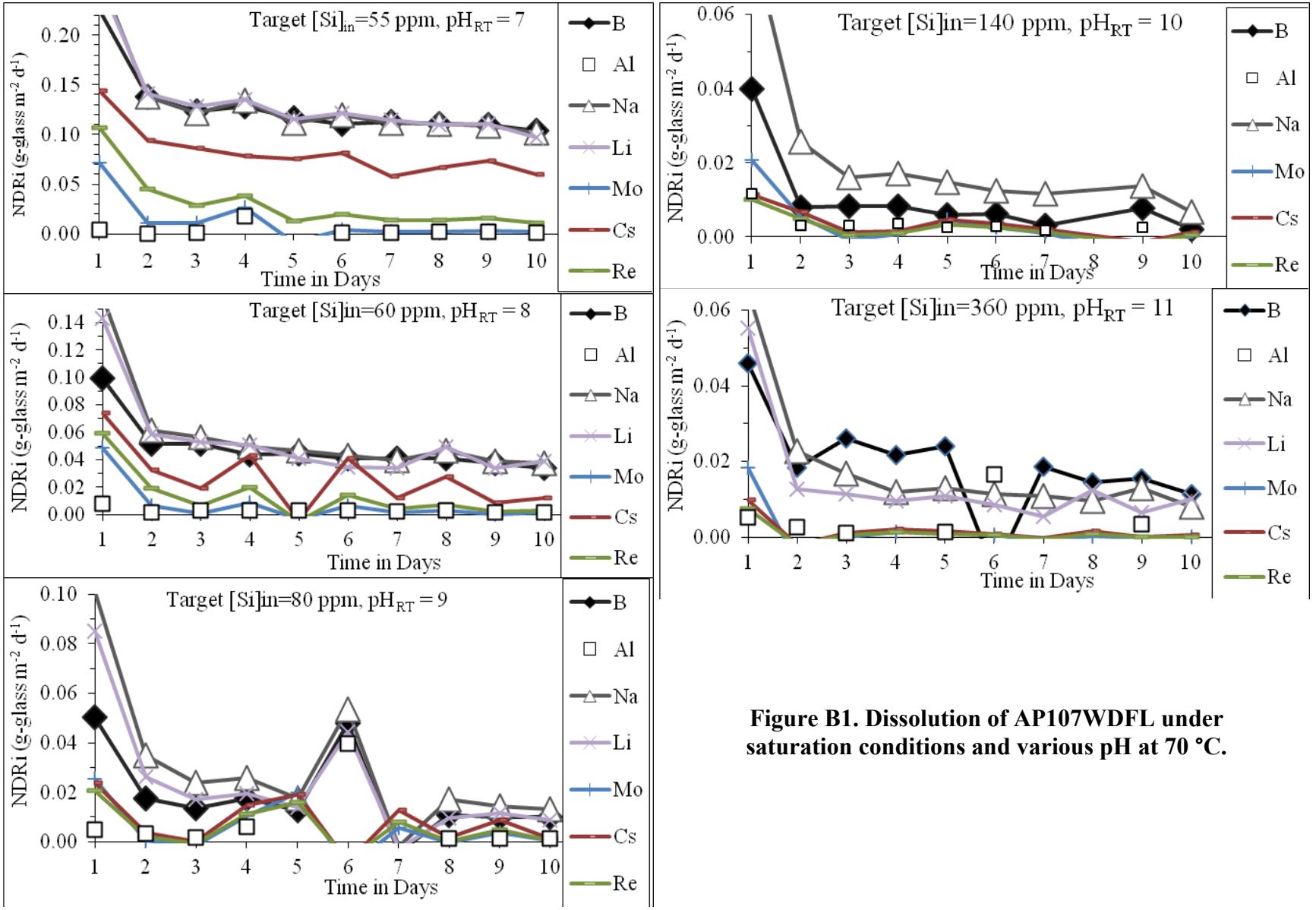

Figure B1. Dissolution of AP107WDFL under saturation conditions and various pH at 70 °C.

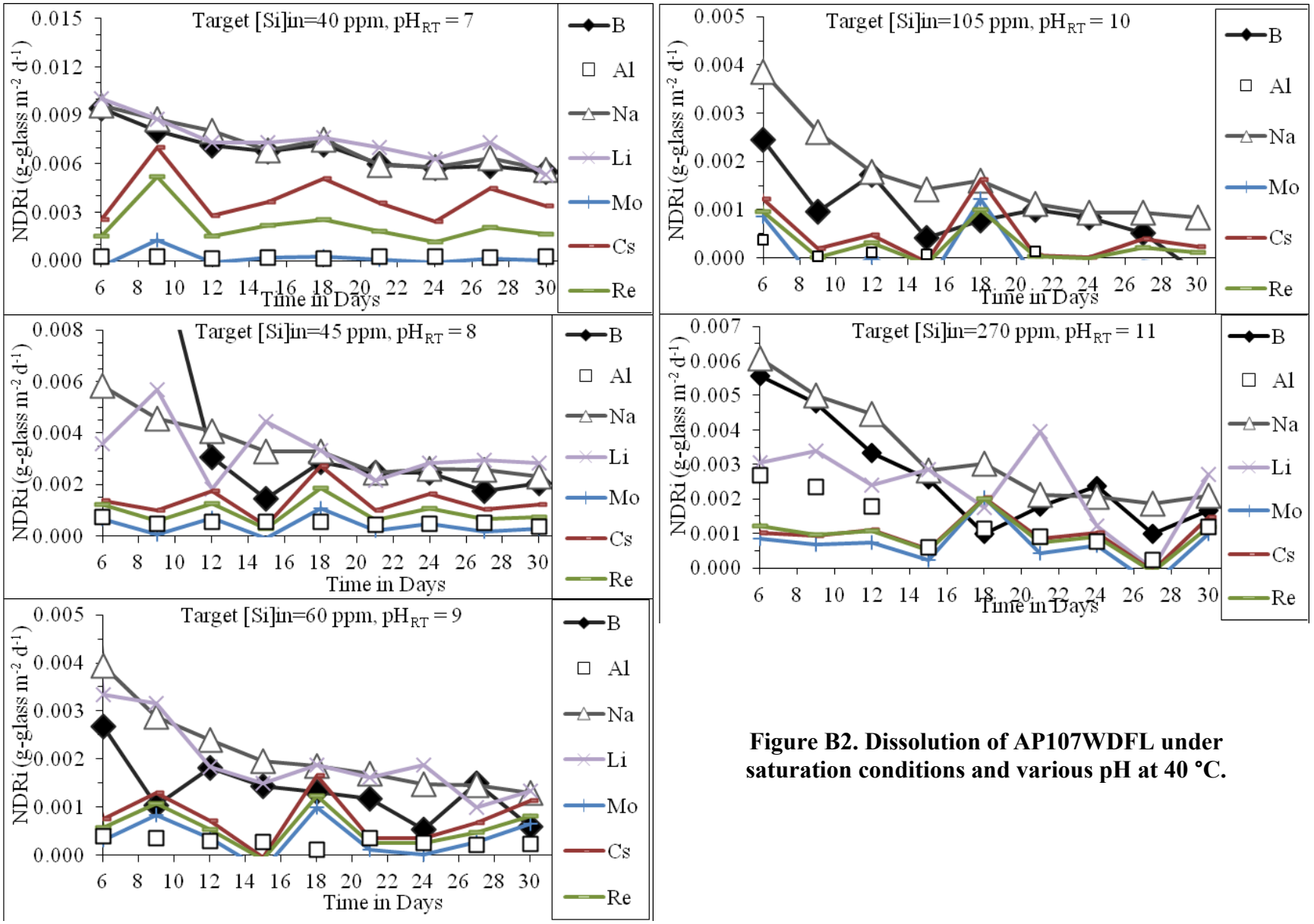

Figure B2. Dissolution of AP107WDFL under saturation conditions and various pH at 40 °C.

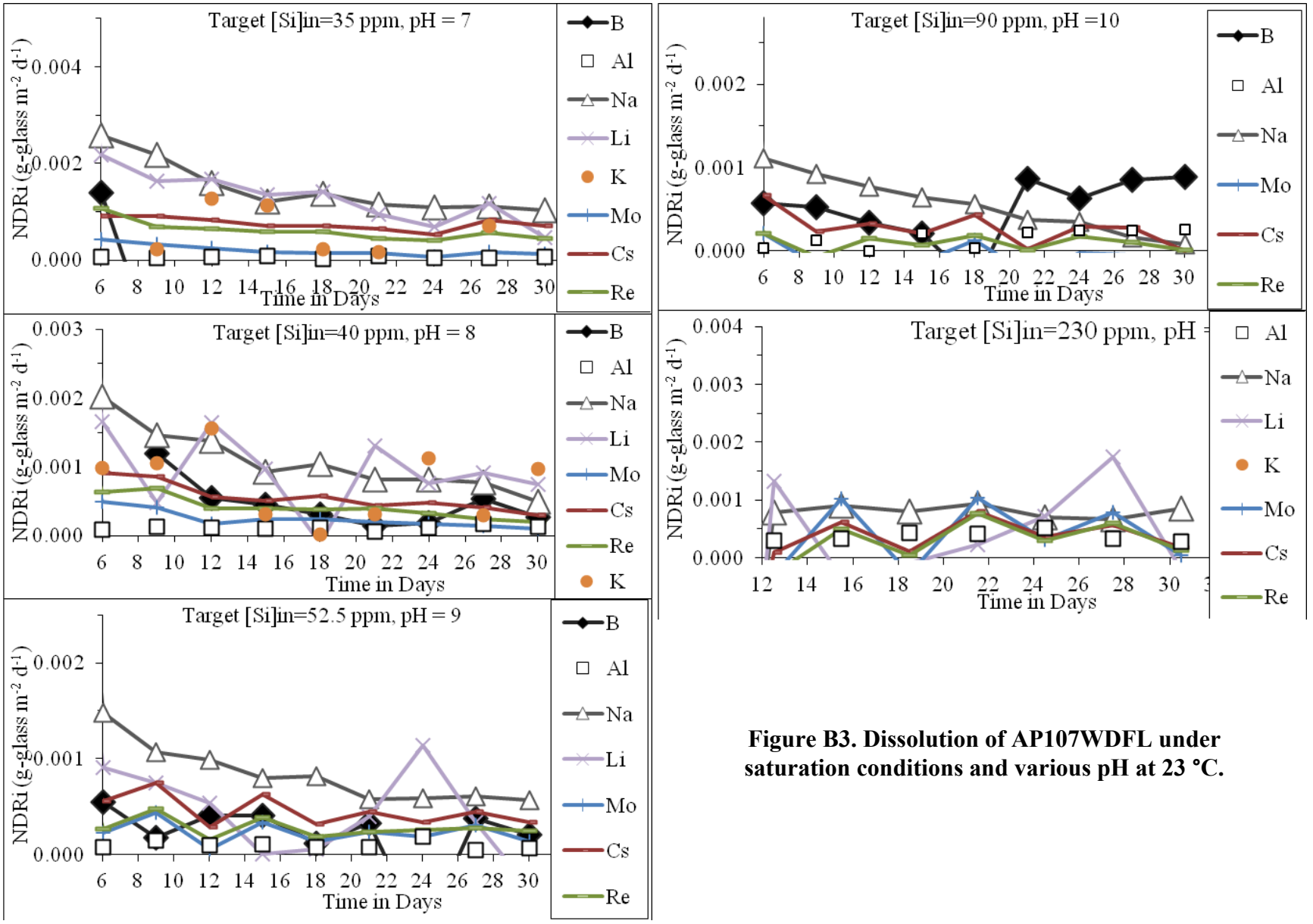

Figure B3. Dissolution of AP107WDFL under saturation conditions and various pH at 23 °C.

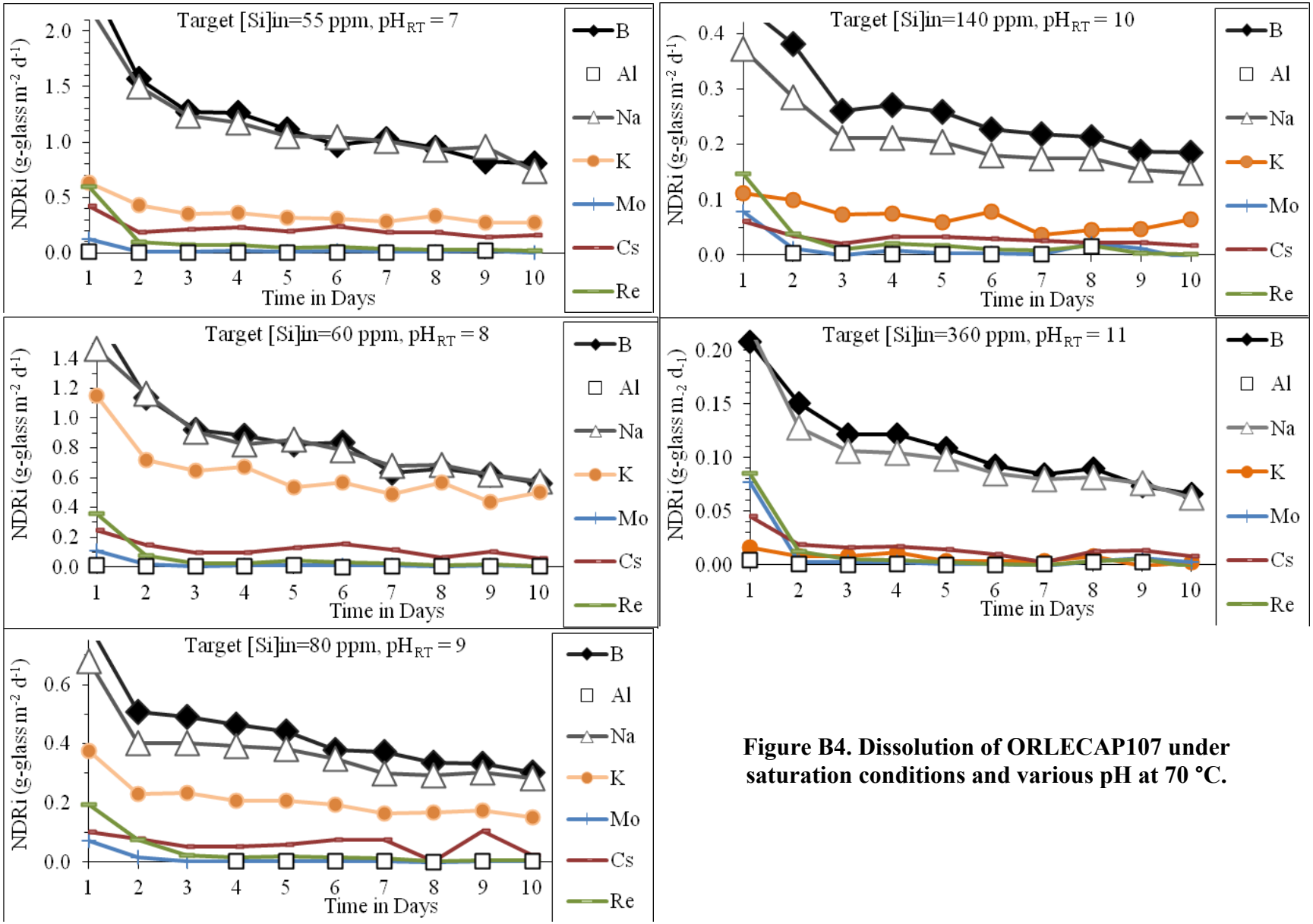

Figure B4. Dissolution of ORLECAP107 under saturation conditions and various pH at 70 °C.

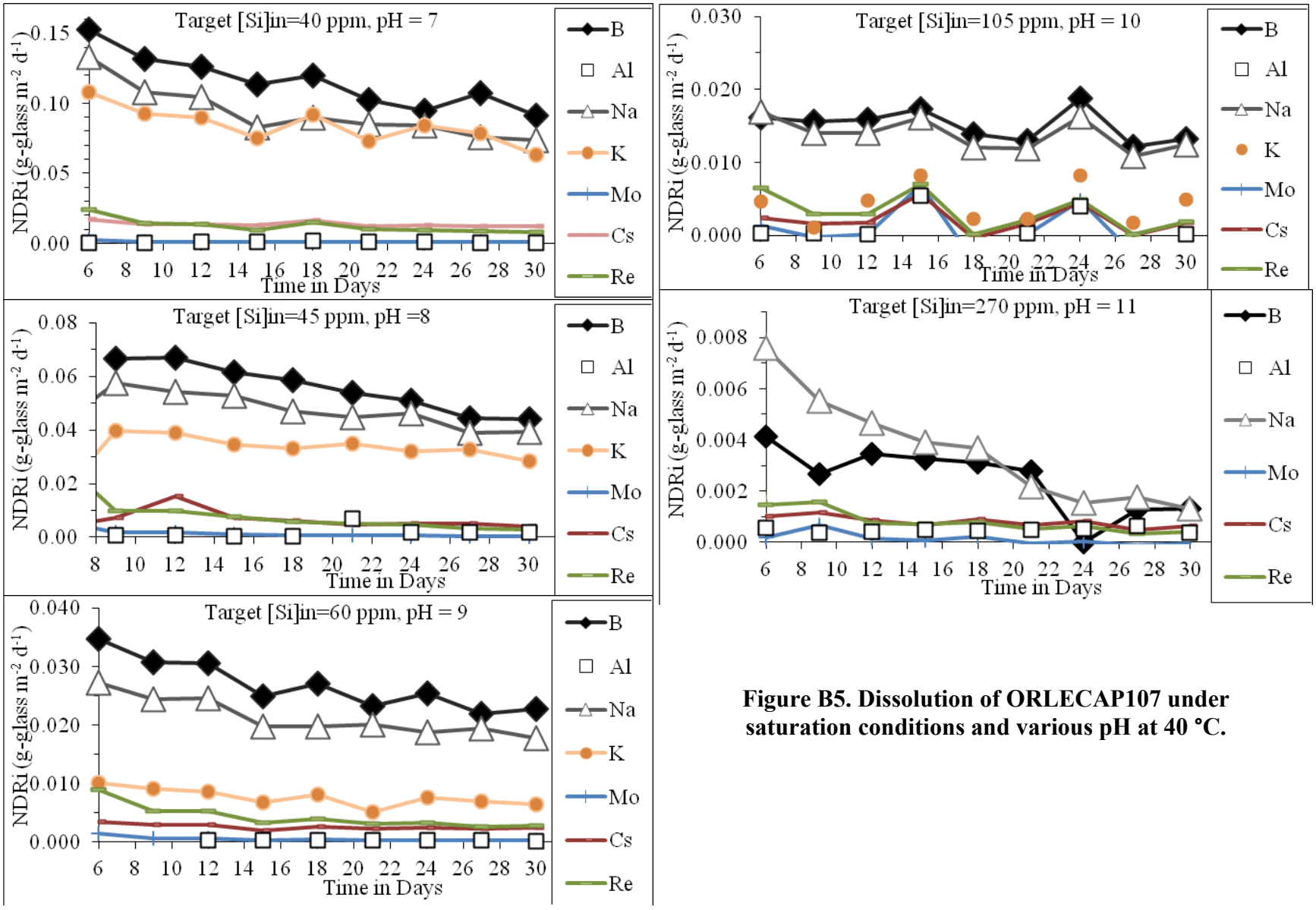

Figure B5. Dissolution of ORLECAP107 under saturation conditions and various pH at 40 °C.

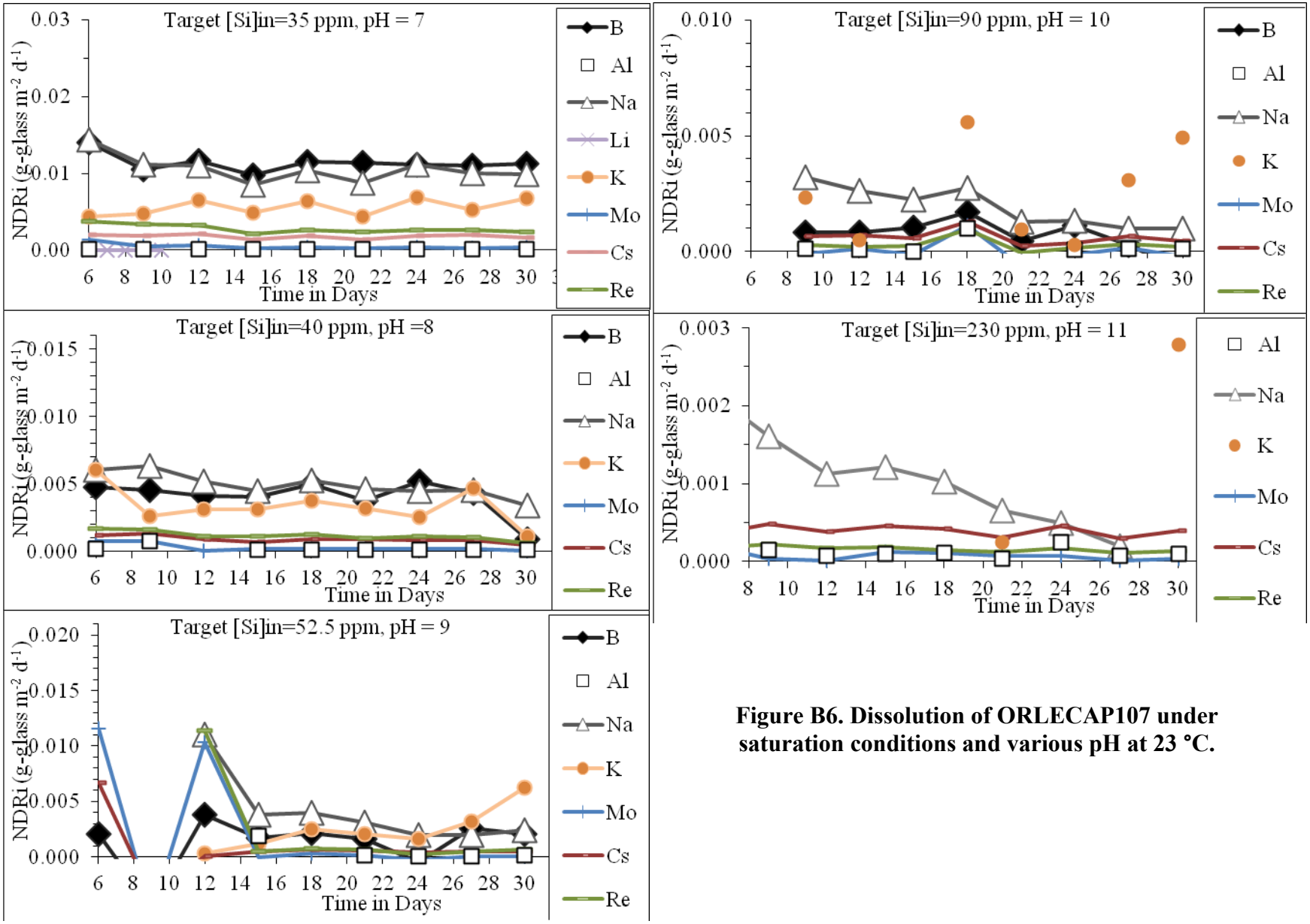

Figure B6. Dissolution of ORLECAP107 under saturation conditions and various pH at 23 °C.

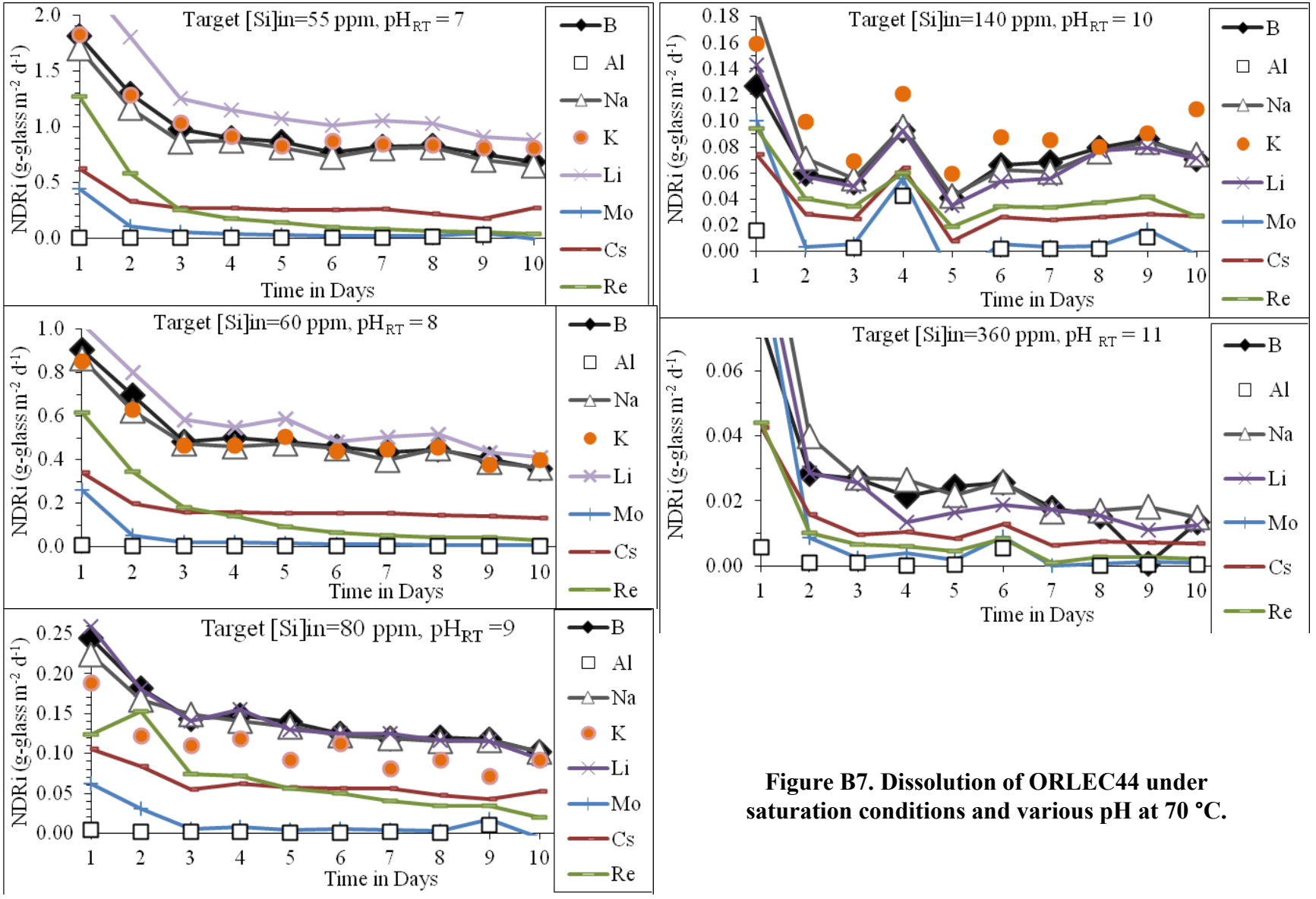

Figure B7. Dissolution of ORLEC44 under saturation conditions and various pH at 70 °C.

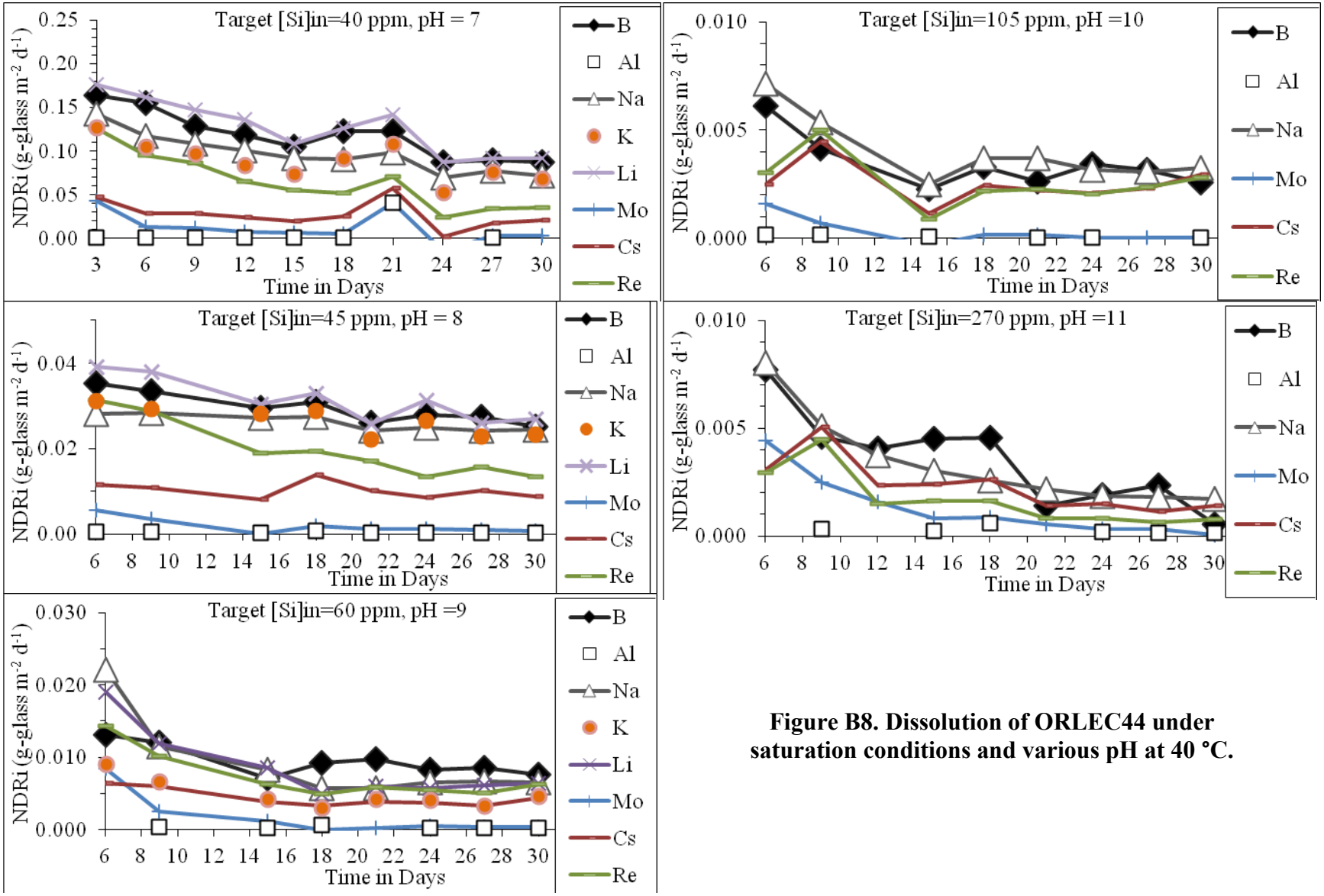

Figure B8. Dissolution of ORLEC44 under saturation conditions and various pH at 40 °C.

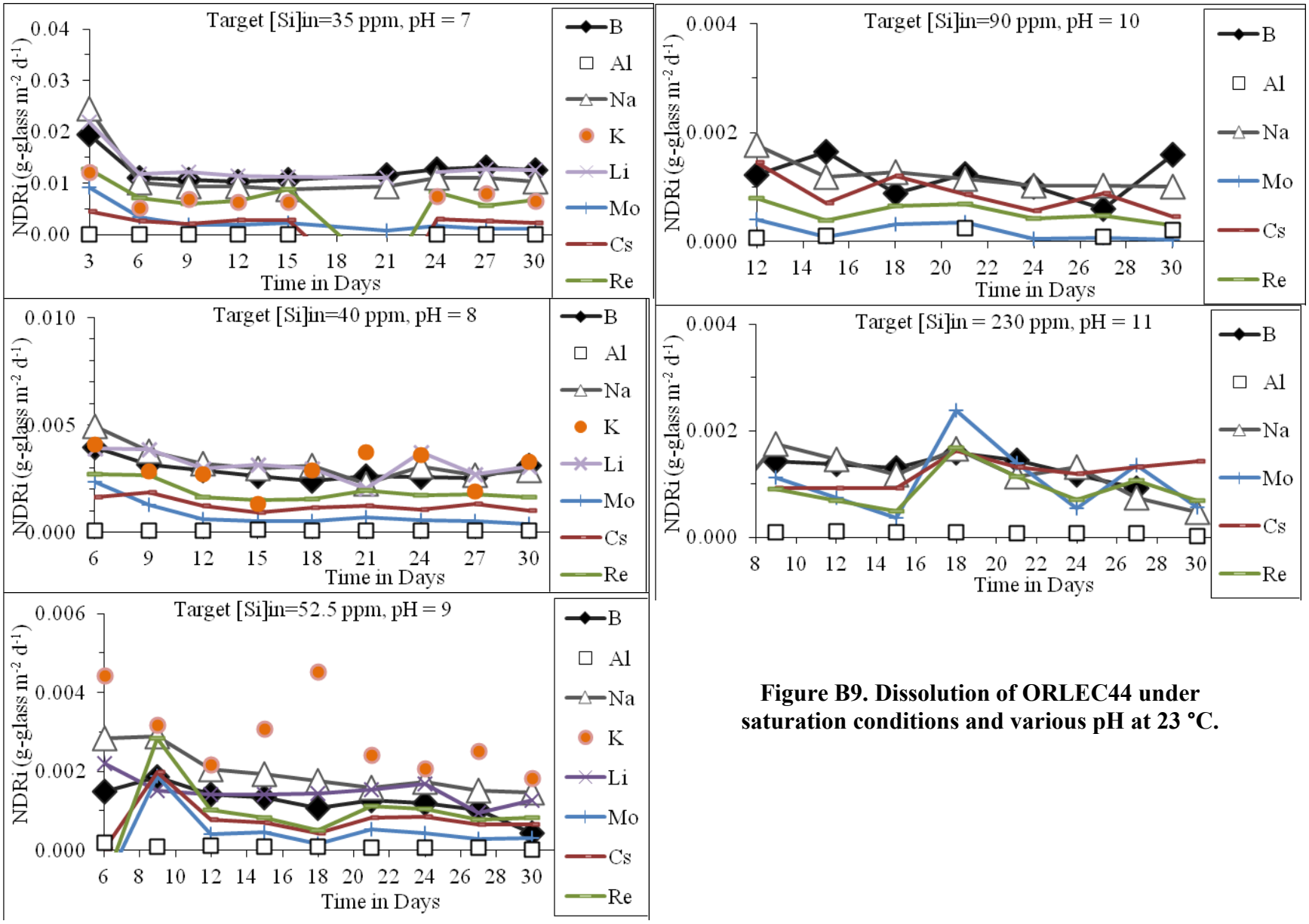

Figure B9. Dissolution of ORLEC44 under saturation conditions and various pH at 23 °C.

APPENDIX C

SODIUM ION-EXCHANGE PLOTS COMPARING THE VALUES BY DIFFERENCE OF NDR_{Na} TO NDR_{B}, NDR_{Re}, AND NDR_{Mo}

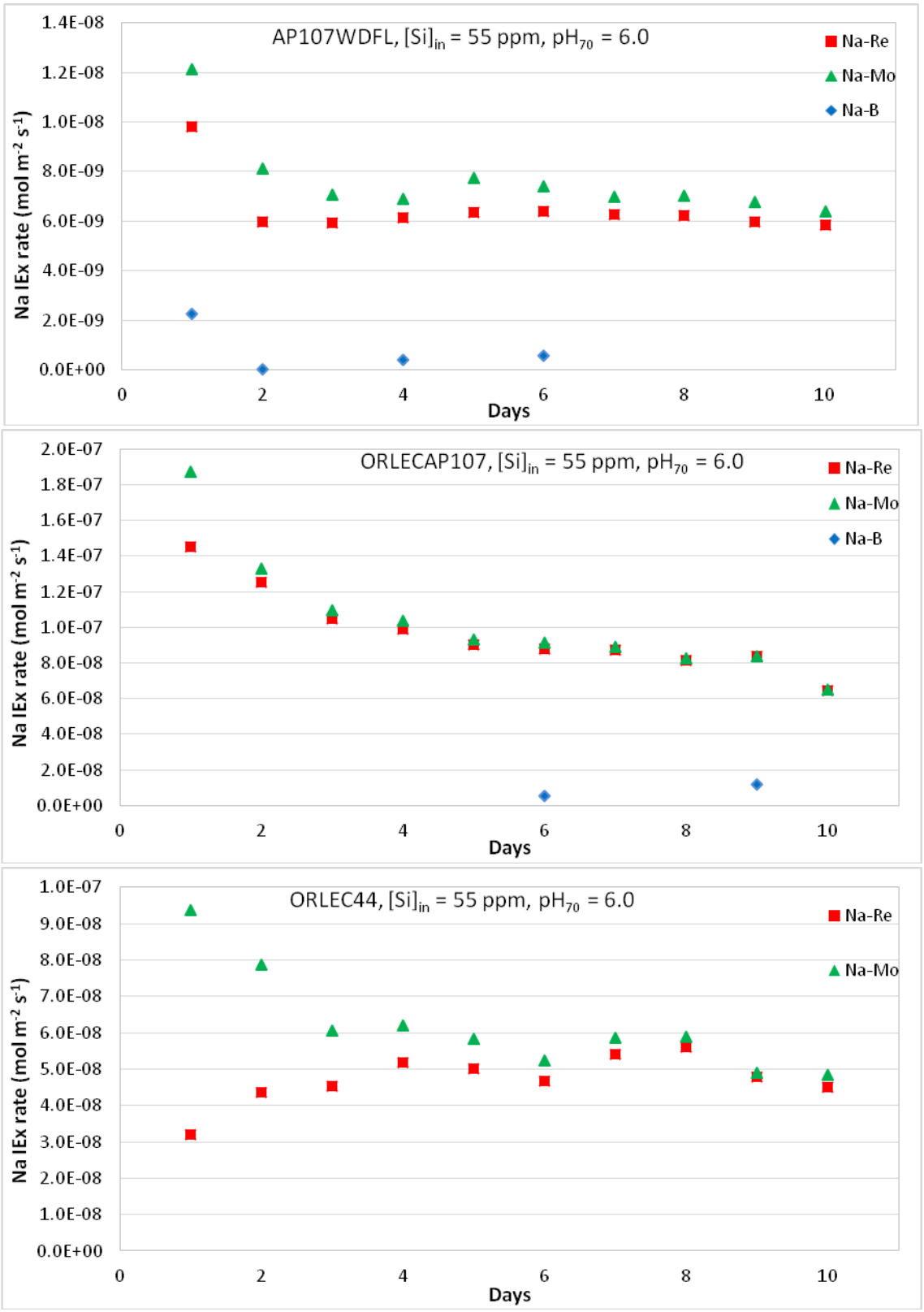

Figure C1. Plot of sodium ion exchange rate calculated from difference of sodium normalized release rate to that of boron, rhenium, or molybdenum, at 70 °C, pH_{23} =7.

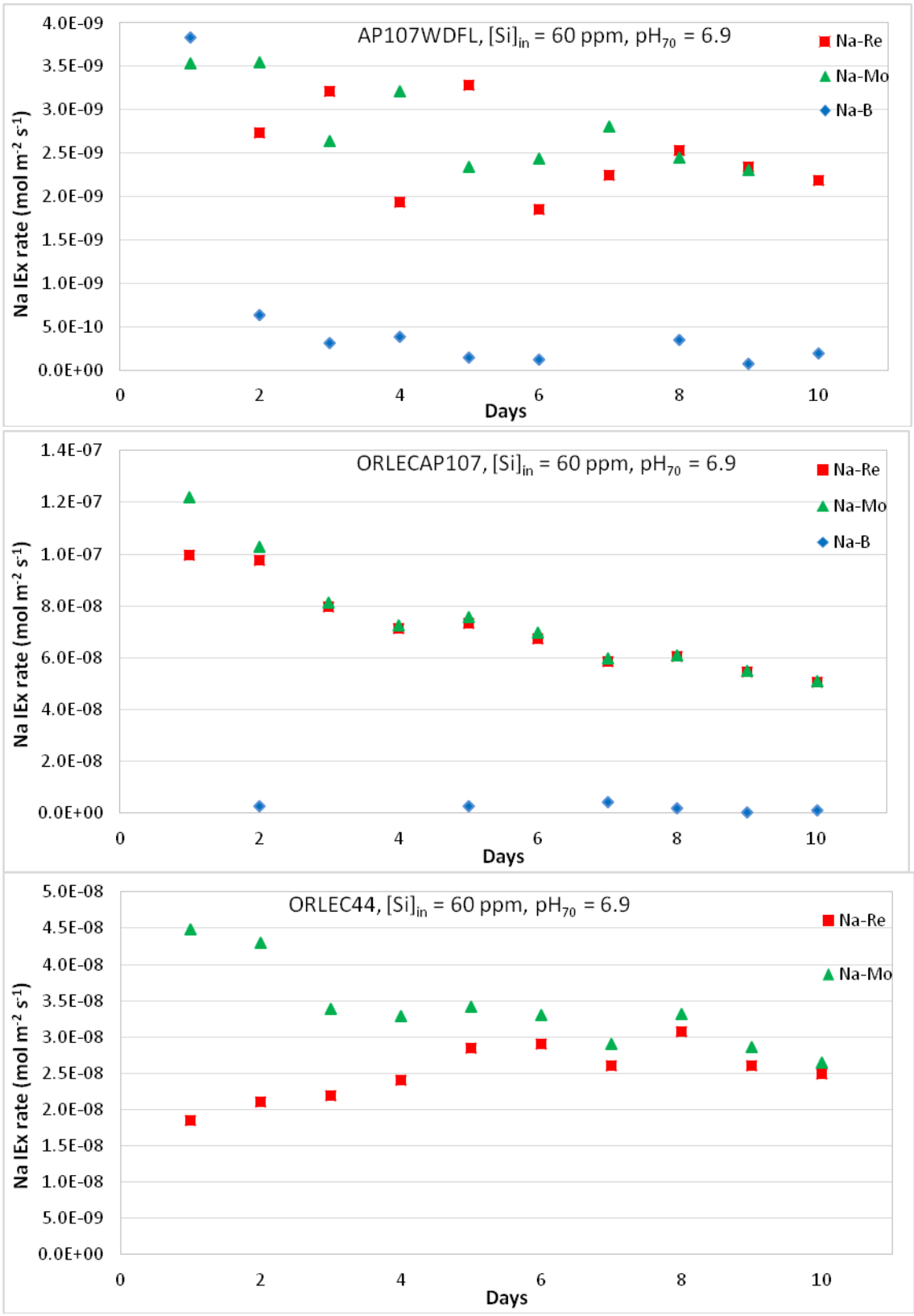

Figure C2. Plot of sodium ion exchange rate calculated from difference of sodium normalized release rate to that of boron, rhenium, or molybdenum, at 70 °C, pH_{23} =8.

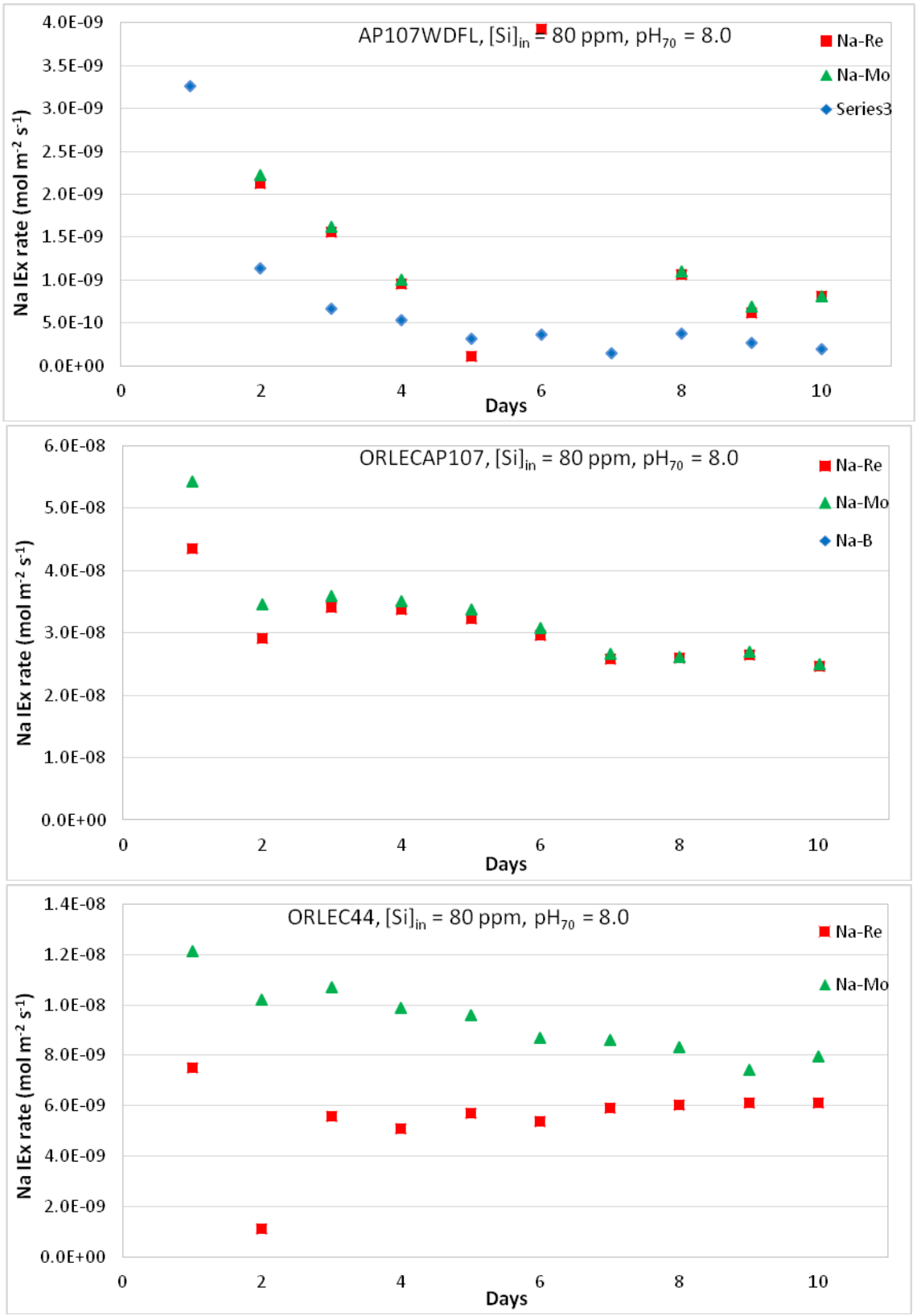

Figure C3. Plot of sodium ion exchange rate calculated from difference of sodium normalized release rate to that of boron, rhenium, or molybdenum, at 70 °C, pH_{23} =9.

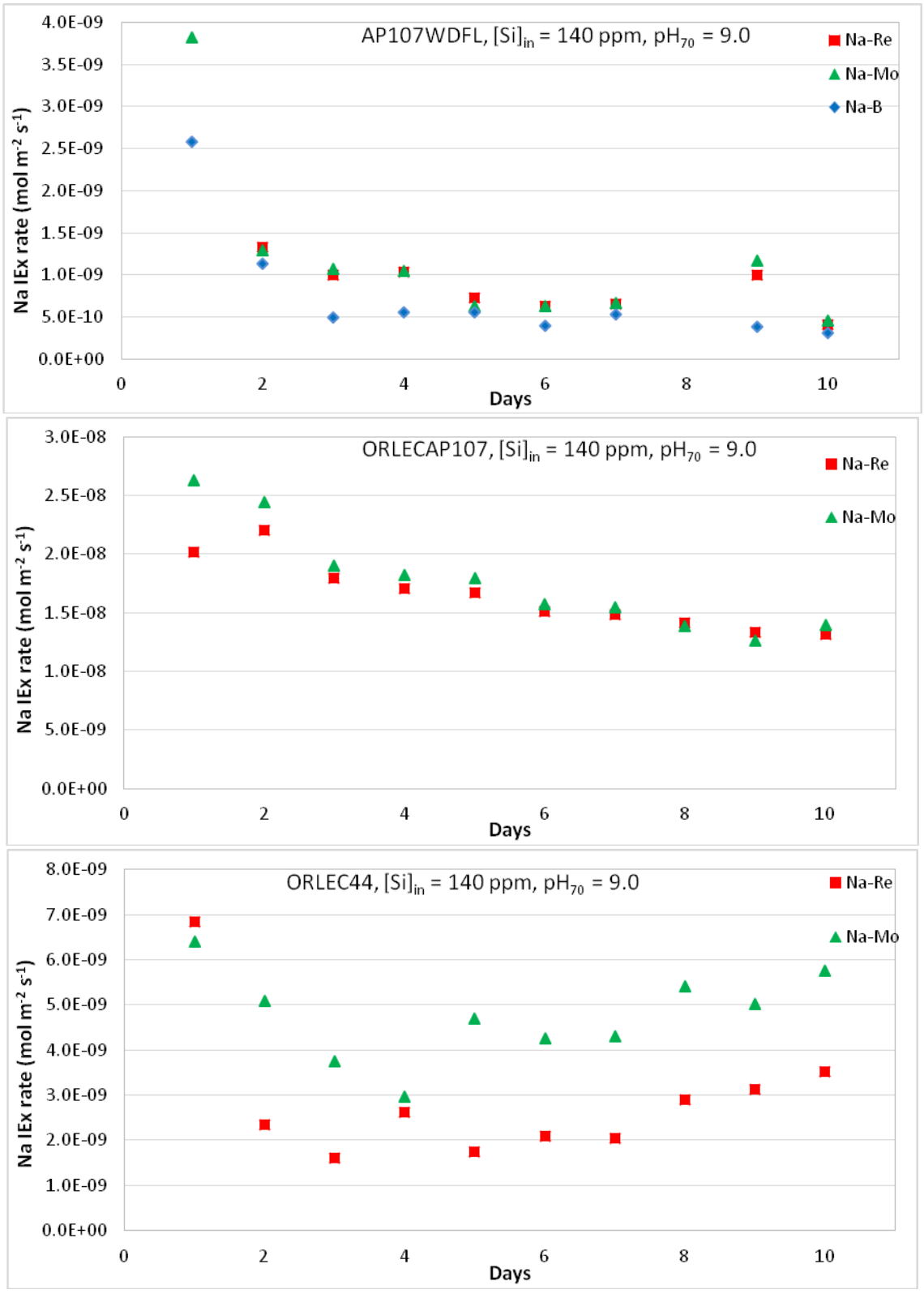

Figure C4. Plot of sodium ion exchange rate calculated from difference of sodium normalized release rate to that of boron, rhenium, or molybdenum, at 70 °C, pH_{23} =10.

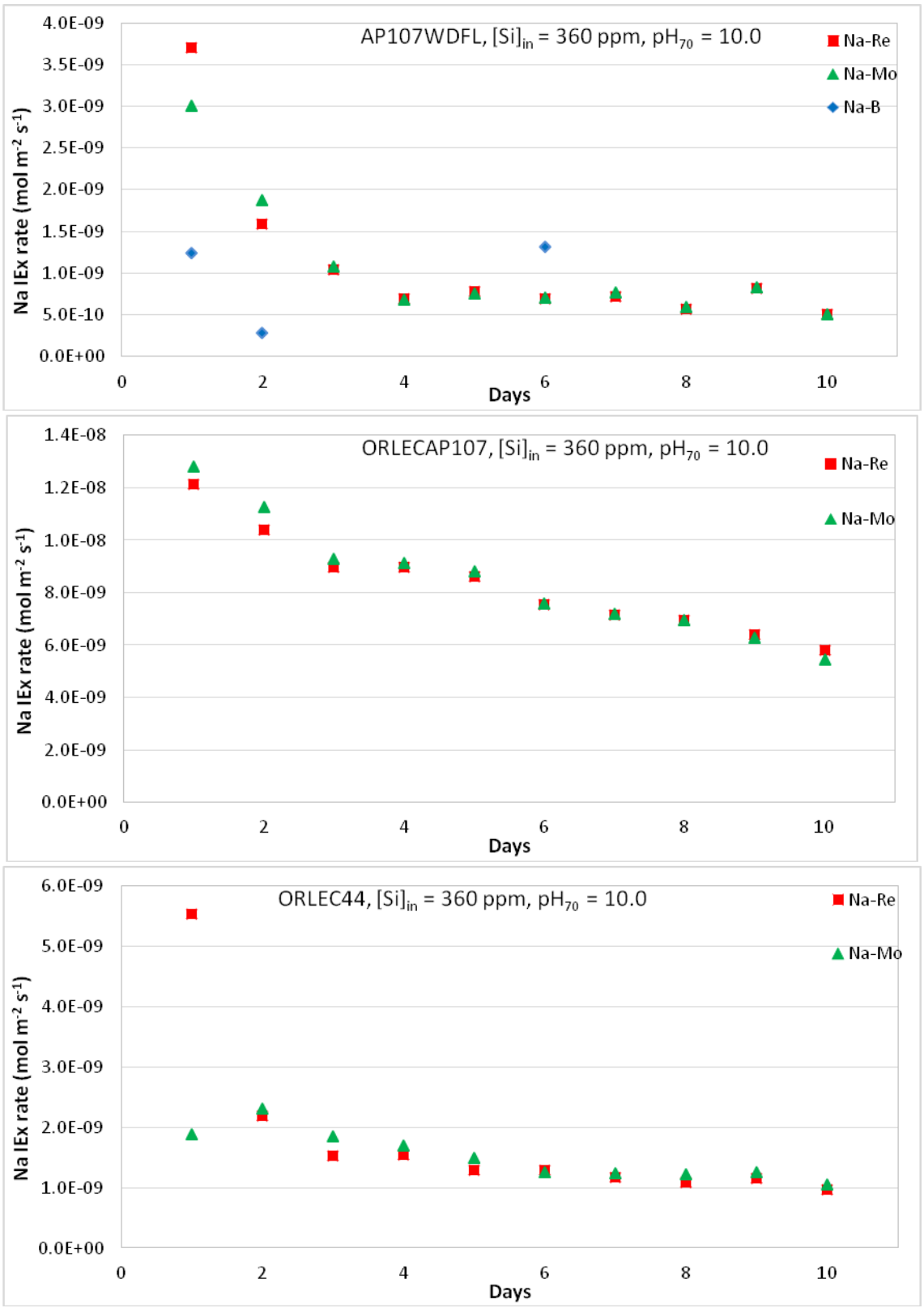

Figure C5. Plot of sodium ion exchange rate calculated from difference of sodium normalized release rate to that of boron, rhenium, or molybdenum, at 70 °C, pH_{23} =11.

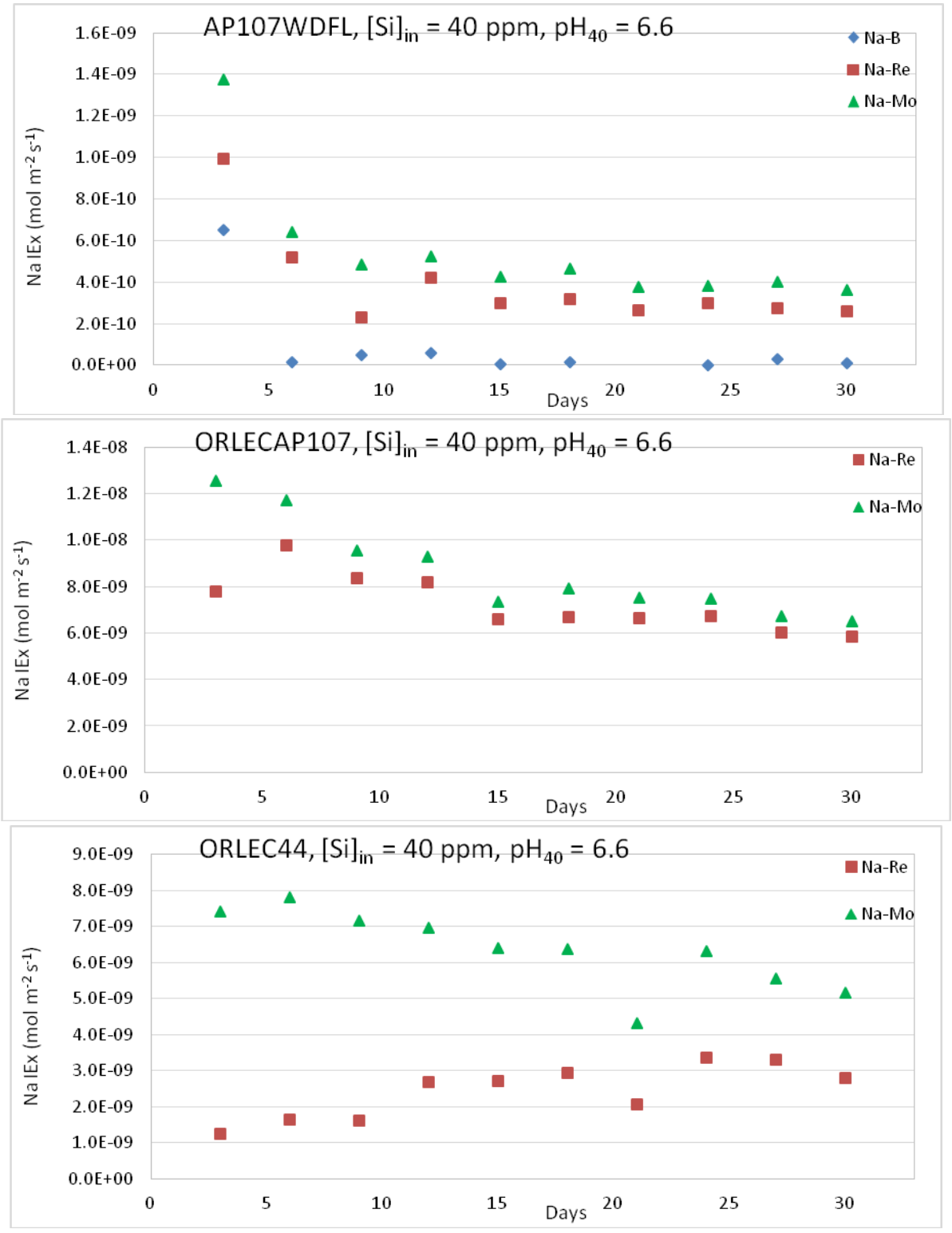

Figure C6. Plot of sodium ion exchange rate calculated from difference of sodium normalized release rate to that of boron, rhenium or molybdenum, at 40 °C, pH_{23} =7.

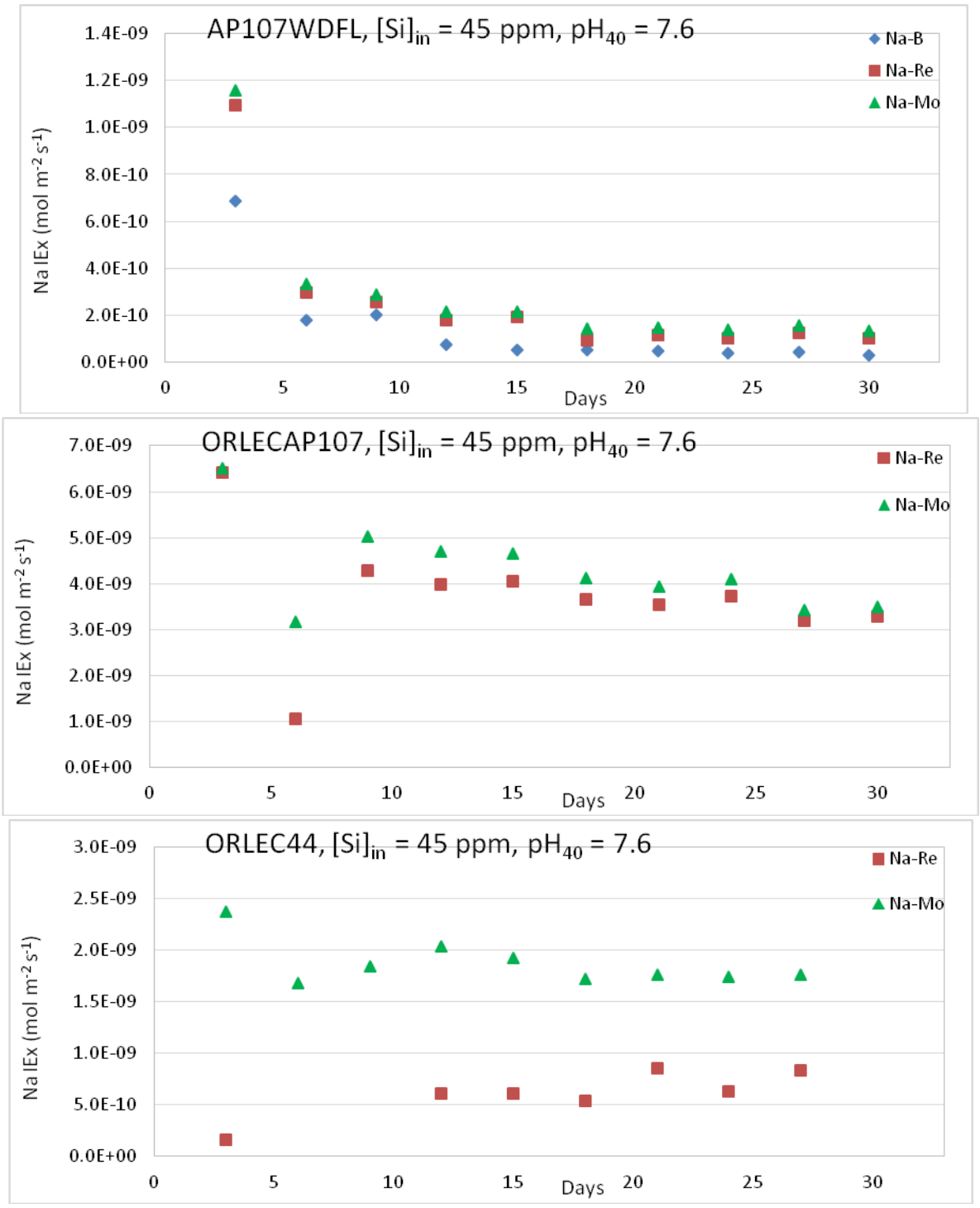

Figure C7. Plot of sodium ion exchange rate calculated from difference of sodium normalized release rate to that of boron, rhenium, or molybdenum, at 40 °C, pH_{23} =8.

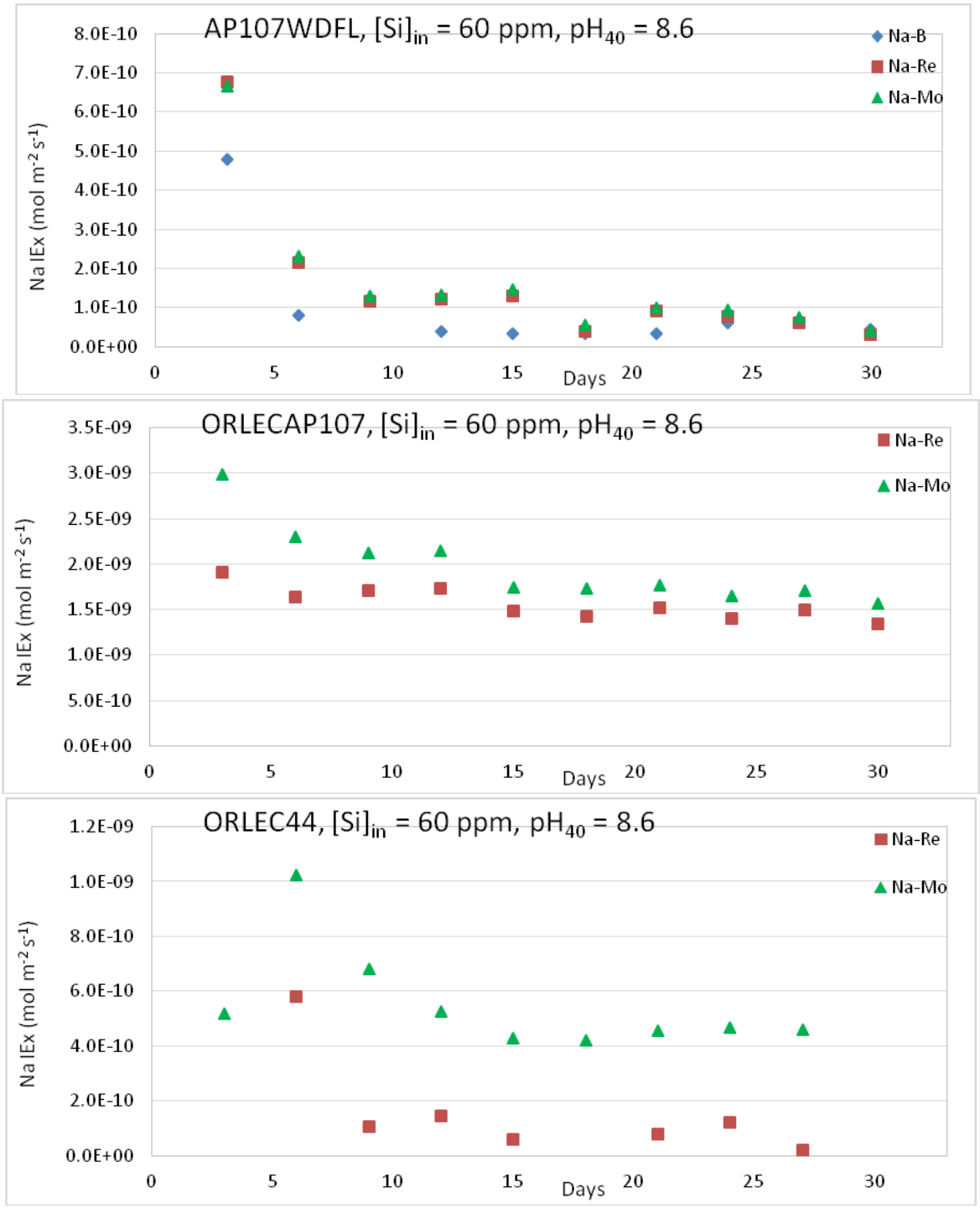

Figure C8. Plot of sodium ion exchange rate calculated from difference of sodium normalized release rate to that of boron, rhenium, or molybdenum, at 40 °C, pH_{23} =9.

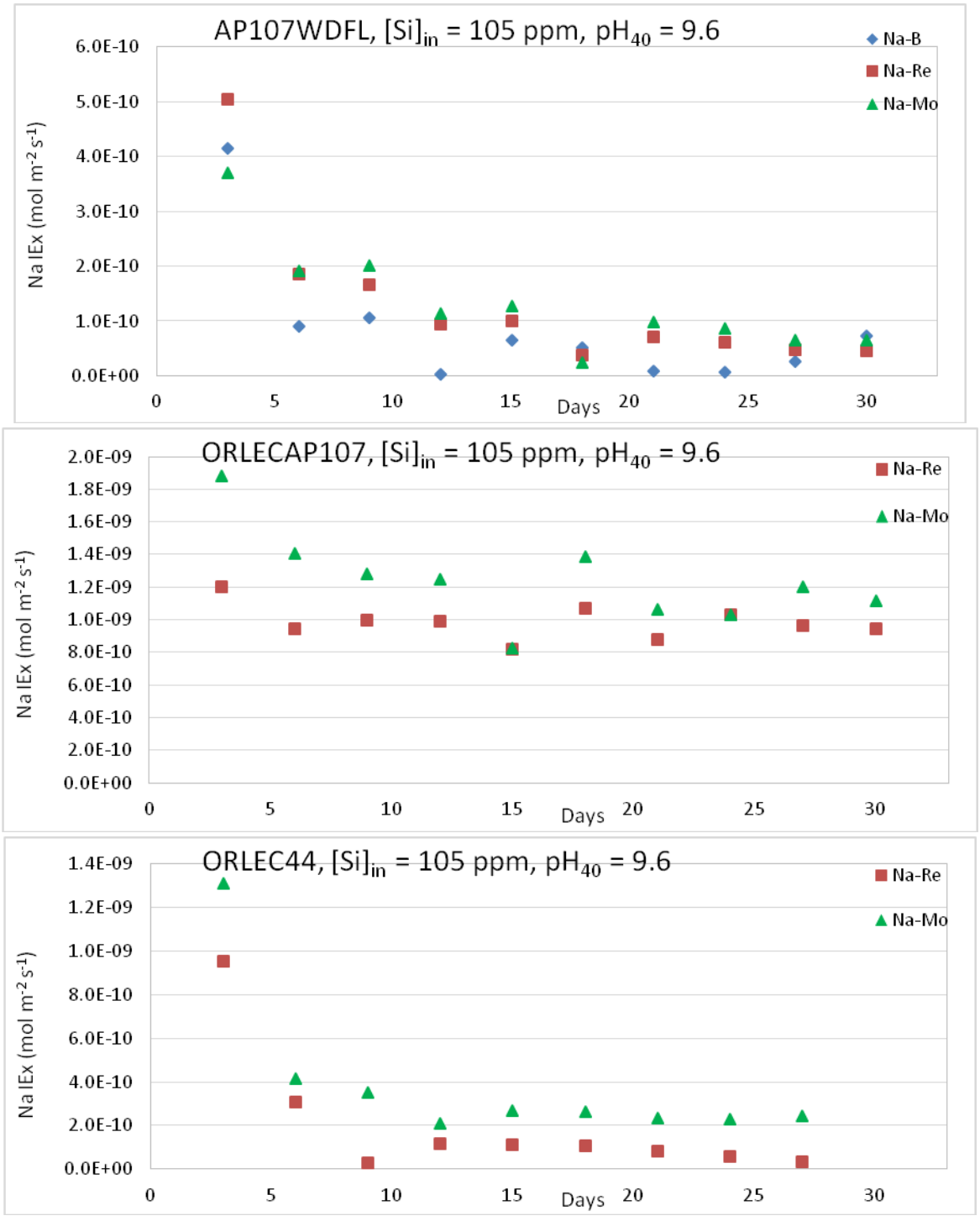

Figure C9. Plot of sodium ion exchange rate calculated from difference of sodium normalized release rate to that of boron, rhenium, or molybdenum, at 40 °C, pH_{23} =10.

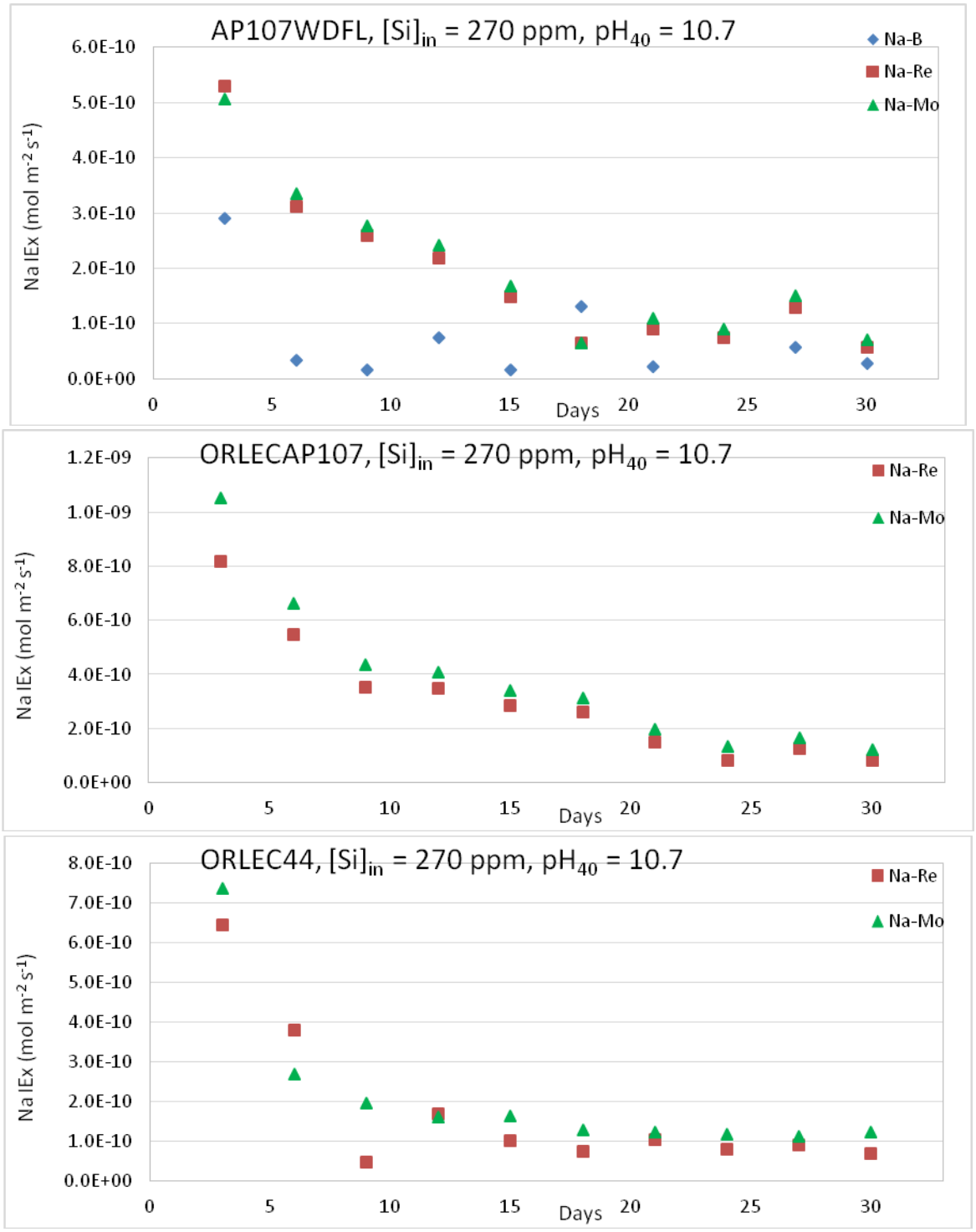

Figure C10. Plot of sodium ion exchange rate calculated from difference of sodium normalized release rate to that of boron, rhenium, or molybdenum, at 40 °C, pH_{23} =11.

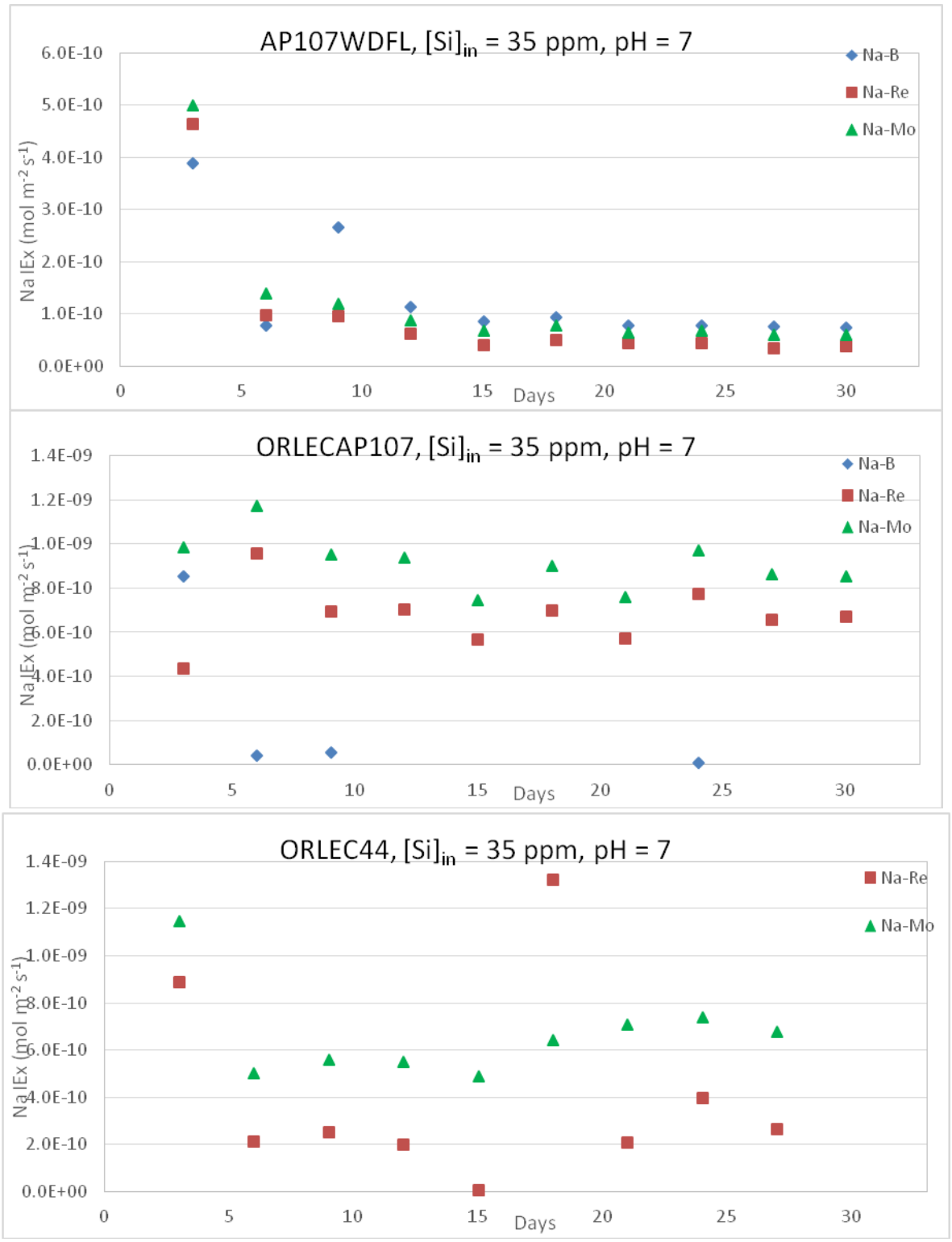

Figure C11. Plot of sodium and lithium ion exchange rate calculated from difference of respective normalized release rates to that of boron, rhenium, or molybdenum, at 23 °C, pH_{23} =7.

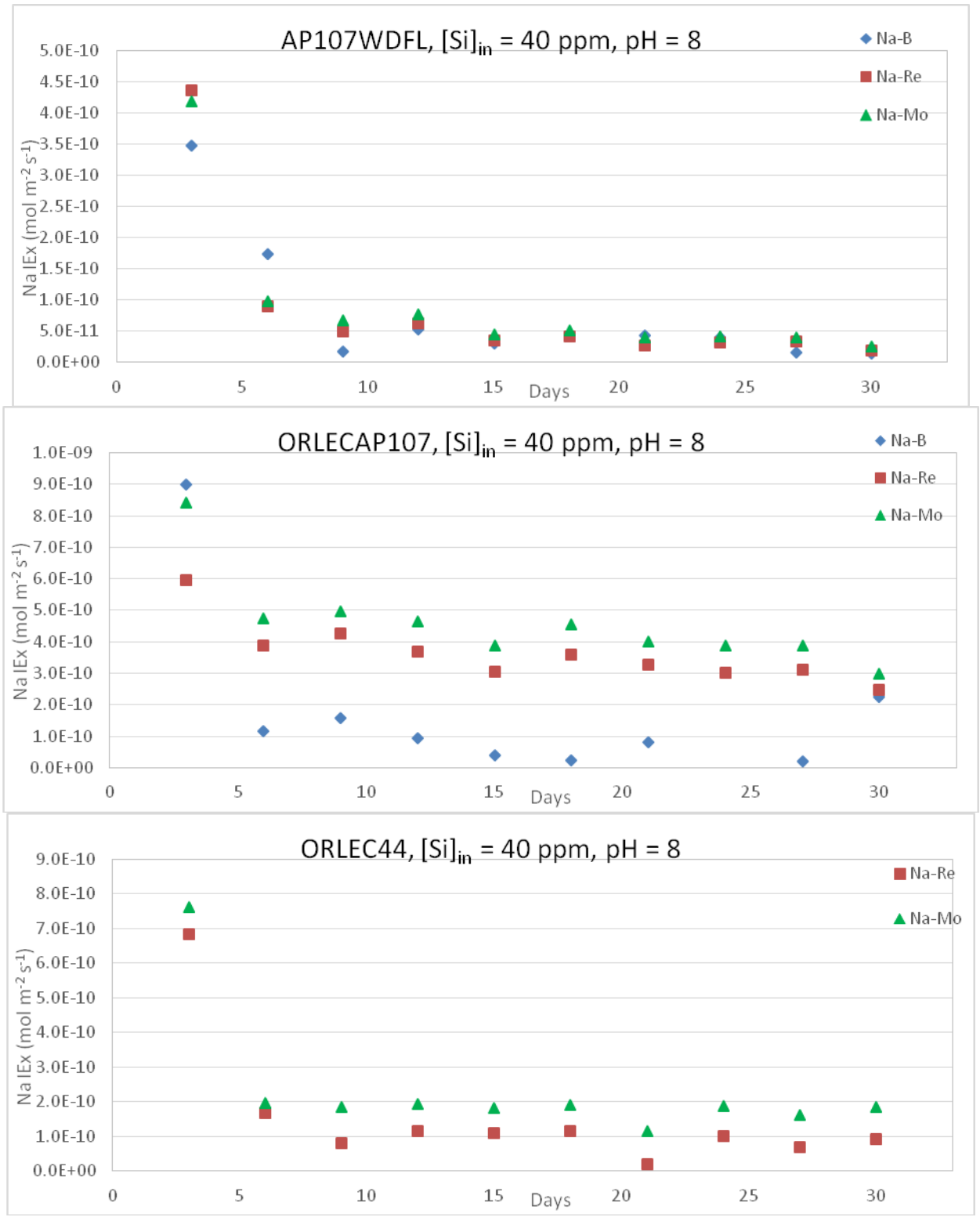

Figure C12. Plot of sodium ion exchange rate calculated from difference of respective normalized release rates to that of boron, rhenium, or molybdenum, at 23 °C, pH_{23} =8.

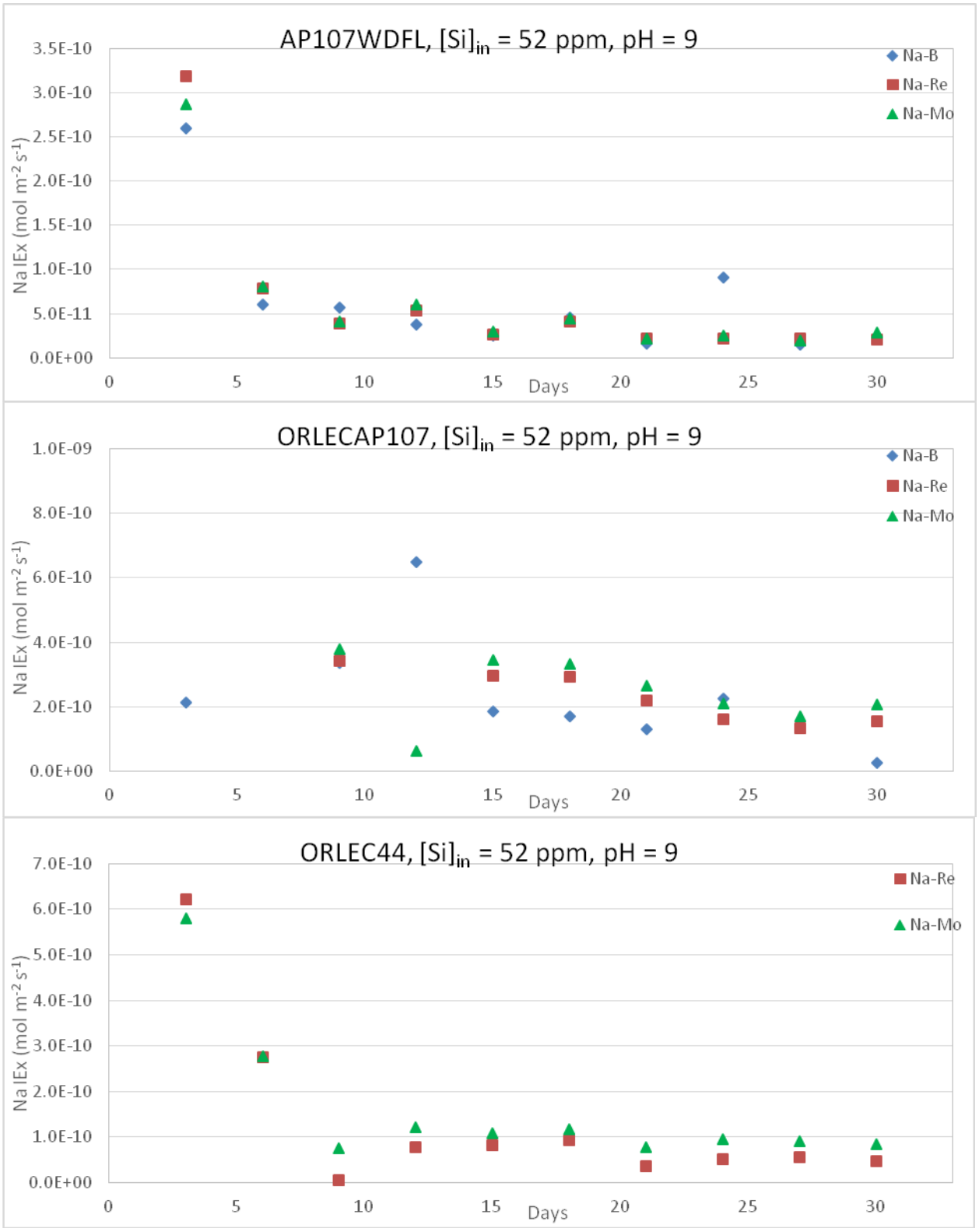

Figure C13. Plot of sodium ion exchange rates calculated from difference of respective normalized release rates to that of boron, rhenium, or molybdenum, at 23 °C, pH23 =9.

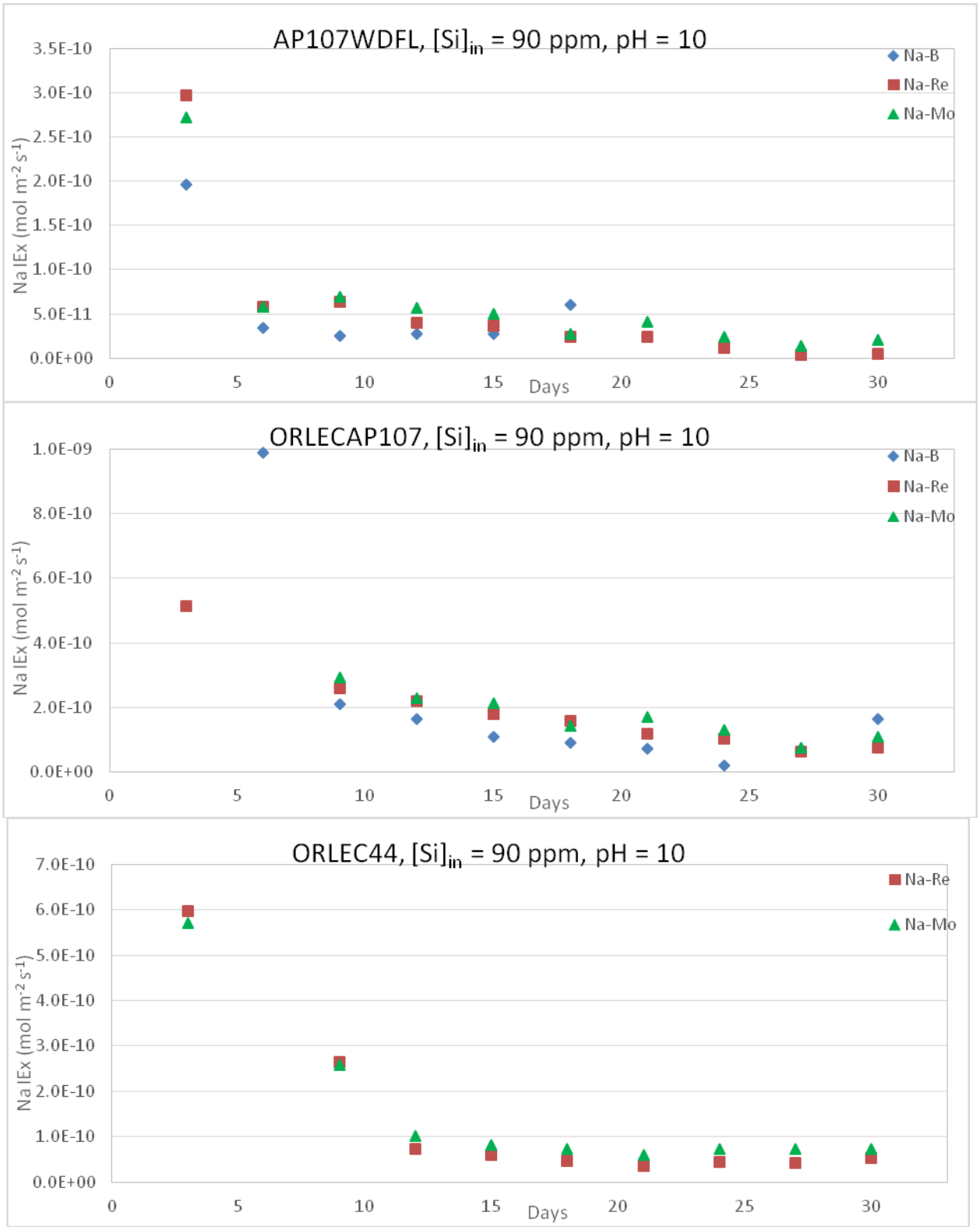

Figure C14. Plot of sodium ion exchange rates calculated from difference of respective normalized release rates to that of boron, rhenium, or molybdenum, at 23 °C, pH_{23} =10.

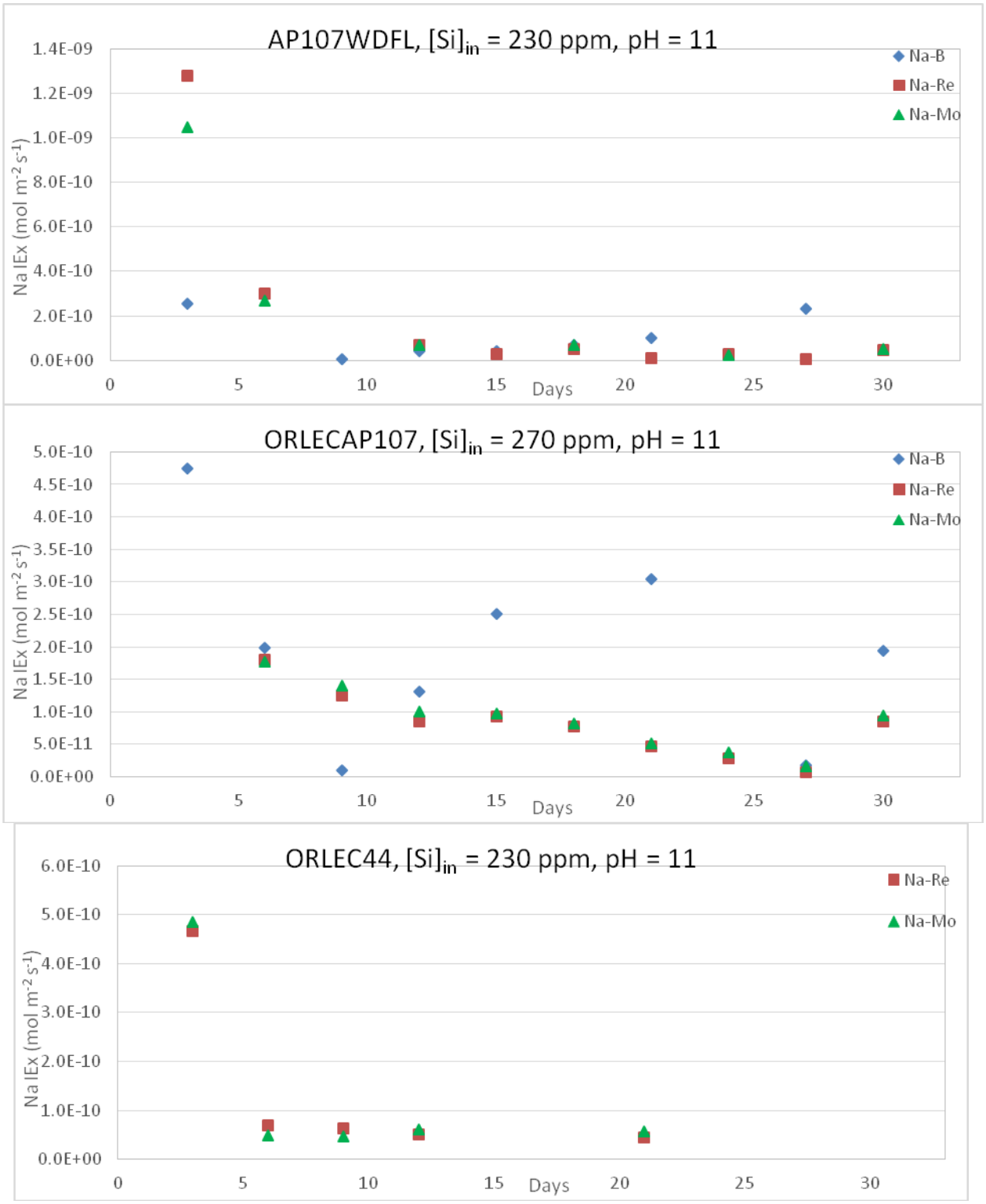

Figure C15. Plot of sodium ion exchange rates calculated from difference of respective normalized release rates to that of boron, rhenium, or molybdenum, at 23 °C, pH_{23} =11.